



MARTIN-LUTHER-UNIVERSITÄT  
HALLE-WITTENBERG

Synthesis and Characterization of  
*N* $\alpha$ -aroyl-*N*-aryl-Phenylalanine Amides  
and Their Activity Against Mycobacteria

## **Kumulative Dissertation**

Zur Erlangung des akademischen Grades  
*Doctor rerum naturalium (Dr. rer. nat.)*

Vorgelegt der  
Naturwissenschaftlichen Fakultät I – Biowissenschaften  
Martin-Luther-Universität Halle-Wittenberg

Von  
Markus Philipp Lang



1. Gutachter/in: Professor Dr. Peter Imming
2. Gutachter/in: PD Dr. habil. Matthias Schmidt
3. Gutachter/in: Professor Dr. Courtney Aldrich

Verteidigung der vorliegenden Arbeit am: 19.12.2024



To my family



---

# Acknowledgements

Completing this doctoral thesis has been a significant milestone in my professional journey, and I could not have shaped it without the support and encouragement of many individuals.

First and foremost, I would like to express my deepest gratitude to my advisors, Professor Dr. Peter Imming and Dr. Adrian Richter, for their guidance, continuous support, and patience and insightful feedback throughout my research.

I am also grateful to the reviewers of my dissertation, PD Dr. Matthias Schmidt and Professor Dr. Courtney Aldrich for their time and expertise.

I would like to express my gratitude to my friends & colleagues of my working group. First and foremost, Lea Mann, for performing a major part of mycobacterial work that is an integral part of this thesis. Many thanks are due to Dr. Rana Abdelaziz, Ruth Feilcke, Paul Robin Palme, Dr. Rüdiger W. Seidel, Dr. Mthandazo Dube, Julia Seiser and Franziska Flesch whose camaraderie, encouragement, and thought-provoking discussions have been a source of inspiration and motivation.

I thank the diploma and master students Ilaria Sequenzia, Leo Dumjahn and Johannes Doering that worked with me on this project.

Furthermore, I thank Antje Herbrich-Peters, Simone Kniesa and Dirk Stolzenhain for their scientific and technical support.

I would also like to thank all of our collaborators, but especially Professor Dr. Thomas Dick for the opportunity to become part of his lab for a short time and Dr. Uday S. Ganapathy for the exceptional introduction to the field of microbiology at the Center for Discovery and Innovation, Nutley and Professor Dr. Elizabeth Campbell and Dr. Barbara Bosch for the insights into RNAP and the inspiring time at The Rockefeller University in Manhattan.

On a personal note, I am deeply thankful to my family and friends for their unconditional love and support. To my parents, Ina and Dietmar, and my grandparents for your encouragement. To my partner, Marten, for your patience, understanding, and belief in me that has been a constant source of strength.

Thank you all for your support and contributions to this significant achievement in my life.

# Table of Contents

<i>Acknowledgements</i> .....	VII
<i>Table of Contents</i> .....	VIII
<i>List of Tables</i> .....	X
<i>List of Figures</i> .....	XI
<i>List of Abbreviations</i> .....	XIII
<b>1) Introduction</b> .....	<b>1</b>
<b>1.1) The Genus of Mycobacteria</b> .....	<b>1</b>
1.1.1) Systematic of Mycobacteria .....	1
Taxonomy of the <i>M. avium</i> complex .....	2
Taxonomy of <i>M. abscessus</i> .....	3
1.1.2) Microbiology of Mycobacteria .....	4
Cell Wall Morphology of Mycobacteria .....	4
Mycobacterial Biofilm Formation .....	6
Mycobacterial Infection of Immune Cells .....	7
The Slow Growth of Mycobacteria .....	7
<b>1.2) Infections &amp; Diseases Caused by NTM</b> .....	<b>9</b>
1.2.1) Transmission & Risk Factors of NTM Infections .....	9
1.2.2) Epidemiology of NTM Pulmonary Disease .....	10
1.2.3) Diagnosis of NTM Pulmonary Disease .....	11
1.2.4) Therapy of NTM Pulmonary Disease .....	12
Resistances & Susceptibility Testing of NTM .....	12
Therapy of <i>M. avium</i> complex Pulmonary Disease .....	14
Therapy of <i>M. abscessus</i> Pulmonary Disease .....	15
Role of RNAP Inhibitors in Therapy Regimens .....	16
<b>1.3) Structure &amp; Function of RNA Polymerases</b> .....	<b>17</b>
1.3.1) Differences of Prokaryotic and Eukaryotic RNA Polymerases .....	17
1.3.2) Structure of Prokaryotic RNA Polymerase .....	19
Comparison of RNAP Core Enzymes of Different Bacteria .....	23
1.3.3) Prokaryotic Transcription .....	24
1.3.3.1) Initiation .....	24
Promoter Recognition and Binding .....	24
Formation of the Open Promoter Complex .....	25
Abortive Initiation & Promotor Escape .....	25
1.3.3.2) Elongation .....	26
1.3.3.3) Termination .....	27

---

<b>1.4) Inhibition of Bacterial RNA Polymerase .....</b>	<b>29</b>
1.4.1) Prokaryotic RNAP as a Drug Target.....	29
1.4.2) Rifamycins .....	30
Chemistry of Rifamycins .....	30
Mechanism of Action & Target Binding .....	31
Resistance of Mycobacteria to Rifamycins .....	32
1.4.3) <i>N</i> -aroyl- <i>N</i> -aryl-phenylalanine amides (AAPs).....	33
Mechanism of Action.....	33
<b>2) Publications .....</b>	<b>37</b>
2.1) Objective of the Project .....	37
2.2) Research Article I.....	39
2.3) Research Article II .....	61
2.4) Research Article III .....	73
<b>3) Summary &amp; Discussion .....</b>	<b>89</b>
3.1) Chemical Derivatization & Structure-Activity Relationship.....	89
3.1.1) General Synthetic Procedure.....	90
3.1.2) Analysis of the Stereo Configuration.....	91
3.1.3) Derivatization of the Amino Acid Core .....	91
3.1.4) Derivatization of the Aroyl-Moiety (R <sup>2</sup> ) .....	91
3.1.5) Derivatization of Morpholinoaniline-Moiety (R <sup>3</sup> ).....	92
3.1.6) Necessity of Tertiary Nitrogen in Morpholine-like Derivatives.....	94
3.1.7) <i>N</i> -Methylation of Amide Bonds .....	94
3.2) Antimycobacterial Activity of AAP Derivatives.....	95
3.3) Metabolic <i>in vitro</i> Stability of AAPs.....	101
3.4) Target, Structural Insights & Binding Mode.....	103
3.5) Conclusion .....	105
<b>4) References .....</b>	<b>107</b>
<b>5) Appendices.....</b>	<b>127</b>
5.1) Comment on Provided Supplementary Information .....	127
5.2) Supplementary Information Publication I .....	129
5.3) Supplementary Information Publication II.....	189
5.4) Supplementary Information Publication III.....	229
<b>Publication List.....</b>	<b>XV</b>
<b>Curriculum Vitae .....</b>	<b>XVII</b>
<b>Eidesstattliche Erklärung .....</b>	<b>XVIII</b>

## List of Tables

<b>Table 1.</b> Runyon classification of NTM [6]. Classes I to III are slow-growing species that need longer than 5 days to form visible colonies on solid agar. ....	2
<b>Table 2.</b> The members of the <i>M. avium</i> complex based on genetic analysis [11]....	3
<b>Table 3.</b> ATS recommended treatment regimens and dosing for <i>M. avium</i> complex pulmonary disease [105]. ....	14
<b>Table 4.</b> Suggested therapy scheme of the ATS for <i>M. abscessus</i> pulmonary disease [83], [98], [115]. Abbreviations: PO, peroral drugs; IV, intravenous drugs; NEB, nebulized drugs.....	15
<b>Table 5.</b> Overview on prokaryotic and eukaryotic RNA polymerases und their functionalities. ....	18
<b>Table 6.</b> Comparison of RNAP core enzyme subunits molecular weights of different bacterial species. <i>E. coli</i> : <i>Escherichia coli</i> ATCC 11775, <i>Mtb</i> : <i>M. tuberculosis</i> : ATCC 25618 / H37Rv; <i>M. abscessus</i> : <i>Mycobacterium abscessus</i> ATCC 19977. Molecular weights rounded to integral kDa. ....	23
<b>Table 7.</b> Sequence homology of RNAP subunits between <i>E. coli</i> : <i>Escherichia coli</i> ATCC 11775 (PATRIC genome ID: 866789.18), <i>Mtb</i> : <i>Mycobacterium tuberculosis</i> ATCC 25618 / H37Rv (sequence extracted from PDB file: 5UHA); <i>Mabs</i> : <i>Mycobacterium abscessus</i> ATCC 19977 (PATRIC genome ID: 36809.5). Sequence homology was determined with Basic local alignment search tool provided by the National Institutes of Health (NIH) [145]. ....	24
<b>Table 8.</b> General chemical structure of rifamycins and associated structures of clinically used rifamycins. Red numbers indicate numbering of carbon atoms. ..	31
<b>Table 9.</b> Selection of synthesized AAP derivatives with the highest activities against <i>M. tuberculosis</i> H37Rv ( <i>Mtb</i> ), <i>M. abscessus</i> ATCC 19977 ( <i>Mabs</i> ) and <i>M. intracellulare</i> ATCC 35761 ( <i>Mintra</i> ). Black compound numbering as in Publication I, Lang et. al., J. Med. Chem., 2023. Blue compound number as in Publication II, Lang et al., ChemMedChem, 2024. Orange compound number as in Publication III, Lang et al., Antibiotics, 2024. ....	96
<b>Table 10.</b> Comparison of MBC and MIC values of a selection of antibiotics and AAP derivatives against <i>M. abscessus</i> . Colors indicate identical compounds analyzed in different publications. ND: not determined. For structures of AAP derivatives see Table 9. ....	98

# List of Figures

<b>Figure 1.</b> Diagram of the mycobacterial cell wall with the thickness of each layer. The blue colored parts of the glycolipids stand for lipophilic chains that interact with the mycolic acids, the red head groups resemble the hydrophilic carbohydrate groups that are oriented to the outside of the bacterial cell and play an important role in bacteria-host interaction. ....	4
<b>Figure 2.</b> An exemplary $\alpha$ -mycolic acid. ....	5
<b>Figure 3.</b> Scheme of a prokaryotic RNAP holoenzyme. ....	19
<b>Figure 4.</b> Different perspectives of a crystallized <i>M. tuberculosis</i> transcription initiation complex (PDB: 5UHE, 4.04 Å resolution). The data and graphics were processed using Chimera X [131]. ....	20
<b>Figure 5.</b> Clipped depiction of a crystallized <i>M. tuberculosis</i> transcription initiation complex (PDB: 5UHE, 4 Å resolution) limited to the $\beta$ and $\beta'$ subunits exposing the cleft incorporating the three main channels of bacterial RNAP as well as the active center. The data and graphics were processed using Chimera X [131].....	21
<b>Figure 6.</b> Binding interactions between the RNAP holoenzyme and the DNA promotor region. ....	25
<b>Figure 7.</b> Depiction of a crystallized <i>M. tuberculosis</i> transcription initiation complex (PDB: 5UHE, 4 Å resolution). The RNA exit channel is blocked by the $\sigma_4$ resulting in abortive initiation cycles in which short RNA transcripts are produced. The data and graphics were processed using Chimera X[131].....	26
<b>Figure 8.</b> Depiction of an <i>M. tuberculosis</i> RNAP elongation complex (PDB: 8EOS, electron microscopic data, resolution: 3.10 Å). View into the catalytic cleft ( $\beta$ subunit excluded). Trigger loop (T1008-P1029), Bridge helix (L847-S881) and F-Loop (A818-V846) are highlighted in different colors. The data and graphics were processed using Chimera X [131]. ....	27
<b>Figure 9.</b> The binding site of AAPs is located between the <i>N</i> -terminal end of the bridge helix and the F loop in a distance of $\sim 30$ Å to the catalytic center. The $\beta$ subunit is omitted for clarity. Depiction based on PDB: 8EOS, electron microscopic data, resolution: 3.10 Å.....	34
<b>Figure 10.</b> Structural comparison of the AAP screening hit MMV688845 and D-AAP1 with the CBR compound CBR703. Chemical moieties that form concordant target interactions are marked with the same colors. The $\beta$ and $\beta'$ subunits in <i>M. tuberculosis</i> RNAP form three lipophilic pockets that can accommodate the	

three aromatic systems of AAPs. One of these pockets is absent in the RNAP of gram-negative bacteria, explaining AAP inactivity. CBR compounds lack one aromatic system at that particular site, which is responsible for restoring activity against gram-negative bacteria. .... 35

**Figure 11.** Overview of substituents that were introduced to the AAP chemical scaffold in the present publications. Arrows indicate the overall effect on biological activity. Letters indicate in which publication the respective moieties were used for derivatization. .... 90

**Figure 12.** Selection of clinically used compounds with S-oxides as structural elements. .... 93

**Figure 13.** Overview of MIC<sub>50</sub> values determined against strains of the *M. abscessus* complex, the *M. avium* complex and a set of different other NTM. CLR: clarithromycin; Compound 3: Improved AAP derivative; compound 3 in publication III [188]; MMV: MMV688845. ....100

**Figure 14.** Preliminary 2.5 Å cryo-EM structure of *M. tuberculosis* RNAP together with compound 24 (Lang *et al.*, J. Med. Chem., 2023) bound to the AAP target site (unpublished). ....104

# List of Abbreviations

Abbreviations used in the publications presented in this work are excluded from this list and can be found in the respective publication.

AAP	<i>N</i> $\alpha$ -aroyl- <i>N</i> -aryl-phenylalanine amides
ABC	ATP binding cassette
ADP	Adenosine diphosphate
ATCC	American Type Culture Collection
ATP	Adenosine triphosphate
ATS	American Thoracic Society
bp	Base pair
CFTR	Cystic fibrosis transmembrane conductance regulator
CLSI	Clinical and Laboratory Standards Institute
COPD	Chronic obstructive pulmonary disease
DNA	Desoxyribonucleic acid
<i>E. coli</i>	<i>Escherichia coli</i>
EC	Ternary elongation complex
EM	Electron microscopy
GPL	Glycopeptidolipid
IDSA	Infectious Diseases Society of America
<i>M. species name</i>	<i>Mycobacterium species name</i>
MBC	Minimal bactericidal concentration
MIC	Minimal inhibitory concentration
MRSA	Methicillin resistant <i>Staphylococcus aureus</i>
NAC	Nucleotide addition cycle
NIH	National Institutes of Health
NTM	Non-tuberculous mycobacteria
NTP	Nucleoside triphosphate
PATRIC	Pathosystems Resource Integration Center
PDB	Protein data base
RNA	Ribonucleic acid
RNA Pol I/II/III	Eucaryotic RNA polymerases I/II/III
RNAP	RNA polymerase
RP <sub>c</sub>	Closed promoter complex
RP <sub>o</sub>	Open promoter complex
TB	Tuberculosis
$\alpha_2\beta\beta'\omega$	RNAP core enzyme



# 1) Introduction

## 1.1) *The Genus of Mycobacteria*

The genus *Mycobacterium* encompasses a wide spectrum of bacteria, with more than 190 species identified to date [1]. Of these, the *Mycobacterium tuberculosis* (*M. tuberculosis*) complex is the most well-known and stands out as it includes the bacteria responsible for tuberculosis (TB), a disease that has had a profound impact on global health [2]. In addition to TB-causing bacteria, this genus also includes *M. leprae* and *M. lepromatosis*, which are known to cause leprosy, an infectious disease that remains particularly prevalent in regions such as India, Brasil and Indonesia [3], [4].

In addition to these infamous pathogens, another group of mycobacteria is drawing the attention of health systems: Non-tuberculous mycobacteria (NTM) represent a group of mycobacterial species, which are causing infectious diseases that are challenging to treat. This introduction gives an overview of the biology and clinical importance of mycobacteria with a focus on NTM, thus allowing the reader to gain an understanding of the effects of these microorganisms on public health and the obstacles encountered in developing novel medicinal chemistry strategies to combat them.

### 1.1.1) Systematic of Mycobacteria

The genus *Mycobacterium* can be divided into three distinct groups. The first of these is the *M. tuberculosis* complex, which contains a number of obligate pathogens that cause the infectious disease TB in various human and non-human host species. Based on recent comparative genetic analysis, the classical taxonomy of the *M. tuberculosis* complex has been revised, with the result that many species do not meet the criteria of autonomous species [5]. The former species names (present in humans; *M. tuberculosis (sensu strictu)*, *M. africanum*, *M. bovis*, *M. caprae* and *M. canetti*; [6]), have been classified as synonyms or strains of *M. tuberculosis*.

Secondly, *M. leprae* and *M. lepromatosis*, which are distinguished from other mycobacteria due to extensive evolutionary genome decay [7].

Lastly, there is the group of NTM. The first attempt to categorize NTM was made by Runyon in 1959, who used phenotypic characteristics of the bacteria for differentiation, resulting in a 4-class system summarized in **Table 1**.

**Table 1.** Runyon classification of NTM [8]. Classes I to III are slow-growing species that need longer than 5 days to form visible colonies on solid agar.

Runyon class			
I Photochromogens	II Scotochromogens	III Non- Chromogens	IV Fast-growing
Slow-growing			
Produce pigments under the influence of light	Produce pigments even without light	Never produce pigments	Form colonies on solid agar within 5 days or less
Examples			
<i>M. kansasii</i> <i>M. marinum</i> <i>M. simiae</i> <i>M. szulgai</i> *	<i>M. xenopi</i> <i>M. gordonae</i> <i>M. szulgai</i> *	<i>M. avium</i> complex <i>M. ulcerans</i>	<i>M. fortuitum</i> <i>M. abscessus</i> <i>M. chelonae</i> <i>M. smegmatis</i>

\* *M. szulgai* belongs to class I when grown at 24 °C and to class II when grown at 37 °C.

While the power of genetic analysis has reshaped the phylogeny and taxonomy of mycobacteria [1], [9], the phenotypic classification into fast- and slow-growing mycobacteria is in use up to this day. The most common genetic tool for species identification is by sequencing the 16S rRNA gene. Secondary gene targets for identification are the *hsp65* and the *rpoB* genes [10].

In 2018, Gupta *et al.* implemented a new taxonomic system of mycobacteria that divided the former genus of *Mycobacterium* into five distinct genera based on genetic analysis [11]. This new system provoked a dispute within the scientific community, with the consensus to largely ignore the proposed changes [12].

#### Taxonomy of the *M. avium* complex

The slow-growing *M. avium* complex consisted of two mycobacterial species, *M. avium* and *M. intracellulare*. Van Ingen *et al.* defined a revised classification system that includes more species, based on their genetic identity to each other [13]. The system is shown in **Table 2**. The organism with the highest clinical relevance for humans within the *M. avium* complex is *M. avium* subsp. *hominissuis* (“the one that infects human and pigs”) and both *M. intracellulare* subspecies. The other species are rarely found in humans.

**Table 2.** The members of the *M. avium* complex based on genetic analysis [13].

Species	Subspecies	Clinical relevance in humans
<i>M. avium</i>	<i>avium</i>	Rarely infectious for humans, bird related
	<i>hominissuis</i>	Pulmonary disease, lymphadenitis, disseminated disease, osteomyelitis, skin and soft tissue infection
	<i>silvaticum</i>	No relevance, virulent in birds
	<i>paratuberculosis</i>	No relevance, virulent in cattle, discussed to be related to human Crohns disease [14]
<i>M. intracellulare</i>	<i>intracellulare</i>	Pulmonary disease, lymphadenitis, disseminated disease, osteomyelitis, skin infections
	<i>chimaera*</i>	Pulmonary disease, osteomyelitis, endocarditis, skin infections
<i>M. arosiense</i>	-	Pulmonary disease, osteomyelitis, skin infections
<i>M. colombiense</i>	-	Disseminated disease
<i>M. vulneris</i>	-	Lymphadenitis, Skin infections
<i>M. marseillense</i>	-	No clinical data
<i>M. bouchedurhonense</i>	-	No clinical data
<i>M. timonense</i>	-	No clinical data
<i>M. yongonense**</i>	-	Pulmonary disease
<i>M. paraintracellulare</i>	-	Pulmonary disease
<i>M. lepraemurium</i>	-	No relevance

\* Van Ingen *et al.* classify *M. chimaera* as a separate species; however, in literature it is often found as a subspecies of *M. intracellulare*, *e.g.* [15], [16]

### Taxonomy of *M. abscessus*

The taxonomy of the *M. abscessus* has also evolved with advancements in molecular techniques. Initially classified as a single species, it has been redefined into three distinct subspecies based on genetic and phenotypic differences: *M. abscessus* subsp. *abscessus*, *M. abscessus* subsp. *bolletii*, and *M. abscessus* subsp. *massiliense*. The designation of *M. abscessus* as a complex of its subspecies should be avoided as the sole presence of subspecies does not justify the taxonomical formation of a complex [17]. The interesting and turbulent history of *M. abscessus* taxonomy is summarized by Lopeman *et al.* [18]. The fact that the three subspecies are genetically very similar, but develop distinct phenotypical

differences, was the reason for vibrant scientific discussions [19]. This is reflected by the presence of unique resistance mechanisms to commonly used antibiotics, complicating therapeutic approaches. These aspects are discussed in section 1.2.4).

### 1.1.2) Microbiology of Mycobacteria

Mycobacteria represent a group of bacteria that exhibit unique physiological and biological characteristics, setting them apart from other bacteria. These traits contribute significantly to their resilience and the challenges associated with treating infections caused by them.

#### Cell Wall Morphology of Mycobacteria

Mycobacteria have a cell envelope that is different in structure and composition when compared to the cell walls of Gram-positive and Gram-negative bacteria [20]. The generally more robust mycobacterial cell walls consist of different layers with distinct functions. A schematic diagram of these layers and their dimensions is given in Figure 1.

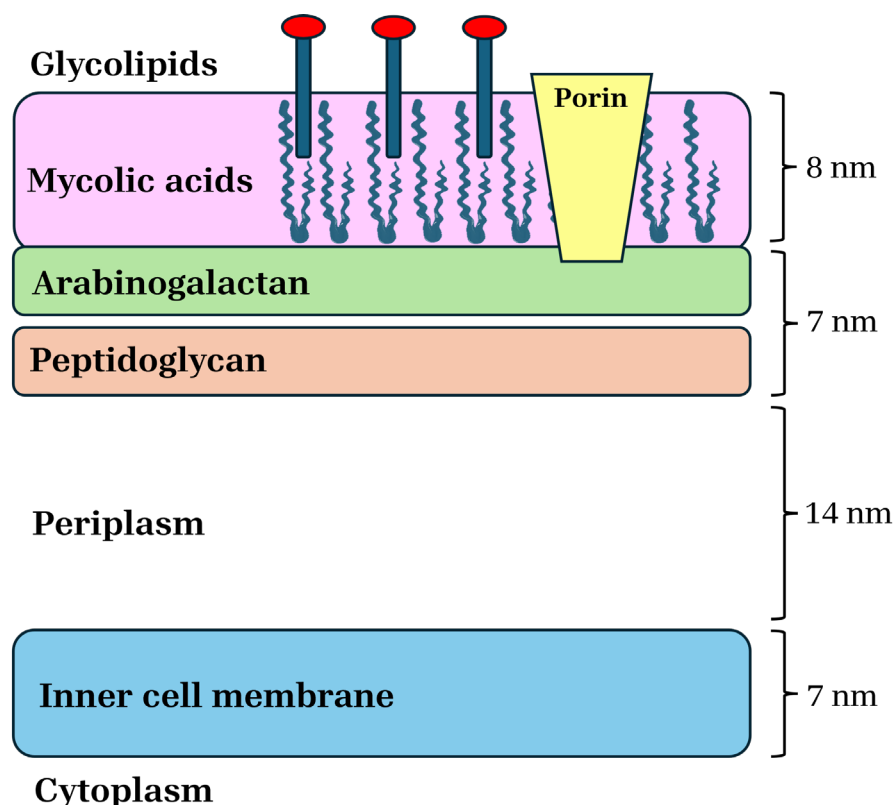


**Figure 1.** Diagram of the mycobacterial cell wall with the thickness of each layer. The blue colored parts of the glycolipids stand for lipophilic chains that interact with the mycolic acids, the red head groups resemble the hydrophilic carbohydrate groups that are oriented to the outside of the bacterial cell and play an important role in bacteria-host interaction.

The inner cell membrane of mycobacteria is bordering the periplasmic space, which is rich in enzymes that are necessary for the assembly and regulation of the cell wall structure [21].

Adjacent to the periplasm is the layer of mesh-like peptidoglycan that provides structural integrity and shape to the bacterial cell. The peptidoglycan is built up from alternating *N*-acetyl glucosamine and *N*-acetyl muramic acid monomers that can be modified [22]. The chains are interconnected by short peptide sidechains (8 amino acids per connection) that form the rigid mesh. The *N*-acetyl moiety attached to the muramic acid moiety is sometimes oxidized in mycobacteria to form *N*-glycolyl muramic acid [23], which is discussed to strengthen the peptidoglycan mesh because it provides additional hydrogen bonding capacities [24]. The structure giving function of peptidoglycan is supported by embedded arabinogalactan, which is a polysaccharide mainly composed of arabinose and galactose. It is connected to the peptidoglycan by phosphodiester bonds to provide additional strength [22].

This arabinogalactan-peptidoglycan matrix provides an anchor for the mycomembrane that is attached on the outside. It is organized as a double layer that mostly contains highly lipophilic mycolic acids. The inner layer is covalently bound to the arabinogalactan. These  $\beta$ -hydroxy- $\alpha$ -alkyl fatty acids are made up of two long aliphatic branches that can vary in length as displayed in **Figure 2**. In addition to the structure shown, oxygenated mycolic acids that carry keto or methoxy functionalities instead of the distal cyclopropane ring in the merochain are present in mycobacteria [25]. They adopt different conformations in the mycomembrane which probably contribute to antibiotic tolerance, as their absence caused an improvement in antibiotic activity [26]. The high hydrophobicity of mycolic acids makes mycobacteria generally less permeable for most antibiotics, causing resistance. Jarlier *et al.* showed that the influx of  $\beta$ -lactams in *M. chelonae* is reduced up to 3 orders of magnitude in comparison to *Pseudomonas aeruginosa* because of this permeability barrier [27].

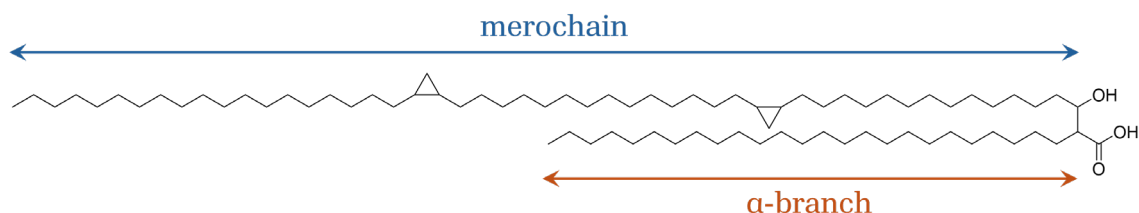


**Figure 2.** An exemplary  $\alpha$ -mycolic acid.

While absent in *M. tuberculosis*, in NTM the outer leaflet of the mycomembrane contains glycopeptidolipids (GPLs) that populate the outer surface [28]. These lipids play an important role in host interactions and can mask the antigens present in the bacterial cell walls from recognition, thereby modulating the hosts immune responses [29], [30]. Additionally, the presence or absence of GPLs affects the morphotype of NTM the way they form biofilms or infect immune cells, as described below.

### Mycobacterial Biofilm Formation

The ability of some mycobacterial species to adhere to biological and artificial surfaces to form confluent biofilms has been analyzed [31], [32]. For NTM, suitable environments such as waterpipes, household water sources and showerheads are suspect for the formation of biofilms, which can be a continuous reservoir for bacteria [33]. Their extraordinary cell wall morphology distinguishes biofilm formation from other bacterial taxa [34]. Their lack of cell extensions, like pili or fimbriae that usually ensures initial surface attachment, are replaced by other adhesion strategies. Especially for NTM, the GPLs protruding from the outer capsule of the bacterial cells play an important role in their attachment and mobility on the surface, as shown for *M. smegmatis* [35]. Additionally, the extracellular matrix that interconnects the cells and that gives the bacterial community structure is of different composition, as mycobacteria seem unable to excrete exopolysaccharides that are often present in biofilms [36]. Instead, free mycolic acids, which are shorter than the ones that build up the cell wall, appear to be an integral part of mycobacterial biofilm matrices [37]. Their involvement provides an additional layer of hydrophobicity and defense onto the bacteria, which is already recognized as another parameter that complicates therapeutic intervention [38].

*M. abscessus*, as well as other NTM, can undergo a transition from a smooth to a rough morphotype, which is also affecting their ability to form biofilms [39]. These two morphologies are adopted by the bacteria depending on the amount of GPLs expressed on their outer surface. The smooth morphotypes capsules are highly populated with these lipids allowing them to form biofilms [40], [41]. In the case of *M. abscessus* pulmonary disease, this morphotype is considered to be more infectious, mainly due to the formation of difficult to eradicate biofilms in the respiratory tract that evade the host immune response [40]. The rough morphotype lacks GPLs, and instead of forming biofilms, bacteria of this morphotype form long, cord-like aggregates that are associated with severe tissue destruction and inflammation [42].

### Mycobacterial Infection of Immune Cells

Immune cells like macrophages establish the primary line of defense against bacteria. They employ phagocytosis and intracellular lysosomal processes to eradicate invading bacteria and stop infection. The remarkable resilience of mycobacteria allows them to survive and modulate these mechanisms. This infection of immune cells is especially well understood for *M. abscessus*, which can replicate inside of these cells in contrast to *M. smegmatis* and *M. fortuitum* [43]. The content of GPLs and the resulting morphotypes of *M. abscessus* control the way the bacteria are ingested by macrophages. Rough morphotypes, that form large aggregates, cannot be engulfed by macrophages and persist in peripheral areas [44]. Only small aggregates are ingested and form social phagosomes inside the macrophages. This type of phagosome strongly stimulates macrophage apoptosis, releasing bacteria that can initiate replication to cause tissue damage and inflammation [43]. Smooth morphotypes that are rich in GPLs are phagocytized as individual bacteria. The maturation process of these loner phagosomes to lysophagosomes seems to be inhibited by the smooth *M. abscessus* bacteria, preventing them from being lysed [43]. That way, smooth *M. abscessus* strains can survive inside of macrophages for a long time. It has been proposed that infected macrophages are stimulated to secrete cytokines, which results in the recruitment of other immune cells, ultimately leading to the formation of granulomas [43], [45].

### The Slow Growth of Mycobacteria

One of the most notable characteristics of mycobacteria is that they exhibit exceptionally low growth rates in comparison to other bacteria. Even within the genus *Mycobacterium*, growth rates can vary considerably. Fast-growing mycobacteria, such as *M. smegmatis*, *M. abscessus*, or *M. fortuitum*, can form visible colonies on solid agar in three to five days. In contrast, slow-growing species, such as the *M. avium* complex, *M. kansasii*, and *M. malmoense* require more than seven days, while some species, including *M. simiae*, *M. szulgai*, and *M. xenopi*, require up to 15 days. *M. ulcerans* and the *M. tuberculosis* require up to 28 days to form visible colonies [46].

There are many reasons why mycobacteria have low growth rates. It has been discussed that the low permeability of mycobacterial cell walls for hydrophilic solutes also restricts the amount of nutrients that are available for bacterial metabolism [47]. The expression of porins could be the only proper pathway for hydrophilic substances to enter the bacterial cell [48]. Therefore, high expression levels may be correlated with high growth rates. Sharbati-Tehrani *et al.* demonstrated that *MspA*-mediated expression of porins, which are naturally

present in the fast-growing *M. smegmatis*, can increase the growth rate of *M. bovis* by up to four-fold [49]. The lower amount of substrate specific ABC importers compared to fast-growing organisms like *Escherichia coli* (*E. coli*) [50] and the generally lower synthetic performance of nucleic acid products are also discussed as reasons for low growth rates [51].

It is striking that the apathogenic and low-risk bacteria tend to have faster growth rates, while highly pathogenic mycobacteria such as *M. tuberculosis* and *M. leprae* grow exceptionally slowly. Therefore, the causality between growth rate and virulence is often discussed. Higher virulence may be due to the ability of slow-growing mycobacteria to efficiently persist within granulomas, areas of limited nutrient supply [52].

## **1.2) Infections & Diseases Caused by NTM**

Unlike the *M. tuberculosis* complex, which evolved as a specialized pathogen in humans [53], NTM are ubiquitous environmental bacteria, that can be found in soil, natural sources, and in various biofilms within human made plumbing systems [54], [55]. The only two NTM species that are considered as obligate pathogens are *M. marinum*, the causative agent of the swimming pool granuloma [56], and *M. ulcerans*, which is causing the Buruli ulcer disease [57], while other NTM species only cause disease in individuals suffering from certain risk factors (see 1.2.1).

The clinical relevance of NTM infections has surged in recent decades due to an increase in susceptible populations, advances in diagnostic methods, and heightened clinical awareness [58]. NTM infections present as a wide spectrum of manifestations, ranging from asymptomatic colonization [59], soft tissue infections [60], lymphadenitis [61], and disseminated disease. However, the most common clinical presentation is a severe but slowly progressing pulmonary disease, which is characterized by TB-like symptoms such as fever, chronic cough with sputum production, shortness of breath, fatigue, and unplanned weight loss. The following sections focus on this predominant clinical manifestation.

### **1.2.1) Transmission & Risk Factors of NTM Infections**

There are several ways in which NTM can enter the human body to cause infections. The main route appears to be human contact with environmental sources. Biofilms in the water supply system [62] as well as contaminated shower heads [63] are reservoirs of NTM that persons at risk are in continuous contact with [64]. In addition, the usage of indoor swimming pools is largely recognized as a potential source of infection and the use should be limited in susceptible populations [65]. Aerosolization of water and subsequent inhalation of contaminated droplets is considered as the most common way of infection. Other infectious materials are potting soils and fomites, which are naturally inhabited by NTM [66]. Patient-to-patient transmission is controversially disputed but does not seem to play a major role for epidemiology [67], [68].

Certain populations are at a higher risk for NTM pulmonary disease. These include individuals with preexisting lung diseases, such as bronchiectasis [69] and COPD [70] as well as those with weakened immune systems due to conditions like HIV/AIDS [71], [72], or immunosuppressive treatments [73]. Additionally, patients that suffer from cystic fibrosis, show an increased susceptibility to NTM infections. A genetic irregularity causes the expression of a dysfunctional cystic fibrosis transmembrane conductance regulator (CFTR), a chloride channel which is

regulating the electrolyte homeostasis of lung epithelia cells [74]. This causes the cells to excrete thick mucus, which impairs mucociliary clearance and promotes invasion of NTM [75], [76], [77].

### 1.2.2) Epidemiology of NTM Pulmonary Disease

The epidemiology of NTM pulmonary disease varies significantly across different geographic regions and populations. The prevalence of NTM infections appears to be rising globally, with notable increases in developed countries. This is likely due to improved diagnostic capabilities, heightened awareness, and changes in environmental factors. In many of these countries, the incidence of NTM pulmonary disease is estimated to be higher than that of TB. For the United States a TB incidence rate of 2.5 per/100,000 was reported in 2022 [78], while for NTM disease an overall incidence rate of 3.13 – 4.73 was reported for the period between 2008 and 2015 [79]. In Japan the number of new TB cases is decreasing since years (incidence: 2010: 15 per/100,000; 2021: 7.5 per/100,000) [80], but the rate of new NTM cases is steadily increasing. The most recent incidence rate that was reported for NTM pulmonary disease is 14.9 per/100,000 in the year of 2014 which is a doubling in cases since the year 2000 [81]. It is notable that the highest incidences of NTM pulmonary disease occur in regions that have tropic temperatures and high humidity. For the United States, Hawaii and Florida have a higher reported burden of NTM pulmonary disease than other states [82], [83]. Countries in south-east Asia (Japan, Taiwan, South Korea, China) and Australia (Queensland), have a particularly high burden [79]. The amount of data regarding NTM pulmonary disease surveillance is very low for African regions. The available diagnostic tools and lack of awareness in routine care suggest that a significant part of NTM infections is misdiagnosed as TB [79].

The distribution of different NTM species also differs substantially within different regions. A comprehensive and recent review on this topic was published by Prevots *et al.* [79]. For most countries and regions, the *M. avium* complex is the most common species causing NTM pulmonary disease ranging from ~50% to ~90% of reported cases. *M. abscessus* is the other predominant infectious agent, ranging between 5% and 10% of cases in many countries. Exceptions with higher *M. abscessus* infection rates are Mexico City (27 % of cases) and French Guiana (16% of cases) [79]. Exceptions can be found in Japan where *M. chelonae* is most often encountered. Serbia and Croatia have a particularly high burden reported for *M. xenopi* pulmonary disease [79]. The United States, Poland and Brazil suffer from high numbers of *M. kansasii* pulmonary disease [79]. Other NTM that are causing pulmonary disease less often are *M. malmoense*, which seems to be prevalent in northern European regions [84], *M. szulgai* [85], [86], and *M. simiae* [87].

### 1.2.3) Diagnosis of NTM Pulmonary Disease

Diagnosing NTM pulmonary disease requires a combination of clinical, radiological, and microbiological criteria. The American Thoracic Society (ATS) together with the Infectious Diseases Society of America (IDSA) give recommendations on which tests should be performed as a minimum evaluation to decide whether the definition of NTM pulmonary disease is met [88]:

- **Clinical:**
  - Pulmonary TB-like symptoms like cough, decline in lung function or systematic symptoms
  - Exclusion of other diseases, especially TB
- **Radiological:**
  - Chest radiography or alternatively high-resolution computed tomography to check for lung involvement (cavitation, bronchiectasis, nodules)
- **Microbiological:**
  - At least two NTM-positive expectorated sputum samples from different time points  
*or*
  - One NTM-positive culture from a bronchial lavage  
*or*
  - Histopathologic identification of mycobacterial features like granulomatous inflammation together with positive culture from the same biopsy specimen

If these criteria are fulfilled, the species of the encountered NTM should be identified [89]. Most of the stated criteria and recommendations apply best for infections that are caused by the *M. avium* complex, *M. abscessus* and *M. kansasii* as these are the most common in the United States. It remains unclear whether the same thresholds should be applied when less frequently encountered NTM are the infectious agents [90].

Because the infectious agents are ubiquitous in the environment, it is common for tests to be positive in the absence of pathological signs. To determine whether a patient has a manifest disease or a sole contamination/colonization of the lung, the recommended multidomain approach for diagnosis should be followed whenever an NTM infection is suspected [84].

### 1.2.4) Therapy of NTM Pulmonary Disease

Pharmacotherapy for NTM infections is usually realized with a combination of multiple antibiotics, tailored based on the specific NTM species and patient factors. The primary drugs used include macrolides (such as clarithromycin and azithromycin), rifamycins (such as rifampin and rifabutin), ethambutol, and aminoglycosides (such as amikacin and streptomycin). For more resistant species and strains, agents like clofazimine, linezolid, and bedaquiline may be employed [90]. Treatment regimens are often prolonged, typically lasting months to years, and require careful monitoring for efficacy and adverse effects. Sawka *et al.* give an overview on the side effects of drugs that are in use against NTM infections and how they should be monitored during the course of therapy [91].

The complexity of NTM pharmacotherapy is further complicated by the need for individualized treatment plans, considering factors such as drug-drug interactions, patient comorbidities, and potential for adverse reactions. Often, NTM are resistant to a degree that makes eradication impossible, and the therapy can only suppress further progression of the disease. Still, instead of “watchful waiting” clinical experts recommend initiation of antibiotic therapy when the diagnostic criteria discussed above are met.

Emerging resistance patterns and the limited availability of effective drugs underscore the urgent need for ongoing research and development of new therapeutic options. The following sections discuss general considerations regarding resistance and susceptibility of *M. abscessus* and the *M. avium* complex, as these are the two groups with the highest global impact, followed by the recommended treatment regimens for these two groups.

#### Resistances & Susceptibility Testing of NTM

While *in vitro* susceptibility testing of *M. tuberculosis* is common and usually promises better clinical outcomes, its value for NTM infection treatment is controversial, as in the past it has been observed that the *in vitro* results often do not correlate sufficiently with the clinical response, with notable interspecies differences [90]. This may be due to the ability of mycobacteria to enter a persistent state as a result of the influence of antibiotic chemotherapeutics and microenvironmental conditions within the host, such as nutritional starvation and low oxygen levels, e.g. in granulomas [92]. The Clinical and Laboratory Standards Institute (CLSI) provides protocols and methods for comparable antimicrobial susceptibility testing of mycobacteria and clinical breakpoints [93], [94].

Routine susceptibility testing of the *M. avium* complex is only recommended for macrolides [95] and amikacin, as these antibiotics show clear *in vitro* – *in vivo* correlation. Macrolide resistances are usually due to spontaneous point mutations

that occur in the peptidyltransferase region of the 23S rRNA gene (*rrl*) [96], [97], rather than an inducible mechanism. Amikacin resistance roots in point mutations of the 16S rRNA gene *rrs* which occur after extensive exposure to aminoglycosides [98].

The susceptibility of *M. abscessus* should likewise be tested and considered for macrolides and amikacin, as the correlation of *in vitro* results with clinical outcomes is well established for these antibiotics [99], [100]. Macrolide resistance of *M. abscessus* can be due to similar point mutations as in the *M. avium* complex or due to an inducible resistance mechanism. The presence of erythromycin resistant methylases (*erm*) induces resistance by methylating an adenine residue located at the macrolide target site within the 23S rRNA [101]. Various NTM [102], [103], [104] and *M. tuberculosis* [105] show active *erm* variants. One of the most clinically relevant *erm* genes for NTM infections is *erm(41)*, which is present in the most common subspecies *M. abscessus* subsp. *abscessus* (encountered in ~45-70% of cases depending on the region) and in *M. abscessus* subsp. *bolletii* (~10-15% of cases) [106]. The *erm(41)* gene is not functional in *M. abscessus* subsp. *massiliense* (~20-55% of cases) due to the deletion of gene sections, making macrolide therapy less problematic in this case. This shows that investigation of genetics down to the subspecies level can complement therapy benefits. An alternative method for determining macrolide susceptibility is through prolonged *in vitro* incubation of mycobacterial strains with macrolides for up to 14 days. This approach allows for the observation of *erm*-induced macrolide resistance, which only emerges after a period of three days [107]. Common panels of antibiotics for susceptibility testing against *M. abscessus* furthermore include cefoxitin, imipenem, linezolid, doxycycline, tigecycline, ciprofloxacin, and moxifloxacin [108]. If susceptible, these antibiotics may be considered for therapy, but with low certainty of clinical effects [90]. Rifamycins are usually not tested, as *M. abscessus* is equipped with intrinsic resistance mechanisms against this drug class, see 1.4.2) Resistance of Mycobacteria to Rifamycins, although recent derivatives have demonstrated activity [109], [110]. *M. abscessus* also shows intrinsic resistance to ethambutol (nucleotide differences at target site compared to other susceptible mycobacteria; [111]) and highly variable susceptibility to  $\beta$ -lactams [112]. Recently, tebipenem in combination with the  $\beta$ -lactamase inhibitor avibactam proved effective in an *in vivo* mouse model [113]. Nevertheless, the clinical experience with the treatment of *M. abscessus* pulmonary disease justifies its designation as an antibiotic nightmare [18], [114].

### Therapy of *M. avium* complex Pulmonary Disease

For patients with NTM pulmonary disease caused by macrolide-susceptible *M. avium* complex, the ATS recommends the treatment regimens specified in **Table 3** and its continuation for at least 12 months after culture conversion [90], [115]. With this 3-drug regimen, an average proportion of culture conversions of 61.4% was reported [116]. In case of macrolide resistance, the administration of macrolides should be discontinued, another drug should be added to the regimen based on susceptibility testing, and surgical intervention should be considered [115]. For macrolide resistant *M. avium* complex pulmonary disease, the rate of culture conversion was reported to be as low as 21% [117],

The role of rifampicin in the recommended regimen is questioned as its use is associated with high recurrence rates and toxicity [118]. Van Ingen *et al.* review the efficacy of rifampicin against *M. avium* complex pulmonary disease and conclude that there is no rationale behind its use as pharmacokinetic and pharmacodynamic criteria for a successful therapy are not met with the addition of rifampicin to the regimen [118]. The authors rather recommend a mindful review of dosages and the substitution of rifampicin for clofazimine.

**Table 3.** ATS recommended treatment regimens and dosing for *M. avium* complex pulmonary disease [115].

Drugs	Dosing frequency & Dosage	
	Thrice weekly	Daily
	Basic regimen for nodular-bronchiectatic lung involvement	Intensified regimen for cavitary lung involvement and refractory disease
<b>Azithromycin<sup>a</sup></b>	500 mg	250-500 mg
<b>Rifampicin<sup>b</sup></b>	600 mg	450-600 mg
<b>Ethambutol</b>	25 mg/kg per day	15 mg/kg per day
In case of <i>cavitary disease</i> add:		
<b>Amikacin</b>	15-25 mg/kg IV for 2-3 months	10-15 mg/kg IV for 2-3 months
In case of <i>refractory disease</i> (defined as no sputum conversion after 6 months of therapy) amikacin IV may be replaced by:		
<b>Amikacin</b>	N/A	Liposomal suspension 590 mg inhaled

**a:** Azithromycin preferred to clarithromycin due to lower rifampicin/p450 interaction

**b:** May be substituted by rifabutin when tolerated by the patient as it shows slightly better *in vitro* activity or when drug-drug-interactions of rifampicin and antiretroviral therapy is suspected [119]

### Therapy of *M. abscessus* Pulmonary Disease

Up to today, there is no canonical, best-practice pharmacotherapy against *M. abscessus* pulmonary disease. The combinations used are only considered treatment approaches. The selection of drugs, duration of therapy and the techniques of administration remain unclear. The current opinion of expert clinicians is that a biphasic therapy approach together with susceptibility based antibiotic selection offers the best prognosis [106]. **Table 4** shows the therapy scheme suggested by the ATS. An initial, intensified period of therapy that includes intravenous administration of antibiotics is followed by a continuation phase of orally administered drugs, that are usually taken until 12 months after culture conversion, which is often achieved for macrolide-susceptible specimen, but for macrolide resistant strains the rates of positive outcomes are abysmal. Only 8% of patients achieve culture conversion after an average therapy duration of 24 months *and* surgical intervention [120], [121]. This shows the urgent need for new therapy options against *M. abscessus* pulmonary disease. The expansion of the drug pipeline against *M. abscessus* with new small molecules and new inhibition mechanisms can be complimented by careful repurposing and repositioning of known antibiotics and the evaluation of combination therapies of the same [122], [123], [124].

**Table 4.** Suggested therapy scheme of the ATS for *M. abscessus* pulmonary disease [90], [106], [125]. Abbreviations: PO, peroral drugs; IV, intravenous drugs; NEB, nebulized drugs.

Phase	Macrolide-susceptible	Inducible or mutational macrolide resistance
Initial, intensive phase (undefined length, minimum 4 weeks)	<b>1-2 IV</b> drugs <b>2 PO</b> drugs (priority for macrolides)	<b>2-3 IV</b> drugs <b>2-3 PO</b> drugs
Continuation phase (until 12 months after culture conversion)	<b>2-3 PO/NEB</b> drugs (priority for macrolides)	<b>2-3 PO/NEB</b> drugs

IV drugs:	PO drugs:	NEB drugs:
Amikacin Imipenem Cefoxitin Tigecycline	Azithromycin Clarithromycin Clofazimine Linezolid	Amikacin

### Role of RNAP Inhibitors in Therapy Regimens

The presented guidelines for the most common groups of clinically relevant NTM show that the role of rifamycins in the treatment regimens is not definitively established. Against *M. avium* complex pulmonary infections the guidelines still recommend the use of rifampicin, although the benefit of this regimen is highly questioned [118]. Against *M. abscessus* pulmonary disease, rifampicin shows no activity, although rifabutin appears to be effective in animal models, probably due to its insensitivity to naphthohydroquinone oxidation, and should be considered as an alternative to rifampicin [110]. Furthermore, rifamycins are currently the most effective first-line anti-TB drugs [2]. However, the emergence of multi-drug resistant and extensively multi-drug resistant *M. tuberculosis* strains in clinical settings has complicated the treatment of TB [126], [127]. The various resistance mechanisms that mycobacteria employ to evade the effects of rifamycins are discussed in a later section (1.4.2).

The only other approved non-rifamycin RNAP inhibitor, fidaxomicin, is active against *M. tuberculosis* [128] and NTM [129] *in vitro* but is only used against gastrointestinal *Clostridium difficile* infections because it does not show adequate systematic resorption.

This lack of effective RNAP inhibitors is a major drawback for current antimycobacterial therapy options. The next section of the introduction gives an overview of the general biological function and structure of prokaryotic RNAP, its value as a target for antimycobacterial therapy, and a review of various aspects of rifamycins. It then introduces AAPs as the primary focus of this thesis.

### ***1.3) Structure & Function of RNA Polymerases***

DNA-dependent RNA polymerases are enzyme complexes that play an essential role in pro- and eukaryotic organisms. They participate in the highly regulated processes that transcribe DNA into RNA, which is then translated into proteins necessary for survival, growth and environmental adaptability. These enzymes have complex structures, made up of multiple subunits with specific roles and functions, which are explained in the following sections.

#### **1.3.1) Differences of Prokaryotic and Eukaryotic RNA Polymerases**

Prokaryotic and eukaryotic RNA polymerases (RNAPs), while sharing a high degree of conservation, exhibit structural and functional differences that reflect their adaptation to different cellular environments and transcriptional needs. **Table 5** gives a comparison of the different RNAPs that are present in eukaryotes and prokaryotes.

Prokaryotes rely on a single RNAP enzyme that produces all RNA products that are necessary for their metabolism and survival, whereas eukaryotes utilize three different RNAPs. These eukaryotic variants - RNA Pol I, II, and III – perform specific functions and have a higher number of subunits compared to the prokaryotic RNAP (see **Table 5**). Despite these differences, pro- and eukaryotic RNAPs share similar core subunits, indicating a conserved mechanism of RNA synthesis across the different life forms [130]. For instance, the gene encoding the RPB2 subunit of *Saccharomyces cerevisiae* RNA polymerase II shows a significant sequence homology with the  $\beta$  subunit of *Escherichia coli* RNA polymerase, suggesting similar roles in RNA synthesis [131].

In prokaryotes, the initiation of transcription is regulated by  $\sigma$  factors of different families that interact with the RNA polymerase to initiate transcription at specific promoters [132]. This mechanism is different from the complex system of DNA modifications, transcription factors and coactivators required by eukaryotic RNA polymerases for transcription initiation [133].

**Table 5.** Overview on prokaryotic and eukaryotic RNA polymerases und their functionalities.

	<i>Function</i>	<i>Number of Subunits</i>	<i>Homologous subunits</i>				
<b>Prokaryotic RNAP</b> [132], [134]	Production of all prokaryotic RNA products	5	$\alpha^1$	$\alpha^2$	$\beta$	$\beta'$	$\omega$
<b>Eukaryotic RNAPs</b> [135]							
RNA Pol I [136]	Production of ribosomal RNA	14	RPC5	RPC9	RPA2	RPA1	RPB6
			+ 9 other subunits				
RNA Pol II [137]	Production of precursor mRNA and small regulatory RNA products	12	RPB3	RPB11	RPB2	RPB1	RPB6
			+ 7 other subunits				
RNA Pol III [138]	Production of tRNA and regulatory RNAs	17	RPC5	RPC9	RPC2	RPC1	RPB6
			+ 12 other subunits				

### 1.3.2) Structure of Prokaryotic RNA Polymerase

The prokaryotic RNAP core enzyme is an assembly of five different subunits: two identical  $\alpha$  subunits, one  $\beta$  subunit, one  $\beta'$  subunit, and the  $\omega$  subunit [134]. This core enzyme ( $\alpha_2\beta\beta'\omega$ ) is catalytically competent and capable of binding to the DNA template strand [132], [139]. Homologs of this core enzyme structure can be found in all bacterial species. In *Thermus aquaticus* the spatial extent of the RNAP core was determined to be  $150 \text{ \AA} \times 115 \text{ \AA} \times 110 \text{ \AA}$  [132]. To initiate RNA transcription, the core enzyme must first interact with a transcription factor known as the  $\sigma$  factor, resulting in the formation of the RNAP holoenzyme [132]. **Figure 3** shows a schematic depiction of an RNAP holoenzyme and **Figure 4** shows an X-ray crystal structure of a fully assembled RNAP transcription initiation complex extracted from *M. tuberculosis*.

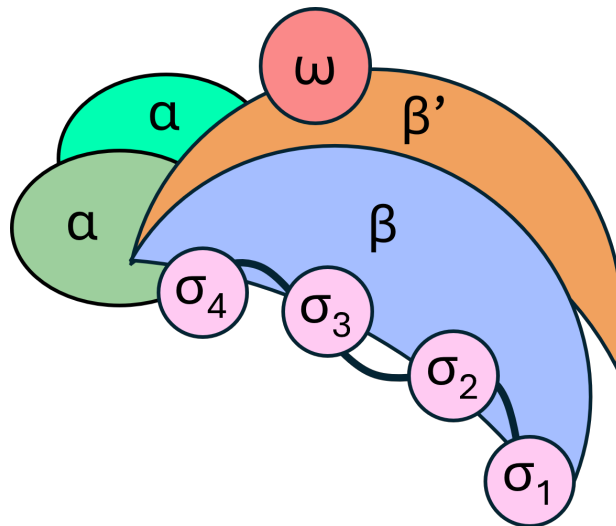


**Figure 3.** Scheme of a prokaryotic RNAP holoenzyme.

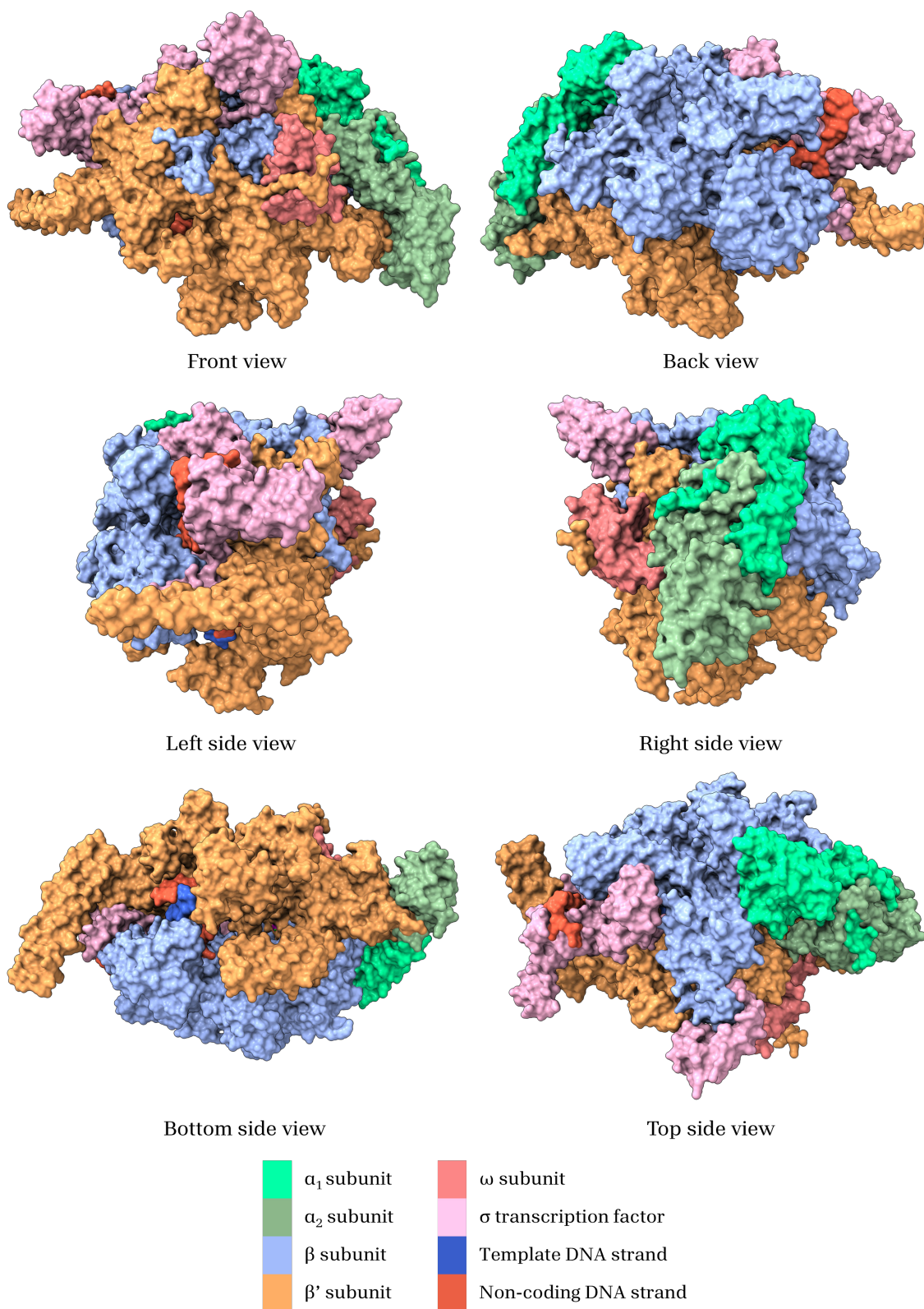


**Figure 4.** Different perspectives of a crystallized *M. tuberculosis* transcription initiation complex (PDB: 5UHE, 4.04 Å resolution). The data and graphics were processed using Chimera X [140].

The  $\alpha$  subunits are organized as a homodimer and assist the assembly of the complete core enzyme as the combined *N*-terminal domains act as a mounting site for the  $\beta$  and  $\beta'$  subunits [130]. Furthermore, the  $\alpha$  subunits play an important role in promoter recognition. The sequence in which the subunits are brought together is:  $\alpha + \alpha \rightarrow \alpha_2 \rightarrow \alpha_2\beta \rightarrow \alpha_2\beta\beta' \rightarrow \alpha_2\beta\beta'\omega$ . Other domains of the  $\alpha$  subunits are also relevant for transcription factor interaction and promoter DNA binding [141].

Often the RNAP structure is referred to as a “crab claw” whereas the two biggest subunits,  $\beta$  and  $\beta'$ , form its two pincers. The spacious cleft between these two subunits forms three distinct channels: The primary channel, which accommodates the DNA and the DNA-RNA hybrid, the nucleoside triphosphate (NTP)-entry channel and the RNA-exit channel [142]. The intersection of these channels harbors the catalytically active site of the enzyme which is located at the closed end of the claw at the bottom of the pincers [143].

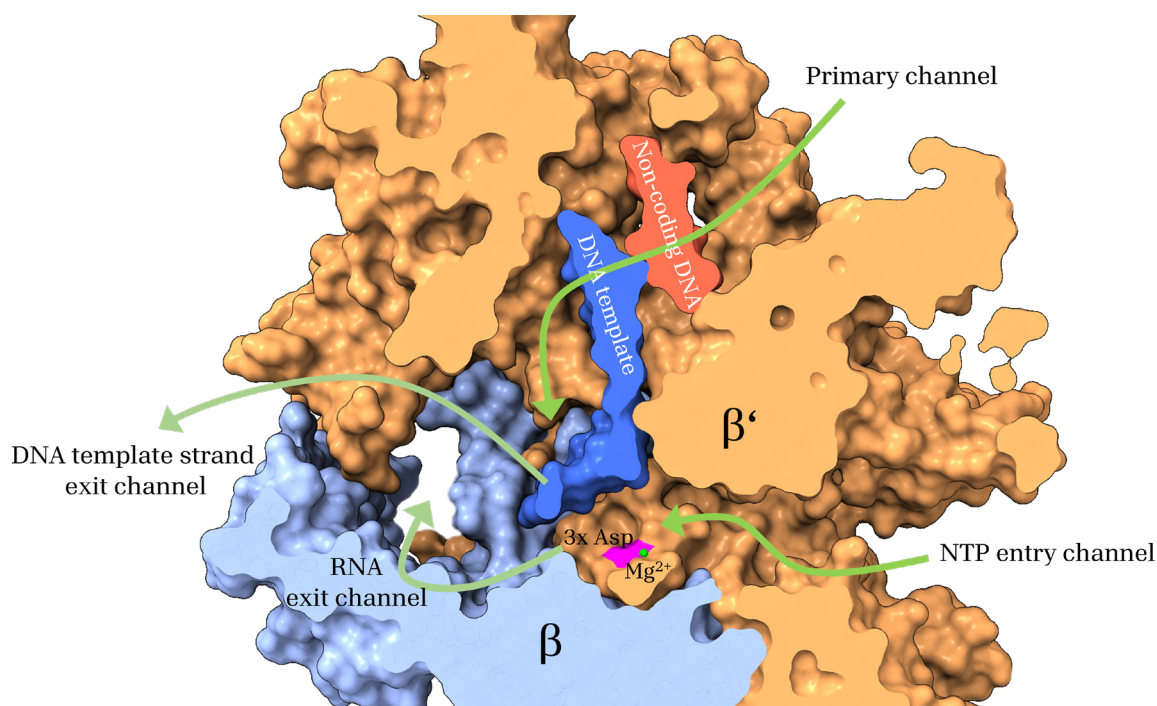


**Figure 5.** Clipped depiction of a crystallized *M. tuberculosis* transcription initiation complex (PDB: 5UHE, 4 Å resolution) limited to the  $\beta$  and  $\beta'$  subunits exposing the cleft incorporating the three main channels of bacterial RNAP as well as the active center. The data and graphics were processed using Chimera X [140].

Within the  $\beta'$  subunit the highly conserved sequence **DFDGD** forms the active center of the enzyme. The sequence contains three aspartate amino acids which coordinate a magnesium ion that mediates the catalysis [144] making this subunit crucial for transcription initiation and elongation.

The  $\beta'$  subunit is characterized by its high conformational flexibility. It accommodates the RNAPs “switch region”. The conformation of this domain

swings open to make space for loading the template DNA to the active center making it essential for transcription initiation [145]. Upon reversal of this open conformation the molten DNA is secured in the cleft for elongation. Another important domain is the “Trigger loop” which is located in close proximity to the active center. It exists in a folded (“Trigger helix”) or unfolded (“Trigger loop”) state, modifying different process steps. The folded state opens the active center, making it accessible for entering NTPs and allowing the elongation complex to translocate to the next position. The unfolded conformation of the Trigger loop initiates catalysis by precisely positioning the NTPs with the side chain of a histidine which is thought to literally “trigger” the formation of the new phosphodiester bond of the nascent RNA [146], [147]. The folding of the trigger loop is strongly assisted by a domain called the “F loop” which is in close contact with the trigger loop and is therefore crucial for the catalytic cycle. The impairment of the structural integrity of the F loop reduces the rate of nucleotide addition significantly [148]. The “Bridge helix” is a flexible  $\alpha$ -helix of the  $\beta'$  subunit located downstream of the active center. It is in close contact with the  $\beta$  subunit and the Trigger loop and directly connected to the F loop. It functions as a part of the ratchet-like mechanism that enables the RNAP to move DNA through the primary channel [149], [150]. The Bridge helix modulates that functionality by entering a “kinked” conformation which blocks the catalytically active site causing the RNAP complex to pause elongation [151].

The group of  $\sigma$  factors plays a crucial role in the transcriptional regulation of bacteria. They modulate the RNAP core enzyme’s ability to initiate transcription at  $\sigma$  factor specific promoters. Each kind of  $\sigma$  factor has a specific set of target genes, forming regulons that respond to environmental signals, thus enabling the bacterium to survive under various stress conditions and within the host. Therefore,  $\sigma$  factors are essential for adapting to changing environments but also for virulence [152]. The genome of *M. tuberculosis* encodes thirteen  $\sigma$  factors, with several being critical for its ability to cause disease [153]. For instance, the  $\sigma$  factor SigH is involved in the global gene expression response to oxidative stress and heat shock, indicating its role in stress responses [154]. Another  $\sigma$  factor, SigE, regulates genes crucial for the integrity and function of the bacterial cell envelope during infection, highlighting its importance in interacting with the host immune system [155].

### Comparison of RNAP Core Enzymes of Different Bacteria

Although the DNA-dependent RNAP is a highly conserved enzyme complex within the realm of bacteria, certain differences between the structures and sizes of the core enzymes can be found, especially when the compared bacterial taxa are phylogenetically distinct from each other. An example can be found in **Table 6** where the core enzyme's subunits of *E. coli*, *M. tuberculosis* and *M. abscessus* are compared in regard of their molecular weight. While the rather small  $\alpha$  and  $\omega$  subunits of the mycobacterial species are comparable in size to the subunits of *E. coli*, bigger differences can be found within the  $\beta$  and the  $\beta'$  subunits, which show a reduced size in comparison to *E. coli*. The difference is more pronounced in the  $\beta$  subunit which shows a size reduction of  $\sim 14\%$  for *M. tuberculosis* and even  $\sim 18\%$  for *M. abscessus*. It becomes evident that small molecule inhibition of these enzyme complexes varies greatly due to differences in binding modes resulting from structural differences.

**Table 6.** Comparison of RNAP core enzyme subunits molecular weights of different bacterial species. *E. coli*: *Escherichia coli* ATCC 11775, *Mtb*: *M. tuberculosis*: ATCC 25618 / H37Rv; *Mabs*: *M. abscessus* ATCC 19977. Molecular weights rounded to integral kDa.

	$\alpha$	$\beta$	$\beta'$	$\omega$	Total weight ( $\alpha_2\beta\beta'\omega$ )
<b><i>E. coli</i></b>	37 kDa	151 kDa	155 kDa	10 kDa	390 kDa
<b><i>Mtb</i></b>	38 kDa	130 kDa	147 kDa	12 kDa	365 kDa
<b><i>Mabs</i></b>	38 kDa	124 kDa	147 kDa	11 kDa	358 kDa

A more detailed look at the sequence homology (**Table 7**) of the three different species reveals another crucial aspect. As expected, the homology between *E. coli* and the two mycobacterial species is rather low. More so, the subunits that were found to be comparable in size differ greatly in sequence homology, e.g. the 37 kDa  $\alpha$  subunit of *E. coli* only shows a sequence homology of 44% and 45% to 38 kDa subunits of *M. tuberculosis* and *M. abscessus*, respectively.

Comparing *M. tuberculosis* and *M. abscessus* shows less divergence in sequence homology. The values range from 77% to 93% homology throughout the subunits of the core enzyme, indicating that even between two species that share the same genus differences can occur that may result in different interactions with small molecule inhibitors.

**Table 7.** Sequence homology of RNAP subunits between *E. coli*: *Escherichia coli* ATCC 11775 (PATRIC genome ID: 866789.18), *Mtb*: *Mycobacterium tuberculosis* ATCC 25618 / H37Rv (sequence extracted from PDB file: 5UHA); *Mabs*: *Mycobacterium abscessus* ATCC 19977 (PATRIC genome ID: 36809.5). Sequence homology was determined with Basic local alignment search tool provided by the National Institutes of Health (NIH) [156].

	<i>E. coli</i>		<i>Mtb</i>		<i>Mabs</i>	
<i>E. coli</i>	x		44 %	58 %	45 %	59 %
			51 %	33 %	52 %	38 %
<i>Mtb</i>	44 %	58 %	x		93 %	90 %
	51 %	33 %			90 %	77 %
<i>Mabs</i>	45 %	59 %	93 %	90 %	x	
	52 %	38 %	90 %	77 %		

$\alpha$	$\beta$
$\beta'$	$\omega$

### 1.3.3) Prokaryotic Transcription

The complex process of the production of RNA from a DNA template can be divided into three main steps: Initiation, elongation and termination. The following sections give a comprehensive overview of the steps necessary to produce RNA products within the realm of bacteria.

#### 1.3.3.1) Initiation

##### Promoter Recognition and Binding

Before the highly regulated step of transcription initiation can start, the  $\sigma$  factor has to anneal to the  $\beta$  and  $\beta'$  subunits of the RNAP core enzyme forming the RNAP holoenzyme  $\alpha_2\beta\beta'\omega\sigma$ , because the core enzyme is not capable of binding and melting double stranded DNA alone. After the assembly, the contact between DNA and the RNAP holoenzyme is established at certain domains of the  $\alpha$  subunit and the four domains of the  $\sigma$  factor [157]. A schematic overview of the binding interactions is given in **Figure 6**. Most distal from the starting position of transcription, the  $\alpha$  subunits interacts with the 20 base pair (bp) long UPE promoter region about -40 to -60 bps upstream the DNA double strand. Other interactions form between the -35 element (TTGACA) and the  $\sigma_4$ , the -10 element (Pribnow-Box) and  $\sigma_2$ , in some promoters accompanied by  $\sigma_3$ , and the discriminator promoter region that binds to  $\sigma_1$ , closest to the transcription starting point. The resulting assembly is referred to as the closed promoter complex (RP<sub>C</sub>).

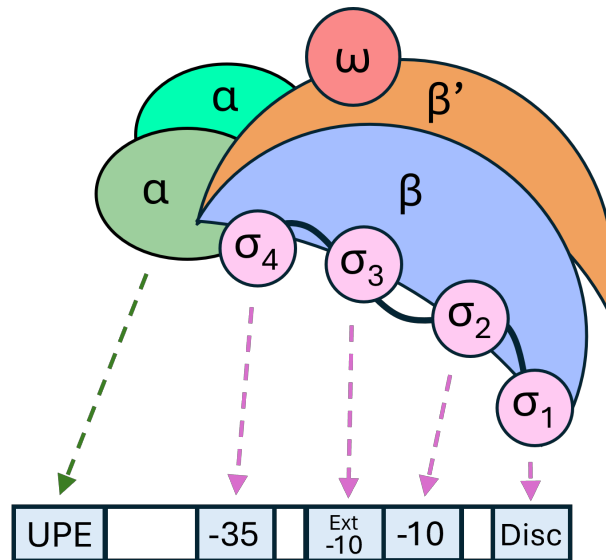


**Figure 6.** Binding interactions between the RNAP holoenzyme and the DNA promoter region.

#### Formation of the Open Promoter Complex

After the promoter DNA is bound to the holoenzyme the catalytically active site is still blocked by  $\sigma_1$  and the DNA is still wound into a double strand. By conformational isomerization of the  $\sigma$  factor,  $\sigma_1$  is displaced from the active site and  $\sigma_2$  facilitates the melting the DNA double strand into its respective single strands from positions -12 to +2, forming the transcription bubble. This configuration of the enzymatic system is called the open promoter complex ( $RP_0$ ).

#### Abortive Initiation & Promotor Escape

After the formation of the transcription bubble and stabilization of the open promoter complex the first NTPs can enter the catalytic site to be fused together by the formation of phosphodiester bonds. In this state, the  $\sigma_4$  domain is blocking the RNA exit channel resulting in steric clashes with the nascent RNA strain (**Figure 7**) and the template DNA that accumulates within the catalytic site as the DNA pulled in (DNA scrunching). This can cause cycles of abortion of the catalyzed reaction and the release of small RNA transcripts with lengths of 9 to 10 nucleotides without leaving the promoter region. Only when a critical chain length of 11 to 15 nucleotides is reached, the transcript can displace the  $\sigma_4$  domain giving room for the growing RNA. After the RNAP dislocates or “escapes” from the DNA promoter region, the RNAP core enzyme releases the  $\sigma$  factor from the enzyme complex forming the ternary elongation complex (EC) to start productive elongation.

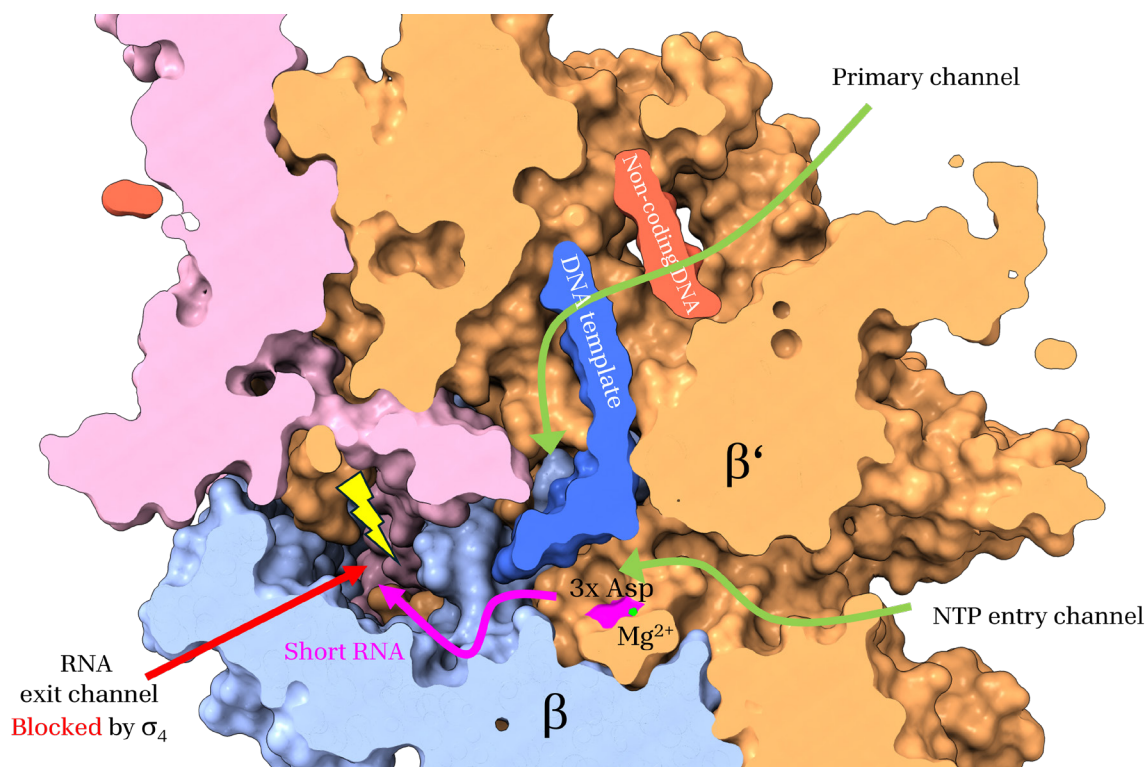


**Figure 7.** Depiction of a crystallized *M. tuberculosis* transcription initiation complex (PDB: 5UHE, 4 Å resolution). The RNA exit channel is blocked by the  $\sigma_4$  resulting in abortive initiation cycles in which short RNA transcripts are produced. The data and graphics were processed using Chimera X[140].

### 1.3.3.2) Elongation

During the step of elongation, the EC synthesizes the RNA strand by adding ribonucleotides in 5' to 3' direction, matching the DNA template strand's nucleotides with their RNA counterparts. A representative view of the EC and the transcription bubble is displayed in **Figure 8**.

The nucleotide addition cycle (NAC) is a crucial part of elongation, that involves several steps: the correct NTP entering the RNA polymerase active site, incorporation into the growing RNA chain if the NTPs correctly pair with the DNA template, and the translocation of the RNA polymerase exposing the next DNA base for another addition. The  $S_N2$  nucleophilic attack of the ribose 3' hydroxyl group (chelated by the  $Mg^{2+}$  of the catalytic center) at the  $\alpha$ -phosphate of the NTP forms the phosphodiester bond and releases pyrophosphate [158]. The reaction is dependent on the mobility of the trigger loop, the F loop and the Bridge helix, as conformational changes align the reaction partners for efficient reaction. This cycle repeats, allowing the RNA strand to be elongated one nucleotide at a time. While the nascent RNA strain is elongating, the transcription bubble remains at a constant size of usually  $12 \pm 1$  nucleotides [159]. The DNA/RNA hybrid that forms within the transcription bubble during addition of NTPs is 9 to 10 base pairs long [160].

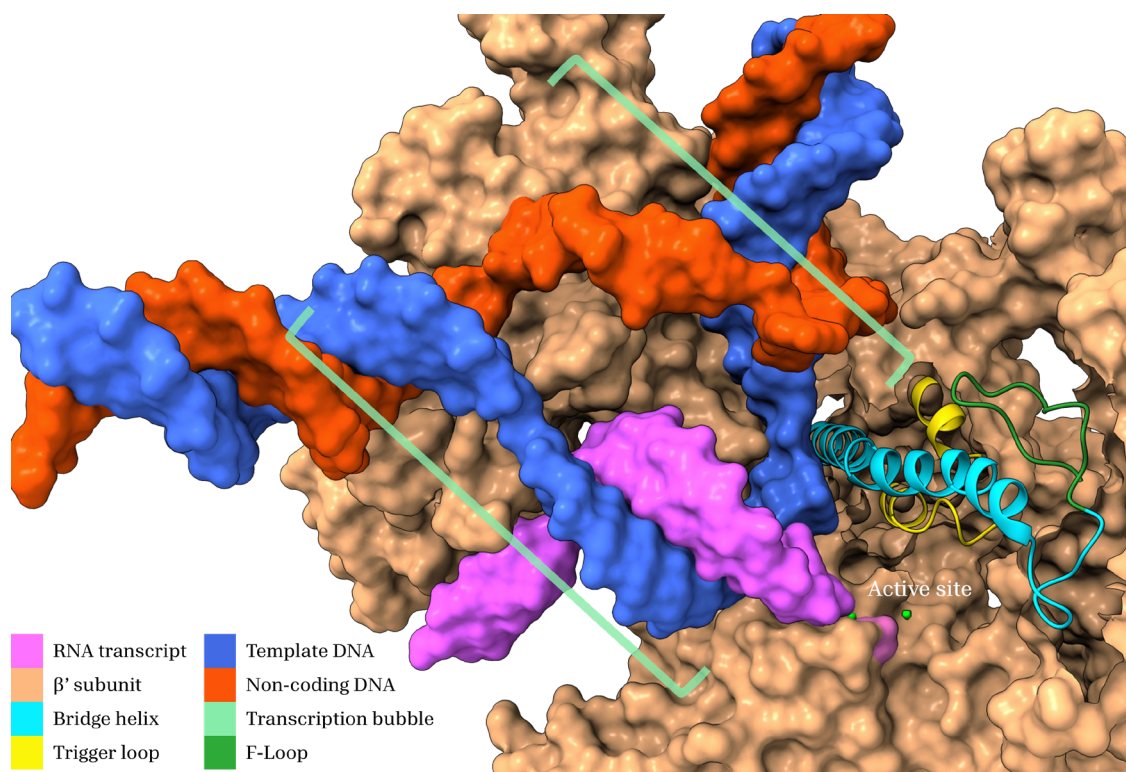


**Figure 8.** Depiction of an *M. tuberculosis* RNAP elongation complex (PDB: 8EOS, electron microscopic data, resolution: 3.10 Å). View into the catalytic cleft ( $\beta$  subunit excluded). Trigger loop (T1008-P1029), Bridge helix (L847-S881) and F-Loop (A818-V846) are highlighted in different colors. The data and graphics were processed using Chimera X [140].

### 1.3.3.3) Termination

Termination in prokaryotic transcription is a critical process that marks the end of the RNA synthesis. This process can occur by two main mechanisms: Rho-dependent and Rho-independent termination [161], [162]. In Rho-dependent termination, the protein Rho recognizes specific RNA sequences and causes the RNA polymerase to detach from the DNA template [163]. In Rho-independent termination, the formation of a hairpin-loop structure in the RNA transcript, followed by a series of uracil nucleotides, leads to the dissociation of the RNA polymerase from the DNA. Both mechanisms ensure that transcription is accurately concluded, allowing the newly synthesized RNA molecule to undergo further processing and fulfill its role within the cell.



## ***1.4) Inhibition of Bacterial RNA Polymerase***

### **1.4.1) Prokaryotic RNAP as a Drug Target**

The prokaryotic RNA polymerase is an essential enzyme responsible for transcription in bacteria. Without the production of RNA from DNA, bacteria would not be able to produce the diverse spectrum of enzymes and proteins required for nearly every aspect of their metabolism and structural integrity. This central role of RNAP in bacterial growth and survival makes it a significant target for antibacterial chemotherapy. Blocking the bacteria's ability to sustain their metabolism at a fundamental stage also reduces their capacity to adapt to caused imbalances of their cellular homeostasis, e.g. by up- or downregulating certain regulatory RNA products, enzymes and proteins. This displays a significant advantage of RNAP inhibition as a concept of antimicrobial drug development.

A key challenge in designing rational antimicrobial RNAP inhibitor is to create substances that selectively target prokaryotic RNAP without affecting eukaryotic RNAPs, to reduce their potential toxicity for human cells. Although enzymes for RNA production are similar in all living organisms, prokaryotic RNAP displays features that differ from its eukaryotic counterparts, which offers a possibility for the development of antibiotics (see 1.3.1). However, the catalytically active site of prokaryotic RNAP is hard to exploit as a target site because of its highly conserved character even between eukaryotes and prokaryotes. Fortunately, the generally different shape and surface properties of the subunits in combination with the complex regulation of transcription processes, give room for a manifold of different inhibition concepts.

Numerous small molecule scaffolds have been under investigation to identify novel RNAP inhibitors. The generation and validation of new RNAP drug targets is a significant area of research that was summarized in the comprehensive review published by Kirsch *et al.* recently. It provides an excellent overview of substances, binding sites, and mechanisms that have already been investigated in the context of RNAP inhibition [159]. Despite all the efforts required to identify and characterize promising candidate molecules, only a few RNAP inhibitors have reached the development stage, and even less are approved and currently in clinical use. This shows the significant challenge of translating potential compounds from the chemical laboratory to clinical application.

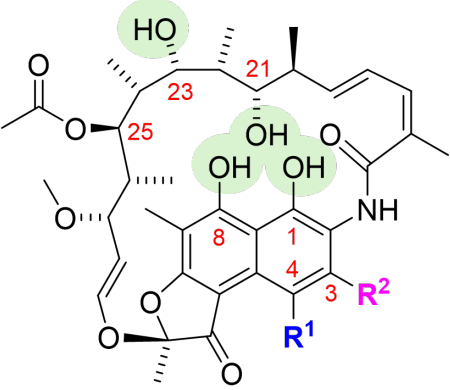
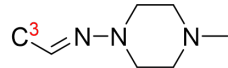
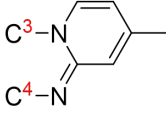
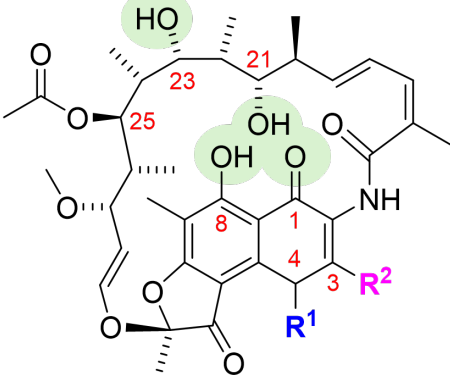
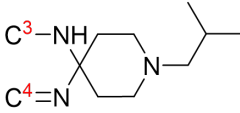
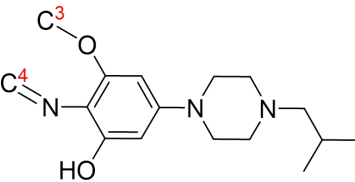
### 1.4.2) Rifamycins

Rifamycins, the most important clinically used RNAP inhibitors, have significantly impacted the treatment of bacterial infections since their discovery in 1957 [164]. The compound group originates from the soil bacterium *Amycolatopsis mediterranei* (since 2004 named *A. rifamycinica* [165]) and was first identified and isolated in the laboratories of Dow-Lepetit Pharmaceuticals (Milan, Italy) [164]. Named after the contemporary movie *Rififi* [166], these antibiotics are known for their potent activity against a wide range of Gram-positive and some Gram-negative bacteria, particularly their efficacy in treating mycobacterial infections such as tuberculosis and leprosy [167], [168], as well as infections with NTM [109], [123]. Rifamycins have also been employed in treating other severe infections, like those caused by methicillin-resistant *Staphylococcus aureus* (MRSA) [169], [170]. Rifamycin SV, the first rifamycin that showed clinical success was introduced in 1963, followed by Rifampicin in 1968, which is still a cornerstone of many therapy regimens [164].

#### Chemistry of Rifamycins

Rifamycins are macrocyclic molecules that combine an aromatic naphthalene system with a polyketide chain, called the *ansa* loop, that forms an arch over the naphthalene structure. Natural rifamycins generally show a low bioavailability as well as antibacterial activity and can be cytotoxic [164], [171], making a chemical derivatization of the chemical scaffold imperative for the development of this drug class. Both structural moieties can be decorated with various functional groups for structure diversification. A structural overview of rifamycins that gained clinical importance is given in **Table 8**. In engineered rifamycins, the naphthohydroquinone core can be retained or is being exchanged by its oxidated form, a naphthoquinone, in the cases of Rifabutin and Rifalazil.

**Table 8.** General chemical structure of rifamycins and associated structures of clinically used rifamycins. Red numbers indicate numbering of carbon atoms.

	<b>R<sup>1</sup></b>	<b>R<sup>2</sup></b>	<b>Name</b>
		OH	H
	OH		Rifampicin
	OH		Rifapentine
			Rifaximin
			Rifabutin
			Rifalazil

It has long been suspected that the only promising derivatizations could be performed at C3 and C4 of the naphthalene core [171], and indeed, up to today all clinically used rifamycins only differ at these positions. The discovery of kanglemycins, however, showed that even sterically demanding substitutions alongside the *ansa* bridge can yield RNAP inhibitors with substantial activities that also occupy the rifamycin binding site and share key target interactions with rifamycins [172]. Another example for a successful derivatization of the *ansa* bridge was presented by Lan *et al.* by variation of the C25 ester [173].

### Mechanism of Action & Target Binding

The effect of rifamycins on bacterial transcription was first recognized in 1965 [174], until the mechanism of action was experimentally proven in 1978 [175], and much later in 2001 the target binding was further elucidated by Campbell *et al.* by co-crystallization of rifampicin with the RNAP of *Thermophilus aquaticus* [176]. Rifamycins bind to the  $\beta$ -subunit 12 Å in distance from the catalytically active center, sterically blocking the exit channel of the nascent RNA. The consequence of

this blockage is that the RNAP can only produce unfunctional RNA up to a length of two or three nucleotides until the RNA strand collides with the bound rifamycin [176]. The length of the RNA products that are synthesized differ depending on the substitution pattern at C3 and C4, as these moieties are oriented towards the active center [177]. Key target interactions are formed by four oxygen atoms at C1, C8, C21, and C23 that act as either hydrogen bond donors or acceptors [176].

### Resistance of Mycobacteria to Rifamycins

Despite the initial success of rifamycins, the emergence of rifamycin-resistant *M. tuberculosis* strains and resistant non-tuberculous mycobacteria like *M. abscessus* poses a significant clinical challenge, necessitating ongoing research and development to enhance their efficacy and combat resistance [178]. The harsh reality shows that approximately 4% of patients without a TB treatment history and approximately 20 % of patients that have been treated for TB before [2] are infected with a rifampicin resistant *M. tuberculosis* strain.

The use of rifamycins against NTM is equally concerning. Rifampicin, rifabutin and rifapentine were tested against *M. avium* complex clinical isolates *in vitro* using a hollow fiber model in a single-drug regimen [179]. The substances initially killed the bacteria but then failed to control the growth of the investigated *M. avium* complex strains due to emerging resistance after 4 days [179]. The attempt to use rifampicin in combination with other antimycobacterial drugs to reduce the occurrence of antibiotic resistance fails against *M. avium* complex and the role of rifampicin is questioned [180]. The infamous *M. abscessus* is inherently resistant to rifampicin [181].

Mycobacteria employ a manifold of different resistance mechanisms to adapt to rifamycins. In *M. tuberculosis*, the most common form of rifamycin resistance is induced by mutations that can occur in the *rpoB* gene, which encodes the  $\beta$ -subunit, directly altering the rifamycin binding site. The cluster in which these mutations usually occur corresponds to the amino acids 426 – 453 in *M. tuberculosis* [176]. The resistance mutations that are clinically most relevant are D435V, H445Y and S450L [182].

Another important mechanism of rifamycin resistance is the expression of ADP-ribosyl transferase encoded by the *arr* gene. Fortunately, *arr* is absent in *M. tuberculosis*, explaining the high activity of rifamycins [183]. Being present in *M. abscessus* and other mainly fast-growing mycobacteria [184], this enzyme renders rifamycins less effective (*M. abscessus* MIC<sub>90</sub> of rifampicin 0.22  $\mu$ M (without functional *arr*) to 9.5  $\mu$ M (wild type)) by adding an ADP-ribosyl group to the free hydroxyl group at C23 [181]. An important step forward has been achieved

lately. By redesigning the rifamycin scaffold at C25 the ADP-ribosylation can be blocked, opening new pathways for new rifamycins [173], [185].

An additional resistance mechanism is mediated by a naphthohydroquinone oxidase, present in *M. abscessus*, that oxidizes the naphthalene moiety resulting in reduced activities of rifamycins that carry a hydroxyl group at C1. In contrast, rifabutin and rifalazil with their already oxidized naphthoquinone core are less susceptible for oxidation and show higher activities against *M. abscessus* (MIC<sub>90</sub> rifabutin 1.9 μM in comparison to MIC<sub>90</sub> of rifampicin 9.5 μM) [186].

### 1.4.3) *N*α-aroyl-*N*-aryl-phenylalanine amides (AAPs)

This cumulative thesis is concerned with investigating the compound class of AAPs. The presented publications highlight the potential of AAPs as antimycobacterial RNAP inhibitors and provide detailed insights into the medicinal chemistry efforts, structural elucidation methods, microbiological evaluation, pharmacokinetic and physicochemical analysis that were utilized to develop this compound class. For a broad overview of AAPs, we refer the reader to our recent review [187].

This introductory section will provide a comprehensive overview on the proposed mechanism of action of AAPs, as this important aspect is not sufficiently addressed in the published material to gain understanding of it.

#### Mechanism of Action

The first valuable insights into the RNAP target site and the mechanism of action of AAPs were provided by the research group of Richard Ebright (Rutgers University, New Jersey, USA). In the published studies, they were able to determine the drug-target interactions of AAPs. By selecting spontaneously resistant *M. smegmatis* mutants and subsequent RNAP sequencing, the binding region was narrowed down [188] until the binding site was verified by X-ray diffraction analysis of a co-crystal of the *M. tuberculosis* RNAP RP<sub>o</sub> and the AAP named D-AAP1 (PDB code: 5UHE) [189].

The knowledge of the functional moieties of RNAP to which AAPs bind provided the initial basis for the assumption of their mechanism of action. The compound binds to both the β and β' subunit. Key interacting amino acids belong to the bridge helix and the F loop of the β' subunit [189]. A schematic depiction of the AAP binding site with its named functional regions is given in **Figure 9**. The amino acids that interact with the AAP scaffold are depicted in Publication I and Publication III [190], [191].

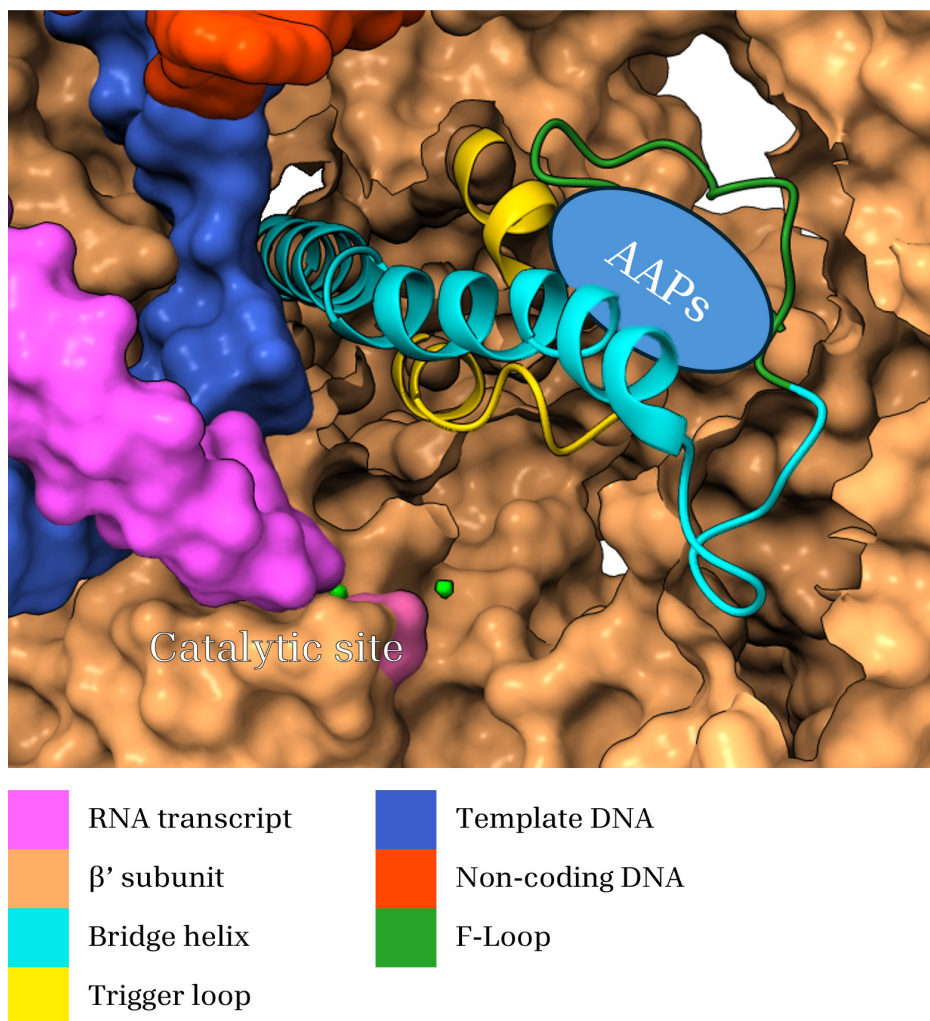


**Figure 9.** The binding site of AAPs is located between the N-terminal end of the bridge helix and the F loop in a distance of  $\sim 30$  Å to the catalytic center. The  $\beta$  subunit is omitted for clarity. Depiction based on PDB: 8EOS, electron microscopic data, resolution: 3.10 Å.

The binding of AAPs results in impaired conformational dynamics of the bridge helix and the F loop. It is proposed that bound AAPs constrain the bridge helix in a straight conformation [188] interfering with its normal function of assisting the trigger loop with the catalytic reaction, alignment and translocation during the NAC as described earlier.

In 2003, the Landick Lab (University of Wisconsin) published insights of a novel class of antibacterial RNAP inhibitors called the CBR compounds [192]. These compounds not only show a structural resemblance to AAP compounds in regard of their aromatic systems, but also share identical binding regions with the difference that CBRs are able to inhibit the RNAP of gram-negative bacteria like *E. coli* but not mycobacterial RNAP [193]. A comparison of AAP and CBR regarding chemical structures and their binding is displayed in **Figure 10**. Because of the identical binding site, it can be assumed that the mechanism of action of AAPs is at

least similar to the well-studied ways in which CBRs inhibit the growth of non-mycobacteria [194], [195]. However, there is still need for a valid verification. The established interference results in the trigger loop being frozen in its catalytically active state, which has a decreased translocation capability. This causes pausing of the NAC and subsequent over-termination, which ultimately results in unfunctional RNA products [194], [195].

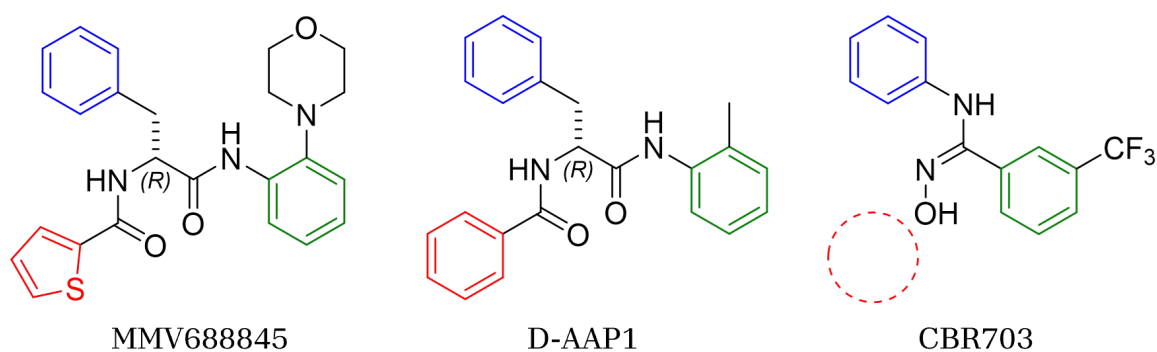


**Figure 10.** Structural comparison of the AAP screening hit MMV688845 and D-AAP1 with the CBR compound CBR703. Chemical moieties that form concordant target interactions are marked with the same colors. The  $\beta$  and  $\beta'$  subunits in *M. tuberculosis* RNAP form three lipophilic pockets that can accommodate the three aromatic systems of AAPs. One of these pockets is absent in the RNAP of gram-negative bacteria, explaining AAP inactivity. CBR compounds lack one aromatic system at that particular site, which is responsible for restoring activity against gram-negative bacteria.

In conclusion, AAPs do not act orthosterically or by sterical occlusion of RNAP channels in a manner similar to rifamycins. Instead, they exert their effect allosterically, by hampering enzyme dynamics.



## 2) Publications

### 2.1) Objective of the Project

The primary objective of this research project is to develop and optimize AAPs as potent inhibitors of RNAP for the treatment of mycobacterial infections, including those caused by *M. tuberculosis* and NTM, such as *M. abscessus* and the *M. avium* complex.

This project aims to:

1. **Synthesize New AAP Derivatives:** Establishing a straightforward, synthetic pathway that considers the problem of conservation of the crucial stereo configuration of AAPs to avoid the need for preparative chiral separation. The design of the scaffold should be guided by known drug-target interactions and aided by molecular docking techniques.
2. **Assess Antimycobacterial Activity:** The novel AAP derivatives should have enhanced *in vitro* activity and bactericidal activity against mycobacteria. The aim was to conduct comprehensive *in vitro* studies, like growth inhibition assays or macrophage infection models, to evaluate the efficacy of AAPs against a broad spectrum of mycobacterial species, including clinical isolates of *M. tuberculosis* and various NTM with a focus on *M. abscessus*.
3. **Establishing Structure-Activity-Relationship:** Another objective of the synthetic efforts is to gain insight into the relationship between the employed derivatization of the chemical scaffold of AAPs and the resulting biological activity and compound properties.
4. **Optimize Pharmacokinetic Properties:** Improve the pharmacokinetic profile of AAPs through structural modifications, ensuring sufficient, solubility, plasma stability and microsomal stability which eventually increases bioavailability for potential clinical use.
5. **Assess Possible Cytotoxic Effects:** The cytotoxicity of new derivatives should be as low as possible.

Through these objectives, the project seeks to address the critical need for new and effective treatments for mycobacterial infections, particularly in the face of rising drug resistance and the lack of effective RNA inhibitors against NTM.



## 2.2) Research Article I

# Synthesis and Characterization of Phenylalanine Amides Active against *Mycobacterium abscessus* and Other Mycobacteria

Markus Lang, Uday S. Ganapathy, Lea Mann, Rana Abdelaziz, Rüdiger W. Seidel, Richard Goddard, Ilaria Sequenzia, Sophie Hoenke, Philipp Schulze, Wassihun Wedajo Aragaw, René Csuk, Thomas Dick, Adrian Richter

American Chemical Society Publishing

Journal of Medicinal Chemistry

*J. Med. Chem.*, 2023, 66, 7, 5079–5098

Publication Date: March 31, 2023

DOI: 10.1002/cmdc.202300593

### Summary

The study reports the comprehensive investigation of the AAP parent compound MMV688845 to explore the structure-activity relationships that govern antimycobacterial activity, selectivity and drug disposition properties. We established a robust synthetic pathway for AAP derivatization which preserves the essential *R* configuration throughout synthesis which is confirmed by an X-ray crystal structure of MMV688845 and other derivatives. Changes to the amino acid core are tolerated for phenylalanine and tyrosine. The most flexible moiety is the morpholine structure of the hit compound. The best synthesized candidate 24 harbors a thiomorpholine sulfone instead of morpholine and has nanomolar MIC<sub>90</sub> values of down to 0.78 μM against *M. abscessus* and 0.2 μM against *M. tuberculosis* (12-fold and 4-fold better than MMV688845). Thiomorpholine sulfoxide containing derivatives demonstrate 5-fold increased aqueous solubility and retain activity against *M. abscessus*. Bactericidal effects demonstrate a significant reduction in viable bacteria without cytotoxic effects against mammalian cell lines. On-target mechanism was validated using AAP resistant mutants. These studies validate AAP as a promising compound for development of a new class of antibiotics targeting RNAP.

### Own contributions

Synthesis and characterization of compounds, analysis of structure-activity relationship, determination of solubilities, conceptualization of the draft, original draft preparation, review and editing, preparation of figures

Synthesis and Characterization of Phenylalanine Amides Active against *Mycobacterium abscessus* and Other Mycobacteria

Markus Lang, Uday S. Ganapathy, Lea Mann, Rana Abdelaziz, Rüdiger W. Seidel, Richard Goddard, Ilaria Sequenzia, Sophie Hoenke, Philipp Schulze, Wassihun Wedajo Aragaw, René Csuk, Thomas Dick, and Adrian Richter\*

Cite This: *J. Med. Chem.* 2023, 66, 5079–5098

Read Online

ACCESS |



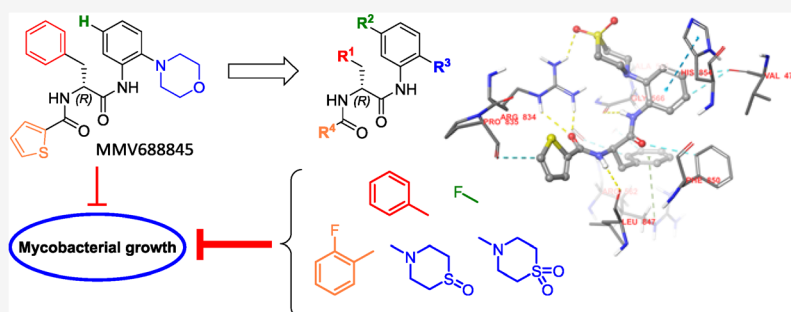
Metrics &amp; More



Article Recommendations



Supporting Information



**ABSTRACT:** *N*α-2-thiophenyl-D-phenylalanine-2-morpholinoanilide [MMV688845, Pathogen Box; Medicines for Malaria Venture; IUPAC: (2*R*)-*N*-(1-((2-morpholinophenyl)amino)-1-oxo-3-phenylpropan-2-yl)thiophene-2-carboxamide)] is a hit compound, which shows activity against *Mycobacterium abscessus* (MIC<sub>90</sub> 6.25–12.5 μM) and other mycobacteria. This work describes derivatization of MMV688845 by introducing a thiomorpholine moiety and the preparation of the corresponding sulfones and sulfoxides. The molecular structures of three analogs are confirmed by X-ray crystallography. Conservation of the essential *R* configuration during synthesis is proven by chiral HPLC for an exemplary compound. All analogs were characterized in a MIC assay against *M. abscessus*, *Mycobacterium intracellulare*, *Mycobacterium smegmatis*, and *Mycobacterium tuberculosis*. The sulfone derivatives exhibit lower MIC<sub>90</sub> values (*M. abscessus*: 0.78 μM), and the sulfoxides show higher aqueous solubility than the hit compound. The most potent derivatives possess bactericidal activity (99% inactivation of *M. abscessus* at 12.5 μM), while they are not cytotoxic against mammalian cell lines.

## 1. INTRODUCTION

Infections with mycobacteria are difficult to treat, as they often require prolonged antibiotic therapy, which can be accompanied by severe side effects. Whereas drug-susceptible tuberculosis can usually be treated successfully within six months,<sup>1–4</sup> the therapy of infections with multidrug-resistant (MDR) *Mycobacterium tuberculosis* (*Mtb*) strains and nontuberculous mycobacteria (NTM)<sup>5,6</sup> is protracted and cure rates are often low (25–58% for *Mycobacterium abscessus*<sup>7,8</sup> (*Mabs*) infections<sup>9–11</sup>). For infections with MDR *Mtb*, progress has already been made in recent years. Research efforts have led to the approval of two new drugs: bedaquiline and pretomanid.<sup>12–14</sup> Bedaquiline acts by inhibiting mycobacterial ATP synthase, while pretomanid has a rather complex mechanism of action. Under normoxic conditions, pretomanid is converted into reactive intermediates that interfere with mycolic acid synthesis, while in anaerobic environments, it acts as an NO donor that effectively poisons the respiration of mycobacteria.<sup>15,16</sup> By combining bedaquiline,

pretomanid, and linezolid, a new therapeutic regimen for treatment of MDR tuberculosis has been established.<sup>17</sup>

NTM have come into scientific focus in recent years, owing to the fast-growing, multidrug-resistant *Mabs* and the *Mycobacterium avium* complex (MAC), which have emerged as problematic opportunistic pathogens.<sup>18–21</sup> They possess numerous intrinsic resistance mechanisms, which render classical anti-tubercular drugs and many other common antibiotics ineffective.

Currently, the RNA polymerase (RNAP) inhibitor rifampicin (RIF) is a cornerstone of antimycobacterial therapy. As a result,

Received: January 2, 2023

Published: March 31, 2023



ACS Publications

© 2023 American Chemical Society

5079

<https://doi.org/10.1021/acs.jmedchem.3c00009>  
*J. Med. Chem.* 2023, 66, 5079–5098

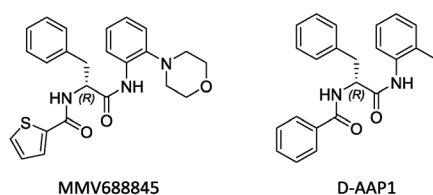
mycobacteria with acquired or intrinsic resistance to rifamycins, e.g., MDR *Mtb* or *Mabs*, are a particular threat. Mycobacteria use different mechanisms to counteract the effect of RIF. In *Mtb*, 95% of the resistant strains possess acquired mutations in the target of RIF, the  $\beta'$  subunit of the RNAP. Less frequently, the expression of efflux pumps influences RIF resistance.<sup>22</sup> In contrast, RIF resistance in *Mabs* is caused by other mechanisms. *Mabs* has the ability to covalently modify RIF through the enzyme ADP-ribosylase<sup>23</sup> and thereby inactivate it. In addition, naphthoquinone oxidation increases resistance.<sup>24</sup> Certain rifamycins, such as rifabutin, are less susceptible to these mechanisms of resistance, which is reflected in improved efficacy *in vitro* and *in vivo*.<sup>25,26</sup> Recent advances in rifamycin research made it possible to completely block ADP-ribosylation while retaining its antimycobacterial activity. The redesign of the C25-O-acyl position was crucial for these improvements of the rifamycin structures.<sup>27,28</sup>

Despite the promising attributes of rifabutin, a synthetic RNAP inhibitor that exhibits no cross-resistance with rifamycins is of interest for antimycobacterial drug development. The *N* $\alpha$ -aryl-*N*-aryl-phenylalanine amide (AAP) MMV688845 (*N* $\alpha$ -2-thiophenyl-*D*-phenylalanine-2-morpholinoanilide), discovered as an anti-*Mtb* hit,<sup>29</sup> has been shown to be active against *Mabs* (ATCC19977) by screening of the Pathogen Box library<sup>30</sup> (Medicines for Malaria Ventures, MMV). Analogs of MMV688845 have been shown to be inhibitors of *Mtb* RNAP that bind to the  $\beta$  and  $\beta'$  subunits but address a different binding site than rifamycins.<sup>31</sup> In addition, derivatives of MMV688845 are described in a patent,<sup>32</sup> although these were not investigated against NTM including *Mabs*. Based on the promising screening experiments, we have developed a synthesis for MMV688845, yielding the active enantiomer with *ee*-values of >99% and investigated its stereospecific activity against *Mabs*, as well as its cytotoxicity.<sup>33</sup> In parallel, the RNAP was validated as target in *Mabs*, and a detailed *in vitro* profiling of the hit compound was performed.<sup>34</sup> Motivated by these encouraging results, a series of MMV688845 derivatives was synthesized with the aim of increasing *in vitro* activity against NTM, improving physicochemical properties such as solubility and getting a first insight into *in vitro* metabolism properties of this compound class.

## 2. RESULTS AND DISCUSSION

**2.1. Docking Studies.** To explore which structural alternations of the hit molecule MMV688845 may be favourable for target binding, a molecular docking was conducted based on the published crystallographic structure of *Mtb* RNAP (PDB code: 5UHE). We used the X-ray structure of the crystallized protein with the model compound D-AAP1 as a reference for our modeling approaches.<sup>31</sup> The chemical diagrams of both substances are given in Scheme 1.

**Scheme 1. Structures of the Hit Compound MMV688845 and D-AAP1**



According to Lin et al., D-AAP1 offers space for six additional nonhydrogen atoms at the position of the methyl group, while it is coordinated to its target enzyme, offering potential for structure-based hit to lead optimization.<sup>31</sup> In MMV688845, the methyl group is replaced by a morpholine ring, introducing five additional nonhydrogen atoms while retaining activity.<sup>30</sup> The docking study of MMV688845 and RNAP<sub>*Mtb*</sub> (Figure 1A) indicates a hydrogen bond between the morpholine oxygen atom and arginine residue R834 of the  $\beta'$  subunit. Motivated by this finding, we were eager to find other hydrogen bond acceptor groups, which exploit the potential additional hydrogen bond for drug–target interactions and possibly lead to different physicochemical properties.

As the results of Lin et al. suggest only limited space for derivatization (five of the six proposed nonhydrogen atoms are already part of MMV688845), we chose to investigate structures that offer the desired properties while keeping the size of the relevant part of the molecule almost unchanged with only one or two additional atom(s). Our docking studies indicate that substitution of the morpholine part with a thiomorpholine and its respective oxidation products (sulfoxide and sulfone) will lead to a similar binding mode as observed for MMV688845. Figure 1B,C depicts the modeled complexes with MMV688845 derivatives containing sulfone and sulfoxide groups. The modeling data suggest that the oxygen atom(s) of the sulfone or sulfoxide can act as hydrogen bond acceptors for R834, whereas clashes with the target protein could not be observed. A superimposed visualization of D-AAP1 and substance 20 can be found in the Supporting Information (Figure S1).

In addition, our docking experiments revealed that a *p*-hydroxy group of a tyrosine analog of MMV688845 is positioned to form an additional hydrogen bond to the backbone of the target protein at P477 (Figure 1D) without any calculated clashes.

To check whether the proposed binding modes also have relevance in the RNAP of *Mabs*, a protein–protein BLAST (Basic Local Alignment Search Tool) was used to align and compare the *Mtb*  $\beta$  and  $\beta'$  RNAP subunits with their respective relatives in *Mabs*. The sequence homology was found to be 90.4% for the  $\beta$  subunits and 89.9% for the  $\beta'$  subunits, while the amino acids that are relevant for drug–target interaction in *Mtb* RNAP are highly conserved (only exception: A563 in *Mtb* to G512 in *Mabs*, a list of the relevant amino acids can be found in the Supporting Information, Table S1), making a similar binding mode in *Mabs* RNAP probable.

**2.2. Synthesis.** The objective of the synthetic work described in this study is the derivatization of MMV688845. For this purpose, a synthetic route based on a published synthesis of the hit compound<sup>33</sup> was designed. Starting from Boc-protected amino acids, the preparation of analogs is possible in three steps, as shown in Scheme 2. This modified synthetic route allows targeted derivatization of MMV688845 without racemization of the amino acid stereocenter.

In the first step (general procedure A), an amide bond is synthesized using the phosphonic acid anhydride T3P in a mixture of EtOAc and pyridine,<sup>35</sup> followed by removal of the Boc-protecting group using TFA. The second amide bond in the molecule is formed using the coupling reagent DEPBT,<sup>36</sup> for which the amine is reacted with an aromatic carboxylic acid.

The synthesis and modification of aniline building blocks were crucial for the desired derivatization, for which the 2-morpholinoaniline in MMV688845 was the starting point. Using the syntheses shown in Scheme 3, thiomorpholine and its

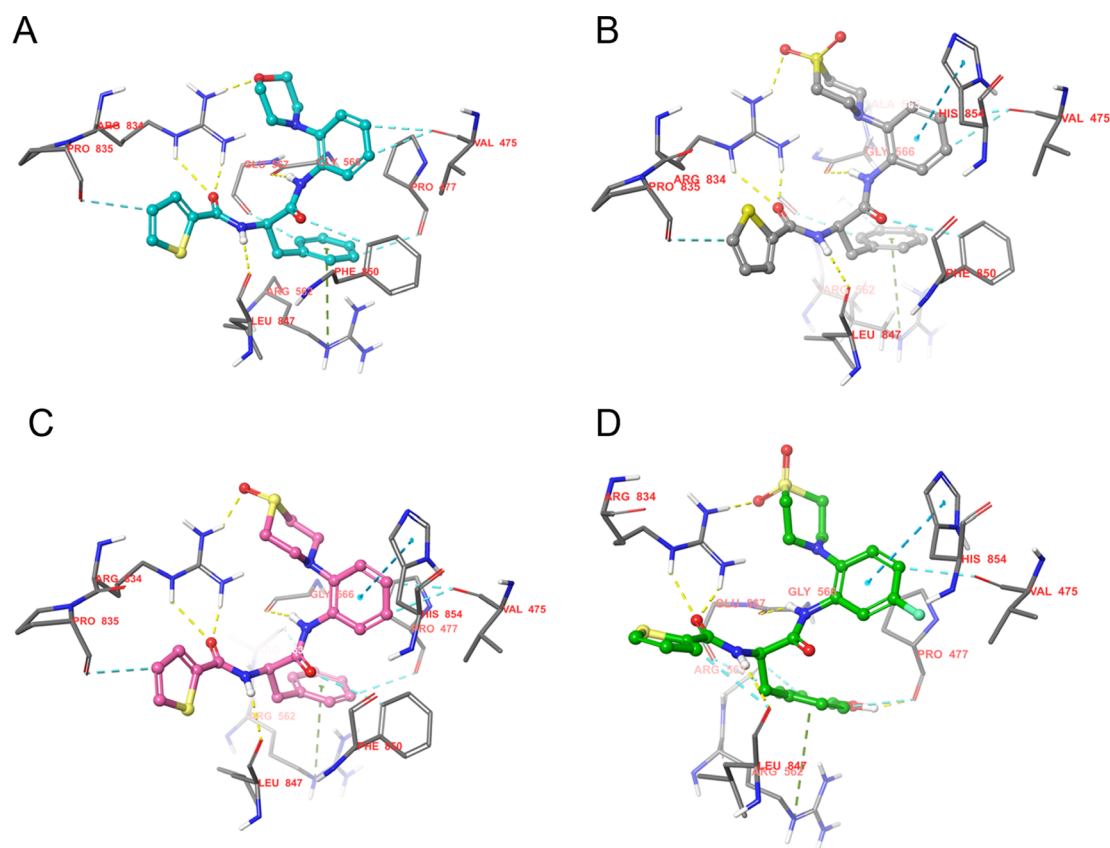
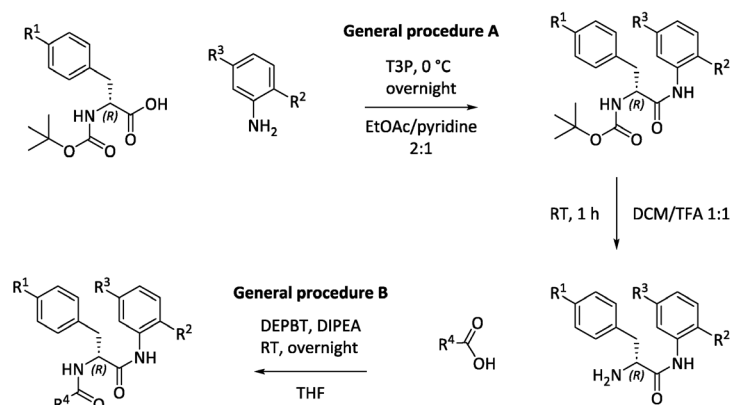


**Figure 1.** Docking poses of MMV688845 (A), compound 20 (B), compound 14 (C) and the  $\beta$  and  $\beta'$  subunits of RNAP<sub>Mtb</sub> and compound 39 after exchange of phenylalanine for tyrosine (D). Hydrogen bonds are displayed as yellow dashed lines. 2D visualizations of the shown interactions can be found in the Supporting Information (Figure S2). Visualization generated with the Maestro graphical interface (Schrödinger Release 2022-3: Maestro, Schrödinger, LLC, New York, NY, 2021).

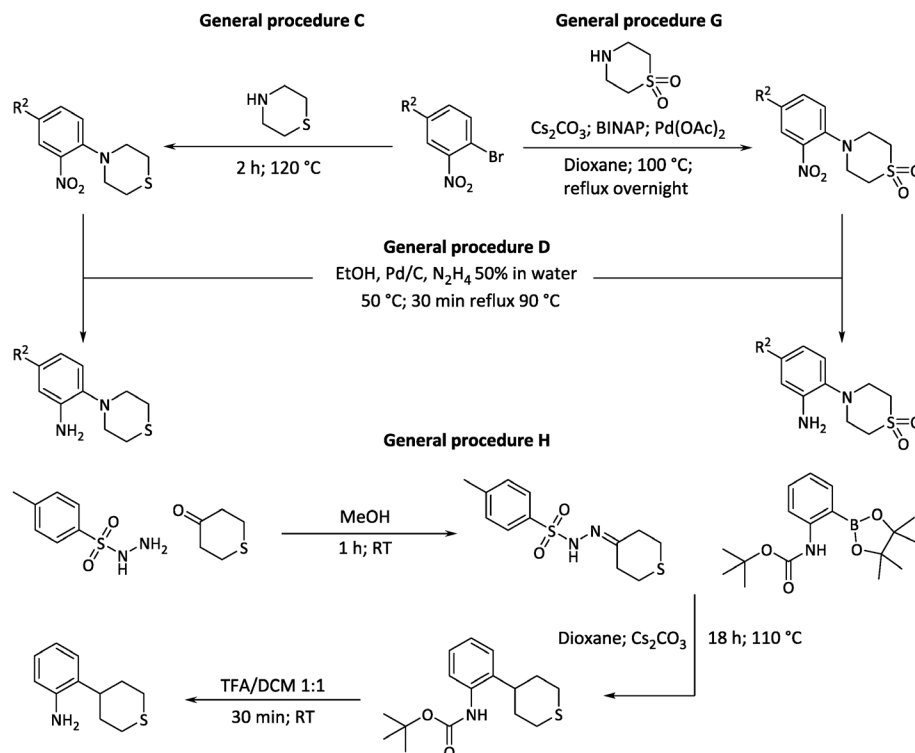
**Scheme 2. Synthetic Pathway for Derivatization of MMV688845 Analogues (T3P: Propanephosphonic Acid Anhydride, TFA: Trifluoroacetic Acid, DEPBT: 3-(Diethoxyphosphoryloxy)-1,2,3-benzotriazin-4(3H)-one, DIPEA: *N,N*-Diisopropylethylamine)**



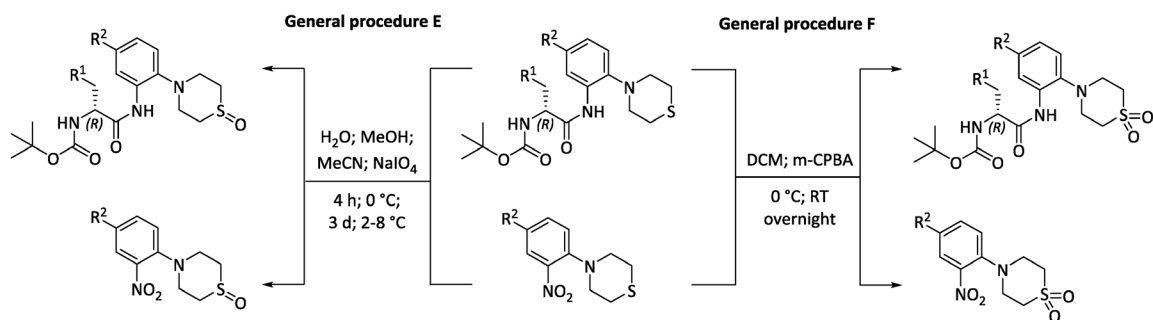
oxidation products, i.e., sulfone and sulfoxide, were introduced as substituents for derivatization. The introduction of thiomorpholine was achieved by a nucleophilic substitution on 2-bromonitrobenzene (general procedure C) and subsequent

reduction of the nitro group by hydrazine (general procedure D). In the case of 21, we tried to couple commercially available thiomorpholine dioxide to 1-bromo-2-nitrobenzene to avoid the use of oxidizing agents completely, because oxidation could

**Scheme 3. Preparation of the Aniline Building Block (BINAP: 2,2'-Bis(diphenylphosphino)-1,1'-binaphthyl; TFA: Trifluoroacetic Acid)**



**Scheme 4. Synthesis of Thiomorpholine Sulfoxides and Sulfones (m-CPBA: meta-Chloroperoxybenzoic Acid)**



also occur at the aniline nitrogen atom to form its *N*-oxide. General procedure C did not yield the desired product in this case. A reason for this could be the electron-withdrawing effect of the two oxygen atoms, which makes the nitrogen of thiomorpholine dioxide less nucleophilic preventing the substitution. A BINAP and transition metal-aided coupling was investigated, which produced the desired aniline in a yield of 32%. Thus, we eventually decided against this latter approach as it is more expensive and less efficient than the nucleophilic substitution approach.<sup>37</sup>

For the synthesis of 2-(tetrahydro-2*H*-thiopyran-4-yl) anilines, a different synthetic strategy was necessary (general procedure H in Scheme 3). The desired derivatives were prepared by C-C coupling of 4-oxothiane and Boc-2-amino-

phenylboronic acid pinacol ester.<sup>38</sup> For this synthetic method, 4-oxothiane was transformed to a sulfonylhydrazone using tosylhydrazide. In the subsequent step, the C-C coupling was carried out by reaction of the sulfonylhydrazone with the boronic acid pinacol ester in the presence of  $\text{Cs}_2\text{CO}_3$ . The final Boc cleavage was performed in TFA/DCM. Barluenga et al. postulated that the tosylhydrazones formed like that decompose thermally forming a diazo intermediate (Bamford–Stevens reaction), which reacts with the boronic acid or its ester.<sup>39</sup>

The oxidation of the thioether moiety was carried out according to general procedures E and F as shown in Scheme 4. By using different oxidizing agents, sulfone and sulfoxides were selectively obtained. The oxidation was conducted on the products of general procedure A or on the substituted nitro

building blocks. Starting from the thiomorpholine derivatives, sulfoxides were prepared using  $\text{NaIO}_4$ , while the analogous sulfones were obtained by oxidation with *m*-CPBA. The molecular structures of the oxidation products were unambiguously determined by X-ray crystallography, as described below. Oxidizing the sulfur in the 4-(4- $\text{R}^2$ -2-nitro-phenyl)-thiomorpholine intermediates is an alternative way to achieve oxidation (for example, see synthesis of **47** (sulfoxide) or **25** (sulfone)). S-Oxidation of the nitro building block has the disadvantage that the more polar groups (especially the sulfoxides) are present in subsequent synthetic steps, which complicates purification of the products by normal phase column chromatography. S-Oxidation after the final coupling step has not been investigated since the thiophene groups are also prone to oxidation.<sup>40</sup>

**2.2.2. Stereochemical Evaluation of the Synthetic Pathway.** It is known that only the *R* enantiomer of MMV688845 shows activity against *Mabs*, whereas the *S* enantiomer is inactive.<sup>31,33</sup> The synthetic procedure described by Ebright *et al.*<sup>32</sup> required preparative chiral HPLC separation of the enantiomers in the racemic mixture of the final compounds. To avoid the necessity of enantiomer separation, an important goal in the design of the synthesis was to start with reactants containing the required *R* configuration and preserve that configuration throughout the synthesis. Boc-protected (*R*)-phenylalanine is a readily available and inexpensive starting material for most compounds. In our previous study, we made important steps toward the realization of this goal.<sup>33</sup> To determine the stereochemistry of the reactions, (*R*)-MMV688845, (*S*)-MMV688845, and (*rac*)-MMV688845 were synthesized starting from the (*R*)-, (*S*)-, or (*rac*)-phenylalanine using the new synthetic procedure.

Although phenylalanine is not known for its susceptibility to racemization, like e.g., phenylglycine containing peptides,<sup>41</sup> literature shows that phenylalanine racemization can occur even in relatively mild amidation procedures.<sup>33,42–45</sup> To achieve mild reaction conditions, we adapted the T3P (*n*-propanephosphonic acid anhydride<sup>46</sup>) coupling method published by Dunetz *et al.*<sup>35</sup> The authors showed that a mixture of EtOAc and pyridine at 0 °C yielded the lowest degree of racemization. Another advantage of T3P is that the side products formed in the coupling reactions are water-soluble and hence can be readily separated by extraction during work up. The intermediate and final compounds were analyzed by chiral HPLC (see the Supporting Information). The *ee*-values are listed in Table 1.

All products that were synthesized from enantiopure Boc-phenylalanine derivatives showed *ee*-values higher than 99% indicating that virtually no racemization occurs under the reaction conditions used. Specific optical rotations have been

**Table 1. *ee*-Values of the Starting Materials (Boc-Protected Amino Acids), the Intermediates 1-(*R*), 1-(*S*), and 1-(*rac*) Being the Intermediates after Anilide Formation; 2A-(*R*), 2A-(*S*), and 2A-(*rac*) Being the Boc-Deprotected Intermediate and Final Compounds 2B-(*R*), 2B-(*S*), and 2B-(*rac*) during a Synthetic Route**

substance	<i>ee</i> -value [%]			
	Boc-Phe-	1-	2A-	2B-
( <i>R</i> )	99.82	99.80	99.92	99.70
( <i>S</i> )	100.00	99.34	99.84	99.79
( <i>rac</i> )	0.24	0.64	0.47	0.06

determined for the compounds in Table 1 and can be found in the Supporting Information.

**2.2.3. Structural Elucidation.** To prove that oxidation indeed occurred at the S atom of the thiomorpholine moiety only, an X-ray crystal structure analysis was conducted on a selection of compounds, viz. **6**, **14**, and **20**, because the formation of thiomorpholine *N*-oxide is also conceivable under the conditions used.<sup>47</sup> We recently described the crystal and molecular structure of racemic MMV688845 (CSD refcode: BALNUB),<sup>33</sup> while the investigated compound set for this study represents the direct thiomorpholine analog of MMV688845 **6**, its sulfoxide derivative **14** and its sulfone derivative **20**.

We obtained colorless crystals of enantiopure **6** and **20** suitable for X-ray diffraction from a chloroform/heptane solvent system. Interestingly, two crystallographically independent homochiral molecules of **6** (Figure 2A) form a hydrogen-bonded dimer about a *pseudo* center of symmetry in the reported crystal structure (triclinic system, space group *P1*) analogous to the crystallographic center of symmetry observed for racemic MMV688845 (monoclinic system, space group *P2*<sub>1</sub>/*n*). The crystal structure of **20** is isomorphous with that of **6**.

The corresponding sulfoxide **14** crystallized as a sesquihydrate from aqueous methanol. The homochiral molecules likewise constitute a hydrogen-bonded dimer through N–H...O hydrogen bonds formed between the phenylalanine amide moieties. The dimer is, however, not *pseudo* centrosymmetric as in **6** and **20** but exhibits a crystallographic 2-fold rotation axis (monoclinic system, space group *I2*). N–H...O hydrogen bond parameters within dimers in are essentially comparable in **6**, **20**, and **14** (see the Supporting Information).

Bearing in mind that single-crystal X-ray diffraction does not prove the homogeneity of the bulk material, the molecular structures and absolute configurations of the sulfone **20** (Figure 2B) and the sulfoxide **14** (Figure 2C) were also confirmed by X-ray crystallography, indicating oxidation of the sulfur atom in the isolated products without formation of thiomorpholine *N*-oxides.

**2.3. Microbiology. 2.3.1. In Vitro Activity Determination against NTM and *Mtb*.** The *in vitro* activity of MMV688845 analogs described in this study was determined as MIC<sub>90</sub> against a panel of NTM (*Mabs*, *Mycobacterium intracellulare* and *Mycobacterium smegmatis*) and *Mtb*—the most prevalent mycobacterial pathogen worldwide. The mycobacteria were selected to ensure comparability of our data (where applicable) to other publications,<sup>31,33,50,51</sup> for their clinical relevance<sup>52</sup> in both pulmonary<sup>53</sup> and extrapulmonary<sup>54</sup> clinical presentations, and in view of the severity and treatability<sup>55</sup> of the infections.

Since *Mabs* has become a serious problem in the clinic,<sup>19</sup> we particularly focused on this species. The activity was therefore analyzed against two different *Mabs* strains, namely, the reference strain ATCC 19977 and clinical isolate *Mabs* Bamboo. To assess possible effects of the growth medium on the *in vitro* activity, the assays were performed in both Middlebrook 7H9 and cation-adjusted Mueller-Hinton II broth medium (MHII).

As *Mabs* is capable of infecting human macrophages and actively proliferates intracellularly by evading certain immune defense mechanisms,<sup>55</sup> activity was also determined in a fluorescence based macrophage infection assay<sup>59</sup> (for detailed method description, see the Supporting Information).

*M. intracellulare* ATCC 35761 (*Mintra*) was chosen to represent the clinically relevant *M. avium* complex (MAC).<sup>56</sup> Studies in the United States have shown that MAC is the most

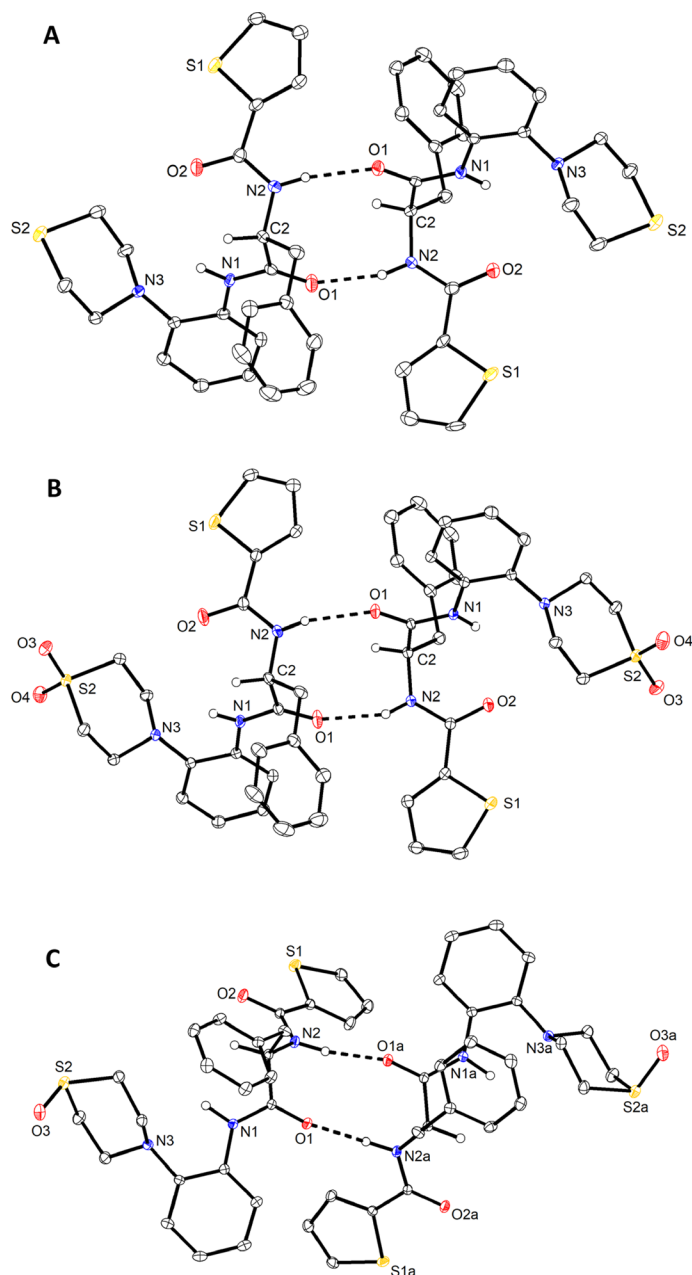


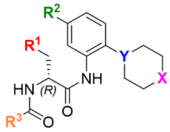
**Figure 2.** Molecular structures of **6** (A), **20** (B), and **14** (C), as determined by X-ray crystallography. Displacement ellipsoids are drawn at the 50% probability level. Hydrogen atoms on nitrogen and the chirality center are represented by small spheres of arbitrary radius otherwise omitted for clarity. Dashed lines represent N–H···O hydrogen bonds. Minor positional disorder of thiophene rings (ca. 6%) in **6** (A) and **20** (B) is also not shown for the sake of clarity. Solvent water in the crystal structure of **14** (C): 1.5 H<sub>2</sub>O is not shown (suffix a denotes symmetry-related atoms). The structure of **14** (C) was refined with aspherical atomic scattering factors using NoSpherA2.<sup>48,49</sup>

frequently isolated NTM in both pulmonary lung disease<sup>53</sup> and extrapulmonary infections.<sup>57</sup>

*M. smegmatis* (*Msmeg*) is a fast-growing mycobacterium generally considered nonpathogenic and often used as a surrogate organism for *Mtb*.<sup>50,51</sup> To demonstrate a broad spectrum of activity against fast-growing mycobacteria and to

analyze species-dependent differences in efficacy, *M. smegmatis* mc<sup>2</sup> 155 was included in the selection of mycobacteria. We report the results of broth microdilution MIC<sub>90</sub> assays for each substance in Table 2.

Optical density-derived and RFP-fluorescence-derived MIC<sub>90</sub> values were similar. Although OD measurement is a well-

Table 2. Antimycobacterial Activity of MMV688845 (abbr. MMV845) Derivatives<sup>a</sup>


	R <sup>1</sup>	R <sup>2</sup>	X, Y	R <sup>3</sup>	MIC <sub>90</sub>					MIC <sub>50</sub>	MIC <sub>30</sub>	MIC <sub>50</sub>	MIC <sub>30</sub>		
					Msmeg mc <sup>2</sup> 155 <sup>b</sup>	Mtb H37Rv <sup>c</sup>	Mabs ATCC19977 <sup>d</sup>	Mabs ATCC19977 <sup>e</sup>	Mintra ATCC 35761 <sup>f</sup>	Mabs Bamboo <sup>g</sup>	Mabs ATCC 19977 + THP1 <sup>h</sup>				
					7H9	7H9	7H9	MHII	7H9	7H9	OD	RFP	RFP	RPMI	RFP
MMV845	Phenyl	H	O, N	2-Thiophenyl	0.78	0.78	6.25	12.5	0.78	1.7	4.4	1.56	12.5		
6	Phenyl	H	S, N	2-Thiophenyl	3.13	6.25	12.5	50	0.78	2.5	14	12.5	> 100		
7	Phenyl	H	S, N	2-Fluorophenyl	3.13	6.25	12.5	50	0.78	3	18	12.5	> 100		
11	Phenyl	F	S, N	2-Thiophenyl	3.13	1.56	25	50	0.78	1.4	14	3.13	> 100		
12	Phenyl	F	S, N	2-Fluorophenyl	6.25	1.56	25	25	0.78	1.15	12	3.13	100		
14	Phenyl	H	S=O, N	2-Thiophenyl	1.56	0.4	3.13	6.25	0.1	0.33	2	3.13	25		
15	Phenyl	H	S=O, N	2-Fluorophenyl	0.78	0.78	6.25	3.13	0.1	0.4	2.1	0.78	12.5		
17	Phenyl	F	S=O, N	2-Thiophenyl	1.56	0.4	1.56	3.13	0.05	0.28	1.9	0.78	25		
18	Phenyl	F	S=O, N	2-Fluorophenyl	1.56	0.78	3.31	3.13	0.2	0.52	2	0.39	12.5		
20	Phenyl	H	O=S=O, N	2-Thiophenyl	1.56	0.2	3.13	3.13	0.1	0.24	1.7	0.78	6.25		
24	Phenyl	H	O=S=O, N	2-Fluorophenyl	0.78	0.2	0.78	1.56	0.05	0.23	4.3	0.39	6.25		
28	Phenyl	F	O=S=O, N	2-Thiophenyl	1.56	0.78	6.25	3.13	0.2	0.43	6.5	0.39	3.13		
29	Phenyl	F	O=S=O, N	2-Fluorophenyl	1.56	0.78	3.13	3.13	0.1	0.4	4.5	0.39	3.13		
32	Phenyl	H	S, CH	2-Thiophenyl	6.25	> 25	50	100	6.25	21	44	> 100	> 100		
34	Phenyl	H	S=O, CH	2-Thiophenyl	6.25	> 25	25	50	3.13	6	20	> 100	> 100		
36	<i>p</i> -Hydroxyphenyl	F	S, N	2-Thiophenyl	12.5	0.78	12.5	50	0.1	1.6	15	12.5	50		
37	<i>p</i> -Hydroxyphenyl	F	S, N	2-Fluorophenyl	6.25	1.56	25	50	0.2	1.7	15	6.25	25		
39	<i>p</i> -Hydroxyphenyl	F	O=S=O, N	2-Thiophenyl	6.25	0.78	6.25	3.13	0.05	0.4	9	6.25	25		
40	<i>p</i> -Hydroxyphenyl	F	O=S=O, N	2-Fluorophenyl	6.25	0.78	6.25	6.25	0.2	1.1	13	3.13	25		
42	3-Thiophenyl	H	O, N	2-Thiophenyl	1.56	3.13	12.5	12.5	1.56	2.3	7	12.5	50		
43	3-Thiophenyl	H	O, N	2-Fluorophenyl	1.56	3.13	12.5	12.5	0.78	1.9	7	6.25	25		
45	2-Thiophenyl	H	O, N	2-Thiophenyl	1.56	6.25	12.5	12.5	1.56	2.4	9	12.5	> 100		
46	2-Thiophenyl	H	O, N	2-Fluorophenyl	1.56	3.13	6.25	12.5	0.78	2	7	6.25	25		
50	3-Thiophenyl	H	S=O, N	2-Thiophenyl	3.13	6.25	6.25	12.5	0.2	3.4	15	12.5	100		
51	3-Thiophenyl	H	S=O, N	2-Fluorophenyl	1.56	3.13	6.25	12.5	0.2	1.5	4.4	6.25	50		
53	2-Thiophenyl	H	S=O, N	2-Thiophenyl	3.13	3.13	12.5	12.5	0.2	1.3	5.8	12.5	100		
54	2-Thiophenyl	H	S=O, N	2-Fluorophenyl	1.56	1.56	6.25	12.5	0.2	1.8	6.5	6.25	50		

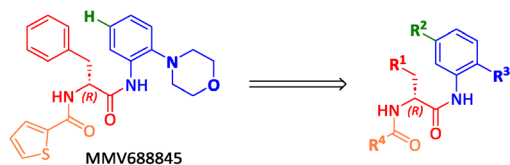
<sup>a</sup>Color coding: For each tested mycobacterial strain, the colors show the difference to the average activity value, dark green: lowest MIC value; light green: below average; white: closest to average; light red: above average, dark red: highest MIC value. For detailed information on the methodology of the assays, see the Supporting Information. <sup>b</sup>Incubated for three days at 37 °C (*Msmeg* and *Mabs*) or five days (*Mintra*). Performed in duplicate, results were averaged. Data were obtained via RFP measurement (shown here) or OD measurement (see the Supporting Information). <sup>c</sup>Incubated for seven days at 37 °C. Data were obtained via OD measurement. Performed in duplicate, results were averaged. <sup>d</sup>Incubated for three days at 37 °C. Data were obtained via OD measurement. Performed in duplicate, results were averaged. <sup>e</sup>Incubated for three days (37 °C, 5% CO<sub>2</sub>). Performed in duplicate, results were averaged.

established method to analyze bacterial growth, RFP assay data often offer higher sensitivity and specificity.<sup>58,59</sup> Nevertheless, in our case, the OD and RFP values correlate well and the MIC<sub>90</sub> values of the reference compound do not differ substantially.

The MIC<sub>90</sub> values for MMV688845 determined in this study are consistent with values found in the literature. Low *et al.* determined a MIC<sub>90</sub> value against *Mabs* of 7 μM, and we found 6.25 μM in Middlebrook 7H9 medium. To investigate culture media independency, the growth inhibitory effect was analyzed in MHII and a MIC<sub>90</sub> value of 12.5 μM was determined indicating culture medium independency. The MIC<sub>90</sub> value we determined against *Mtb* is slightly lower (0.78 μM) than that of Low *et al.* (1.2 μM).

Derivatization of the parent compound MMV688845 was performed at the residues R<sup>1</sup>–R<sup>3</sup> as shown in Scheme 5.

#### Scheme 5. AAP Base Scaffold and Derivatized Residues



5085

<https://doi.org/10.1021/acs.jmedchem.3c00009>  
J. Med. Chem. 2023, 66, 5079–5098

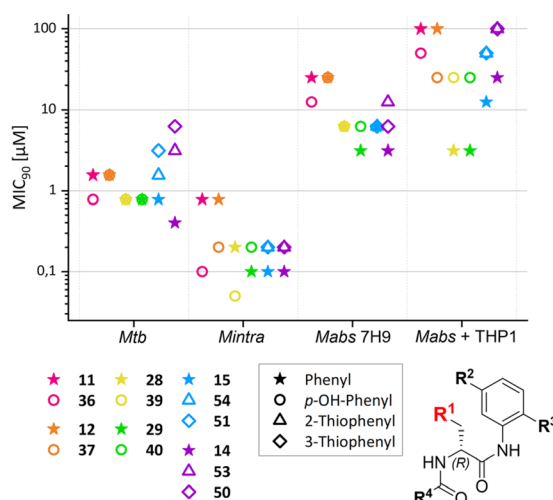


**Figure 3.** Comparison of MIC<sub>90</sub> values of compounds that only differ in R<sup>1</sup>. Compounds that only differ in R<sup>1</sup> are shown in the same color; the symbols represent the respective R<sup>1</sup> substituent. Displayed values were generated by RFP measurement. Only *Mtb* MIC<sub>90</sub> values were generated by OD measurement. Compounds that only differ in R<sup>1</sup> are displayed in the same color.

decrease in activity when a *p*-Hydroxyphenyl group is present. Possibly, these results are based on the higher polarity of the *p*-Hydroxyphenyl group leading to lower permeability through the membranes of both the macrophages and bacteria.

In *Msmeg*, MIC<sub>90</sub> values show a 4-fold increase when a *p*-Hydroxyphenyl group is introduced into the molecule.

Interestingly, the MIC<sub>90</sub> values against *Mintra* show an opposite trend. A comparison of **28** and **39** shows that the *p*-Hydroxyphenyl group has a positive effect on the MIC<sub>90</sub> values with a 2-to-4-fold increase in activity. Currently, we have no well-founded explanation for this result, although structural differences between the RNAPs of *Mabs* and *Mintra* and the interaction of R<sup>1</sup> with the target may play a role.

The MIC<sub>90</sub> values determined against *Mtb* show that *p*-Hydroxyphenyl as a substituent is never inferior to phenyl. In the case of compounds **11** and **36**, *p*-Hydroxyphenyl substitution shows a better activity against *Mtb*.

Although the change from phenyl to 2- or 3-thiophenyl is very small regarding the chemical and electronic properties of the molecule, it leads to activity loss in every single species investigated, showing that R<sup>1</sup> is indeed sensitive to even minor changes in the substituent R<sup>1</sup>.

The primary intent of derivatizing R<sup>2</sup> was to sterically shield the anilide to prevent hydrolysis and to slow down or prevent metabolism of the morpholino-anilide moiety of the molecule. To this end, we introduced a fluorine atom in the *para* position to the morpholine moiety and determined whether this resulted in lower MIC<sub>90</sub> values. An overview of compounds only different at R<sup>2</sup> is given in Figure 4.

The introduction of the fluorine atom results in a tendency for higher MIC<sub>90</sub> values. It is worth noting that, for *Mabs*, a 2-to-4-fold increase in MIC<sub>90</sub> values was observed (e.g., **6/11** or **24/29**). Interestingly, this behavior is reversed when R<sup>3</sup> contains a thiomorpholine sulfoxide group. Both thiomorpholine sulfoxide structures (**14/17**, **15/18**) show 2-fold increased MIC<sub>90</sub> values against *Mabs*. This effect is not observed for the respective

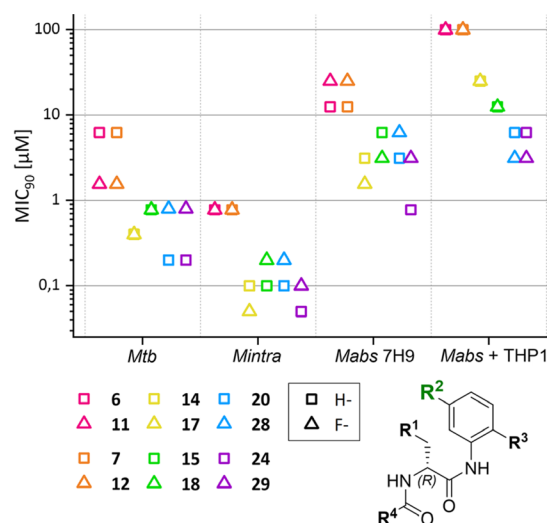


**Figure 4.** Comparison of MIC<sub>90</sub> values of compounds that only differ in R<sup>2</sup>. Compounds that only differ in R<sup>2</sup> are shown in the same color; the symbols represent the respective R<sup>2</sup> substituent. Displayed values were generated by RFP measurement. Only *Mtb* MIC<sub>90</sub> values were generated by OD measurement.

sulfones. For example, the *Mabs* and *Mtb* MIC<sub>90</sub> values of the most active compound **24** are increased 4-fold on addition of the fluorine substituent. A similar effect was observed in the other sulfones, **20/28**.

The MIC<sub>90</sub> values determined for *Mabs* in the macrophage infection model decreased upon introduction of the fluorine substituent. The effect is more pronounced in the MIC<sub>50</sub> values. Here, a 2-to-4-fold decrease for all substances with the fluorine substituent was found.

The main R<sup>3</sup> variation of the compound set presented here is the exchange of the morpholine group of MMV688845 by a thiomorpholine group and the respective oxides (1λ<sup>4</sup>-thiomorpholin-1-one (thiomorpholine-sulfoxide) and 1λ<sup>6</sup>-thiomorpholine-1,1-dione (thiomorpholine-sulfone)). Tetrahydrothiopyran and its sulfone were included to check on the necessity of an aromatic amine structure within R<sup>3</sup>. An overview of the MIC values is given in Figure 5.

MIC<sub>90</sub> determination against *Msmeg* revealed a decrease (4-fold) in activity when morpholine was exchanged for thiomorpholine in MMV688845. An increase of activity was seen for the respective oxides (2-fold increase). For all other comparison groups, S-oxidation had no strong effect on the MIC<sub>90</sub> values.

In *Mtb*, however, oxidation to the sulfone in **20** resulted in a 4-fold decrease in the MIC<sub>90</sub> values (**20**, MIC<sub>90</sub> down to 200 nM) in comparison to MMV688845. The respective sulfoxide also showed better activity than the hit compound (2-fold decrease in the MIC<sub>90</sub> values).

For *Mabs*, a similar behavior was observed: in comparison to MMV688845, a 2-to-4-fold increase in activity was observed, the sulfone leading to lower MIC values. The same is true for all other compared groups that contain either phenyl or *p*-hydroxyphenyl as R<sup>1</sup>. In these groups, improvements of MIC<sub>90</sub> values of down to 0.78 μM (**24**) were achieved. Groups that contain 2- or 3-thiophenyl as R<sup>1</sup> did not benefit from the oxidation. The same effects are seen with the clinical isolate

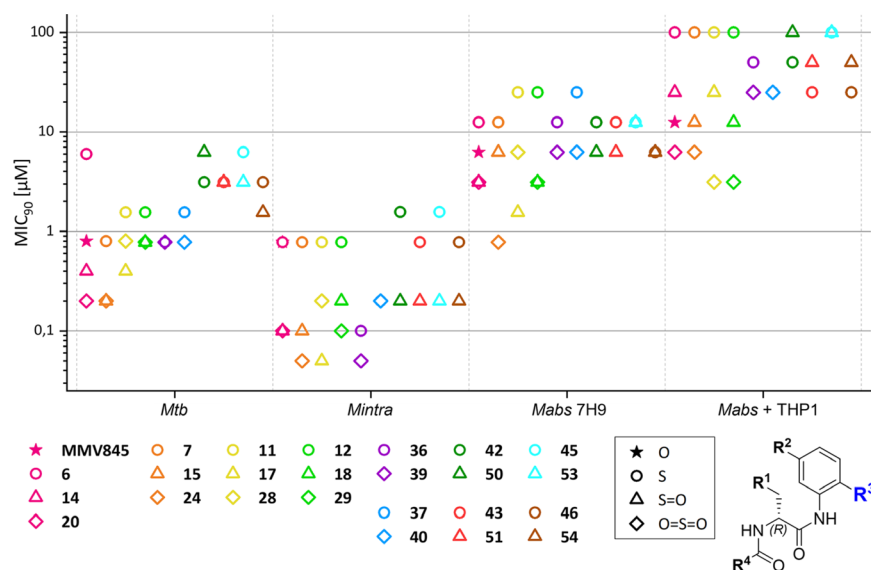


**Figure 5.** Comparison of MIC<sub>90</sub> values of compounds that only differ in R<sup>3</sup>. Compounds that only differ in R<sup>3</sup> are shown in the same color; the symbols represent the respective R<sup>3</sup> substituent. Displayed values were generated by RFP measurement. Only *Mtb* values were generated by OD measurement. Compounds 32 and 34 were excluded in this figure. MMV845 abbr. MMV688845.

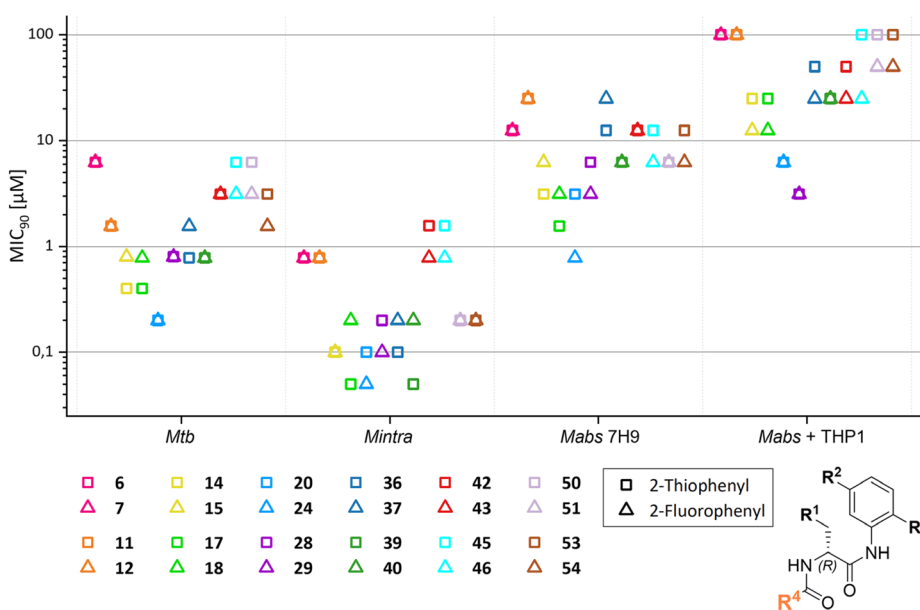


**Figure 6.** Comparison of MIC<sub>90</sub> values of compounds that only differ in R<sup>4</sup>. Compounds that only differ in R<sup>4</sup> are shown in the same color; the symbols represent the respective R<sup>4</sup> substituent. Displayed values were generated by RFP measurement. Only *Mtb* values were generated by OD measurement.

*Mabs* Bamboo, even though the most active substances do not reach as low MIC<sub>90</sub> values as those that we observed with the *Mabs* ATCC 19977 strain. Nevertheless, the respective sulfones and sulfoxides offer submicromolar MIC<sub>50</sub> values and low-micromolar MIC<sub>90</sub> values. Within the macrophage infection model, we noted that the oxides are still more potent than MMV688845 but with less of a difference. The difference between the sulfoxides used and their respective sulfones is

remarkable: sulfoxides show a strong decrease in activity when tested in the macrophage infection model. This could be due to their high polarity, which could negatively affect their ability to cross biological bilayer membranes. The need to pass two membranes (macrophage and bacterium) rather than one may have magnified this effect.

Against *Mintra*, thiomorpholine oxidation also increases activity. MIC<sub>90</sub> values are decreased by a factor of 4 in

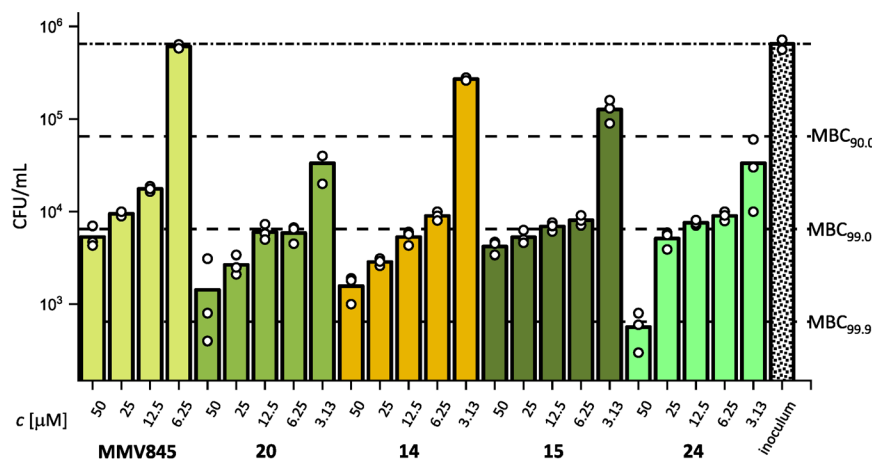


**Figure 7.** MBC determination against *Mabs* ATCC19977 of MMV688845 (abbr. MMV845) and a selection of AAP derivatives. Bacteria reduction levels are displayed as dashed horizontal lines. Substances were analyzed in triplicates as indicated by the white dots.

comparison to MMV688845. In other groups, oxidation resulted in compounds that have  $MIC_{90}$  values down to 50 nM (24 and 39), which is equivalent to an 8-fold increase in activity.

For varying  $R^4$ , we considered the thiophene-2-carboxamide (same as in the hit compound MMV688845) and the 2-fluorophenyl and 2-thiophenyl demonstrate similar activity levels within a maximum 2-fold difference with the tendency that the 2-fluorophenyl compounds achieve slightly lower  $MIC_{90}$  values. Only in 17 of 84 direct comparisons (throughout all bacterial species tested), 2-thiophenyl compounds exhibit lower values than their respective 2-fluorophenyl compounds. In the macrophage infection assay, the 2-thiophenyl compounds were always inferior to the 2-fluorophenyl compounds.

**Figure 6** shows the comparison of  $MIC_{90}$  values against the different mycobacterial strains of compounds that differ only in  $R^4$ .  $MIC_{90}$  values of the displayed compounds do not differ substantially depending on the  $R^4$  substituent. In most of the cases, 2-fluorophenyl and 2-thiophenyl demonstrate similar activity levels within a maximum 2-fold difference with the tendency that the 2-fluorophenyl compounds achieve slightly lower  $MIC_{90}$  values. Only in 17 of 84 direct comparisons (throughout all bacterial species tested), 2-thiophenyl compounds exhibit lower values than their respective 2-fluorophenyl compounds. In the macrophage infection assay, the 2-thiophenyl compounds were always inferior to the 2-fluorophenyl compounds.

**2.3.2. Bactericidal.** The ability to kill mycobacteria instead of forcing them into a dormant or quiescent state is a crucial property of effective antimycobacterial treatments, in particular for the therapy of *Mabs* infections.<sup>61</sup> To find out whether the AAP derivatives kill *Mabs*, a minimum bactericidal concentration (MBC) evaluation was conducted. Typically, an MBC is defined as the concentration at which the level of colony forming units in an inoculum is reduced by three logarithmic units, or in other words, a killing rate of 99.9% of the bacteria that was present at the start of the experiment. In mycobacteriology, this threshold was redefined for reasons of reproducibility and accuracy and is currently set at 99.0% as mycobacteria need inconveniently longer incubation times for high killing rates of 99.9%.<sup>62</sup>

MBC testing against *Mabs* ATCC19977 was conducted for a selection of the most active compounds as well as MMV688845, **Figure 7**. MMV688845 did not reduce viable bacteria at a concentration below 12.5  $\mu$ M. At its  $MIC_{90}$  value of 6.25  $\mu$ M, no reduction of viable bacteria was observed. It achieves its  $MBC_{99}$  at a concentration of 50  $\mu$ M ( $MBC_{99}$  at 8X  $MIC_{90}$ ). In contrast,

the new derivatives reported here show a higher reduction of viable bacteria at lower concentration levels. **14** and **15** (both including a sulfoxide moiety) show a reduction at 3.13  $\mu$ M but stay below 90% reduction (58 and 81% respectively), while the sulfones **20** and **24** both reach a reduction of 95% at the same concentration levels. For all tested derivatives, concentration levels of 6.25  $\mu$ M and higher result in a reduction of 99% or only slightly above that threshold making them about 4 times more bactericidal than the hit compound. Compounds **20** and **15** achieved their respective  $MBC_{99}$  at 2X  $MIC_{90}$ . This is a significant improvement in cidal activity over MMV688845.

**2.3.3. Testing against MMV688845-Resistant Mutants.** To verify on-target the activity of the analogs described in this study, compounds **14**, **15**, and **24** were tested against the MMV688845-resistant strain *Mabs* Bamboo 845<sup>R</sup>-2.1. The strain and its resistance to MMV688845 were previously described.<sup>34</sup> The data presented in **Table 3** show evidence

**Table 3.** Activity Data against the MMV688845-Resistant Strain *Mabs* Bamboo 845<sup>R</sup>-2.1<sup>a</sup>

compound	MIC <sub>90</sub> ( $\mu$ M)
	<i>Mabs</i> Bamboo 845 <sup>R</sup> -2.1
CLR	0.27
RFB	1.1
MMV688845	>100
<b>24</b>	42
<b>14</b>	>100
<b>15</b>	100

<sup>a</sup>Generated by selecting at 50  $\mu$ M MMV688845 using *Mabs* Bamboo. This strain is resistant to MMV688845 and has a rpoB/ $\beta$  subunit P473L mutation.<sup>34</sup> The observed frequency of resistance (FoR) was  $5.83 \times 10^{-8}$  CFU<sup>-1</sup>. CLR: clarithromycin; RFB: rifabutin.

that the target is the  $\beta$  subunit of the bacterial RNAP, because *Mabs* Bamboo 845<sup>R</sup>-2.1. harbors a P473L mutation of the  $\beta$  subunit, which is located directly at the binding site of the phenylalanine amides that was proposed by Lin et al.<sup>31</sup> and used for the herein described modeling study (2.1).

Similar to MMV688845, the three tested analogs suffered from a severe activity loss by at least factor 10 indicating the bacterial RNAP is involved in the molecular activity of the newly synthesized phenylalanine amides. Rifabutin, a RNAP inhibitor with a different binding site, achieved a MIC<sub>90</sub> value of 3 μM in a former activity determination against the MMV688845-sensitive *Mabs* Bamboo.<sup>25</sup> The results of the present study show no decline in activity against the resistant strain, which indicates that the probability of cross resistance between the two RNAP inhibitors is low.

**2.4. In Vitro Plasma and Microsomal Stability.** Former investigations on MMV688845 revealed low drug plasma levels after oral administration in Sprague Dawley male rats<sup>30</sup> and CD 1 mice,<sup>34</sup> which could be due to low metabolic stability. To narrow down the reasons why MMV688845 seems to exhibit low plasma levels, we conducted plasma stability and microsomal stability assays on the hit compound and the most active derivative, compound 24. The substances were tested in both human and murine plasma and microsomes. The plasma stability is given as a %-remaining concentration versus time plot in Figure 8. Microsomal stability is displayed in Table 4.

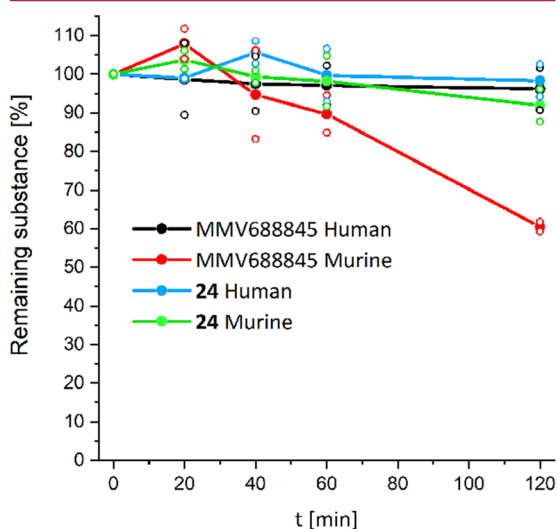


**Figure 8.** Plasma stability of MMV688845 (abbr. MMV845) and compound 24 in human and murine plasma over five different time points. Substances were analyzed in duplicates. Empty circles depict the measured values, filled circles show the respective mean.

The results show that both tested substances are stable in human plasma throughout the tested time frame. In murine plasma, MMV688845 shows a stronger decline in concentration than compound 24. A possible explanation for this behavior is that the fluorine atom in the phenyl moiety of 24 sterically shields the amide bond of compound 24 from being a target for

murine carboxyesterases (CES), leaving it uncleaved. As CES do not seem to be abundant in human plasma,<sup>63</sup> the stability of both substances in human plasma could be higher.

The determined half-lives show that both substances suffer from severe instability in a liver microsome assay, which is probably the reason for the low bioavailability *in vivo* described above. A rapid degradation of the phenylalanine amides by oxidation (e.g., hydroxylation) or hydrolytic activity of the microsomes seems to us a probable explanation for this observation.<sup>64–66</sup>

**2.5. Cytotoxicity.** MMV688845 was tested for cytotoxicity using the HEP 93 liver cancer cell line and found to be noncytotoxic.<sup>29,33</sup> In our study, we extended cytotoxicity testing of MMV688845 and all synthesized compounds to seven mammalian cell lines using a colorimetric microculture assay that utilized sulforhodamine-B as a staining agent. The methodology of this assay is described in various references.<sup>67–69</sup>

The EC<sub>50</sub> values are listed in Table 5. We confirmed the noncytotoxic properties of MMV688845, which was not cytotoxic for all tested cell lines at concentrations of up to 30 μM. The same was true for most variants of MMV688845. Only a few of the analogs showed very weak cytotoxicity against the tested cell lines. Most potent compounds can be considered as unproblematic since the MIC values are far below the EC<sub>50</sub> cytotoxicity values.

**2.6. Determination of Kinetic Solubilities and cLogP Values.** Solubility is a crucial parameter for the development of new drug candidates and their *in vivo* efficacy, especially for oral administration.<sup>70</sup> The calculated LogP value is considered as a predictive parameter to estimate compound solubility and/or permeability (cLogP values between 2 and 3 are desirable for pharmaceutical compounds).<sup>71</sup>

The kinetic solubilities of the new MMV688845 derivatives in PBS were experimentally determined by a nephelometric method described by Bevan and Lloyd.<sup>72</sup> (see the Supporting Information).

Figure 9A shows the relation between the calculated LogP values and measured solubilities of the synthesized compounds. Compounds with cLogP values higher than 3.5 usually have solubilities lower than 50 μM, making them hard to handle in biological assays and giving them undesirable biopharmaceutical properties. At cLogP values below 3, the solubilities show a much higher variability. In this region, six compounds show high aqueous solubilities of up to 431 μM.

Figure 9B,C shows the MIC<sub>90</sub> values determined against *Mabs* in the standard microdilution assay as well as in the macrophage infection model. Compounds with a cLogP between 2 and 3 achieve the lowest MIC<sub>90</sub> values. Within the macrophage infection model, a general increase in MIC<sub>90</sub> values is observed as described above. Nevertheless, the most active compounds possess a cLogP value between 2 and 3, verifying a desirable LogP range of 2–3 for the development of the AAP compound class.

**Table 4.** Half-Times and Intrinsic Clearance Values after Incubation of MMV688845 (abbr. MMV845) and Compound 24 with Human and Murine Liver Microsomes over 40 min<sup>a</sup>

substance	$t_{1/2}$ [min]	human microsomes	Cl <sub>int</sub> [ $\mu\text{L}/\text{min} \times \text{mg}$ ] human microsomes	$t_{1/2}$ [min]	murine microsomes	Cl <sub>int</sub> [ $\mu\text{L}/\text{min} \times \text{mg}$ ] murine microsomes
MMV845	1.7		1366	0.9		1837
24	1.5		1113	1.8		1562

<sup>a</sup>Experiment has been performed in duplicate.

Table 5. EC<sub>50</sub> Values [ $\mu\text{M}$ ] of AAP Analogs against Seven Different Mammalian Cell Lines<sup>a</sup>

compound	A375 <sup>a</sup>	HT29 <sup>b</sup>	MCF7 <sup>c</sup>	A2780 <sup>d</sup>	NIH 2T3 <sup>e</sup>	HeLa <sup>f</sup>	HEK293 <sup>g</sup>
MMV688845	>30	>30	>30	>30	>30	>30	n.d.
6	>30	>30	16.4 $\pm$ 1.7	19.8 $\pm$ 2.0	>30	>30	19.1 $\pm$ 2.4
7	18.6 $\pm$ 4.2	>30	13.6 $\pm$ 1.4	14.9 $\pm$ 1.6	>30	>30	6.3 $\pm$ 1.2
11	>30	>30	>30	>30	>30	>30	n.d.
12	29.4 $\pm$ 1.4	>30	>30	28.3 $\pm$ 1.4	28.5 $\pm$ 2.0	28.3 $\pm$ 1.5	n.d.
14	>30	>30	>30	>30	>30	>30	>30
15	>30	>30	>30	>30	>30	>30	>30
17	>30	>30	>30	>30	>30	>30	n.d.
18	>30	>30	>30	>30	>30	>30	n.d.
20	>30	>30	>30	23.6 $\pm$ 2.2	>30	>30	>30
24	>30	>30	>30	>30	>30	>30	n.d.
28	>30	>30	23.2 $\pm$ 2.8	24.0 $\pm$ 5.2	26.9 $\pm$ 5.0	>30	>30
29	>30	>30	25.9 $\pm$ 2.7	23.2 $\pm$ 4.4	24.2 $\pm$ 4.2	>30	>30
32	>30	>30	>30	>30	>30	>30	n.d.
34	>30	>30	>30	>30	>30	29.8 $\pm$ 1.3	n.d.
36	>30	>30	>30	>30	>30	>30	n.d.
37	>30	>30	>30	>30	>30	>30	n.d.
39	>30	29.8 $\pm$ 1.7	>30	29.7 $\pm$ 1.2	>30	>30	n.d.
40	>30	>30	>30	>30	>30	>30	>30
42	>30	>30	>30	>30	>30	>30	n.d.
43	>30	>30	>30	>30	>30	>30	n.d.
45	>30	29.8 $\pm$ 1.9	>30	29.5 $\pm$ 2.0	29.0 $\pm$ 1.3	>30	n.d.
46	>30	>30	>30	>30	>30	>30	n.d.
50	>30	>30	>30	>30	>30	>30	n.d.
51	>30	>30	>30	>30	>30	>30	n.d.
53	>30	>30	>30	>30	>30	>30	n.d.
54	29.3 $\pm$ 1.5	>30	28.9 $\pm$ 1.8	29.0 $\pm$ 1.7	>30	>30	n.d.

<sup>a</sup>Melanoma. <sup>b</sup>Colon cancer. <sup>c</sup>Breast cancer. <sup>d</sup>Ovarian cancer <sup>e</sup>Mouse fibroblasts <sup>f</sup>Cervical cancer. <sup>g</sup>Human embryonic kidney cancer. <sup>h</sup>The assay was performed in triplicate. Standard deviations are displayed if applicable.

Table 6 summarizes the solubilities and cLogP values for the compounds synthesized. Introduction of thiomorpholine lowers the solubility of the compounds in PBS buffer by factor 2 to 3. This may be attributed to the lower electronegativity of the sulfur atom in comparison to oxygen, which reduces the polarity within the molecule. A strong improvement in solubility is observed when thiomorpholine sulfoxides are present. For instance, the solubility of **15** is approximately 5 times higher than the solubility of the hit compound MMV688845. The improvement is not as prominent when thiomorpholine is oxidized to the respective sulfone (e.g., **20**, **24**, **28**). In this case, a 2-fold increase in solubility was observed in comparison to their respective thioethers. The difference in solubility between sulfoxides and sulfones can be explained by the fact that sulfoxide itself is asymmetric since the free electron pair of the sulfur atom is still present. This provides a strong dipole moment to the molecule and increases its polarity. It should be noted that cLogP values are not a good predictor for the high difference in solubility of sulfones and sulfoxides since the cLogP values only differ by a value of 0.05. The results show that the highest increase in solubility is achieved by introduction of the sulfoxide group.

The aqueous solubility can otherwise be increased when R<sup>1</sup> is exchanged for a polar *p*-hydroxyphenyl group. This resulted in a doubling of the solubility of thiomorpholine containing compounds (**11**/37  $\mu\text{M}$  to **36**/78  $\mu\text{M}$ ; **12**/31  $\mu\text{M}$  to **37**/58  $\mu\text{M}$ ). This is also the case for their respective sulfone derivatives (**36**/78  $\mu\text{M}$  to **39**/170  $\mu\text{M}$ ; **37**/58  $\mu\text{M}$  to **40**/158  $\mu\text{M}$ ).

In summary, based on a straightforward synthetic route, systematic derivatization made it possible to obtain an overview

of the influence of the different substituents on the antimycobacterial activity of AAPs and hence important structure–activity relationship information as summarized in Scheme 6.

### 3. CONCLUSIONS

We have shown that synthetic RNAP inhibitors derived from MMV688845 have the potential to reach *in vitro* MIC<sub>90</sub> values of below 1  $\mu\text{M}$  against pathogenic mycobacteria, e.g., *Mtb* and *Mabs*. In addition to the improved activity against mycobacteria and the absence of cytotoxicity, the new analogs display bactericidal activity (99% CFU reduction) against *Mabs* at concentrations below 10  $\mu\text{M}$ . Compounds **20** and **15** achieved MBC<sub>99</sub> at 2X MIC<sub>90</sub>, giving them higher cidal activity than MMV688845 (MBC<sub>99</sub> at 8X MIC<sub>90</sub>). Systematic derivatization based on a straightforward synthetic route made it possible to obtain important structure–activity relationship information. It is worth noting that the oxidized thiomorpholine derivatives, sulfoxide and sulfone, result in an increase in activity in comparison to MMV688845 reaching submicromolar activities against *Msmeg*, *Mintra*, and even *Mabs*. Sulfones show higher activities than sulfoxides across the board. Sulfoxides are interesting for further research because of their higher aqueous solubility. The data show that anti-*Mabs* targeting of MMV688845 is possible and that attractive MIC values can be achieved with this compound class, warranting further preclinical investigation. Since MMV688845 analogs do not exhibit cross-resistance with rifamycin-resistant mycobacteria, further investigation is of scientific interest to develop an RNAP inhibitor that is effective against these resistant pathogens.

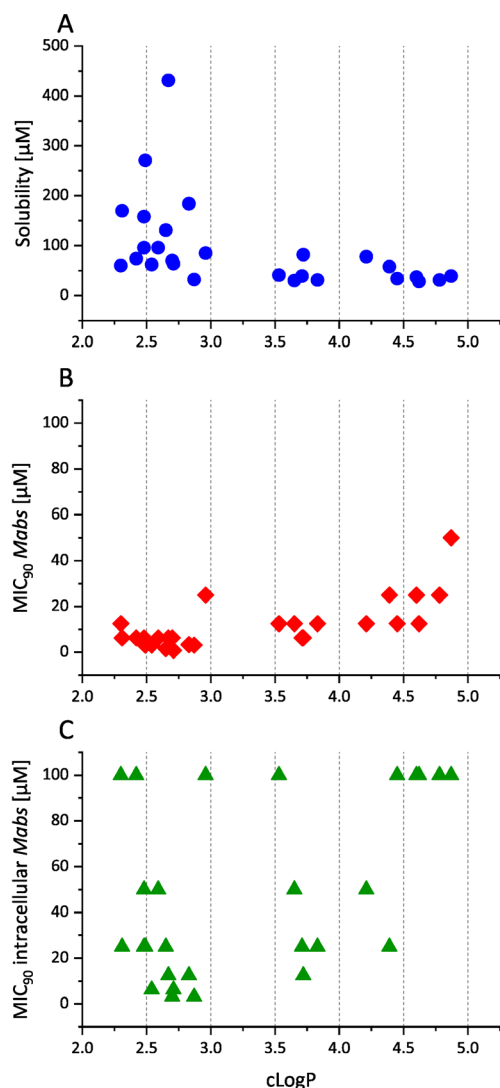


**Figure 9.** Relationship of cLogP values and their corresponding kinetic solubilities of all the synthesized AAP analogs (A). Relationship of cLogP values and their corresponding MIC<sub>90</sub> values against *Mabs* of all the synthesized AAP analogs (B). Relationship of cLogP values and their corresponding MIC<sub>90</sub> values against *Mabs* within the macrophage infection model of all the synthesized AAP analogs (C). The cLogP values were calculated with ChemDraw (Perkin Elmer Informatics Inc.).

Particular attention should be paid to NTM, such as *Mabs*, as there are species-dependent differences in the structure–activity relationships, as shown in this study. In addition to further derivatization with the aim of increasing activity, the investigation of hepatic metabolism, pharmacokinetics, and activity of MMV688845 derivatives *in vitro* and *in vivo* should be addressed. In this study, it was possible to show that compound **24** has an improved stability against mouse plasma *in vitro* than the hit compound MMV688845, but the very rapid degradation by liver microsomes is a drawback of the compound class.

Elucidation of the hepatic metabolism of phenylalanine amides is desirable in future research, as this should help developing analogs with improved hepatic stability.

#### 4. MATERIALS AND METHODS

**4.1. General.** Starting materials were purchased and used as received. Solvents used for either synthetic or purification purposes were distilled and stored over 4 Å molecular sieves. Glassware was oven-dried at 110 °C prior to use. For the determination of *R<sub>f</sub>* values and other analytical purposes such as qualitative chromatography, Merck TLC silica gel 60 on aluminum sheets with fluorescent indicator F254 were used. Flash chromatography was performed with a puriFlash 430 instrument (Interchim, Montluçon, France). Columns were packed in either 8 g (*v* = 10 mL/min), 45 g (*v* = 30 mL/min), or 90 g (*v* = 40 mL/min) cartridges with 40–63 µm normal phase silica gel produced by Carl Roth. Column loading was performed with the dry load method. NMR spectra were recorded on an Agilent Technologies VNMRs 400 MHz spectrometer. Chemical shifts are reported relative to the residual solvent signal (CDCl<sub>3</sub>: δ<sub>H</sub> = 7.26 ppm; δ<sub>C</sub> = 77.36 ppm; CD<sub>3</sub>OD δ<sub>H</sub> = 3.31 ppm). <sup>13</sup>C NMR spectral data were generally determined as attached-proton-test spectra (APT). Spectra have been cut, baseline and phase corrected, and analyzed utilizing MestreNova 11.0 software (Mestrelab Research, S.L., Spain). APCI-MS (atmospheric pressure chemical ionization) was performed using an expression CMS mass spectrometer (Advion Inc., Ithaca, NY, USA), with both ASAP (atmospheric solids analysis probe) sampling and with the help of the Plate Express TLC-plate extractor. ESI measurements have been conducted on the same expression CMS mass spectrometer with an ESI ionization module and direct injection sampling. HRMS was carried out using an LTQ Orbitrap XL mass spectrometer (Thermo Fisher Scientific Inc., Waltham, MA, USA).

**4.2. HPLC.** All described final compounds were confirmed to be of >95% purity. Purity was measured by UV absorbance at 254 nm. The HPLC apparatus consists of an XTerra RP18 column (3.5 µm, 3.9 mm × 100 mm) from the manufacturer Waters (Milford, MA, USA) and two LC-10 AD pumps, a SPD-M10A VP PDA detector, and a SIL-HT autosampler, all from the manufacturer Shimadzu (Kyoto, Japan).

Compounds used for stereochemical analyses (Boc-Phe-(R); **1**-(R), **2A**-(R), and **2B**-(R); Boc-Phe-(S); **1**-(S), **2A**-(S), and **2B**-(S); Boc-Phe-(rac); **1**-(rac), **2A**-(rac), and **2B**-(rac)) were checked for purity using an Agilent 1260 HPLC instrument equipped with UV diode array detector (50 mm Eclipse Plus C18 1.8 µm, i.d. 4.6 mm, *v* = 1.0 mL min<sup>-1</sup>, λ<sub>used</sub> = 220 nm). Elution systems: [Boc-Phe-(R); Boc-Phe-(S); Boc-Phe-(rac): acetonitrile/water 35:65; 0.1% v/v TFA]; [**1**-(R); **1**-(S); **1**-(rac): acetonitrile/water 55:45]; [**2A**-(R); **2A**-(S); **2A**-(rac): methanol/water 20 mM NH<sub>4</sub>HCO<sub>3</sub> pH 9 55:45]; [**2B**-(R); **2B**-(S); **2B**-(rac): acetonitrile/water 45:55].

For preparative tasks, an XTerra RP18 column (7 µm, 19 mm × 150 mm) manufactured by Waters (Milford, MA, USA) and two LC-20 AD pumps (Shimadzu, Kyoto, Japan) were used. The mobile phase was in all cases a gradient of methanol/water (starting at 95% v/v water to 5% v/v water) with 0.05% v/v TFA added.

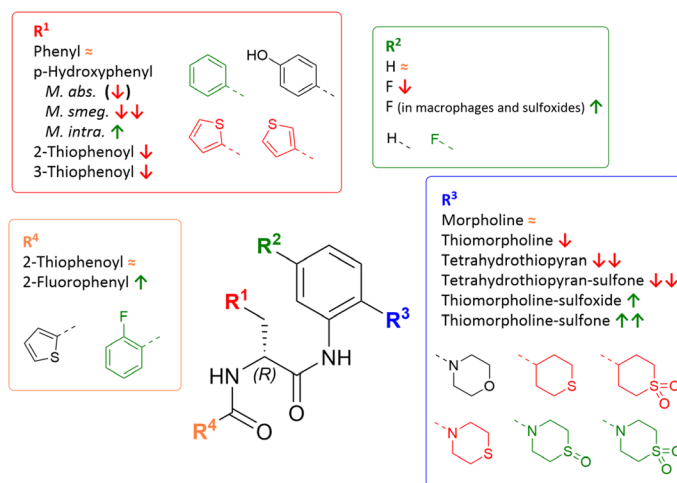
The determination of *ee*-values was conducted using a Shimadzu Prominence LC-20A HPLC instrument with diode array detection (*v* = 1.0 mL min<sup>-1</sup>, λ<sub>used</sub> = 220 nm). The utilized elution systems and chiral columns differ according to the structure that had to be analyzed: [Boc-Phe-(R); Boc-Phe-(S); Boc-Phe-(rac): 150 mm Chiralpak IA-3, 4.6 mm i.d.; acetonitrile/water 30:70; 0.1% v/v TFA]; [**1**-(R); **1**-(S); **1**-(rac): 150 mm Chiralpak IB N-3, 4.6 mm i.d.; acetonitrile/water 55:45]; [**2A**-(R); **2A**-(S); **2A**-(rac): 150 mm Chiralpak IG-3, 4.6 mm i.d.; *n*-heptane/*iso*-propanol 90:10]; [**2B**-(R); **2B**-(S); **2B**-(rac): 150 mm Chiralcel OJ-3R, 4.6 mm i.d.; acetonitrile/water 40:60].

**4.3. X-ray Crystallography.** Details of the X-ray intensity data collections, structure solutions and refinements, and hydrogen bond parameters can be found in the Supporting Information. X-ray crystallography structures have been determined for compounds **6**, **14**, and **20**. CCDC 2231845–2231847 contains the supplementary crystallographic data for this paper. The data can be obtained free of

Table 6. Kinetic Solubilities and cLogP Values of MMV688845 (abbr. MMV845) and All Synthesized AAP Derivatives<sup>a</sup>

	MMV845	6	7	11	12	14	15
Solubility [ $\mu\text{M}$ ]	82	34	28	37	31	271	431
cLogP	3.72	4.45	4.62	4.6	4.78	2.49	2.67
	17	18	20	24	28	29	32
Solubility [ $\mu\text{M}$ ]	131	184	62	64	70	32	39
cLogP	2.65	2.83	2.54	2.71	2.7	2.87	4.87
	34	36	37	39	40	42	43
Solubility [ $\mu\text{M}$ ]	85	78	58	170	158	30	31
cLogP	2.96	4.21	4.39	2.31	2.48	3.65	3.83
	45	46	50	51	53	54	
Solubility [ $\mu\text{M}$ ]	41	39	74	96	60	96	
cLogP	3.53	3.71	2.42	2.59	2.3	2.48	

<sup>a</sup>Color coding: the colors show the difference to the average kinetic solubility of all tested compounds, dark blue: highest solubility, light blue: above average, white: closest to average, light red: below average, dark red: lowest kinetic solubilities of the tested compound set.

Scheme 6. Overview of the Influence of the Different Substituents on the Antimycobacterial Activity of AAPs<sup>a</sup>

<sup>a</sup>Red arrows indicate a loss in activity; green arrows indicate an increased activity caused by the respective residues.

charge from the Cambridge Crystallographic Data Centre via [www.ccdc.cam.ac.uk/structures](http://www.ccdc.cam.ac.uk/structures).

**4.4. General Procedure A—Amide Coupling T3P.** A solution of the Boc-protected  $\alpha$ -amino acid (1.1 equiv) and the aniline (1 equiv) in a 1:2 mixture of pyridine (distilled) and EtOAc (distilled) was cooled to  $-20\text{ }^{\circ}\text{C}$  with an isopropanol/dry ice bath. If the compounds did not dissolve completely at  $-20\text{ }^{\circ}\text{C}$ , additional pyridine/EtOAc mixture was added until complete dissolution. A 50% m/v solution of T3P in EtOAc (2 equiv) was added to the mixture subsequently. After 10 min, the dry ice bath was removed and replaced by an ice/water bath to keep the temperature at  $0\text{ }^{\circ}\text{C}$  overnight.<sup>46</sup> Afterward, a reasonable amount of EtOAc was added to the reaction mixture to wash it with 0.25 M  $\text{KH}_2\text{PO}_4$  solution three times in a separation funnel. The organic phase was collected and dried with  $\text{Na}_2\text{SO}_4$ , and the solvent was removed under reduced pressure. As a general purification procedure, flash chromatography was performed with varying gradient eluting systems on 40–63  $\mu\text{m}$  normal phase silica gel (see respective synthesis documentation in the [Supporting Information](#)).

**4.5. General Procedure B—Amide Coupling DEPBT.** The formation of the anilide bond (general procedure A) was followed by the cleavage of the Boc-protecting group using TFA. For this purpose,

the purified Boc- $\alpha$ -amino anilides were dissolved in DCM and an equal volume of TFA was added under stirring. The solution was stirred for 30 min at room temperature and checked for the complete Boc-cleavage using thin-layer chromatography (TLC). The DCM/TFA mixture was removed under reduced pressure after complete conversion. The crude product was redissolved in EtOAc and washed with saturated  $\text{NaHCO}_3$  solution three times. The organic phase was collected, and the solvents were evaporated under reduced pressure.

The formation of the second amide bond was achieved with the coupling reagent DEPBT. For this synthetic step, the Boc-deprotected amino acid was dissolved in THF with the respective aromatic carboxylic acid and DEPBT. After complete dissolution, DIPEA was added, and the solution was stirred overnight at room temperature. Afterward, the reaction mixture was washed successively once with 0.25 M  $\text{KH}_2\text{PO}_4$ , water, saturated  $\text{NaHCO}_3$ , water, and brine. The organic phase was dried with  $\text{Na}_2\text{SO}_4$ , and the solvents were removed under reduced pressure. For purification, a flash chromatography was performed with varying gradient eluting systems on 40–63  $\mu\text{m}$  normal phase silica gel (see respective synthesis documentation in the [Supporting Information](#)).

**4.6. General Procedure C—Nucleophilic Substitution of Thiomorpholine.** 1-Bromo-2-nitrobenzene or the respective deriva-

tives were dissolved in thiomorpholine without addition of solvents in a small glass flask. The mixture was heated to 120 °C and stirred for 2 h. After cooling down to room temperature, the precipitated solid was filtered out, the filter was washed thoroughly with DCM, and the solid was discarded. DCM was evaporated under reduced pressure to obtain the bright-orange oily crude products. For purification, flash chromatography was performed with varying gradient eluting systems on 40–63  $\mu\text{m}$  normal phase silica gel (see respective synthesis documentation in the Supporting Information).

**4.7. General Procedure D—Reduction of 4-(2-Nitrophenyl)thiomorpholines.** 4-(4- $R^2$ -2-Nitro-phenyl)thiomorpholines were dissolved in ethanol. One third of the total amount of palladium 10% m/m on active charcoal was added, and the mixture was then heated to 50 °C and stirred vigorously. A 50% v/v solution of hydrazine in water was added very slowly. The remaining amount of catalyst was added to the mixture in portions. Afterward, the temperature was increased to 90 °C and the mixture was refluxed for 30 min. The bright orange-yellow solution turned to a clear and colorless solution. The mixture was cooled down to room temperature and filtered to remove the catalyst. The filter was washed thoroughly with ethanol to extract residual product. Completion of the reaction and purity were checked with TLC. Solvents were then removed under reduced pressure. The crude product was used for the next synthesis without further purification when applicable (for exceptions see respective synthesis documentation in the Supporting Information).

**4.8. General Procedure E—Oxidation of Thiomorpholines to Sulfoxides.** Sodium periodate was dissolved in water and cooled to 0 °C. 4-(4- $R^2$ -2-Nitro-phenyl)thiomorpholines or their respective Boc-amino acid coupled derivatives were dissolved in methanol. This solution was then added to sodium periodate solution under stirring. If a precipitate formed, acetonitrile was added until full dissolution occurred. The mixture was then stirred at 0 °C for 4 h, before it was stored in the fridge for three days. Subsequently, the mixture was extracted with DCM three times. The organic phases were collected, and the solvents were evaporated under reduced pressure. For purification, flash chromatography was performed with varying gradient eluting systems on 40–63  $\mu\text{m}$  normal phase silica gel (see respective synthesis documentation).

**4.9. General Procedure F—Oxidation of Thiomorpholines to Sulfones.** 4-(4- $R^2$ -2-Nitro-phenyl)thiomorpholines or their respective Boc-amino acid coupled derivatives were dissolved in DCM. The mixture was cooled to 0 °C before a solution of *m*-chloroperbenzoic acid in DCM was added over 30 min with a syringe. The reaction mixture was stirred overnight at room temperature. After completion of the reaction, the mixture was washed three times with saturated  $\text{NaHCO}_3$  solution. The organic phase was collected, the solvent was evaporated under reduced pressure, and a dryload was prepared for purification with flash chromatography (see respective synthesis documentation).

**4.10. General Procedure G—Nucleophilic Substitution of Thiomorpholinedioxides.** 1-Bromo-2-nitrobenzene and thiomorpholinedioxide were dissolved in dioxane. Then, palladium(II) acetate, BINAP, and  $\text{Cs}_2\text{CO}_3$  were added. The mixture was then ultrasonically degassed; the flask was flushed with argon and then refluxed at 100 °C overnight. After the reaction mixture had cooled down to room temperature, it was filtered through Celite and the filter was washed thoroughly with EtOAc. The solvents were evaporated under reduced pressure. For purification, flash chromatography utilizing an EtOAc/heptane gradient was used (see respective synthesis documentation).

**4.11. General Procedure H—C-C Coupling of 4-Oxothiane and Boc-2-aminophenylboronic Acid Pinacol Ester.** 4-Oxothiane was added to a solution of *p*-toluenesulfonylhydrazide in methanol. The reaction mixture was stirred at room temperature for 1 h and was then monitored until full conversion using TLC. The solvent was removed under reduced pressure, and the crude product was used in the next step without further purification.

The sulfonylhydrazone formed in the first step, Boc-2-aminophenylboronic acid pinacol ester, and cesium carbonate were added to a three-necked Schlenk flask attached to a condenser. The apparatus was put under vacuum and backfilled with argon three times, while the

mixture of solids was stirred with a magnetic stirrer. Dry and ultrasonic-degassed dioxane was added through a septum with a syringe before the reaction was heated to 110 °C for 18 h. After cooling to room temperature, the reaction was quenched with saturated  $\text{NaHCO}_3$  solution. The mixture was then extracted with DCM three times. Solvents were removed under reduced pressure, and the crude product was prepared for purification with flash chromatography.

The purified product was then dissolved in DCM, and an equal volume of TFA was added under stirring. The solution was stirred for 30 min at room temperature and checked for the complete Boc-cleavage by TLC. The DCM/TFA mixture was removed under reduced pressure after complete conversion. The crude product was reconstituted in EtOAc and washed with saturated  $\text{NaHCO}_3$  solution three times. The organic phase was collected, and solvents were evaporated under reduced pressure. The crude product was used for the subsequent reactions without further purification.

**4.12. Microbiological Assays.** 4.12.1. *Bacteria and Culture Media.* *M. smegmatis* mc<sup>2</sup> 155 pTEC27, *M. intracellulare* ATCC 35761 pTEC27, and *M. abscessus* ATCC 19977 pTEC27 expressing tomato RFP were used for the activity assays. Stocks of the bacteria grown in Middlebrook 7H9 medium +10% v/v ADS +0.05% v/v polysorbate 80 + 400  $\mu\text{g}/\text{mL}$  hygromycin were stored in approximately 15% v/v glycerol at –80 °C. Using an inoculation loop, bacteria were streaked on 7H10 agar plates (containing hygromycin 400  $\mu\text{g}/\text{mL}$ ) and grown for five days in an incubator at 37 °C.

Bacteria were grown in complete 7H9 broth supplemented with 10% v/v ADS and 0.05% v/v polysorbate 80, respectively, in MHII broth supplemented with 0.05% v/v polysorbate 80. The culture volume was 10 mL in a 50 mL Falcon tube. The tubes were covered to protect the photosensitive hygromycin and shaken in an incubator at 37 °C. Solid cultures were grown on a 7H10 medium supplemented with 0.5% v/v glycerol and 10% v/v ADS containing 400  $\mu\text{g}/\text{mL}$  hygromycin.

*M. abscessus* Bamboo was isolated from the sputum of a patient with amyotrophic lateral sclerosis and bronchiectasis and was provided by Wei Chang Huang, Taichung Veterans General Hospital, Taichung, Taiwan. *M. abscessus* Bamboo whole-genome sequencing showed that the strain belongs to *M. abscessus* subsp. *abscessus* and harbors an inactive clarithromycin-sensitive erm41 C28 sequevar. *M. tuberculosis* H37Rv (ATCC 27294) was obtained from the American Type Culture Collection.

For general bacteria culturing and certain MIC experiments, Middlebrook 7H9 broth (BD Difco) was supplemented with 0.5% m/v albumin, 0.2% m/v glucose, 0.085% m/v sodium chloride, 0.0003% m/v catalase, 0.2% v/v glycerol, and 0.05% v/v polysorbate 80. Unless otherwise stated, solid cultures were grown on Middlebrook 7H10 agar (BD Difco) supplemented with 0.5% m/v albumin, 0.2% m/v glucose, 0.085% m/v sodium chloride, 0.5% v/v glycerol, 0.0003% m/v catalase, and 0.006% v/v oleic acid. All drugs were prepared as 10 mM stocks in dimethyl sulfoxide (DMSO).

4.12.2. *THP-1 Cells and Culture Media.* THP-1 cells were put in 90% v/v FBS + 10% v/v DMSO and stored in liquid nitrogen. THP-1 cells were grown in a complete RPMI medium. The cells were grown in a tissue culture flask with a minimum volume of 30 mL and a maximum volume of 40 mL and were incubated in an atmosphere of 95% air and 5% carbon dioxide ( $\text{CO}_2$ ) at a temperature of 37 °C. The cell density was kept between 0.25 million and 1 million cells/mL. Every two or three days, the cells were counted and diluted to 0.25 million cells/mL. The cells doubled every 48 h. A culture from nitrogen stock could be subcultured for up to three months; after this time, a change in morphology and growth behavior was observed. For culturing of THP-1 cells, the RPMI 1640 medium supplemented with 5% v/v fetal bovine serum (FBS), 2% m/v glutamine, and 1% v/v nonessential amino acids.

4.12.3. *MIC Determination against M. smegmatis mc<sup>2</sup> 155 pTEC27, M. intracellulare ATCC 35761 pTEC27, and M. abscessus ATCC 19977 pTEC27.* MIC values were determined by the broth microdilution method. 96-well flat bottom tissue culture plates (Sarstedt, 83.3924.500) were used.<sup>73</sup> In the third well of each column two times the desired highest concentration of each compound was added in the respective assay medium. Each compound was diluted 2-fold in a nine-point serial dilution. The concentration of the starting

inoculum was  $5 \times 10^5$  cells/mL. The starting inoculum was diluted from a preculture at the mid-log phase ( $OD_{600}$ , 0.3 to 0.7), and an  $OD_{600}$  of 0.1 was correlated to  $1 \times 10^8$  CFU/mL. The plates were sealed with Parafilm, placed in a container with moist tissue, and incubated for three days at 37 °C (*M. smegmatis* and *M. abscessus*) or five days (*M. intracellulare*). Each plate had eight negative controls (1% v/v dimethyl sulfoxide) and eight positive controls (100  $\mu$ M amikacin). After incubation, the plates were monitored by OD measurement at 550 nm (BMG labtech Fluostar Optima) and by measurement of fluorescence ( $\lambda_{ex}$  = 544 nm,  $\lambda_{em}$  = 590 nm). The assay was performed in duplicate, and the results were averaged.

**4.12.3.1. Data Analysis.** Every assay plate contained eight wells with dimethyl sulfoxide (1% v/v) as a negative control, which corresponds to 100% bacterial growth and eight wells with amikacin (100  $\mu$ M) as a positive control in which 100% inhibition of bacterial growth was reached. Controls were used to monitor the assay quality through determination of the  $Z'$  score. The  $Z'$  factor was calculated as follows:

$$Z' = 1 - \frac{3(SD_{\text{amikacin}} + SD_{\text{DMSO}})}{|M_{\text{amikacin}} - M_{\text{DMSO}}|}$$

where SD is standard deviation and  $M$  is mean.

The percentage of growth inhibition was calculated by the equation:

$$\% \text{growth inhibition} = -100\% \times \frac{\text{signal}_{\text{sample}} - \text{signal}_{\text{DMSO}}}{\text{signal}_{\text{DMSO}} - \text{signal}_{\text{amikacin}}}$$

**4.12.4. MIC Determination against *M. abscessus* Bamboo.** MIC value determination by optical density at 600 nm [ $OD_{600}$ ] was carried out in 96-well plate format. 96-well plates were initially set up with 100  $\mu$ L of 7H9 per well. For each compound, a 10-point 2-fold dilution series starting at twice the desired highest concentration was dispensed onto the 96-well plates using a Tecan D300e Digital Dispenser, with the DMSO concentration normalized to 2% v/v. A bacteria culture grown to mid-log-phase ( $OD_{600}$ , 0.4 to 0.6) was diluted to  $OD_{600} = 0.1$  ( $1 \times 10^7$  CFU/mL). The resulting bacteria suspension (100  $\mu$ L) was dispensed onto the 96-well plates containing the sample compounds to give a final volume of 200  $\mu$ L per well with an initial  $OD_{600} = 0.05$  ( $5 \times 10^6$  CFU/mL) and a final DMSO concentration of 1% v/v. Final compound concentration ranges were typically 50–0.098  $\mu$ M or 6.25–0.012  $\mu$ M. Untreated control wells, which contained bacteria suspension and 1% v/v DMSO, were included on each plate. Plates were sealed with Parafilm, stored in boxes with wet paper towels, and incubated at 37 °C with shaking (110 rpm) for three days.

To determine growth,  $OD_{600}$  was measured using a Tecan Infinite M200 plate reader on day 0 and day 3. Two biological replicates were performed. Clarithromycin was included in each experiment as a positive control. For each well on the 96-well plate, bacterial growth was calculated by subtracting the day 0  $OD_{600}$  value from the day 3  $OD_{600}$  value. For each compound series, the bacterial growth values for the untreated control wells were averaged to give the average drug-free bacterial growth. For compound-containing wells, percentage growth was calculated by dividing their growth values by the average drug-free bacterial growth for the compound series and multiplying by 100. For each compound series, we plotted percentage growth versus compound concentration. By visual inspection of the dose–response curve, we determined the MIC of a compound as the compound concentrations that would result in 90% growth inhibition. The MIC determination was performed two times with different starter cultures. The MIC values shown in this article are the averaged results of biological duplicates.

**4.12.5. MIC Determination against *M. tuberculosis* H37Rv.** MICs were determined as described previously with slight modifications.<sup>74</sup> Briefly, compounds were serially diluted in flat-bottom 96-well plates, and a mid-log-phase culture was mixed with the compound-containing broth (final  $OD_{600} = 0.05$ ). Plates were sealed with a Breathe-Easy sealing membrane (Sigma), placed in humidified plastic boxes, and incubated at 37 °C for seven days, shaking at 80 rpm. Growth was monitored by measuring turbidity at 600 nm using a Tecan Infinite 200 Pro microplate reader (Tecan).  $MIC_{90}$  values were deduced from the

generated dose–response curves. The MIC values shown in the script are the averaged results of the two biological replicates.

**4.12.6. MIC Determination in the Macrophage Infection Model.** For the infection assay, an *M. abscessus* pTEC27 culture ( $OD$ , 0.2–0.8, mid-log phase) was centrifuged (4000 rpm, RT, 10 min), washed with 7H9 medium with 0.05% v/v polysorbate 80 (about 10 mL), and vortexed. After a second centrifugation (4000 rpm, RT, 10 min), the 7H9 medium was replaced by the RPMI medium (the same volume or a little less to concentrate the bacteria), vortexed, and incubated at RT for 5 min. After incubation, the bacterial suspension was filtered through a 5  $\mu$ M pore-size filter to remove the clumps. The  $OD_{600}$  was determined after filtration ( $OD = 0.1$  corresponds to  $1 \times 10^8$  CFU/mL). The appropriate number of bacteria was incubated in the presence of 10% v/v human serum at 37 °C for 30 min for opsonization. A cell suspension of THP-1 cells ( $1 \times 10^6$  cells/mL) in the RPMI incomplete medium was incubated with the opsonized *M. abscessus* single-cell suspension (MOI, 5:1) and PMA (40 ng/mL) for 4 h at 37 °C under constant agitation. After infection, the THP-1 cell suspension was centrifuged (750 rpm, RT, 10 min) and washed with the RPMI medium. A 10-point 2-fold serial dilution of each compound was then prepared in 96-well flat bottom plates that had been tissue culture treated (Sarstedt, 3924). Column one of the 96-well plate included eight negative controls (1% v/v DMSO) and column two eight positive controls (1.5  $\mu$ M bedaquiline). The plates were then inoculated with the infected cells ( $1 \times 10^5$  THP-1 cells/well), sealed with Parafilm, and incubated for four days (37 °C, 5%  $CO_2$ ). After incubation, the cells were fixed with paraformaldehyde (PFA; 4% m/v in PBS) for 30 min. After removal of the PFA, the cells were stained with DAPI readymade solution (Sigma, MBD0015). The plates were washed twice with the RPMI medium. Image acquisition (DAPI 386–23 nm, RFP 560–25 nm, brightfield) and analysis were done with a CellInsight CXS (ThermoFisher). The mean CircSpotAvgArea of the RFP channel was used for calculations of growth inhibition.

MIC values were determined against *M. abscessus* ATCC 19977 pTEC27 by the microdilution method in RPMI incomplete media (RPMI 1640 medium supplemented with 5% v/v FBS, 1% m/v glutamine, and 1% v/v nonessential amino acids) with 70  $\mu$ M amikacin in the assay medium. A 10-point 2-fold serial dilution of each compound was prepared in 96-well flat bottom plates that had been tissue culture treated (Sarstedt, 3924). Column one of the 96-well plate included eight negative controls (1% v/v DMSO) and column two eight positive controls (1.5  $\mu$ M bedaquiline).

**4.12.6.1. Data Analysis.** Every assay plate contained eight wells with DMSO (1% v/v) as a negative control, which correspond to 100% bacterial growth, and eight wells with bedaquiline (1.5  $\mu$ M) as a positive control, in which 100% inhibition of bacterial growth was reached. The controls were used to monitor assay quality through determination of the  $Z$ -score and for normalizing the data on a plate basis. The  $Z$ -factor was determined using the following equation:

$$Z' = 1 - \frac{3(SD_{\text{bedaquiline}} + SD_{\text{DMSO}})}{|M_{\text{bedaquiline}} - M_{\text{DMSO}}|}$$

where SD is standard deviation and  $M$  is mean.

Percent inhibition was calculated as follows:

$$\% \text{growth inhibition} = -100\% \times \frac{\text{signal}_{\text{sample}} - \text{signal}_{\text{DMSO}}}{\text{signal}_{\text{DMSO}} - \text{signal}_{\text{bedaquiline}}}$$

**4.12.7. MBC Determination against *M. abscessus* ATCC 19977 pTEC27.** For MBC determination, *M. abscessus* ATCC19977 was incubated in a microplate dilution assay for four days as described above. Subsequently, the MBC was determined by CFU counting: for this purpose, 6-well plates were used, each filled with 4 mL 7H10 agar supplemented with 0.5% v/v glycerol, 10% v/v ADS, and 400  $\mu$ g/mL hygromycin. From the drug concentrations where growth inhibition was detected in the microplate dilution assay, 10  $\mu$ L (undiluted or diluted 1:100) were plated into one well of the 6-well plates. The colonies were counted after four days of incubation at 37 °C, and the experiment was carried out in triplicate. Based on the result, the

concentration of CFUs per mL was calculated. The number of CFUs was also determined in the inoculum prior to the four-day incubation.

**4.13. Plasma Stability.** Plasma stability in human and murine plasma was determined at five different time points over 120 min using HPLC-MS/MS analytic. Pooled human plasma, anticoagulated with trisodium citrate, and nonsterile murine plasma, anticoagulated with Li-heparin, were used. The plasma stability is given as the percentage of substance remaining in plasma over time. All measurements were performed using the Shimadzu Prominence HPLC system including a vacuum degasser, gradient pumps, reverse phase column (ZORBAX Extend-C18 column, 2.1x50 mm, 5  $\mu$ m), column oven, and autosampler. The HPLC system was coupled with tandem mass API 3000 (AB Sciex). Both positive and negative ion modes of the TurboIonSpray ion source were used. Acquisition and analysis of the data were performed using Analyst 1.6.3 software (PE Sciex).

Incubations of every compound + references (verapamil and propantheline bromide) were carried out in five aliquots of 60  $\mu$ L each (one for each time point), in duplicates. Plasma was spiked with test compounds from a 10 mM DMSO stock solution to yield a test concentration of 1  $\mu$ M, final DMSO concentration 1% v/v. The aliquots were incubated at 37 °C with shaking at 100 rpm. Five time points over 120 min were analyzed. The reactions were stopped by adding 300  $\mu$ L of methanol containing the internal standard with subsequent plasma proteins sedimentation by centrifuging at 6000 rpm for 4 min. Supernatants were analyzed by the HPLC system that was coupled with a tandem mass spectrometer. The percentage of the test compounds remaining after incubation in plasma and their half-lives ( $t_{1/2}$ ) were calculated.

**4.14. Microsomal Stability.** Microsomal stability was determined at five different time points over 40 min using HPLC-MS/MS analytic. Pooled, mixed gender human liver microsomes (XenoTech, H0630/lot N#2010065) and murine liver microsomes (pooled, male BALB/c mice, XenoTech, M3000/lot #1810163) were used.

Microsomal incubations were carried out in 96-well plates in five aliquots of 30  $\mu$ L each (one for each time point). The liver microsomal incubation medium composed of phosphate buffer (100 mM, pH 7.4), MgCl<sub>2</sub> (3.3 mM), NADPH (3 mM), glucose-6-phosphate (5.3 mM), and glucose-6-phosphate dehydrogenase (0.67 units/mL) with 0.42 mg of liver microsomal protein per mL. In the control reactions, the NADPH-cofactor system was substituted with phosphate buffer. Test compounds (2  $\mu$ M, final solvent concentration 1.6% v/v) were incubated with microsomes at 37 °C, shaking at 100 rpm. Five time points over 40 min were analyzed. The reactions were stopped by adding five volumes of 90% v/v acetonitrile with the internal standard to incubation aliquots, followed by protein sedimentation by centrifuging at 5500 rpm for 3 min. Each reaction was performed in duplicates.

Analysis of supernatants was performed using a Shimadzu HPLC system including a vacuum degasser, gradient pumps, reverse phase HPLC column, column oven, and autosampler. Mass spectrometric analysis was performed using an API 3000 mass spectrometer from Applied Biosystems/MDS Sciex (AB Sciex) with a Turbo V ion source and TurboIonSpray interface. The TurboIonSpray ion source was used in both positive and negative ion modes. The data acquisition and system control were performed using Analyst 1.6.3 software from AB Sciex.

The microsomal stability is presented as the substances half-life times and intrinsic clearance calculated from their respective elimination constants with the following formula:

$$k_{el} = -\text{slope}$$

$$t_{1/2} = \frac{0.693}{k_{el}}$$

$$Cl_{int} = \frac{0.693}{t_{1/2}} \times \frac{\mu\text{L}_{incubation}}{\text{mg}_{microsomes}}$$

Eliminations constants were determined in an ln(AUC) versus time plot using linear regression analysis.

**4.15. Determination of Cytotoxicity.** Cytotoxicity was determined using a colorimetric microculture test with sulforhodamine-B (Kiton-Red S, ABCR) as the staining agent. Cells were transferred to a 96-well plate to treat them with increasing compound concentrations (1, 3, 7, 12, 20, and 30  $\mu$ M) after 24 h. DMSO/DMF concentrations never exceeded 0.5% v/v, which is nontoxic for the cells. The supernatant was discarded after 72 h; the cells were fixed with 10% v/v TFA and left to rest for 24 h at 4 °C. After washing the cells with a strip, washed cells were stained with a 10  $\mu$ M sulforhodamine-B solution (200  $\mu$ L) for 20 min before they were washed again with 1% v/v acetic acid solution to remove excess dye. Cells were air-dried overnight. Absorption was determined using a 96-well plate reader (Tecan spectra). Three-independent experiments in triplicate for each were conducted for the given compounds. The averaged data resulted in semilogarithmic dose–effect curves, which were fitted with the Hill equation (GraphPad Prism 5).

**4.16. Nephelometry Solubility Screen.** The solubilities of the final compounds were determined nephelometrically using a NEPHELOstar Plus (BMG Labtech GmbH, GER) device. Stock solutions (25 mM) in DMSO of the compounds were prediluted in pure DMSO. Then, 5  $\mu$ L of the predilutions were furtherly diluted in flat-bottom 96-well plates in 245  $\mu$ L of phosphate buffered saline (PBS) and mixed and measured immediately (2% v/v DMSO in measured sample). In this way, concentrations of 0.78, 1.56, 3.13, 6.25, 12.5, 25, 50, 100, 150, 200, 250, 300, 350, 400, 450, and 500  $\mu$ M were measured. The blank corrected raw data were interpreted with a segmental regression fit utilizing the Omega software (BMG Labtech GmbH, GER). Each compound was analyzed as a quadruplet prepared from the same stock solution.

## ■ ASSOCIATED CONTENT

### Supporting Information

The Supporting Information is available free of charge at <https://pubs.acs.org/doi/10.1021/acs.jmedchem.3c00009>.

Additional information on the molecular docking studies; 2D visualizations of 3D structures; experimental details of X-ray crystallography; sequence alignment details for *Mtb* and *Mabs* RNAP; antimycobacterial activity of all MMV688845 derivatives derived from OD measurements (not RFP measurements); chemical structures; synthetic protocols, molar equivalents of all reactants, purification procedures, and percentage yields for each synthetic experiment; TLC  $R_f$  values for all synthesized compounds, <sup>1</sup>H-NMR spectra for all synthesized compounds, and respective written documentation; APT-NMR spectra for all *in vitro* tested compounds and respective written documentation; HPLC-purity and respective HPLC traces for all *in vitro* tested; atmospheric pressure chemical ionization mass spectrometry data for all synthesized compounds; high-resolution mass spectrometry data for all *in vitro* tested compounds; molecular formula strings for all described substances; and PDB files for the presented crystal structures (PDF)

Smiles list, synthesis, and characterization of phenylalanine amides active against *Mycobacterium abscessus* and other mycobacteria (CSV)

Docking substance 14 (PDB)

Docking substance 20 (PDB)

Docking substance 39 (PDB)

Docking substance MMV688845 (PDB)

## ■ AUTHOR INFORMATION

### Corresponding Author

Adrian Richter – Institut für Pharmazie, Martin-Luther-Universität Halle-Wittenberg, Halle (Saale) 06120,

Germany; [orcid.org/0000-0002-0062-7896](https://orcid.org/0000-0002-0062-7896);  
Email: [adrian.richter@pharmazie.uni-halle.de](mailto:adrian.richter@pharmazie.uni-halle.de)

## Authors

Markus Lang – Institut für Pharmazie, Martin-Luther-Universität Halle-Wittenberg, Halle (Saale) 06120, Germany

Uday S. Ganapathy – Center for Discovery and Innovation, Hackensack Meridian Health, Nutley, New Jersey 07110, United States

Lea Mann – Institut für Pharmazie, Martin-Luther-Universität Halle-Wittenberg, Halle (Saale) 06120, Germany

Rana Abdelaziz – Institut für Pharmazie, Martin-Luther-Universität Halle-Wittenberg, Halle (Saale) 06120, Germany

Rüdiger W. Seidel – Institut für Pharmazie, Martin-Luther-Universität Halle-Wittenberg, Halle (Saale) 06120, Germany; [orcid.org/0000-0003-3438-4666](https://orcid.org/0000-0003-3438-4666)

Richard Goddard – Max-Planck-Institut für Kohlenforschung, Mülheim an der Ruhr 45470, Germany; [orcid.org/0000-0003-0357-3173](https://orcid.org/0000-0003-0357-3173)

Ilaria Sequenzia – Institut für Pharmazie, Martin-Luther-Universität Halle-Wittenberg, Halle (Saale) 06120, Germany

Sophie Hoenke – Institut für Chemie, Martin-Luther-Universität Halle-Wittenberg, Halle (Saale) 06120, Germany

Philipp Schulze – Max-Planck-Institut für Kohlenforschung, Mülheim an der Ruhr 45470, Germany

Wassihun Wedajo Aragaw – Center for Discovery and Innovation, Hackensack Meridian Health, Nutley, New Jersey 07110, United States

René Csuk – Institut für Chemie, Martin-Luther-Universität Halle-Wittenberg, Halle (Saale) 06120, Germany; [orcid.org/0000-0001-7911-290X](https://orcid.org/0000-0001-7911-290X)

Thomas Dick – Center for Discovery and Innovation, Hackensack Meridian Health, Nutley, New Jersey 07110, United States; Department of Medical Sciences, Hackensack Meridian School of Medicine, Nutley, New Jersey 07110, United States; Department of Microbiology and Immunology, Georgetown University, Washington, District of Columbia 20007, United States

Complete contact information is available at:  
<https://pubs.acs.org/10.1021/acs.jmedchem.3c00009>

## Funding

This work was funded by the Deutsche Forschungsgemeinschaft (DFG, German Research Foundation)—432291016 (to A.R.), the National Institute of Allergy and Infectious Diseases of the National Institutes of Health under award number R01AI132374, and Mukoviszidose Institut gGmbH (Bonn, Germany) project number 2202 (to A.R.), the research and development arm of the German Cystic Fibrosis Association Mukoviszidose e. V.

## Notes

The authors declare no competing financial interest.

## ACKNOWLEDGMENTS

We would like to thank Dr. Nadine Taudte and Dr. Jens-Ulrich Rahfeld for providing and maintaining the biosafety level 2 facility, Professor Christian W. Lehmann for providing access to the X-ray diffraction facility at the Max-Planck-Institut für Kohlenforschung (Mülheim an der Ruhr, Germany), Elke Dreher and Heike Schucht for technical assistance, Dr. Christian Ihling and Antje Herbrich-Peters for measuring the HRMS spectra, and Gudrun Hahn for specific rotation measurements.

We are grateful to Wei Chang Huang (Taichung Veterans General Hospital, Taichung, Taiwan) for providing *M. abscessus* Bamboo. Thanks are due to Dr. Dieter Ströhl for the NMR spectroscopy.

## ABBREVIATIONS

AAP, *N* $\alpha$ -aroyl-*N*-aryl-phenylalanine amide; ADP, adenosine diphosphate; APT, attached proton test; ATCC, American type culture collection; BINAP, (2,2'-bis(diphenylphosphino)-1,1'-binaphthyl); BLAST, Basic Local Alignment Search Tool; Boc, *tert*-butoxycarbonyl; CES, carboxylesterase; CFU, colony forming units; CLR, clarithromycin; cLogP, calculated logarithmic octanol–water partition coefficient; DCM, dichloromethane; DIPEA, *N,N*-diisopropylethylamine; DMF, dimethylformamide; DMSO, dimethylsulfoxide; *ee*-values, enantiomeric excess values; EtOAc, ethyl acetate; EtOH, ethanol; FBS, fetal bovine serum; LogP, logarithmic octanol–water partition coefficient; *Mabs*, *Mycobacterium abscessus*; MAC, *Mycobacterium avium* complex; MBC, minimum bactericidal concentration; *m*-CPBA, *m*-chloroperbenzoic acid; MDR, multidrug resistant; MHII, Miller-Hinton broth II; MIC, minimum inhibitory concentration; *Mintra*, *Mycobacterium intracellulare*; MMV, medicines for malaria ventures; MOI, multiplicity of infection; *Msmeg*, *Mycobacterium smegmatis*; *Mtb*, *Mycobacterium tuberculosis*; NTM, nontuberculous mycobacteria; OD, optical density; PBS, phosphate buffered saline; PFA, paraformaldehyde; PMA, phorbol-12-myristate-13-acetate; RFB, rifabutin; RFP, red fluorescent protein; RIF, rifampicin; RNAP, RNA polymerase; RT, room temperature; SAR, structure–activity relationship; T3P, *n*-propanephosphonic acid anhydride; TFA, trifluoroacetic acid; THF, tetrahydrofuran; TLC, thin-layer chromatography

## REFERENCES

- (1) World Health Organization. *Module 4: Treatment Drug-Susceptible Tuberculosis Treatment*; World Health Organization, 2022. <https://www.who.int/publications/i/item/9789240048126> (accessed 2023-02-21).
- (2) World Health Organization. *Global Tuberculosis Report 2022*; World Health Organization 2022. <https://www.who.int/publications/i/item/9789240061729> (accessed 2023-01-02).
- (3) Dartois, V. A.; Rubin, E. J. Anti-Tuberculosis Treatment Strategies and Drug Development: Challenges and Priorities. *Nat. Rev. Microbiol.* **2022**, *20*, 685–701.
- (4) Sharma, A.; de Rosa, M.; Singla, N.; Singh, G.; Barnwal, R. P.; Pandey, A. Tuberculosis: An Overview of the Immunogenic Response, Disease Progression, and Medicinal Chemistry Efforts in the Last Decade toward the Development of Potential Drugs for Extensively Drug-Resistant Tuberculosis Strains. *J. Med. Chem.* **2021**, *64*, 4359–4395.
- (5) Ahmed, I.; Tiberi, S.; Farooqi, J.; Jabeen, K.; Yeboah-Manu, D.; Migliori, G. B.; Hasan, R. Non-Tuberculous Mycobacterial Infections—A Neglected and Emerging Problem. *Int. J. Infect. Dis.* **2020**, *92*, S46–S50.
- (6) Dartois, V.; Dick, T. Drug Development Challenges in Nontuberculous Mycobacterial Lung Disease: TB to the Rescue. *J. Exp. Med.* **2022**, *219*, No. e20220445.
- (7) Gupta, R. S.; Lo, B.; Son, J. Phylogenomics and Comparative Genomic Studies Robustly Support Division of the Genus *Mycobacterium* into an Emended Genus *Mycobacterium* and Four Novel Genera. *Front. Microbiol.* **2018**, *9*, 67.
- (8) Tortoli, E.; Brown-Elliott, B. A.; Chalmers, J. D.; Cirillo, D. M.; Daley, C. L.; Emler, S.; Andres Floto, R.; Garcia, M. J.; Hoefsloot, W.; Koh, W. J.; Lange, C.; Loebinger, M.; Maurer, F. P.; Morimoto, K.; Niemann, S.; Richter, E.; Turenne, C. Y.; Vasireddy, R.; Vasireddy, S.

Wagner, D.; Wallace, R. J.; Wengenack, N.; van Ingen, J. Same Meat, Different Gravy: Ignore the New Names of Mycobacteria. *Eur. Respir. J.* **2019**, *54*, 1900795.

(9) Koh, W. J.; Jeong, B. H.; Kim, S. Y.; Jeon, K.; Park, K. U.; Jhun, B. W.; Lee, H.; Park, H. Y.; Kim, D. H.; Huh, H. J.; Ki, C. S.; Lee, N. Y.; Kim, H. K.; Choi, Y. S.; Kim, J.; Lee, S. H.; Kim, C. K.; Shin, S. J.; Daley, C. L.; Kim, H.; Kwon, O. J. Mycobacterial Characteristics and Treatment Outcomes in Mycobacterium Abscessus Lung Disease. *Clin. Infect. Dis.* **2017**, *64*, 309–316.

(10) Jarand, J.; Levin, A.; Zhang, L.; Huitt, G.; Mitchell, J. D.; Daley, C. L. Clinical and Microbiologic Outcomes in Patients Receiving Treatment for Mycobacterium Abscessus Pulmonary Disease. *Clin. Infect. Dis.* **2011**, *52*, 565–571.

(11) Jeon, K.; Kwon, O. J.; Nam, Y. L.; Kim, B.-J.; Kook, Y.-H.; Lee, S.-H.; Young, K. P.; Chang, K. K.; Koh, W.-J. Antibiotic Treatment of Mycobacterium Abscessus Lung Disease. *Am. J. Respir. Crit. Care Med.* **2009**, *180*, 896–902.

(12) Stover, C. K.; Warrenner, P.; VanDevanter, D. R.; Sherman, D. R.; Arain, T. M.; Langhorne, M. H.; Anderson, S. W.; Towell, J. A.; Yuan, Y.; McMurray, D. N.; Kreiswirth, B. N.; Barry, C. E.; Baker, W. R. A Small-Molecule Nitroimidazopyran Drug Candidate for the Treatment of Tuberculosis. *Nature* **2000**, *405*, 962–966.

(13) Diacon, A. H.; Pym, A.; Grobusch, M. P.; de los Rios, J. M.; Gotuzzo, E.; Vasilyeva, I.; Leimane, V.; Andries, K.; Bakare, N.; de Marez, T.; Haxaire-Theeuwes, M.; Lounis, N.; Meyvisch, P.; de Paep, E.; van Heeswijk, R. P. G.; Dannemann, B. Multidrug-Resistant Tuberculosis and Culture Conversion with Bedaquiline. *N. Engl. J. Med.* **2014**, *371*, 723–732.

(14) Diacon, A. H.; Pym, A.; Grobusch, M.; Patientia, R.; Rustomjee, R.; Page-Shipp, L.; Pistorius, C.; Krause, R.; Bogoshi, M.; Churchyard, G.; Venter, A.; Allen, J.; Palomino, J. C.; de Marez, T.; van Heeswijk, R. P. G.; Lounis, N.; Meyvisch, P.; Verbeeck, J.; Parys, W.; de Beule, K.; Andries, K.; Neeley, D. F. M. The Diarylquinoline TMC207 for Multidrug-Resistant Tuberculosis. *N. Engl. J. Med.* **2009**, *360*, 2397–2405.

(15) Mudde, S. E.; Upton, A. M.; Lenaerts, A.; Bax, H. I.; de Steenwinkel, J. E. M. Delamanid or Pretomanid? A Solomonic Judgement! *J. Antimicrob. Chemother.* **2022**, *77*, 880–902.

(16) Manjunatha, U.; Boshoff, H. I. M.; Barry, C. E. The Mechanism of Action of PA-824. *Commun. Integr. Biol.* **2009**, *2*, 215–218.

(17) Conradie, F.; Diacon, A. H.; Ngubane, N.; Howell, P.; Everitt, D.; Crook, A. M.; Mendel, C. M.; Egizi, E.; Moreira, J.; Timm, J.; McHugh, T. D.; Wills, G. H.; Bateson, A.; Hunt, R.; van Niekerk, C.; Li, M.; Olugbosi, M.; Spigelman, M. Treatment of Highly Drug-Resistant Pulmonary Tuberculosis. *N. Engl. J. Med.* **2020**, *382*, 893–902.

(18) Brode, S. K.; Daley, C. L.; Marras, T. K. The Epidemiologic Relationship between Tuberculosis and Non-Tuberculous Mycobacterial Disease: A Systematic Review. *Int. J. Tuberc. Lung Dis.* **2014**, *18*, 1370–1377.

(19) Lopeman, R. C.; Harrison, J.; Desai, M.; Cox, J. A. G. *Mycobacterium Abscessus*: Environmental Bacterium Turned Clinical Nightmare. *Microorganisms* **2019**, *7*, 90.

(20) Boudehen, Y. M.; Kremer, L. Mycobacterium Abscessus. *Trends Microbiol.* **2021**, *29*, 951–952.

(21) Victoria, L.; Gupta, A.; Gómez, J. L.; Robledo, J. Mycobacterium Abscessus Complex: A Review of Recent Developments in an Emerging Pathogen. *Front. Cell. Infect. Microbiol.* **2021**, *11*, 338.

(22) Malenfant, J. H.; Brewer, T. F. Rifampicin Mono-Resistant Tuberculosis—A Review of an Uncommon But Growing Challenge for Global Tuberculosis Control. *Open Forum Infect. Dis.* **2021**, *8*, ofab018.

(23) Rominski, A.; Roditscheff, A.; Selchow, P.; Böttger, E. C.; Sander, P. Intrinsic Rifampicin Resistance of Mycobacterium Abscessus Is Mediated by ADP-Ribosyltransferase MAB\_0591. *J. Antimicrob. Chemother.* **2017**, *72*, 376–384.

(24) Ganapathy, U. S.; Lan, T.; Krastel, P.; Lindman, M.; Zimmerman, M. D.; Ho, H. P.; Sarathy, J. P.; Evans, J. C.; Dartois, V.; Aldrich, C. C.; Dick, T. Blocking Bacterial Naphthohydroquinone Oxidation and Adpribosylation Improves Activity of Rifamycins against Mycobacterium Abscessus. *Antimicrob. Agents Chemother.* **2021**, *65*, e0097821.

(25) Aziz, D. B.; Low, J. L.; Wu, M. L.; Gengenbacher, M.; Teo, J. W. P.; Dartois, V.; Dick, T. Rifabutin Is Active against Mycobacterium Abscessus Complex. *Antimicrob. Agents Chemother.* **2017**, *61*, e00155–e00117.

(26) Dick, T.; Shin, S. J.; Koh, W. J.; Dartois, V.; Gengenbacher, M. Rifabutin Is Active against Mycobacterium Abscessus in Mice. *Antimicrob. Agents Chemother.* **2020**, *64*, e00155–e00117.

(27) Lan, T.; Ganapathy, U. S.; Sharma, S.; Ahn, Y.-M.; Zimmerman, M.; Molodtsov, V.; Hegde, P.; Gengenbacher, M.; Ebright, R. H.; Dartois, V.; Freundlich, J. S.; Dick, T.; Aldrich, C. C. Redesign of Rifamycin Antibiotics to Overcome ADP-Ribosylation-Mediated Resistance. *Am. Ethmol.* **2022**, *134*, No. e202211498.

(28) Paulowski, L.; Beckham, K. S. H.; Johansen, M. D.; Berneking, L.; Van, N.; Degefu, Y.; Staack, S.; Sotomayor, F. V.; Asar, L.; Rohde, H.; Aldridge, B. B.; Aepfelbacher, M.; Parret, A.; Wilmanns, M.; Kremer, L.; Combrink, K.; Maurer, F. P. C25-Modified Rifamycin Derivatives with Improved Activity against Mycobacterium Abscessus. *Proc. Natl. Acad. Sci. U. S. A.* **2022**, *1*, 1–13.

(29) Ballell, L.; Bates, R. H.; Young, R. J.; Alvarez-Gomez, D.; Alvarez-Ruiz, E.; Barroso, V.; Blanco, D.; Crespo, B.; Escibano, J.; González, R.; Lozano, S.; Huss, S.; Santos-Villarejo, A.; Martín-Plaza, J. J.; Mendoza, A.; Rebollo-Lopez, M. J.; Remuñán-Blanco, M.; Lavandera, J. L.; Pérez-Herran, E.; Gamó-Benito, F. J.; García-Bustos, J. F.; Barros, D.; Castro, J. P.; Cammack, N. Fueling Open-Source Drug Discovery: 177 Small-Molecule Leads against Tuberculosis. *ChemMedChem* **2013**, *8*, 313–321.

(30) Low, J. L.; Wu, M. L.; Aziz, D. B.; Laleu, B.; Dick, T. Screening of TB Actives for Activity against Nontuberculous Mycobacteria Delivers High Hit Rates. *Front. Microbiol.* **2017**, *8*, 1539.

(31) Lin, W.; Mandal, S.; Degen, D.; Liu, Y.; Ebright, Y. W.; Li, S.; Feng, Y.; Zhang, Y.; Mandal, S.; Jiang, Y.; Liu, S.; Gigliotti, M.; Talae, M.; Connell, N.; Das, K.; Arnold, E.; Ebright, R. H. Structural Basis of Mycobacterium Tuberculosis Transcription and Transcription Inhibition. *Mol. Cell* **2017**, *66*, 169–179.

(32) Ebright, Richard H.; Ebright, Yon W.; Mandal, Soma; Wilde, Richard; Li, S. Preparation of N-Alpha-Aroyl-N-Aryl-Phenylalaninamides as Inhibitors of Bacterial RNA Polymerase and as Antibacterials. WO2015120320 A1 2015-08-13, 2015.

(33) Mann, L.; Lang, M.; Schulze, P.; Halz, J. H.; Csuk, R.; Hoenke, S.; Seidel, R. W.; Richter, A. Racemization-Free Synthesis of  $\alpha$ -2-Thiophenyl-Phenylalanine-2-Morpholinoanilide Enantiomers and Their Antimycobacterial Activity. *Amino Acids* **2021**, *53*, 1187–1196.

(34) Mann, L.; Ganapathy, U. S.; Abdelaziz, R.; Lang, M.; Zimmerman, M. D.; Dartois, V.; Dick, T.; Richter, A.; Tiwari, S. In Vitro Profiling of the Synthetic RNA Polymerase Inhibitor MMV688845 against Mycobacterium Abscessus. *Microbiol. Spectrum* **2022**, *10*, e0276022.

(35) Dunetz, J. R.; Xiang, Y.; Baldwin, A.; Ringling, J. General and Scalable Amide Bond Formation with Epimerization-Prone Substrates Using T3P and Pyridine. *Org. Lett.* **2011**, *13*, 5048–5051.

(36) Li, H.; Jiang, X.; Ye, Y.-H.; Fan, C.; Romoff, T.; Goodman, M. 3-(Diethoxyphosphoryloxy)-1,2,3-Benzotriazin-4(3H)-One (DEPBT): A New Coupling Reagent with Remarkable Resistance to Racemization. *1999*, *1*, 91–94.

(37) Brewster, W. K. Thieno-Pyrimidine Compounds Having Fungicidal Activity. US 2006/0089370 A1, 2006.

(38) Allwood, D. M.; Blakemore, D. C.; Brown, A. D.; Ley, S. v. Metal-Free Coupling of Saturated Heterocyclic Sulfonylhydrazones with Boronic Acids. *J. Org. Chem.* **2014**, *79*, 328–338.

(39) Barluenga, J.; Tomás-Gamasa, M.; Aznar, F.; Valdés, C. Metal-Free Carbon–Carbon Bond-Forming Reductive Coupling between Boronic Acids and Tosylhydrazones. *Nat. Chem.* **2009**, *1*, 494–499.

(40) Thiemann, T. Thiophene S-Oxides. *Chalcogen Chem; IntechOpen* 2019, .

(41) Elsayy, M. A.; Hewage, C.; Walker, B. Racemisation of N-Fmoc Phenylglycine under Mild Microwave-SPPS and Conventional Stepwise SPPS Conditions: Attempts to Develop Strategies for Overcoming This. *J. Pept. Sci.* **2012**, *18*, 302–311.

- (42) Sturabotti, E.; Vetica, F.; Toscano, G.; Calcaterra, A.; Martinelli, A.; Migneco, L. M.; Leonelli, F. N-Acetyl-L-Phenylalanine Racemization during TBTU Amidation: An In-Depth Study for the Synthesis of Anti-Inflammatory 2-(N-Acetyl)-l-Phenylalanyl-amido-2-Deoxy-d-Glucose (NAPA). *Molecules* **2023**, *28*, 581.
- (43) Al-Warhi, T. I.; Al-Hazimi, H. M. A.; El-Faham, A. Recent Development in Peptide Coupling Reagents. *J. Saudi Chem. Soc.* **2012**, *16*, 97–116.
- (44) Bodanszky, M. *Principles of Peptide Synthesis*; Springer.
- (45) Antonovics, I.; Young, G. T. Amino-Acids and Peptides. Part XXV. The Mechanism of the Base-Catalysed Racemisation of the p-Nitrophenyl Esters of Acylpeptides. *J. Chem. Soc. C* **1967**, *99*, 595–601.
- (46) García, A. L. L. T3P: A Convenient and Useful Reagent in Organic Synthesis. *Synlett* **2007**, *2007*, 1328–1329.
- (47) Harada, H. Azolecarboxamide Derivative. WO 2007/123269 A1, 2017.
- (48) Midgley, L.; Bourhis, L. J.; Dolomanov, O. v.; Grabowsky, S.; Kleemiss, F.; Puschmann, H.; Peyerimhoff, N. Vanishing of the Atomic Form Factor Derivatives in Non-Spherical Structural Refinement - a Key Approximation Scrutinized in the Case of Hirshfeld Atom Refinement. *Acta Crystallogr., Sect. A: Found. Adv.* **2021**, *77*, 519–533.
- (49) Kleemiss, F.; Dolomanov, O. v.; Bodensteiner, M.; Peyerimhoff, N.; Midgley, L.; Bourhis, L. J.; Genoni, A.; Malaspina, L. A.; Jayatilaka, D.; Spencer, J. L.; White, F.; Grundkötter-Stock, B.; Steinhauer, S.; Lentz, D.; Puschmann, H.; Grabowsky, S. Accurate Crystal Structures and Chemical Properties from NoSpherA2. *Chem. Sci.* **2021**, *12*, 1675–1692.
- (50) Chaturvedi, V.; Dwivedi, N.; Tripathi, R. P.; Sinha, S. Evaluation of Mycobacterium Smegmatis as a Possible Surrogate Screen for Selecting Molecules Active against Multi-Drug Resistant Mycobacterium Tuberculosis. *J. Gen. Appl. Microbiol.* **2007**, *53*, 333–337.
- (51) T, J. A. S.; J, R.; Rajan, A.; Shankar, V. Features of the Biochemistry of Mycobacterium Smegmatis, as a Possible Model for Mycobacterium Tuberculosis. *J. Infect. Public Health* **2020**, *13*, 1255–1264.
- (52) Tortoli, E. Microbiological Features and Clinical Relevance of New Species of the Genus Mycobacterium. *Clin. Microbiol. Rev.* **2014**, *27*, 727–752.
- (53) Weiss, C. H.; Glassroth, J. Pulmonary Disease Caused by Nontuberculous Mycobacteria. *Expert Rev. Respir. Med.* **2012**, *6*, 597–613.
- (54) Henkle, E.; Hedberg, K.; Schafer, S. D.; Winthrop, K. L. Surveillance of Extrapulmonary Nontuberculous Mycobacteria Infections, Oregon, USA, 2007–2012. *Emerging Infect. Dis.* **2017**, *23*, 1627–1630.
- (55) To, K.; Cao, R.; Yegiazaryan, A.; Owens, J.; Venketaraman, V. General Overview of Nontuberculous Mycobacteria Opportunistic Pathogens: Mycobacterium Avium and Mycobacterium Abscessus. *J. Clin. Med.* **2020**, *9*, 2541.
- (56) Koh, W. J.; Jeong, B. H.; Jeon, K.; Lee, N. Y.; Lee, K. S.; Woo, S. Y.; Shin, S. J.; Kwon, O. J. Clinical Significance of the Differentiation Between Mycobacterium Avium and Mycobacterium Intracellulare in M Avium Complex Lung Disease. *Chest* **2012**, *142*, 1482–1488.
- (57) Ricotta, E. E.; Adjemian, J.; Blakney, R. A.; Lai, Y. L.; Kadri, S. S.; Prevots, D. R. Extrapulmonary Nontuberculous Mycobacteria Infections in Hospitalized Patients, United States, 2009–2014. *Emerging Infect. Dis.* **2021**, *27*, 845–852.
- (58) Ollinger, J.; Kumar, A.; Roberts, D. M.; Bailey, M. A.; Casey, A.; Parish, T. A High-Throughput Whole Cell Screen to Identify Inhibitors of Mycobacterium Tuberculosis. *PLoS One* **2019**, *14*, No. e0205479.
- (59) Richter, A.; Shapira, T.; Av-Gay, Y. THP-1 and Dictyostelium Infection Models for Screening and Characterization of Anti-Mycobacterium Abscessus Hit Compounds. *Antimicrob. Agents Chemother.* **2019**, *64*, e01601–e01619.
- (60) Martin-Smith, M.; Reid, S. T. Biological Activity in Compounds Possessing Thiophen Rings. *J. Med. Chem.* **1959**, *1*, 507–564.
- (61) Maurer, F. P.; Bruderer, V. L.; Ritter, C.; Castelberg, C.; Bloemberg, G. v.; Böttger, E. C. Lack of Antimicrobial Bactericidal Activity in Mycobacterium Abscessus. *Antimicrob. Agents Chemother.* **2014**, *58*, 3828–3836.
- (62) Heifets, L. Qualitative and Quantitative Drug-Susceptibility Tests in Mycobacteriology. *Am. Rev. Respir. Dis.* **1987**, *137*, 1217–1222.
- (63) Bahar, F. G.; Ohura, K.; Ogihara, T.; Imai, T. Species Difference of Esterase Expression and Hydrolase Activity in Plasma. *J. Pharm. Sci.* **2012**, *101*, 3979–3988.
- (64) Bathelt, C. M.; Ridder, L.; Mulholland, A. J.; Harvey, J. N. Aromatic Hydroxylation by Cytochrome P450: Model Calculations of Mechanism and Substituent Effects. *J. Am. Chem. Soc.* **2003**, *125*, 15004–15005.
- (65) Cerny, M. A. Prevalence of Non-Cytochrome P450-Mediated Metabolism in Food and Drug Administration-Approved Oral and Intravenous Drugs: 2006-2015. *Drug Metab. Dispos.* **2016**, *44*, 1246–1252.
- (66) Bradshaw, P. R.; Wilson, I. D.; Gill, R. U.; Butler, P. J.; Dilworth, C.; Athersuch, T. J. Metabolic Hydrolysis of Aromatic Amides in Selected Rat, Minipig, and Human In Vitro Systems. *Sci. Rep.* **2018**, *8*, 2405.
- (67) Sommerwerk, S.; Heller, L.; Kuhfs, J.; Csuk, R. Selective Killing of Cancer Cells with Triterpenic Acid Amides - The Substantial Role of an Aromatic Moiety Alignment. *Eur. J. Med. Chem.* **2016**, *122*, 452–464.
- (68) Heller, L.; Knorrscheidt, A.; Flemming, F.; Wiemann, J.; Sommerwerk, S.; Pavel, I. Z.; Al-Harrasi, A.; Csuk, R. Synthesis and Proapoptotic Activity of Oleanolic Acid Derived Amides. *Bioorg. Chem.* **2016**, *68*, 137–151.
- (69) Csuk, R.; Barthel, A.; Szczepek, R.; Siewert, B.; Schwarz, S. Synthesis, Encapsulation and Antitumor Activity of New Betulin Derivatives. *Arch. Pharm. Chem. Life Sci.* **2011**, *344*, 37–49.
- (70) Savjani, K. T.; Gajjar, A. K.; Savjani, J. K. Drug Solubility: Importance and Enhancement Techniques. *Int. Scholarly Res. Not.* **2012**, *2012*, 1–10.
- (71) Congreve, M.; Carr, R.; Murray, C.; Jhoti, H. A “Rule of Three” for Fragment-Based Lead Discovery? *Drug Discovery Today* **2003**, *8*, 876–877.
- (72) Bevan, C. D.; Lloyd, R. S. A High-Throughput Screening Method for the Determination of Aqueous Drug Solubility Using Laser Nephelometry in Microtiter Plates. *Anal. Chem.* **2000**, *72*, 1781–1787.
- (73) Richter, A.; Strauch, A.; Chao, J.; Ko, M.; Av-Gay, Y. Screening of Preselected Libraries Targeting Mycobacterium Abscessus for Drug Discovery. *Antimicrob. Agents Chemother.* **2018**, *62*, 1–11.
- (74) Yang, X.; Wedajo, W.; Yamada, Y.; Dahlroth, S. L.; Neo, J. J. L.; Dick, T.; Chui, W. K. 1,3,5-Triazaspiro[5.5]Undeca-2,4-Dienes as Selective Mycobacterium Tuberculosis Dihydrofolate Reductase Inhibitors with Potent Whole Cell Activity. *Eur. J. Med. Chem.* **2018**, *144*, 262–276.



## 2.3) Research Article II

# Synthesis and *in vitro* Metabolic Stability of Sterically Shielded Antimycobacterial Phenylalanine Amides

Markus Lang, Uday S. Ganapathy, Lea Mann, Rüdiger W. Seidel, Richard Goddard, Frank Erdmann, Thomas Dick, Adrian Richter

European Chemical Society Publishing  
ChemMedChem

*ChemMedChem*, 19(6), e202300593.

Publication Date: 08.02.2024

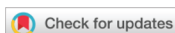
DOI: 10.1002/cmdc.202300593

### Summary

In this article, we report the synthesis and antimycobacterial activity of AAPs designed to combat the metabolic liability of amide hydrolysis of the compound class. Although previously synthesized AAP derivatives were potent growth inhibitors, we observed rapid degradation in microsomal suspensions. The introduction of sterically shielded AAP analogs have been probed, revealing that the introduction of methyl or fluoro substituents near the amide bonds led to enhanced microsomal stability. However, the changes employed close to the anilide bond led to a notable decline in antimycobacterial *in vitro* activity. The findings indicate that the anilide bond of the AAP scaffold is involved in microsomal degradation.

### Own contributions

Synthesis and characterization of compounds, analysis of structure-activity relationship, preparation of figures, conceptualization of the draft, original draft preparation, review and editing



# Synthesis and *in vitro* Metabolic Stability of Sterically Shielded Antimycobacterial Phenylalanine Amides

Markus Lang,<sup>[a]</sup> Uday S. Ganapathy,<sup>[b]</sup> Lea Mann,<sup>[a]</sup> Rüdiger W. Seidel,<sup>[a]</sup> Richard Goddard,<sup>[c]</sup> Frank Erdmann,<sup>[a]</sup> Thomas Dick,<sup>[b, d, e]</sup> and Adrian Richter<sup>\*,[a]</sup>

*N*-α-aryl-*N*-aryl-phenylalanine amides (AAPs) are RNA polymerase inhibitors with activity against *Mycobacterium tuberculosis* and non-tuberculous mycobacteria. We observed that AAPs rapidly degrade in microsomal suspensions, suggesting that avoiding hepatic metabolism is critical for their effectiveness *in vivo*. As both amide bonds are potential metabolic weak points of the molecule, we synthesized 16 novel AAP analogs in which the amide bonds are shielded by methyl or fluoro substituents in close proximity. Some derivatives show improved microsomal stability, while being plasma-stable and

non-cytotoxic. In parallel with the metabolic stability studies, the antimycobacterial activity of the AAPs against *Mycobacterium tuberculosis*, *Mycobacterium abscessus*, *Mycobacterium avium* and *Mycobacterium intracellulare* was determined. The stability data are discussed in relation to the antimycobacterial activity of the panel of compounds and reveal that the concept of steric shielding of the anilide groups by a fluoro substituent has the potential to improve the stability and bioavailability of AAPs.

## Introduction

*Mycobacterium tuberculosis* infections remain a significant global health concern,<sup>[1]</sup> posing challenges to healthcare systems worldwide due to their persistence, potential for drug resistance, and the burden they impose on resources for diagnosis, treatment, and prevention.<sup>[2]</sup> Another growing healthcare concern are non-tuberculous mycobacteria (NTM),<sup>[3]</sup> such as *Mycobacterium abscessus* (*Mabs*), that can cause severe infections of various organs, foremost in the respiratory tract<sup>[4]</sup> that often require different treatment approaches in comparison to tuberculosis.<sup>[5]</sup> Patients with underlying lung conditions, such as chronic obstructive pulmonary disease (COPD), cystic fibrosis (CF),<sup>[6]</sup> or a compromised immune system are partic-

ularly susceptible to NTM infections.<sup>[7]</sup> As the bacteria are commonly found in the environment, NTM are usually acquired from soil and water sources. Patient-to-patient transmission can occur, and this particularly prominent among CF patients.<sup>[8]</sup> Especially when *Mabs* is the causative agent, eradication of NTM infections is difficult owing to its inherent resistance to common antimycobacterial drugs.<sup>[9]</sup> For this reason, new antimycobacterial agents are urgently needed.

MMV688845 (hereafter **MMV**) was first described as a hit structure against *Mycobacterium tuberculosis* (*Mtb*) and provides a potential chemical scaffold for further modification.<sup>[10]</sup> Ebright *et al.* tested MMV anti-NTM properties and displayed *in vitro* activity against *Mycobacterium avium* (*Mavium*).<sup>[11]</sup> Screening the Pathogen Box (Medicines for Malaria Venture, Geneva, Switzerland) against *Mabs* and *Mavium*<sup>[12]</sup> also identified **MMV** (Scheme 1A) as a promising hit compound against NTM.<sup>[12]</sup> The closely related analogs D-AAP1 and D-IX336 were reported to inhibit the mycobacterial RNA polymerase (RNAP) by targeting its β and β' subunits,<sup>[13]</sup> thus inhibiting transcription. The *in vitro* generation and genome sequencing of **MMV** resistant mutants of *Mabs* *Bamboo* suggested that the same holds true for the hit compound.<sup>[14]</sup> Rifamycins such as rifampicin, rifabutin and

[a] M. Lang, L. Mann, Dr. R. W. Seidel, Dr. F. Erdmann, Dr. A. Richter  
Institut für Pharmazie, Martin-Luther-Universität Halle-Wittenberg  
Wolfgang-Langenbeck-Str. 4, 06120 Halle (Saale), Germany  
E-mail: adrian.richter@pharmazie.uni-halle.de

[b] Dr. U. S. Ganapathy, Prof. Dr. T. Dick  
Center for Discovery and Innovation, Hackensack Meridian Health  
111 Ideation Way, 07110 Nutley, New Jersey, USA

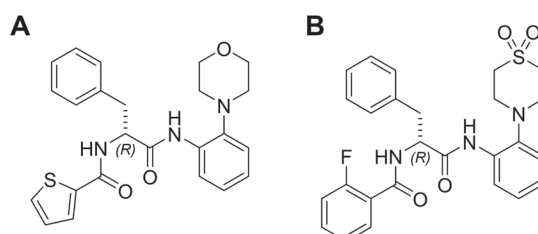
[c] Dr. R. Goddard  
Max-Planck-Institut für Kohlenforschung  
Kaiser-Wilhelm-Platz 1, 45470 Mülheim an der Ruhr, Germany

[d] Prof. Dr. T. Dick  
Department of Medical Sciences, Hackensack Meridian School of Medicine  
123 Metro Blvd, 07110 Nutley, New Jersey, USA

[e] Prof. Dr. T. Dick  
Department of Microbiology and Immunology, Georgetown University  
3900 Reservoir Road, N.W., 20007 Washington DC, USA

Supporting information for this article is available on the WWW under  
<https://doi.org/10.1002/cmdc.202300593>

© 2024 The Authors. ChemMedChem published by Wiley-VCH GmbH. This is an open access article under the terms of the Creative Commons Attribution Non-Commercial NoDerivs License, which permits use and distribution in any medium, provided the original work is properly cited, the use is non-commercial and no modifications or adaptations are made.



Scheme 1. A: Molecular structure of the hit compound **MMV**. B: Molecular structure of **2**.

rifampentine are RNAP inhibitors that are currently in clinical use against many mycobacterial infections. Since *Mabs* exhibits intrinsic resistance mechanisms to rifampicin through C23 ribosylation<sup>[15]</sup> and naphthohydroquinone oxidation<sup>[16]</sup>, a therapy regimen that includes rifamycins is usually not an option. Consequently, there is a need to develop alternative RNAP inhibitors for anti-*Mabs* therapy. Cross-resistance of AAPs with rifamycins is unlikely as the target binding site of AAPs has been shown to be different<sup>[13]</sup> which has also been proven by *in vitro* experiments.<sup>[14]</sup> Furthermore, the hit compound **MMV** was active against a variety of *Mabs* clinical isolates and exhibits bactericidal activity against *Mabs* in broth and in a macrophage infection model.<sup>[5c]</sup> AAPs are also of interest for the treatment of rifampicin-resistant *Mtb*, since they retain the effective bactericidal mechanism of RNAP inhibition while being chemically distinct.

Recently, we prepared analogs of **MMV** and obtained compounds with higher antimycobacterial activity, solubility, and plasma stability than the hit compound.<sup>[17a]</sup> We have established a synthetic pathway that retains the *R* configuration, which is necessary for the desired antimycobacterial activity, with *ee* values of 99%.<sup>[17]</sup> In particular, the introduction of thiomorpholine dioxide instead of morpholine increased the whole cell activity. Compound **2** (Scheme 1B) displays an MIC<sub>90</sub> < 1 μM against *Mabs* and *Mtb*.

Previous investigations on AAPs revealed that **MMV** gave insufficient plasma levels after oral administration in male Sprague Dawley rats.<sup>[12c,18]</sup> We have already presented plasma and microsomal stability data of the hit compound **MMV** and the highly active compound **2** and revealed that **MMV** degraded quickly in murine plasma, whereas **2** was stable in both murine and human plasma.<sup>[17a]</sup> Amide moieties of drug candidates are known to be hydrolyzed in blood plasma to form inactive metabolites.<sup>[19]</sup> The blood plasma of rodents typically exhibits higher and less specific hydrolase activity than human plasma due to differences in plasma esterases and their expression levels.<sup>[20]</sup>

Both **MMV** and **2** were highly unstable during incubation with human and murine liver microsomes.<sup>[17a]</sup> AAPs contain two amide bonds which can undergo enzyme-catalyzed hydrolytic cleavage. The anilide is potentially more susceptible, since C–N π-bond overlap of the amide group is weakened by the conjugation of the nitrogen atom with the phenyl group. Serine esterases such as carboxylesterases, which are predominantly found in the liver, are known to catalyze amide cleavage in humans.<sup>[21]</sup> Another study also presents evidence for anilide cleavage in liver microsomes resulting in formation of an inactive drug candidate metabolite.<sup>[22]</sup>

To address the poor hepatic stability of these compounds, we designed and synthesized a new series of AAP derivatives and performed *in vitro* characterization of plasma and microsomal stability, microbiological activity assessment against a variety of mycobacteria, cytotoxicity testing as well as solubility screening of the new substances.

## Results and Discussion

### Derivatization plan for increased metabolic stability

The derivatization strategy is based on analog **2** (Scheme 1B) that we developed, which shows increased *in vitro* activity against *Mabs* (MIC<sub>90</sub> = 0.78 μM)<sup>[17a]</sup> compared to the initial hit **MMV** (MIC<sub>90</sub> = 6.25 μM). To gain structural insight, we subjected **2** to X-ray crystallography (Figure 1). In the crystal, **2** adopts the same conformation with an intramolecular N–H⋯O hydrogen bond similar to an previously described 2-thiophenoyl analog.<sup>[17a]</sup> Likewise, the molecules form *pseudo* centrosymmetric N–H⋯O hydrogen bond dimers in the solid-state. Owing to the steric demand of the fluorine atom in the *ortho* position, the 2-fluorobenzene moieties are significantly tilted out of the plane of the attached amide groups. The 1,1-dioxo-1λ<sup>5</sup>-thiomorpholin-4-yl moiety appears to be primarily responsible for its increased potency and was therefore retained in the new AAPs.

We systematically derivatized various positions of the scaffold in the proximity of the amide bonds with the aim of sterically shielding the amide linkage and thereby prevent hydrolysis by amidases and esterases. This involved derivatization of positions 2 and 6, *ortho* positions to carbonyl, R<sup>2</sup> and R<sup>3</sup>, of aromatic system A as well as the *ortho* position of aromatic system B (R<sup>1</sup>) adjacent to the anilide bond (Scheme 2A).

This approach was inspired by the development of lidocaine<sup>[24]</sup> in which methyl groups were introduced in order to prevent fast metabolism.<sup>[25]</sup> Introduction of two methyl groups to procaineamide resulted in a conformational change (a twist of the benzene ring) sufficient to sterically shield the amide bond from hydrolysis by amidases.<sup>[25b]</sup> Similar to this approach, the introduction of two *ortho* methyl groups in the aromatic system A could stabilize the amide towards metabolic hydrolysis. The peptides were also *N*-methylated to increase the stability (Scheme 2B). *N*-methylation can lead to higher serum stability of peptide like structures<sup>[26]</sup> and a higher stability

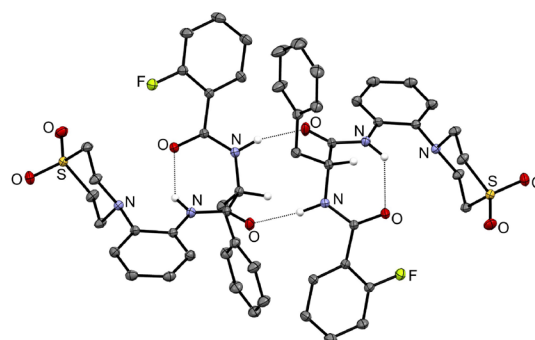
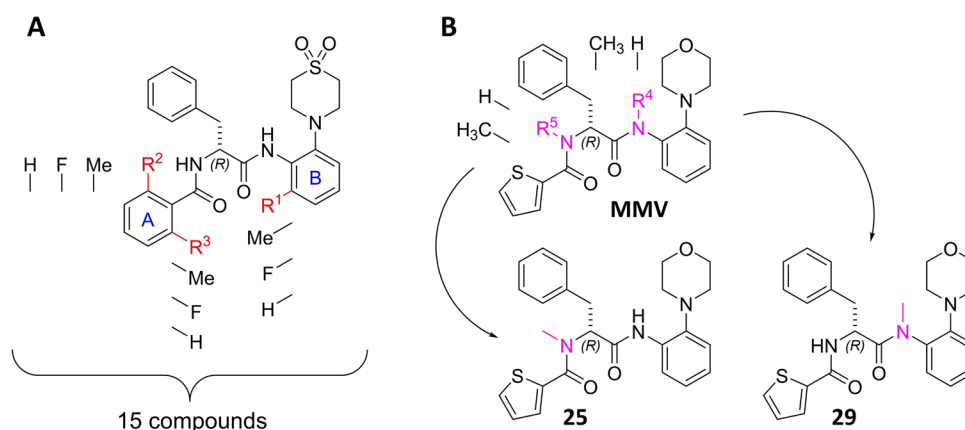


**Figure 1.** Asymmetric unit of **2**. Displacement ellipsoids are drawn at the 50% probability level. Nitrogen-bound hydrogen atoms and the carbon-bound hydrogen atoms attached to centers of chirality are represented by small spheres of arbitrary radius, otherwise hydrogen atoms are omitted for clarity. Dashed lines represent hydrogen bonds. Colour scheme: C, grey; H, white; N, blue; O, red; F, light green; S, yellow. The crystal structure was refined using NoSpherA2.<sup>[23]</sup>



**Scheme 2.** Derivatization strategy of AAPs for increased metabolic stability. **A:** The scaffold of (2*R*)-2-[[2-(2-fluorophenyl)formamido]-*N*-[2-(1,1-dioxo-1- $\lambda$ 6-thiomorpholin-4-yl)phenyl]-3-phenylpropanamide is depicted, and the changes at  $R^1$ ,  $R^2$ , and  $R^3$  are indicated. The synthesized derivatives contain either hydrogen, fluoro, or methyl substituents at the respective positions. All conceivable combinations within this range of substituents were synthesized, resulting in a total of 15 compounds. **B:** Two derivatives of MMV were synthesized by *N*-methylation at positions  $R^4$  and  $R^5$ . One compound was methylated at  $R^4$  (29) and the other one at  $R^5$  (25).

against peptidases like chymotrypsin, as demonstrated by Haviv *et al.* in the synthesis of *N*-methyl leuprolide derivatives.<sup>[27]</sup>

Results from Ebright *et al.* suggest that substituents that are bulkier than hydrogen, fluoro or methyl tend to result in lower antimycobacterial activities (e.g., *o*-chlorine ↓, 4-indolyl ↓, *o*-bromine ↓↓, *o*-ethyl ↓↓↓).<sup>[11]</sup> Thus, we restricted the study to small substituents, preferring fluorine and methyl to chlorine and bromine<sup>[11]</sup> to sterically shield the adjacent amide bond.

To the best of our knowledge, AAPs substituted in the *ortho* position to the anilide bond at aromatic system B (refer to Scheme 2A) have not been reported so far. In accordance with the approach employed in aromatic system A, we also elected to utilize less voluminous substituents to maximize the likelihood of achieving antimycobacterial activity. The addition of a methyl group is expected to result in a greater shielding effect due to its larger size compared to that of a fluorine atom.

#### Synthesis of 4-(2-aminophenyl)-1- $\lambda$ 6-thiomorpholine-1,1-diones

The synthetic sequence commences with the synthesis of an aniline building block substituted with a thiomorpholine dioxide moiety in one *ortho*-position (Scheme 3). The other *ortho*-position is substituted with either hydrogen, fluorine atom, or a methyl group (as explained above).

In the initial step, various halogen-substituted nitrobenzenes were subject to aromatic nucleophilic substitutions. 1,3-Difluoro-2-nitrobenzene reacts smoothly with thiomorpholine dioxide owing to the strong electron deficiency caused by the two fluoro- and nitro substituents (Scheme 3A). The reaction of one equivalent of symmetric 1,3-difluoro-2-nitrobenzene with one equivalent of the nucleophile provides an efficient approach with a 95% yield of the desired product. The mono-substituted product of the reaction did not undergo a second

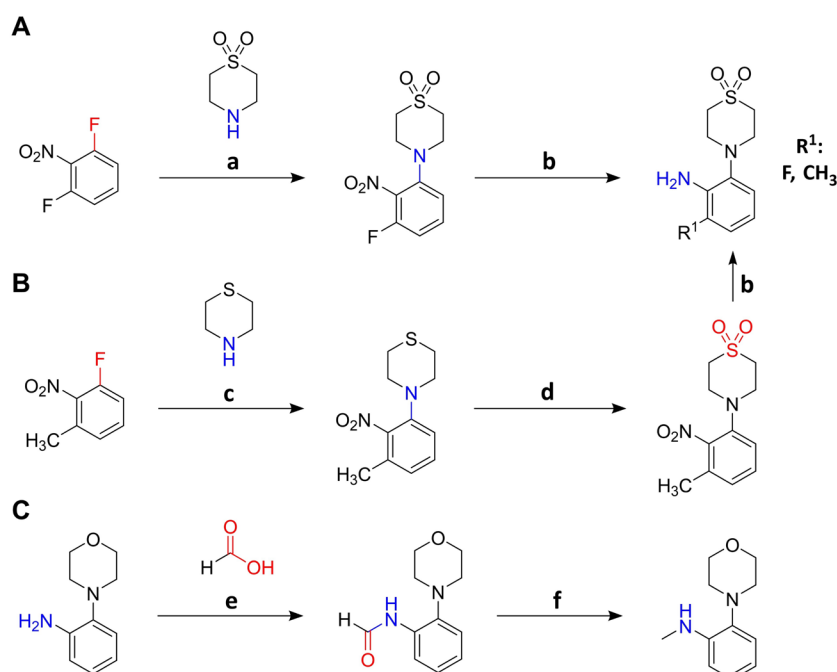
substitution reaction as it was less electrophilic than 1,3-difluoro-2-nitrobenzene.

Thiomorpholine dioxide is less nucleophilic than the corresponding thioether due to the electron-withdrawing effect of the sulfone group. Consequently, the unsubstituted<sup>[17a]</sup> and 3-methyl nitrobenzene which are less electron-deficient than 1,3-difluoro-2-nitrobenzene had to be coupled with nucleophilic thiomorpholine and subsequently oxidized with *m*CPBA (Scheme 3B). Attempted reactions with thiomorpholine dioxide did not result in the desired product.

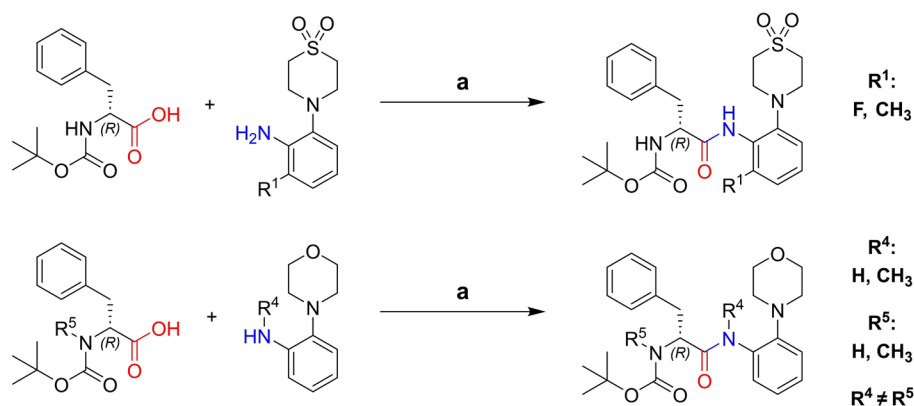
The *N*-methyl aniline moiety was obtained by initial formation of the formic acid amide of 2-morpholinoaniline and subsequent reduction to the secondary amine with  $\text{LiAlH}_4$  (Scheme 3C)

#### Amide coupling with *N*-Boc-(*R*)-phenylalanine

To couple the previously synthesized anilines with *N*-Boc-(*R*)-phenylalanine or *N*-Boc-*N*-methyl-(*R*)-phenylalanine we utilized the coupling agent propane phosphonic acid anhydride (T3P).<sup>[28]</sup> In a former study T3P was found to be highly efficient for the synthesis of the AAP anilide structure while retaining the *R* configuration of the phenylalanine stereocenter<sup>[17a,29]</sup> which is essential for activity.<sup>[17b]</sup> The reaction produced the desired 6-fluoro and 6-methyl derivatives at the  $R^1$  position as well as the *N*-methylated derivatives (Scheme 4). A notable difference was observed in the yields of the reactions. The unsubstituted derivative yielded 99% product, while the 6-fluoro, 6-methyl and *N*-methyl derivatives gave yields of 92%, 56% and 33%, respectively. The particularly low yield of the 6-methyl and the *N*-methyl derivative indicate that the methyl groups sterically hinder the amine from attacking the electrophilic carbon atom.



**Scheme 3.** Synthesis of 4-(2-aminophenyl)-1 $\lambda^5$ -thiomorpholine-1,1-diones and *N*-methyl derivatives. **A:** Synthesis of 3-fluoro derivatives. **B:** Synthesis of 3-methyl derivatives. **C:** Synthesis of *N*-methyl derivatives. **a:** DIPEA, 3 d, 50 °C; **b:** EtOH, H<sub>2</sub>, Pd(OH)<sub>2</sub>/C 20%; **c:** DIPEA, 50 °C, 24 h; **d:** DCM, -20 °C, mCPBA in DCM added over 30 min; **e:** HCOOH, HCOONa, room temperature, overnight; **f:** THF, LiAlH<sub>4</sub> 1 M in THF dropwise over 30 min, argon, 0 °C to room temperature. For quantities and detailed procedures see Supporting Information.

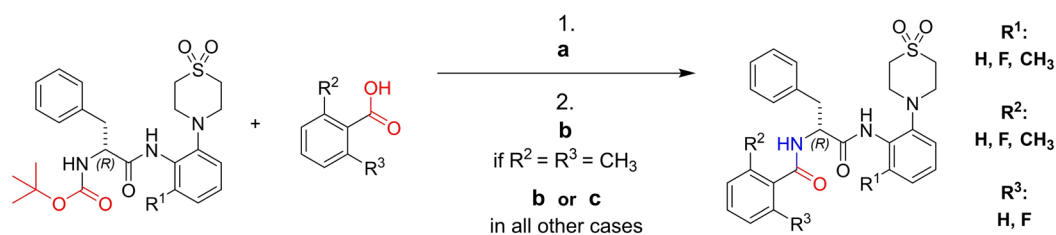


**Scheme 4.** Synthesis of *N*-Boc-(*R*)-phenylalanine anilides (**A**) and *N*-Boc-*N*-methyl-(*R*)-phenylalanine anilides (**B**). **a:** EtOAc + pyridine 2:1, T3P 50% m/v in EtOAc, -20 °C to RT, 20 h. For quantities and detailed procedures see Supporting Information.

#### Amide coupling with different benzoic acids

The final step of the synthetic sequence involves Boc-deprotection of the *N*-Boc-(*R*)-phenylalanine anilides (see Scheme 5) and the *N*-Boc-*N*-methyl-(*R*)-phenylalanine anilides (not shown) and subsequent amide coupling with a benzoic acid derivative. The Boc-deprotected intermediates were used for the amide coupling without further purification. For the

formation of amides, 3-(diethoxyphosphoryloxy)-1,2,3-benzotriazin-4(3*H*)-one (DEPBT) and benzotriazol-1-yloxytriethylphosphonium hexafluorophosphate (PyBOP) were employed as effective and convenient coupling reagents for the synthesis of AAPs<sup>[17]</sup> with retention of the stereochemistry. PyBOP was used when conversion with DEPBT resulted in low yields. The conversion of 2,6-dimethylbenzoic acid proved challenging owing to the high degree of steric hindrance. In preliminary



**Scheme 5.** Synthesis of *N*α-2-phenoyl-(*R*)-phenylalanine-2-anilides. **a:** TFA, DCM, 1 h, RT; **b:** DMF, PyBOP, overnight, RT; **c:** Dioxane, DEPBT, overnight, RT. For synthesis of *N*-methyl compounds methods **a** and **b** were utilized (not depicted). For quantities and detailed procedures see Supporting Information.

experiments, no consumption of the activated 2,6-dimethylbenzoic acid was observed when using DEPBT. Utilizing PyBOP as an alternative coupling reagent<sup>[5b,d]</sup> resulted in the formation of the desired products. Nevertheless, the yields remained relatively low at only 38% in two cases. All final products had >95% purity, as determined by analytical HPLC.

#### *In vitro* plasma stability

All tested substances remained stable in human plasma over the test period of 120 min (as shown in Table 1). **MMV** exhibits a significant decrease in concentration in murine plasma.<sup>[17a]</sup> This result is comparable to the murine plasma stability published by Medicines for Malaria Venture (60% remaining substance after 4 h of incubation).<sup>[18]</sup> The only other compound with a comparable fast degradation in murine plasma was **25**,

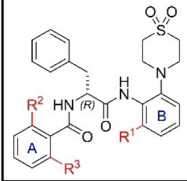
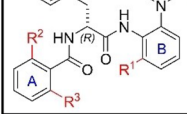
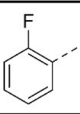
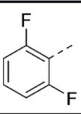
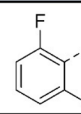
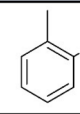
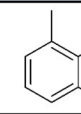
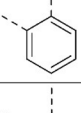
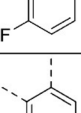
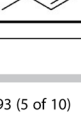
which differs from **MMV** by only one *N*-methyl group ( $R^5$ ). In contrast, **29** did not show a similar drop in concentration, which is possibly due to the *N*-methyl group protecting the anilide ( $R^4$ ).

Our previous study showed a high human and murine plasma stability of **2**.<sup>[17a]</sup> We observed the same for the new derivatives described herein. Altering both the morpholine to thiomorpholine dioxide as well as the *N*α-2-thiophenoyl to *N*α-2-fluorobenzoyl and *N*α-2-methylbenzoyl groups appeared to sufficiently enhance the plasma stability of the compounds.

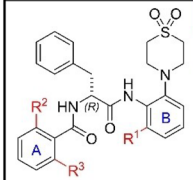
#### *In vitro* microsomal stability

All tested compounds showed a concentration decline in the microsomal suspensions (Table 2) used whereas stability in human microsomal suspensions was higher than in murine

**Table 1.** Remaining relative amounts of AAP derivatives after incubation in human and murine plasma for 120 min. Green marked fields indicate over 90% remaining substance. The values are means of two biological replicates.

Core structure	MMV		25		29		Legend				
	Human	Murine	Human	Murine	Human	Murine	Human	Murine			
	96%	60%	107%	21%	97%	91%					
Aromatic system A											
											
Aromatic system B		<b>2</b>	<b>3</b>	<b>4</b>	<b>5</b>	<b>6</b>					
		98%	92%	100%	101%	99%	99%	94%	89%	96%	92%
		<b>10</b>	<b>11</b>	<b>12</b>	<b>13</b>	<b>14</b>					
		96%	101%	100%	93%	96%	104%	99%	93%	96%	102%
		<b>19</b>	<b>20</b>	<b>21</b>	<b>22</b>	<b>23</b>					
		92%	91%	101%	100%	93%	93%	101%	95%	94%	96%

**Table 2.** Remaining substance [%] of AAP derivatives in murine and human microsomal suspensions after 7 min of incubation. Color coding compares remaining substance in the human and murine assays. Colors show the difference with respect to the average value. Dark green: highest percentage; light green: over average; white: closest to average; light red: below average, dark red: lowest percentage. The displayed values are means of two biological replicates. Propranolol was included as a reference.

Core structure	MMV		25		29		Propranolol (control)		Legend	
	Human after 7 min [%]	Murine after 7 min [%]	Human after 7 min [%]	Murine after 7 min [%]	Human after 7 min [%]	Murine after 7 min [%]	Human after 7 min [%]	Murine after 7 min [%]	Human after 7 min [%]	Murine after 7 min [%]
	Aromatic system A									
	2		3		4		5		6	
	6	1	29	10	20	5	42	6	28	9
	10		11		12		13		14	
	15	1	57	39	53	29	70	26	53	17
	19		20		21		22		23	
46	20	76	53	61	26	73	22	83	42	

microsomal suspensions in every case analyzed (exemplary curves are depicted in Figure 2).

MMV showed particularly low stability in human and murine microsomal suspensions with only 2% and 0% respectively remaining after 7 min. These results differ significantly from those published by Medicines for Malaria Venture for MMV. While they reported half-lives of 129 minutes in human microsomal suspension and 795 minutes in murine microsomal suspension.<sup>[18]</sup> Our study found much lower half-lives of 1.2 and

0.9 minutes, respectively. The observed difference may be due to differences in assay conditions. Medicines for Malaria Venture report briefly on the assay conditions used, including a substrate concentration of 0.5  $\mu\text{M}$ , 0.25 mg/mL microsomal proteins, and 50 mM phosphate buffer at pH 7.4.<sup>[18]</sup> In our assay, we used 2  $\mu\text{M}$  substrate concentration, 0.42 mg/mL microsomal proteins, and 100 mM phosphate buffer at pH 7.4. The authors did not disclose the usage of an NADPH-cofactor system, which is critical for oxidative metabolism catalyzed by microsomal

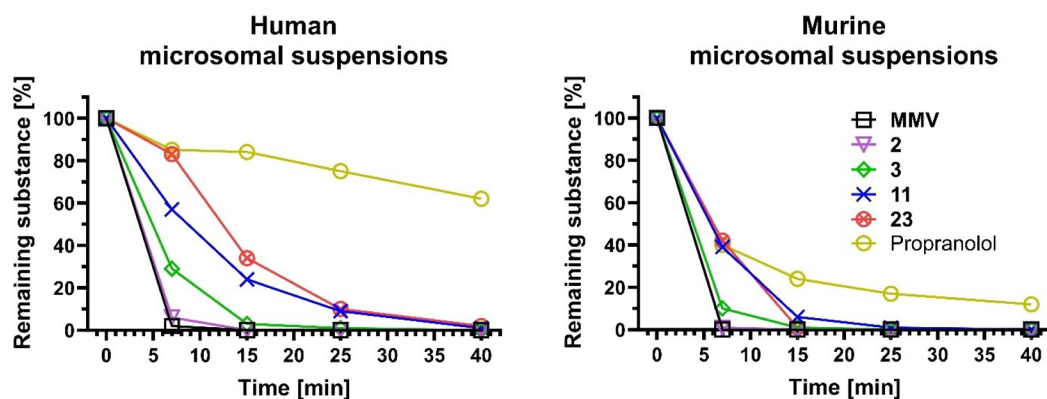


**Figure 2.** Degradation of a selection of compounds in human and murine microsomal suspensions over 40 min. Compounds 11 and 23 are shielded at aromatic system B with a 6-fluoro or 6-methyl substituent respectively and show higher stability than the unshielded derivatives (3). Displayed values are means of two replicates. Propranolol is shown as reference.

enzymes. If this component is not utilized, it could explain the observed difference in microsomal stability.

The *N*-methylated compounds **25** and **29** did not exhibit superior performance to **MMV**. Compound **2**, the starting point for the series reported herein, showed comparably low stabilities. This result shows that the sole replacement of morpholine by thiomorpholine dioxide and thiophene carboxamide by 2-fluoro benzamide does not increase the microsomal stability as was observed for the plasma stability.

Modifying the aromatic system A of **2** to provide further shielding of the adjacent amide bond only showed a slight tendency to increased microsomal stabilities, independent of the substituents introduced. Increased stabilities were however achieved in combination with fluoro- and methyl-substitutions in aromatic system B. There was only a small increase in stability when 2-fluoro benzamide (aromatic system A) was used in combination with a fluoro substituent at aromatic system B (compound **10**). Nevertheless, a tendency to higher stabilities could be observed with a methyl group in aromatic system B (compound **19**).

For all other substitution patterns in aromatic system A, increased stabilities were observed when combined with either methyl or fluoro substitutions in aromatic system B. The highest stability increases in human microsomal suspensions (5.5- to 6.5-fold) were observed for **13** and **22** (a combination of *N*α-2-methylbenzoyl with 6-fluoro or 6-methyl substitutions, respectively). In contrast, the highest stability increases for murine microsomal suspensions (4- to 5-fold) were obtained with the

combination of *N*α-2,6-difluorobenzoyl group together with 6-fluoro or 6-methyl substitutions.

### Antimycobacterial activity assessment

Growth inhibition testing was performed through microdilution assays against a selection of mycobacteria. The results of the assays are depicted in Table 3.

The activities appear to be largely unaffected when aromatic system A was derivatized. Only the *N*α-2,6-dimethylbenzoyl derivative caused an overall decline in activity (see compounds **6** and **14**). All other substitution patterns are well accepted, with the tendency that the *N*α-2,6-difluorobenzoyl containing compounds showed the highest activities with **3** showing the highest activity (all activities in the nanomolar range). Even in combination with the fluoro-substituted aromatic system B, low micromolar activities against *Mavium* and *Mtb* and sub-micromolar activities against *Mycobacterium intracellulare* (*Mintra*) were observed (compound **11**). Particularly striking were the high activities of this compound class against the *Mintra* strain that we tested.

Changing the substitution pattern near and at the amide bonds strongly affected activity against the mycobacterial strains tested. The *N*-methylated compounds **25** and **29** suffered from complete activity loss, independent of the amide bond to which the *N*-methyl group was added. Likewise, derivatization of aromatic system B caused strong declines in

**Table 3.** MIC<sub>90</sub> values of the new AAP derivatives against different mycobacteria. Mabs = Mycobacterium abscessus ATCC 19977; Mintra = Mycobacterium intracellulare ATCC 35761; Mtb = Mycobacterium tuberculosis H37Rv; Mavium = Mycobacterium avium ssp. hominissuis strain 109 (MAC109). Incubation at 37 °C for three days (Mabs), five days (Mintra and Mavium) and seven days (Mtb). Experiments were performed in duplicate, results were averaged. Protocols for different strains differ slightly, for detailed information on the methodology see Supporting Information.

Core structure	MMV		25		29		Legend	
	Mabs	Mintra	Mabs	Mintra	Mabs	Mintra	Mabs	Mintra
Core structure	6.25	0.78	100	> 100	100	> 100		
	0.66	3.02	> 50	> 50	> 50	> 50		
Aromatic system A								
	<b>2</b>	<b>3</b>	<b>4</b>	<b>5</b>	<b>6</b>	<b>7</b>	<b>8</b>	<b>9</b>
Aromatic system B								
	<b>10</b>	<b>11</b>	<b>12</b>	<b>13</b>	<b>14</b>	<b>15</b>	<b>16</b>	<b>17</b>
	0.78	0.05	0.78	0.025	3.13	0.1	1.56	0.4
	0.25	0.99	0.15	0.6	0.66	1.47	0.4	1
	25	1.56	12.5	0.4	25	1.56	12.5	0.8
	16	12.9	5.5	5.43	28	13.5	12	9.8
<b>19</b>	<b>20</b>	<b>21</b>	<b>22</b>	<b>23</b>	<b>24</b>	<b>25</b>	<b>26</b>	
> 100	> 100	> 100	50	> 100	> 100	> 100	> 100	
> 50	> 50	> 50	> 50	> 50	> 50	> 50	> 50	

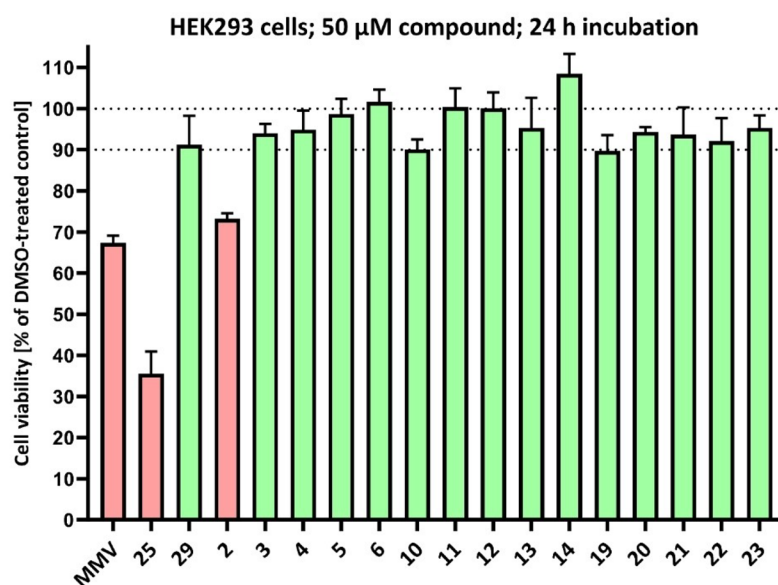


**Figure 3.** Cytotoxicity against human kidney epithelia cells HEK293. Determination of cell viability was performed at a single compound concentration of 50  $\mu$ M after 24 h of incubation relative to DMSO-treated cells. The displayed values are means  $\pm$  SD of triplicates. For detailed information of the protocol, see the Supporting information.

activity. The introduction of a fluoro substituent on the aromatic ring led to increased MIC<sub>90</sub> values, whereas the respective methyl substitution resulted in complete loss of activity. Only derivatives that contained a hydrogen atom next to the amide bond at aromatic system B showed improved MIC<sub>90</sub> values in comparison to the hit compound.

### Cytotoxicity

The compounds synthesized in this study were tested for their single concentration cytotoxicity against the immortalized human kidney epithelia cell line HEK293. To the best of our knowledge, AAPs have not been tested against this cell line so far. Cell viability relative to a DMSO-treated control is depicted in Figure 3.

Only three compounds caused a relative cell viability lower than 90%, including the hit compound **MMV** (67% viability) and also **2** (73% viability), which demonstrated high antimycobacterial activities. Both compounds have been tested against a variety of cell lines and displayed no concerning behavior.<sup>[17,18]</sup> The *N*-methyl compound **25** exhibited the highest cytotoxicity with only 35% viability. In contrast, the other *N*-methyl compound (**29**) did not demonstrate a high degree of cytotoxicity.

### Conclusions

Microsomal stability as a model for hepatic stability was used as an indicator of intrinsic clearance for AAPs. We observed that sterically shielding the amide bonds within the molecular structures of AAPs increases their microsomal stability. In particular, shielding of the anilide bond at the aromatic system B resulted in higher stabilities in microsomal suspensions.

Methyl substituents result in complete loss of whole cell activity, rendering these molecules unsuitable for further efficacy development, although compounds within this group demonstrated improved stabilities against murine (20) and human (22) microsomes. Antimycobacterial activity was observed with fluoro substituents making the respective fluorinated AAPs a valuable option for future efficacy development. The compound **11**, which carries fluorine atoms at all investigated positions, exhibits MIC<sub>90</sub> values between 0.4 and 12.5  $\mu$ M depending on the mycobacterial species combined with improved microsomal stabilities.

Modification of the aromatic system A was tolerated well with regard to the potency of the compounds. *N* $\alpha$ -2,6-dimethylbenzoyl and *N* $\alpha$ -2,6-difluorobenzoyl groups were found to be beneficial for microsomal stability, offering compounds that show higher or equal activities together with higher stabilities in comparison to both the hit compound and the most active compound **2** published so far.

*N*-methylation of the anilide bond resulted in increased plasma stability, whereas *N*-methylation of the *N* $\alpha$ -2-thiophenyl groups did not cause the same effect. This suggests that the

anilide bond of the hit compound is susceptible to hydrolysis and that it is stabilized by an adjacent *N*-methyl group.

Based on these results, we conclude that the AAP derivatives investigated have sufficient plasma stability for activity even without *N*-methylation, which is an improvement compared to the hit compound MMV. Thus, cleavage or metabolism by plasma components probably does not contribute to low *in vivo* plasma levels to a relevant extent.

These findings support the view that the stability issues of AAPs are probably due to the instability of the amide bonds. Useful additional information is provided by the observation that shielding of the anilide bond in aromatic system B results in increased stability. Future studies on the resulting metabolites will aid the design of AAPs for improved stability and activity.

## Supporting Information

CCDC 2293688 contains the supplementary crystallographic data for this paper. These data can be obtained free of charge from the Cambridge Crystallographic Data Centre via [www.ccdc.cam.ac.uk/structures](http://www.ccdc.cam.ac.uk/structures).

The authors have cited additional references within the Supporting Information.<sup>[23,25-42]</sup>

## Acknowledgements

We would like to thank Nadine Jänckel, Dr. Nadine Taudte and Dr. Jens-Ulrich Rahfeld for providing and maintaining the biosafety level 2 facility, Dr. Christian Ihling and Antje Herbrich-Peters for measuring the HRMS spectra, Professor Christian W. Lehmann for providing access to the X-ray diffraction facility and Heike Schrehl for technical assistance.

This work was funded by the Deutsche Forschungsgemeinschaft (DFG, German Research Foundation) – 432291016, the National Institute of Allergy and Infectious Diseases of the National Institutes of Health under award number R01AI132374 and Mukoviszidose Institut gGmbH project number 2202 (Bonn, Germany), the research and development arm of the German Cystic Fibrosis Association Mukoviszidose e. V. Open Access funding enabled and organized by Projekt DEAL.

## Conflict of Interests

The authors declare no conflict of interest.

## Data Availability Statement

The data that support the findings of this study are available from the corresponding author upon reasonable request.

**Keywords:** Phenylalanine amides · AAPs · *Mycobacterium abscessus* · microsomal stability · RNA polymerase · Tuberculosis · NTM

- [1] World Health Organization, "Global Tuberculosis Report 2023," can be found under <https://www.who.int/teams/global-tuberculosis-programme/tb-reports/global-tuberculosis-report-2023>, 2023.
- [2] a) J. H. Malenfant, T. F. Brewer, *Open Forum Infect. Dis.* **2021**, *8*, DOI 10.1093/OFID/OFAB018; b) I. Shah, V. Poojari, H. Meshram, *Indian J. Pediatr.* **2020**, *87*, 833–839; c) B. J. Seaworth, D. E. Griffith, *Microbiol. Spectrum* **2017**, *5*, DOI 10.1128/MICROBIOLSPEC.TNM17-0042-2017; d) F. Conradi, A. H. Diacon, N. Ngubane, P. Howell, D. Everitt, A. M. Crook, C. M. Mendel, E. Egizi, J. Moreira, J. Timm, T. D. McHugh, G. H. Wills, A. Bateson, R. Hunt, C. Van Niekerk, M. Li, M. Olugbosi, M. Spigelman, *N. Engl. J. Med.* **2020**, *382*, 893–902.
- [3] D. R. Prevots, J. E. Marshall, D. Wagner, K. Morimoto, *Clin. Chest Med.* **2023**, DOI 10.1016/J.CCM.2023.08.012.
- [4] M. D. Johansen, J. L. Herrmann, L. Kremer, *Nat. Rev. Microbiol.* **2020**, *18*, 392–407.
- [5] a) M. Yan, S. K. Brode, T. K. Marras, *Clin. Chest Med.* **2023**, DOI 10.1016/j.ccm.2023.06.011; b) C. L. Daley, J. M. Iaccarino, C. Lange, E. Cambau, R. J. Wallace, C. Andrejak, E. C. Böttger, J. Brozek, D. E. Griffith, L. Guglielmetti, G. A. Huit, S. L. Knight, P. Leitman, T. K. Marras, K. N. Olivier, M. Santin, J. E. Stout, E. Tortoli, J. Van Ingen, D. Wagner, K. L. Winthrop, *Eur. Resp. J.* **2020**, *71*, E1–E36. c) M.-V. H. Nguyen, C. L. Daley, *Clin. Chest Med.* **2023**, DOI 10.1016/j.ccm.2023.06.009; d) M. R. Holt, T. Baird, *Clin. Chest Med.* **2023**, DOI 10.1016/j.ccm.2023.06.010.
- [6] T. Baird, S. Bell, *Clin. Chest Med.* **2023**, DOI 10.1016/j.ccm.2023.06.008.
- [7] M. R. Loebinger, J. K. Quint, R. van der Laan, M. Obradovic, R. Chawla, A. Kishore, J. van Ingen, *Chest* **2023**, *164*, 1115–1124.
- [8] a) C. Ruis, J. M. Bryant, S. C. Bell, R. Thomson, R. M. Davidson, N. A. Hasan, J. van Ingen, M. Strong, R. A. Floto, J. Parkhill, *Nat. Microbiol.* **2021**, *6*:10, 1279–1288; b) M. L. Aitken, A. Limaye, P. Pottinger, E. Whimbey, C. H. Goss, M. R. Tonelli, G. A. Cangelosi, M. Ashworth Dirac, K. N. Olivier, B. A. Brown-Elliott, S. McNulty, R. J. Wallace, *Am. J. Respir. Crit. Care Med.* **2012**, *185*, 231–232.
- [9] a) M. M. Johnson, J. A. Odell, *J Thorac Dis* **2014**, *6*, 210; b) R. C. Lopeman, J. Harrison, M. Desai, J. A. G. Cox, *Microorganisms* **2019**, *Vol. 7*, Page 90 **2019**, *7*, 90; c) R. Nessar, E. Cambau, J. M. Reyat, A. Murray, B. Gicquel, *J. Antimicrob. Chemother.* **2012**, *67*, 810–818.
- [10] L. Ballell, R. H. Bates, R. J. Young, D. Alvarez-Gomez, E. Alvarez-Ruiz, V. Barroso, D. Blanco, B. Crespo, J. Escribano, R. González, S. Lozano, S. Huss, A. Santos-Villarejo, J. J. Martin-Plaza, A. Mendoza, M. J. Rebollo-Lopez, M. Remuñan-Blanco, J. L. Lavandera, E. Pérez-Herran, F. J. Gamonito, J. F. García-Bustos, D. Barros, J. P. Castro, N. Cammack, *ChemMedChem* **2013**, *8*, 313–321.
- [11] S. Ebricht, R. H. Ebricht, Y. W. Mandal, S. Wilde, R. Li, *Preparation of N-Alpha-Aroyl-N-Aryl-Phenylalaninamides as Inhibitors of Bacterial RNA Polymerase and as Antibacterials*, **2015**, WO2015120320 A1 2015-08-13.
- [12] a) A. Richter, A. Strauch, J. Chao, M. Ko, Y. Av-Gay, *Antimicrob Agents Chemother* **2018**, *62*, DOI 10.1128/AAC.00828-18; b) J. Jeong, G. Kim, C. Moon, H. J. Kim, T. H. Kim, J. Jang, *PLoS One* **2018**, *13*, e0195595; c) J. L. Low, M. L. Wu, D. B. Aziz, B. Laleu, T. Dick, *Front. Microbiol.* **2017**, *8*, 1539.
- [13] W. Lin, S. Mandal, D. Degen, Y. Liu, Y. W. Ebricht, S. Li, Y. Feng, Y. Zhang, S. Mandal, Y. Jiang, S. Liu, M. Gigliotti, M. Talaue, N. Connell, K. Das, E. Arnold, R. H. Ebricht, *Mol. Cell* **2017**, *66*, 169–179.e8.
- [14] L. Mann, U. S. Ganapathy, R. Abdelaziz, M. Lang, M. D. Zimmerman, V. Dartois, T. Dick, A. Richter, *Microbiol. Spectrum* **2022**, *10*, DOI 10.1128/SPECTRUM.02760-22.
- [15] a) A. Rominski, A. Roditscheff, P. Selchow, E. C. Böttger, P. Sander, *J. Antimicrob. Chemother.* **2017**, *72*, 376–384; b) T. Lan, U. S. Ganapathy, S. Sharma, Y.-M. Ahn, M. Zimmerman, V. Molodtsov, P. Hegde, M. Gengenbacher, R. H. Ebricht, V. Dartois, J. S. Freundlich, T. Dick, C. C. Aldrich, *Angew. Chem.* **2022**, *134*, e202211498; c) M. T. Zaw, N. A. Emran, Z. Lin, *J. Infect. Public Health* **2018**, *11*, 605–610.
- [16] U. S. Ganapathy, T. Lan, P. Krastel, M. Lindman, M. D. Zimmerman, H. P. Ho, J. P. Sarathy, J. C. Evans, V. Dartois, C. C. Aldrich, T. Dick, *Antimicrob. Agents Chemother.* **2021**, *65*, DOI <https://doi.org/10.1128/AAC.00978-21>.
- [17] a) M. Lang, U. S. Ganapathy, L. Mann, R. Abdelaziz, R. W. Seidel, R. Goddard, I. Sequenzia, S. Hoenke, P. Schulze, W. W. Aragaw, R. Csuk, T. Dick, A. Richter, *J. Med. Chem.* **2023**, DOI 10.1021/ACS.JMEDCHEM.3C00009; b) L. Mann, M. Lang, P. Schulze, J. H. Halz, R. Csuk, S. Hoenke, R. W. Seidel, A. Richter, *Amino Acids* **2021**, *53*, 1187–1196.

- [18] Medicines for Malaria Venture, "Biological Data and DMPK Data of the Pathogen Box Compounds," can be found under <https://www.mmv.org/mmv-open/pathogen-box/about-pathogen-box>, 2015.
- [19] A. Beuchel, D. Robaa, D. A. Negatu, A. Madani, N. Alvarez, M. D. Zimmerman, A. Richter, L. Mann, S. Hoenke, R. Csuk, T. Dick, P. Imming, *ACS Med. Chem. Lett.* **2022**, acsmedchemlett.1c00549.
- [20] F. G. Bahar, K. Ohura, T. Ogihara, T. Imai, *J. Pharm. Sci.* **2012**, *101*, 3979–3988.
- [21] P. R. Bradshaw, I. D. Wilson, R. U. Gill, P. J. Butler, C. Dilworth, T. J. Athersuch, *Sci. Rep.* **2018**, *8*, 1–8.
- [22] L. Liu, J. S. Halladay, Y. Shin, S. Wong, M. Coraggio, H. La, M. Baumgardner, H. Le, S. Gopaul, J. Boggs, P. Kuebler, J. C. Davis Jr, X. Charlene Liao, J. W. Lubach, A. Deese, C. Gregory Sowell, K. S. Currie, W. B. Young, S. Cyrus Khojasteh, C. E. C. A. Hop, H. Wong, *Drug Metab. Dispos.* **2011**, DOI 10.1124/dmd.111.040840.
- [23] a) L. Midgley, L. J. Bourhis, O. V. Dolomanov, S. Grabowsky, F. Kleemiss, H. Puschmann, N. Peyerimhoff, *Acta Crystallogr., Sect. A: Found. Crystallogr.* **2021**, *77*, 519–533; b) F. Kleemiss, O. V. Dolomanov, M. Bodensteiner, N. Peyerimhoff, L. Midgley, L. J. Bourhis, A. Genoni, L. A. Malaspina, D. Jayatilaka, J. L. Spencer, F. White, B. Grundkötter-Stock, S. Steinhauer, D. Lentz, H. Puschmann, S. Grabowsky, *Chem. Sci.* **2021**, *12*, 1675–1692.
- [24] Y. Ruetsch, T. Boni, A. Borgeat, *Curr. Top. Med. Chem.* **2001**, *1*, 175–182.
- [25] a) A. Robert, J. R. Schultz, J. E. Nezamis, C. Lancaster, *Gastroenterology* **1976**, *70*, 359–370; b) E. J. Barreiro, A. E. Kümmerle, C. A. M. Fraga, *Chem. Rev.* **2011**, *111*, 5215–5246; c) E. Z. Dajani, D. R. Driskill, R. G. Bianchi, P. W. Collins, R. Pappo, *Am. J. Dig. Dis.* **1976**, *21*, 1049–1057.
- [26] R. H. P. Van Neer, P. K. Dranchak, L. Liu, M. Aitha, B. Queme, H. Kimura, T. Katoh, K. P. Battaile, S. Lovell, J. Inglese, H. Suga, *ACS Chem. Biol.* **2022**, *17*, 2284–2295.
- [27] F. Haviv, T. D. Fitzpatrick, R. E. Swenson, C. J. Nichols, N. A. Mort, E. N. Bush, G. Diaz, G. Bammert, A. Nguyen, N. S. Rhutasel, H. N. Nellans, D. J. Hoffman, E. S. Johnson, J. Greer, *J. Med. Chem.* **1993**, *36*, 363–369.
- [28] A. L. L. García, *Synlett* **2007**, 1328–1329.
- [29] J. R. Dunetz, Y. Xiang, A. Baldwin, J. Ringling, *Org. Lett.* **2011**, *13*, 5048–5051.
- [30] APEX4 v2022.10-0. **2019**, Bruker AXS Inc., Madison, Wisconsin, USA.
- [31] SAINT V8.40B. **2019**, Bruker AXS Inc.: Madison, Wisconsin, USA.
- [32] L. Krause, et al., *J. Appl. Crystallogr.* **2015**, *48*(1), 3–10.
- [33] G. M. Sheldrick, *Acta Crystallogr., Sect. A: Found. Crystallogr.* **2015**, *71*, 3–8.
- [34] G. M. Sheldrick, *Acta Crystallogr., Sect. C: Cryst. Struct. Commun.* **2015**, *71*, 3–8.
- [35] O. V. Dolomanov, et al., *J. Appl. Crystallogr.* **2009**, *42*, 339–341.
- [36] F. Neese, et al., *J. Chem. Phys.* **2020**, *152*, 224108.
- [37] a) A. D. Becke, *J. Chem. Phys.* **1993**, 5648–5652; b) C. Lee, W. Yang, R. G. Parr, *Phys. Rev. B: Condens. Matter* **1988**, *37*, 785–789.
- [38] H. Flack, *Acta Crystallogr., Sect. A: Found. Crystallogr.* **1983**, *39*(6), 876–881.
- [39] R. W. W. Hoof, L. H. Straver, A. L. Spek, *J. Appl. Crystallogr.* **2010**, *43*(4), 665–668.
- [40] C. F. Macrae, et al., *J. Appl. Crystallogr.* **2020**, *53*, 226–235.
- [41] A. L. Spek, *Acta Crystallogr., Sect. D: Biol. Crystallogr.* **2009**, *65*, 148–155.
- [42] X. Yang, W. Wedajo, Y. Yamada, S. L. Dahthroth, J. J. L. Neo, T. Dick, W. K. Chui, *Eur. J. Med. Chem.* **2018**, *144*, 262–276. <https://doi.org/10.1016/J.EJMECH.2017.12.017>.

Manuscript received: October 30, 2023

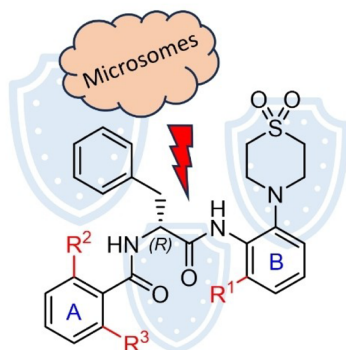
Revised manuscript received: February 6, 2024

Accepted manuscript online: February 8, 2024

Version of record online: ■■■■■

## RESEARCH ARTICLE

*N* $\alpha$ -aroyl-*N*-aryl-phenylalanine amides (AAPs) are active against numerous mycobacteria including *Mycobacterium tuberculosis* and *Mycobacterium abscessus*. As peptides, they are rapidly degraded in human and murine microsomal suspensions. Adding small substituents to the residues adjacent to the amide bonds, in particular at the anilide bond, results in increased stability.



M. Lang, Dr. U. S. Ganapathy, L. Mann,  
Dr. R. W. Seidel, Dr. R. Goddard, Dr. F.  
Erdmann, Prof. Dr. T. Dick, Dr. A.  
Richter\*

1 – 11

Synthesis and *in vitro* Metabolic  
Stability of Sterically Shielded Anti-  
mycobacterial Phenylalanine Amides



## 2.4) Research Article III

# Broad-Spectrum *In Vitro* Activity of *N*-aroyl-*N*-aryl-Phenylalanine Amides against Non-Tuberculous Mycobacteria and Comparative Analysis of RNA Polymerases

Markus Lang, Uday S. Ganapathy, Lea Mann, Rüdiger W. Seidel, Richard Goddard, Frank Erdmann, Thomas Dick, Adrian Richter

MDPI

Antibiotics

*Antibiotics*, 2024, 13(5), 404

Publication Date: 28.04.2024

DOI: 10.3390/antibiotics13050404

### Summary

This article investigates the antimicrobial efficacy of previously published AAPs against 25 NTM isolates of different species, including significant pathogens like *M. abscessus* and *M. avium* complex and further NTM that occur as human pathogens occasionally. The presented results demonstrate that AAPs exhibit activity against the selected mycobacteria, although their effectiveness varies among different species, with *M. ulcerans* showing high susceptibility and *M. xenopi* and *M. simiae* showing a greater level of resistance. A comparative analysis of the RNAP  $\beta$  and  $\beta'$  subunits primary structures revealed strain-specific polymorphisms that may contribute to differences in susceptibility. Given the high degree of conservation in the RNAP target structures, which cannot sufficiently explain the variations in compound activity, the study concludes that the activity must be influenced by factors beyond drug-target interaction, such as different bacterial metabolism and other evasion mechanisms.

### Own contributions

Microbiological testing, Alignment analysis of target structures, preparation of figures, conceptualization of the draft, original draft preparation, review and editing

## Article

# Broad-Spectrum In Vitro Activity of $N\alpha$ -Aroyl- $N$ -Aryl-Phenylalanine Amides against Non-Tuberculous Mycobacteria and Comparative Analysis of RNA Polymerases

Markus Lang <sup>1,2,†</sup>, Uday S. Ganapathy <sup>2,†</sup>, Rana Abdelaziz <sup>1</sup>, Thomas Dick <sup>2,3,4,\*</sup>  and Adrian Richter <sup>1,\*</sup> 

<sup>1</sup> Institut für Pharmazie, Martin-Luther-Universität Halle-Wittenberg, Kurt-Mothes-Straße. 3, 06120 Halle (Saale), Germany; markus.lang@pharmazie.uni-halle.de (M.L.); rana.abdelaziz@pharmazie.uni-halle.de (R.A.)

<sup>2</sup> Center for Discovery and Innovation, Hackensack Meridian Health, 111 Ideation Way, Nutley, NJ 07110, USA; uday.ganapathy@hnh-cdi.org

<sup>3</sup> Department of Medical Sciences, Hackensack Meridian School of Medicine, 123 Metro Boulevard, Nutley, NJ 07110, USA

<sup>4</sup> Department of Microbiology and Immunology, Georgetown University, 3900 Reservoir Road, Washington, DC 20007, USA

\* Correspondence: thomas.dick.cdi@gmail.com (T.D.); adrian.richter@pharmazie.uni-halle.de (A.R.)

† These authors contributed equally to this work.

**Abstract:** This study investigates the in vitro activity of  $N\alpha$ -aroyl- $N$ -aryl-phenylalanine amides (AAPs), previously identified as antimycobacterial RNA polymerase (RNAP) inhibitors, against a panel of 25 non-tuberculous mycobacteria (NTM). The compounds, including the hit compound MMV688845, were selected based on their structural diversity and previously described activity against mycobacteria. Bacterial strains, including the *M. abscessus* complex, *M. avium* complex, and other clinically relevant NTM, were cultured and subjected to growth inhibition assays. The results demonstrate significant activity against the most common NTM pathogens from the *M. abscessus* and *M. avium* complexes. Variations in activity were observed against other NTM species, with for instance *M. ulcerans* displaying high susceptibility and *M. xenopi* and *M. simiae* resistance to AAPs. Comparative analysis of RNAP  $\beta$  and  $\beta'$  subunits across mycobacterial species revealed strain-specific polymorphisms, providing insights into differential compound susceptibility. While conservation of target structures was observed, differences in compound activity suggested influences beyond drug–target interactions. This study highlights the potential of AAPs as effective antimycobacterial agents and emphasizes the complex interplay between compound structure, bacterial genetics, and in vitro activity.

**Keywords:**  $N\alpha$ -aroyl- $N$ -aryl-phenylalanine amides; RNA polymerase; *M. abscessus*; NTM; non-tuberculous mycobacteria; MMV688845; AAPs



**Citation:** Lang, M.; Ganapathy, U.S.; Abdelaziz, R.; Dick, T.; Richter, A. Broad-Spectrum In Vitro Activity of  $N\alpha$ -Aroyl- $N$ -Aryl-Phenylalanine Amides against Non-Tuberculous Mycobacteria and Comparative Analysis of RNA Polymerases. *Antibiotics* **2024**, *13*, 404. <https://doi.org/10.3390/antibiotics13050404>

Academic Editor: Mehran Monchi

Received: 5 April 2024

Revised: 17 April 2024

Accepted: 23 April 2024

Published: 28 April 2024



**Copyright:** © 2024 by the authors. Licensee MDPI, Basel, Switzerland. This article is an open access article distributed under the terms and conditions of the Creative Commons Attribution (CC BY) license (<https://creativecommons.org/licenses/by/4.0/>).

## 1. Introduction

Within the field of infectious diseases, the exploration of mycobacterial infections has always revolved around the formidable presence of *Mycobacterium tuberculosis* (Mtb), rightfully claiming its place as a global health concern [1]. However, amidst this predominant focus, a group of less discussed yet clinically relevant entities is emerging—non-tuberculous mycobacteria (NTM) [2–5]. NTM, comprised of over 190 species, are ubiquitous in the environment, inhabiting soil, water sources, and various organic substrates. These mycobacterial species, distinct from their tuberculosis-causing congener, have garnered increasing attention in recent years due to their diverse clinical manifestations and growing significance in healthcare settings worldwide [6].

While historically deemed harmless environmental dwellers, their potential to cause diseases in immunocompromised populations and individuals with chronic respiratory con-

ditions like cystic fibrosis [7–10] or bronchiectasis [11] has highlighted their clinical relevance. NTM infections manifest across a spectrum of clinical presentations that includes pulmonary, cutaneous [12,13], and disseminated forms. Often characterized by a protracted and subtle onset, these infections cause diagnostic dilemmas that lead to delays in appropriate therapeutic interventions, thereby amplifying patient morbidity and mortality rates.

Epidemiological studies worldwide unveil a rising trend in NTM-associated diseases [14–16], particularly among immunocompromised populations and individuals with chronic respiratory conditions. Moreover, advancements in diagnostic modalities, including molecular techniques and improved culturing methodologies, have unveiled a previously underestimated burden of NTM infections, underscoring the need for heightened clinical vigilance and a deeper understanding of their pathogenic mechanisms.

While the majority of NTM-related pulmonary infections are attributed to species such as the *Mycobacterium avium* complex (MAC) [10,17,18], and *Mycobacterium abscessus* complex (MABC) [19,20], there exist lesser-known species that sporadically provoke pulmonary manifestations. Their occurrence and distribution exhibit notable regional disparities, reflecting diverse environmental reservoirs and varying host susceptibilities across geographical regions [16,21]. Understanding the clinical relevance of these less common NTM species in pulmonary infections is crucial, especially in instances where conventional diagnostic tests may fail to identify the causative organism promptly. Their infrequent occurrence underscores the importance of vigilance among clinicians and microbiologists to consider these NTM species in the differential diagnosis of chronic or refractory pulmonary conditions.

Beyond their clinical impact, the management of NTM infections presents a formidable challenge. Their innate resistance to most anti-tubercular agents and other antibiotics, coupled with variations in susceptibility profiles among different species, necessitates tailored therapeutic regimens based on accurate identification and susceptibility testing as well as new antimycobacterial drugs to secure the treatment of patients.

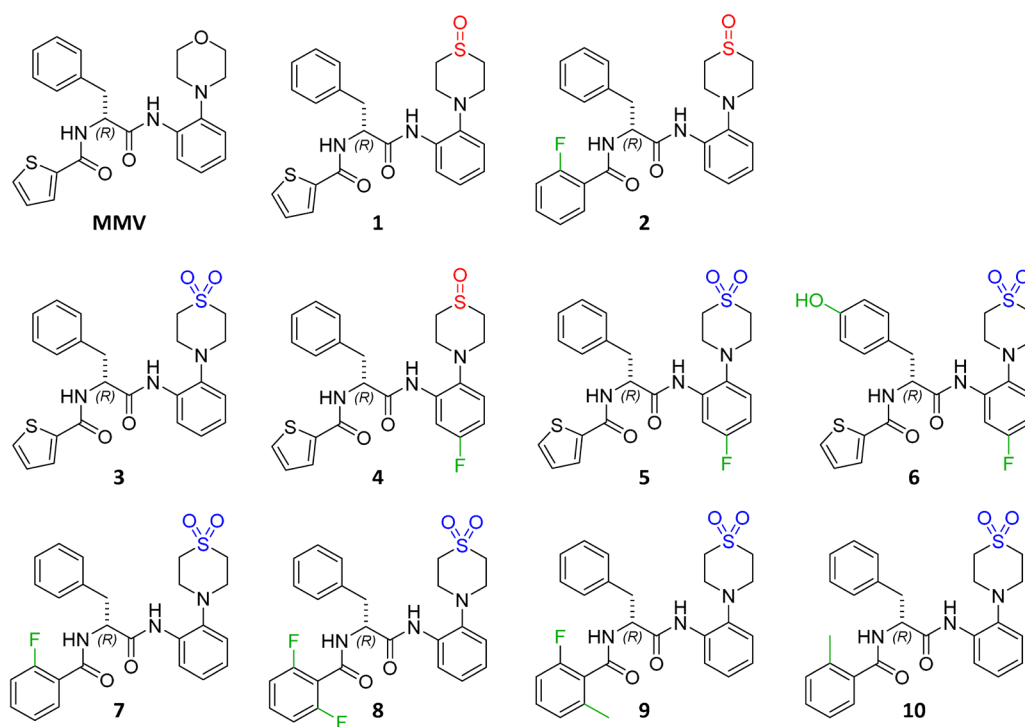
*N*α-aryl-*N*-aryl-phenylalanine amides (AAPs) represent a compound class that has displayed promising activity against *Mtb* and *Mycobacterium abscessus* [22–24], offering a potential avenue for novel therapeutic interventions against these challenging infections. Research exploring the medicinal chemistry [25–27] and antimycobacterial properties [28] of AAPs has shown encouraging results in vitro, demonstrating their ability to inhibit the growth of different mycobacterial species. This compound class's mechanism of action targets the essential mycobacterial RNA polymerase (RNAP) [29], disrupting key cellular processes and counteractions vital for their survival and propagation.

This study attempts to delve into the field of clinically relevant NTM species and their susceptibility to the promising compound class of AAPs. Therefore, a selection of active AAPs was tested against a broad panel of NTM to evaluate the therapeutic potential of the substance class across a broader range of NTM infections. We focused largely on type strains that are available from culture collections to allow for comparability. In addition to the published activity data of AAPs against *M. abscessus* subsp. *abscessus*, the two other subspecies of *M. abscessus*, subsp. *massiliense* and subsp. *bolletii*, are evaluated as well as a panel of clinical isolates of the *M. abscessus* complex. For the *M. avium* complex, two different strains of *M. avium* subsp. *hominissuis* (the most virulent *M. avium* subspecies for humans), *M. intracellulare*, and *M. chimaera* were tested. The set selected for mycobacteria that have occasionally emerged as human pathogens consists of their respective laboratory-type strains. It also contains the two soft tissue pathogens *M. marinum* and *M. ulcerans*, the causative agents of fish tank granuloma [30] and Buruli ulcer [31], respectively. A comparative approach serves as a foundation for unraveling the relationship between bacterial genomic diversity and antibiotic responses, ultimately contributing to the advancement of targeted antimicrobial therapies in the face of evolving mycobacterial resistance.

## 2. Results and Discussion

### 2.1. Selection of *N* $\alpha$ -Aroyl-*N*-Aryl-Phenylalanine Amide Compounds

The compounds selected for assessment against the strains described in this study were synthesized and characterized as described previously [25,32]. The selection of the test set considered their activity against previously tested mycobacteria, as well as diverse structural features that could affect the activity against different NTM species. Compounds 1 to 7 were synthesized during a detailed SAR study that varied the ring systems of the chemical scaffold in the search for better activity against NTM. The morpholine moiety was substituted by thiomorpholine sulfoxides and sulfones, which proved advantageous for the activity and solubility of the compound class, in addition to the exchange of the thiophene carboxylic acid amide to 2-fluorobenzoic acid amides. Compound 6 was included because it showed high activity while harbouring the hydroxyl group [25]. We also wanted to determine the influence of 5-fluoro substitution in para-position to the morpholine moiety (compounds 4 to 6). Compounds 8 to 10 showed high anti-NTM activity and have been synthesized and tested in a previous study with the aim to improve the stability of the compound class by additional sterical hindrance of the amide bonds [32]. The molecular structures of the tested compounds are given in Scheme 1 while their previously published activities against NTM can be found in Table 1. For comparative purposes, the initial hit compound of phenylalanine amides, MMV68845 (MMV), was included. Additionally, clarithromycin (CLR) was used as a positive control due to its clinical relevance.



**Scheme 1.** Chemical structures and identifiers of the AAPs evaluated against the test set of mycobacteria.

**Table 1.** Overview of previously published MIC<sub>90</sub> values for the compound test set utilized in this study. Shown values were calculated from two technical replicates. For detailed information regarding the determination of these values, see the respective reference.

	<i>M. abscessus</i> subsp. <i>abscessus</i> ATCC 19977	<i>M. tuberculosis</i> H37Rv	<i>M. intracellulare</i> subsp. <i>intracellulare</i> ATCC 35761	Ref.
ID	MIC <sub>90</sub> [μM]	MIC <sub>90</sub> [μM]	MIC <sub>90</sub> [μM]	
MMV	6.3	0.78	0.78	
1	3.13	0.40	0.10	
2	6.25	0.78	0.10	
3	3.13	0.20	0.10	[25]
4	3.13	0.40	0.05	
5	6.25	0.78	0.20	
6	6.25	0.78	0.05	
7	0.78	0.20	0.05	[25,32]
8	0.78	0.15	0.025	
9	3.13	0.66	0.10	[32]
10	1.56	0.40	0.40	

## 2.2. Inhibition of *M. abscessus* Complex

All the AAPs that were tested displayed activity against the selected *Mycobacterium abscessus* complex strains. An overview of the calculated MIC<sub>50</sub> values is given in Table 2. As microbial populations are often diverse and different strains may respond differently to antimicrobial agents under assay conditions, we decided to utilize the MIC<sub>50</sub> as a comparative measure of activity, because in some cases, MIC<sub>50</sub> values may reflect a more representative and comparable average than MIC<sub>90</sub> values, as the latter can be influenced by outliers and/or growth and plate effects [33]. The respective MIC<sub>90</sub> values for each compound and strain calculated from the same data sets are displayed in the Supplementary Materials.

**Table 2.** MIC<sub>50</sub> values of a selection of AAPs against type strains of the *Mycobacterium abscessus* complex. Cell shading from green to red indicates high to low activity. The displayed values are average values of two technical replicates.

	<i>M. abscessus</i> subsp. <i>abscessus</i> ATCC 19977	<i>M. abscessus</i> subsp. <i>massiliense</i> CCUG 48898-T	<i>M. abscessus</i> subsp. <i>bolletii</i> CCUG 50184-T
ID	MIC <sub>50</sub> [μM]	MIC <sub>50</sub> [μM]	MIC <sub>50</sub> [μM]
CLR	0.1	0.1	0.3
MMV	1.5	1.9	2.1
1	0.7	0.7	1.5
2	0.4	0.5	1.3
3	0.2	0.3	0.6
4	0.4	0.4	0.8
5	0.4	0.3	0.7
6	0.8	0.4	1.3
7	0.2	0.2	0.7
8	0.2	0.1	0.3
9	0.5	0.3	1.1
10	0.3	0.3	0.6

Testing CLR and the AAP hit compound MMV resulted in MIC<sub>50</sub> values well comparable to those reported in the literature [22,33] (see Figure 1 for exemplary dose–response

curves). The obtained MIC<sub>50</sub> values of the AAPs are generally in the low micromolar concentration range between 0.1  $\mu$ M and 2.1  $\mu$ M. While the MIC<sub>50</sub> values against subsp. *abscessus* were comparable to those against subsp. *massiliense*, there was a pattern of slightly lower activities against subsp. *bolletii*, which was also reported for other antibiotics [34]. Structures containing a sulfone moiety generally exhibit lower MIC<sub>50</sub> values, with compound **8** displaying the highest activity against all subspecies (subsp. *abscessus*: 0.2  $\mu$ M, subsp. *massiliense*: 0.1  $\mu$ M, subsp. *bolletii*: 0.3  $\mu$ M) translating to a 7–19-fold enhancement in activity against the various subspecies when compared to the hit compound MMV. Compound **7** and **8** that exhibited promising in vitro activity (MIC<sub>90</sub> of 0.78  $\mu$ M) against *M. abscessus* subsp. *abscessus* ATCC 19977 were further investigated against a range of clinical isolates of the *M. abscessus* complex, expanding the evaluation to a broader range of genotypes within this species (Table 3). The results demonstrated a comparable potency to the type strains, confirming their potential as effective antimicrobial agents for the treatment of *M. abscessus* infections.

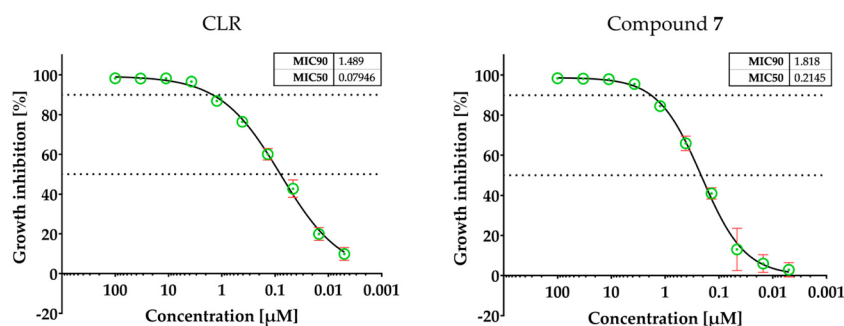


**Figure 1.** Exemplary dose–response curves of Clarithromycin and **7** against *Mycobacterium abscessus* subsp. *abscessus* ATCC 19977. Green data points are average values of two technical replicates. Red error bars display the respective standard deviation. The basis of MIC<sub>50</sub> determination was a curve fit performed with GraphPad Prism 10.0 utilizing a standard variable slope Hill function (bottom asymptote constrained to equal 0).

**Table 3.** MIC<sub>50</sub> values of a selection of AAPs against a panel of *Mycobacterium abscessus* complex clinical isolates. Cell shading from green to red indicates high to low activity. The displayed values are average values of two technical replicates. For detailed information on the origin of clinical isolates, see Section 3.

	<i>M. abscessus</i> subsp. <i>abscessus</i> Bamboo	<i>M. abscessus</i> subsp. <i>abscessus</i> M9	<i>M. abscessus</i> subsp. <i>abscessus</i> M199	<i>M. abscessus</i> subsp. <i>abscessus</i> M337	<i>M. abscessus</i> subsp. <i>abscessus</i> M404
ID	MIC <sub>50</sub> [ $\mu$ M]	MIC <sub>50</sub> [ $\mu$ M]	MIC <sub>50</sub> [ $\mu$ M]	MIC <sub>50</sub> [ $\mu$ M]	MIC <sub>50</sub> [ $\mu$ M]
CLR	0.1	0.2	0.4	0.2	0.1
MMV	1.7	1.8	1.8	1.4	1.7
7	0.4	0.4	0.4	0.3	0.4
8	0.2	0.3	0.3	0.3	0.3

	<i>M. abscessus</i> subsp. <i>abscessus</i> M422	<i>M. abscessus</i> subsp. <i>bolletii</i> M232	<i>M. abscessus</i> subsp. <i>bolletii</i> M506	<i>M. abscessus</i> subsp. <i>massiliense</i> M111
ID	MIC <sub>50</sub> [ $\mu$ M]	MIC <sub>50</sub> [ $\mu$ M]	MIC <sub>50</sub> [ $\mu$ M]	MIC <sub>50</sub> [ $\mu$ M]
CLR	0.2	0.3	0.1	0.05
MMV	1.2	1.9	1.4	0.6
7	0.2	0.4	0.3	0.2
8	0.2	0.4	0.2	0.2

### 2.3. Inhibition of *M. avium* Complex

The examined AAPs demonstrate substantial activity against the selected *M. avium* complex strains, with the determined MIC<sub>50</sub> values being in line with those against the *M. abscessus* complex (Table 4). A promising observation is that these derivatives show potent activity against the *M. avium* complex, with a 5-10-fold improvement in in vitro activity over the hit compound MMV688845. The high clinical relevance of *M. avium* complex infections, for which rifampicin's therapeutic benefits are controversial, emphasizes the potential of AAPs as novel RNAP inhibitors [29,35].

**Table 4.** MIC<sub>50</sub> values of a selection of AAPs against type strains of the *Mycobacterium avium* complex. Cell shading from green to red indicates high to low activity. The displayed values are average values of two technical replicates.

ID	<i>M. avium</i> subsp. <i>hominissuis</i> MAC109	<i>M. avium</i> subsp. <i>hominissuis</i> <i>M. avium</i> 11	<i>M. intracellulare</i> subsp. <i>intracellulare</i> ATCC 13950	<i>M. intracellulare</i> subsp. <i>chimaera</i> CCUG 50989
	MIC <sub>50</sub> [μM]	MIC <sub>50</sub> [μM]	MIC <sub>50</sub> [μM]	MIC <sub>50</sub> [μM]
CLR	0.4	0.4	0.2	0.3
MMV	3.2	1.0	1.0	1.1
1	1.3	0.5	1.6	0.6
2	1.1	0.5	1.0	0.6
3	0.8	0.4	0.6	0.4
4	0.7	0.3	0.6	0.3
5	0.6	0.3	0.5	0.4
6	0.4	0.2	0.7	0.3
7	0.8	0.3	0.4	0.3
8	0.4	0.1	0.2	0.2
9	1.4	0.6	0.7	0.6
10	0.6	0.3	0.4	0.3

### 2.4. Inhibition of Other NTM

The panel of AAPs was tested against a variety of NTM that occasionally occur as human pathogens. The respective MIC<sub>50</sub> values are displayed in Table 5. The selection showed activities in a comparable range to those seen against the *M. abscessus* complex and *M. avium* complex. Notable differences were seen for *M. xenopi* and *M. simiae*, against which activities were reduced. While clarithromycin showed an MIC<sub>50</sub> of 0.03 μM against *M. xenopi*, *M. simiae* was less susceptible (MIC<sub>50</sub> 10.7 μM) to clarithromycin, which is consistent with what has been reported in the literature [36–38]. *M. ulcerans* showed a high susceptibility to AAPs with MIC<sub>50</sub> values as low as 10 nM. A further difference is that certain mycobacterial species react differently to **6**, the only compound in which phenylalanine is replaced by tyrosine. The presence of an additional hydroxyl group reduces the activity in *M. kansasii*, *M. malmoense*, *M. marinum* and *M. szulgai*, with activities always lower than those of the hit compound MMV. For *M. ulcerans* and *M. xenopi*, **6** shows the highest activities among all tested compounds. This suggests that a higher polarity of the compounds may be advantageous for in vitro activity against these strains.

**Table 5.** MIC<sub>50</sub> values of a selection of AAPs against type strains of the different NTM. Cell shading from green to red indicates high to low activity. The displayed values are average values of two technical replicates.

	<i>M. chelonae</i> ATCC 35752	<i>M. fortuitum</i> ATCC 6841	<i>M. szulgai</i> ATCC 35799	<i>M. xenopi</i> ATCC 19250	<i>M. ulcerans</i> S4018	<i>M. marinum</i> ATCC 927	<i>M. simiae</i> ATCC 25275	<i>M. malmoense</i> ATCC 29571	<i>M. kansasii</i> ATCC 12478
ID	MIC <sub>50</sub> [μM]	MIC <sub>50</sub> [μM]	MIC <sub>50</sub> [μM]	MIC <sub>50</sub> [μM]	MIC <sub>50</sub> [μM]	MIC <sub>50</sub> [μM]	MIC <sub>50</sub> [μM]	MIC <sub>50</sub> [μM]	MIC <sub>50</sub> [μM]
CLR	0.1	0.6	0.2	0.03	0.05	1.6	10.7	0.2	0.2
MMV	0.7	1.3	0.4	16.2	0.24	0.5	12.4	1.1	0.3
1	0.3	1.2	0.7	5.9	0.08	1.4	23.0	0.9	0.8
2	0.2	0.7	0.4	4.3	0.05	0.6	9.8	0.7	0.3
3	0.2	0.8	0.4	2.1	0.04	0.4	9.3	0.8	0.3
4	0.2	0.5	0.5	2.1	0.03	0.9	9.1	0.9	0.3
5	0.3	0.4	0.3	1.1	0.03	0.5	4.3	0.8	0.1
6	0.2	0.6	0.7	0.6	0.01	2.0	7.3	1.9	0.6
7	0.1	0.4	0.2	2.0	0.03	0.2	3.9	0.4	0.1
8	0.1	0.2	0.1	0.8	0.01	0.2	2.9	0.2	0.1
9	0.3	1.0	0.4	2.7	0.05	0.7	12.5	0.7	0.3
10	0.2	0.5	0.2	1.5	0.03	0.4	5.5	0.5	0.2

### 2.5. Comparative Analysis of RNAP $\beta$ and $\beta'$ Subunits

In this study, we employed comparative alignment analysis to investigate the genomic diversity among the selected mycobacterial strains and elucidate whether alterations of the protein primary structure within the binding pocket of AAPs could explain the observed differences in AAP susceptibility. By integrating the primary target sequences of the  $\beta$  and  $\beta'$  RNAP subunits from the mycobacterial strains in protein–protein alignment (performed within positions 450–600 and 800–880 for the  $\beta$  and  $\beta'$  subunits, respectively, the complete alignment in this area can be found in the Supplementary Materials), we identified strain-specific amino acid variations in comparison to the reference sequence of a published protein structure of *Mtb* RNAP that was co-crystallized with the AAP [29] analog D-AAP1 (PDB: 5UHE). An overview of the contacts of D-AAP1 and its RNAP binding site based on PDB: 5UHE is given in Figure 2. AAPs are highly active against the *Mtb*-type strain ATCC 25618 H37Rv [22,24,25]. The results of the alignment analysis are displayed in Figure 3. The table was constrained to show amino acid variations located within a 7 Å distance of target-bound D-AAP1 [29] to the surrounding amino acids to limit the analysis to the area around the binding site. *Mtb* RNAP positions that did not show variations for any strain were excluded from the depiction as well as strains that did not show any polymorphisms in these areas.

The overall sequence identity of the *Mtb*  $\beta$  subunit to the NTM  $\beta$  subunits is high (89% to 95%), with the trend that the fast-growing mycobacteria (*M. chelonae*, *M. fortuitum* and *M. abscessus*) show lower identity values (89–91%), while the skin pathogens *M. ulcerans* and *M. marinum* have 95% identity each and even 99% identity in the region that contains the AAP binding site (positions 450–600). *M. chelonae*, *M. fortuitum*, *M. xenopi* and *M. abscessus* all display an alanine-to-glycine variation at position 565 of the  $\beta$  subunit in close proximity to the AAP binding site. However, this variation does not appear to affect their susceptibilities possibly due to the minor differences in volume and polarity between alanine and glycine. In *M. fortuitum*, a leucine to methionine exchange (Grantham’s distance 15, a measure of the similarity of amino acids in protein structures that combines the composition, volume and polarity for comparison, in which small values indicate high similarity and high values indicate low similarity [39]) occurs at position 560, which does not seem to result in lower activities in this case. This particular position reportedly resulted in a resistant *M. abscessus* Bamboo strain after a leucine to proline exchange [28] (Grantham’s distance 98). The leucine at position 560 ensures a transition to a random coil formation (R562-V568) that is in direct contact with AAP structures and is therefore crucial for the right orientation of the binding pocket. As proline disrupts secondary structures, this variation could cause a conformational change in the binding site that cannot be compensated. Additionally, *M. fortuitum* and *M. xenopi* display a proline to serine exchange at position 477, which is an essential lipophilic binding contact to AAP’s anilide aromatic system and the phenylalanine

aromatic system. Its importance for the interaction was demonstrated by the formation of a resistant mutant after a proline to leucine variation [28]. Leucine exhibits similar lipophilic properties as the proline side chain, but its higher spatial demand causes clashes with the anilide aromatic system and the random coil formation (R562-V568), altering the arrangement of the binding pocket and leading to AAP resistance. The proline–serine exchange of *M. fortuitum* and *M. xenopi* leads to a binding pocket that is less hydrophobic but has a similar volume to the native proline conformation, resulting in AAP activity. However, the binding of AAPs could be restricted due to the differences in polarity, which might be a part of the explanation for the slightly lower activities in *M. fortuitum* and the loss of activity against *M. xenopi*.

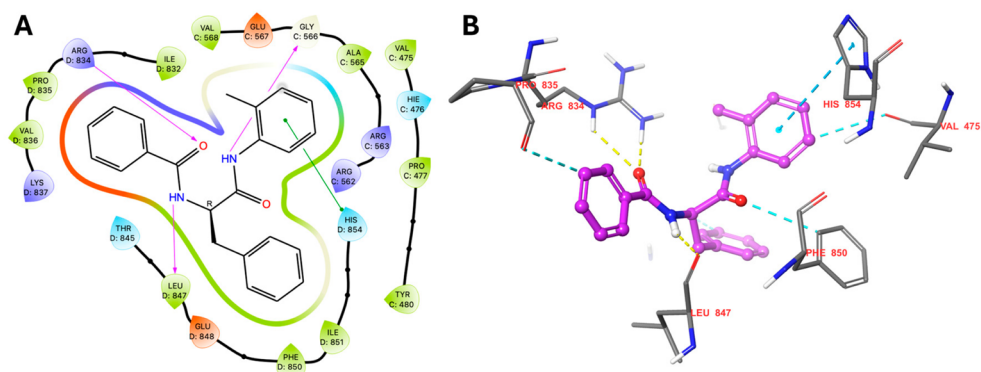


**Figure 2.** D-AAP1 target interactions based on PDB: 5UHE. (A) Two-dimensional summary of interactions. Purple arrows: hydrogen bonds; green lines: pi stacking interaction. (B) Three-dimensional depiction of the binding pose. Yellow dashed lines: hydrogen bonds, blue dashed line: pi stacking interaction; turquoise dashed line: aromatic hydrogen bonds. Visualization generated with the Maestro graphical interface (Schrödinger Release 2022-3: Maestro, Schrödinger, LLC, New York, NY, USA, 2021).

Comparing the sequence identities of the *Mtb*  $\beta'$  subunit with their NTM counterparts, we observed high degrees of homology (90–97% sequence identity), whereas the lowest value of 90% was found for *M. abscessus* and the highest values were again found for *M. ulcerans* and *M. marinum*, which showed 97% each. The  $\beta'$  subunit of *Mtb* shows two clusters of amino acids that build up the binding surface to AAPs. Only two variations were observed within a 7 Å distance to the AAP binding site. A prominent variation that all displayed NTM strains exhibit is the valine to isoleucine exchange at position 836. This position is close to the aryl carboxylic acid amide structure of the AAPs and contributes to the lipophilic surface that interacts with the aromatic system. We do not expect that this amino acid exchange affects activities, as the additional methylene group in isoleucine is not largely affecting the properties of the binding pocket in the matter of polarity. The additional expansion does not appear to influence binding and activity. The only other variation present was found in *M. abscessus* ATCC 19977, where phenylalanine 831 is changed to tyrosine (Grantham's distance 22). However, this alteration does not seem to affect the activity against *M. abscessus* ATCC 19977. The side chain of the phenylalanine is oriented away from the AAP binding site into an unrelated, open cleft resulting in no direct interaction. Phenylalanine and tyrosine share similar properties, making it probable that the same is true for tyrosine. Still, the exchange could lead to differences in the geometry of the binding pocket due to its proximity to the binding site.

	MIC <sub>50</sub> MMV [μM]	Sequence Positions				
		β Subunit			β' Subunit	
		477	560	565	831	836
<i>M. tuberculosis</i> ATCC 25618	< 0.2 <sup>a</sup>	P	L	A	F	V
<i>M. chelonae</i> ATCC 35752	0.7	.	.	G	.	I
<i>M. fortuitum</i> ATCC 6841	1.3	S	M	G	.	I
<i>M. xenopi</i> ATCC 19250	16	S	.	G	.	I
<i>M. abscessus</i> ATCC 19977	1.5	.	.	G	Y	I
<i>M. ulcerans</i> S4018	0.24	.	.	.	.	I
<i>M. marinum</i> ATCC 927	0.5	.	.	.	.	I

**Figure 3.** Variations in β and β' RNAP subunits of mycobacterial strains compared to *Mtb* (sequence numbering refers to *Mtb* β and β' subunits derived from PDB: 5UHE). Violet indicators show positions with direct drug-target contacts. Yellow indicators show positions that resulted in resistant *M. abscessus* Bamboo mutants (P477L; L560P). Dots represent amino acid identity. Green indicates above-average activity of the respective compound, while red indicates below-average activity. a: Published MIC<sub>50</sub> value for *M. tuberculosis* ATCC 25618 [22].

The aromatic system of the phenylalanine part of AAPs extends into a lipophilic cleft of the β subunit. One of the constituents of the surface of this cleft is proline at position 477, which was previously discussed for *M. fortuitum* and *M. xenopi*. This amino acid is in close proximity to the *para* position of the phenylalanine group of AAPs. In *M. xenopi*, the exchange from proline to serine could induce a geometric shift that provides an additional hydrogen bond between the serine backbone and the tyrosine hydroxyl group. This could explain the higher potency of **6**. However, for the strains that show reduced susceptibility to **6**, no variations in the lipophilic cleft were found, making it challenging to explain the difference in activity.

### 3. Materials and Methods

#### 3.1. Bacterial Cultures and Strains

For general bacteria culturing and inhibition experiments, Middlebrook 7H9 broth (BD Difco) was supplemented with 0.5% albumin, 0.2% glucose, 0.085% sodium chloride, 0.0003% catalase, 0.2% glycerol, and 0.05% Tween 80<sup>®</sup>. Most bacterial strains analyzed in this study were purchased as type strains either from the American Type Culture Collection (ATCC) or the Culture Collection University of Goteborg (CCUG) as indicated. *M. abscessus* subsp. *abscessus* Bamboo was isolated from the sputum of a patient with amyotrophic lateral sclerosis and bronchiectasis and was provided by Wei Chang Huang, Taichung Veterans General Hospital, Taichung, Taiwan. Clinical isolates covering the *M. abscessus* complex (M9, M199, M337, M404, M422, M232, M506, and M111) were provided by Jeanette W. P. Teo (Department of Laboratory Medicine, National University Hospital, Singapore). Detailed information on the origin of these isolates is given in reference [40]. *M. avium* subsp. *hominissuis* strain 109 (MAC109) was isolated from the blood of a patient with AIDS and was provided by Petros C. Karakousis (Johns Hopkins University) [41]. *M. avium* subsp. *hominissuis* strain 11 originates from the bone marrow of an AIDS patient suffering from a disseminated infection caused by *M. avium* [22,42]. The isolate was provided by Jung-Yien Chien and Po-Ren Hsueh, National Taiwan University Hospital, Taipei.

### 3.2. Growth Inhibition Assay

Growth inhibition assays were performed in 96-well plate format. The wells were filled with 100  $\mu$ L of supplemented 7H9 medium before dispensing 10 mM compound stock solutions in DMSO into the wells using a Tecan D300e digital dispenser. For each compound, a 10-point 3-fold dilution series or a 10-point 2-fold dilution series was prepared that typically started at a concentration of 100  $\mu$ M. The DMSO concentrations were normalized to 2%. The cultures of the respective bacterial strains were grown to the mid-log phase, which was indicated by a measured OD<sub>600</sub> between 0.4 and 0.6. A sufficient aliquot of the culture was taken from the culture and diluted to an OD<sub>600</sub> of 0.1 with fresh 7H9 medium ( $1 \times 10^7$  CFU/mL). Next, 100  $\mu$ L of the resulting bacterial suspension was used to inoculate the prefilled wells, which resulted in a total volume per well of 200  $\mu$ L with an OD<sub>600</sub> of 0.05 ( $5 \times 10^6$  CFU/mL, 1% DMSO). Each plate included 8 untreated wells containing 1% DMSO and 8 sterile wells for blank corrections. The plates were sealed with Parafilm® (Bemis Company, Nennah, WI, USA), wrapped in damp paper towels, and placed in tight-closing plastic boxes, before incubation at 37 °C and shaking at 110 rpm. Fast-growing NTM (*M. abscessus* and subsp., *M. fortuitum* and *M. chelonae*) were incubated for 3 days as a standard procedure, while the slow-growing strains (all the other strains) were incubated for 5 days. Due to its particularly slow growth rate, *M. ulcerans* was incubated for 10 days.

### 3.3. Determination of MIC Values

To determine the minimal inhibitory concentration at 50% growth inhibition relative to an untreated control (MIC<sub>50</sub>), OD<sub>600</sub> values of each well were measured with a Tecan Infinite M200 plate reader on day 0 and day 3, day 5 or day 10. Before measuring the OD on the final day of analysis, the sedimented bacterial cells were resuspended with either manual pipetting or with the use of an Eppendorf epMotion 5070 pipetting robot. On day 0 and the final day of analysis, the average OD of the sterile wells was subtracted from the remaining wells for blank correction. To generate the bacterial growth values for every well, the blank-corrected day 0 values were subtracted from the blank-corrected day 3/5/10 values. For each compound, the growth values of the two corresponding untreated wells gave the average drug-free growth, which is equal to 100% growth/0% inhibition. To calculate the % growth of each drug-containing well, their growth values were related to their respective drug-free growth values. GraphPad Prism 10.0 was used for graphical analysis, curve fitting and calculations. Dose–response curves were plotted with % inhibition (=100% growth) versus compound concentration. For the calculation of MIC values, the obtained data points were fitted utilizing a standard variable slope Hill function (bottom asymptote value constrained to equal 0). The resulting function was used to calculate MIC<sub>50</sub>. The values were calculated from two technical replicates and averaged for each compound.

### 3.4. Protein–Protein Primary Structure Alignment

To compare the primary structures of the RNAP  $\beta$  and  $\beta'$  subunits of different NTM, we utilized the protein–protein BLAST algorithm provided by NIH (<https://blast.ncbi.nlm.nih.gov/Blast.cgi> (accessed on 4 April 2024)). The primary structures of the type strains were obtained from the Pathosystems Resource Integration Center (PATRIC) database, which is provided by the Bacterial and Viral Bioinformatics Resource Center (BV-BRC, University of Chicago, <https://www.bv-brc.org/> (accessed on 4 April 2024)). Additionally, we retrieved the genome of MAC109 from Matern et al. [41]. The comparative genomics analysis excluded *M. abscessus* subsp. *massiliense*, *M. abscessus* subsp. *bolletii*, *M. abscessus* clinical isolates and *M. avium* subsp. *hominissuis* strain 11.

### 3.5. Visualization of Protein Models

For surface and interaction analysis as well as visualization of the *Mtb* RNAP 3D structure (PDB: 5UHE [29]), we utilized UCSF ChimeraX (Resource for Biocomputing, Visualization, and Informatics at the University of California, San Francisco, CA, USA) [43], as

well as the Maestro graphical interface (Schrödinger Release 2022-3: Maestro, Schrödinger, LLC, New York, NY, USA, 2021).

#### 4. Conclusions

AAPs that emerged as RNAP inhibitors against *Mtb* show promising in vitro activity against a wide range of NTM. In addition to the *M. abscessus* complex and the *M. avium* complex, we demonstrated that AAPs show in vitro activity against a less common yet clinically relevant set of NTM. The majority of NTM were susceptible to AAPs and particularly high activities were observed against *M. marinum* and *M. ulcerans*, while *M. simiae* and *M. xenopi* showed a lower level of susceptibility. The various AAPs that were tested exhibit comparable inhibition tendencies across different mycobacterial species. The data obtained from these other mycobacteria align well with the previously published structure–activity relationships. The comparative analysis of the target sequences of different mycobacterial species, focusing on the binding pocket of AAPs, revealed a high degree of conservation in both the primary and spatial structure within the relevant areas of the  $\beta$  and  $\beta'$  RNAP subunits, showing the potential value of AAPs as broad-spectrum anti-mycobacterial inhibitors. Variations in in vitro activities were observed among compounds with specific structural elements, such as the *para*-hydroxy group in tyrosine (6). However, the observed polymorphisms did not uniformly align with alterations in compound susceptibility, underscoring the multifaceted nature of drug–bacteria interactions.

The study emphasizes the potential of AAPs as versatile antimycobacterial agents. However, the variations in compound activity across different strains indicate the need for further exploration into the interplay between compound structure and bacterial physiology. The study's conclusions are limited by the small number of strains used for each species. Follow-up work should include testing a larger panel of clinical isolates to verify the results, especially for the species that showed conspicuous features. This study offers valuable insights into the susceptibility of NTM to AAPs and provides a basis for the development of more effective treatments against a wide range of mycobacterial infections.

**Supplementary Materials:** The following supporting information can be downloaded at: <https://www.mdpi.com/article/10.3390/antibiotics13050404/s1>, Table S1: MIC<sub>90</sub> values of a selection of AAPs against type strains of the Mycobacterium abscessus complex. The displayed values are average values of two technical replicates. For detailed information on the origin of clinical isolates, see Section 3 of the main manuscript. Table S2: MIC<sub>90</sub> values of a selection of AAPs against a panel of Mycobacterium abscessus complex clinical isolates. Cell shading from green to red indicates high to low activity of the respective compound against the tested clinical isolates. The displayed values are average values of two technical replicates. For detailed information on the origin of clinical isolates, see Section 3 of the main manuscript. Table S3: MIC<sub>90</sub> values of a selection of AAPs against type strains of the Mycobacterium avium complex. Cell shading from green to red indicates high to low activity of the respective compound against the tested NTM species. The displayed values are average values of two technical replicates. For detailed information on the origin of clinical isolates, see Section 3 of the main manuscript. Table S4: MIC<sub>90</sub> values of a selection of AAPs against type strains of the different NTM. Cell shading from green to red indicates high to low activity of the respective compound against the tested clinical isolates. The displayed values are average values of two technical replicates. For detailed information on the origin of clinical isolates, see Section 3 of the main manuscript. Table S5: Alignment of RpoB primary sequences of all tested strains from position 450–600. Position numbering refers to PDB: 5UHE. Dots represent amino acid identity. Table S6: Alignment of RpoC primary sequences of all tested strains from position 500 to 580. Position numbering refers to PDB: 5UHE. Dots represent amino acid identity.

**Author Contributions:** Conceptualization, M.L. and A.R.; methodology, M.L. and U.S.G.; software, M.L.; formal analysis, M.L. and U.S.G.; resources, T.D. and A.R.; data curation, M.L.; writing—original draft preparation, M.L.; writing—review and editing, M.L., U.S.G. and A.R.; visualization, M.L. and R.A.; supervision, T.D. and A.R.; project administration, A.R.; funding acquisition, T.D. and A.R. All authors have read and agreed to the published version of the manuscript.

**Funding:** This work was funded by the Deutsche Forschungsgemeinschaft (DFG, German Research Foundation)—432291016 (to A.R.), the National Institute of Allergy and Infectious Diseases of the National Institutes of Health under award number R01AI132374 (to T.D.), and the Mukoviszidose Institut gGmbH (Bonn, Germany) project number 2202 (to A.R.), the research and development arm of the German Cystic Fibrosis Association Mukoviszidose e.V.

**Institutional Review Board Statement:** Not applicable.

**Informed Consent Statement:** Not applicable.

**Data Availability Statement:** The raw data supporting the conclusions of this article will be made available by the authors upon request.

**Acknowledgments:** We are grateful to Wei Chang Huang (Taichung Veterans General Hospital, Taichung, Taiwan) for providing *M. abscessus* Bamboo, to Jeanette W. P. Teo (Department of Laboratory Medicine, National University Hospital, Singapore) for providing *M. abscessus* clinical isolates and for Jung-Yien Chien and Po-Ren Hsueh (National Taiwan University Hospital, Taipei) for providing *M. avium* subsp. *hominissuis* strain 11. We are also grateful for the development and maintenance of the molecular graphics and analysis software UCSF ChimeraX version 1.7, provided by the Resource for Biocomputing, Visualization, and Informatics at the University of California, San Francisco, with support from the National Institutes of Health R01-GM129325, the Office of Cyber Infrastructure and Computational Biology and National Institute of Allergy and Infectious Diseases. We acknowledge the financial support of the Open Access Publication Fund of the Martin-Luther-University Halle-Wittenberg.

**Conflicts of Interest:** The authors declare no conflicts of interest.

## References

- World Health Organization. Global Tuberculosis Report 2023. Available online: <https://www.who.int/teams/global-tuberculosis-programme/tb-reports/global-tuberculosis-report-2023> (accessed on 18 December 2023).
- Dartois, V.; Sizemore, C.; Dick, T. Editorial: NTM—The new uber-bugs. *Front. Microbiol.* **2019**, *10*, 1299. [CrossRef]
- Wassilew, N.; Hoffmann, H.; Andrejak, C.; Lange, C. Pulmonary Disease Caused by Non-Tuberculous Mycobacteria. *Respiration* **2016**, *91*, 386–402. [CrossRef] [PubMed]
- Ahmed, I.; Tiberi, S.; Farooqi, J.; Jabeen, K.; Yeboah-Manu, D.; Migliori, G.B.; Hasan, R. Non-tuberculous mycobacterial infections—A neglected and emerging problem. *Int. J. Infect. Dis.* **2020**, *92*, S46–S50. [CrossRef] [PubMed]
- Johansen, M.D.; Herrmann, J.L.; Kremer, L. Non-tuberculous mycobacteria and the rise of *Mycobacterium abscessus*. *Nat. Rev. Microbiol.* **2020**, *18*, 392–407. [CrossRef] [PubMed]
- Dahl, V.N.; Mølhave, M.; Fløe, A.; van Ingen, J.; Schön, T.; Lillebaek, T.; Andersen, A.B.; Wejse, C. Global trends of pulmonary infections with nontuberculous mycobacteria: A systematic review. *Int. J. Infect. Dis.* **2022**, *125*, 120–131. [CrossRef] [PubMed]
- Baird, T.; Bell, S. Cystic Fibrosis-Related Nontuberculous Mycobacterial Pulmonary Disease. *Clin. Chest Med.* **2023**, *44*, 847–860. [CrossRef] [PubMed]
- Brugha, R.; Spencer, H. *Mycobacterium abscessus* in cystic fibrosis: Environmental Mycobacteria share genes and evolve to become pathogens. *Science* **2021**, *372*, 465–466. [CrossRef] [PubMed]
- Richards, C.J.; Olivier, K.N. Nontuberculous Mycobacteria in Cystic Fibrosis. *Semin. Respir. Crit. Care Med.* **2019**, *40*, 737–750. [CrossRef]
- Azar, M.; Zimbric, M.; Shedden, K.; Caverly, L.J. Distribution and outcomes of infection of *Mycobacterium avium* complex species in cystic fibrosis. *J. Cyst. Fibros.* **2020**, *19*, 232–235. [CrossRef]
- Park, I.K.; Olivier, K.N. Nontuberculous mycobacteria in cystic fibrosis and non-cystic fibrosis bronchiectasis. *Semin. Respir. Crit. Care Med.* **2020**, *36*, 217–224. [CrossRef]
- Wi, Y.M. Treatment of extrapulmonary nontuberculous mycobacterial diseases. *Infect. Chemother.* **2019**, *51*, 245–255. [CrossRef] [PubMed]
- Piersimoni, C.; Scarparo, C. Extrapulmonary infections associated with nontuberculous mycobacteria in immunocompetent persons. *Emerg. Infect. Dis.* **2009**, *15*, 1351–1358. [CrossRef] [PubMed]
- Prevots, D.R.; Marras, T.K. Epidemiology of Human Pulmonary Infection with Nontuberculous Mycobacteria: A Review. *Clin. Chest Med.* **2015**, *36*, 13–34. [CrossRef]
- Daniel-Wayman, S.; Adjemian, J.; Prevots, D.R. Epidemiology of Nontuberculous Mycobacterial Pulmonary Disease (NTM PD) in the USA. In *Nontuberculous Mycobacterial Disease*; Springer Nature Switzerland AG: Cham, Switzerland, 2019; pp. 145–161. [CrossRef]
- Prevots, D.R.; Marshall, J.E.; Wagner, D.; Morimoto, K. Global Epidemiology of Nontuberculous Mycobacterial Pulmonary Disease: A Review. *Clin. Chest Med.* **2023**, *44*, 675–721. [CrossRef] [PubMed]
- Diel, R.; Nienhaus, A.; Ringshausen, F.C.; Richter, E.; Welte, T.; Rabe, K.F.; Loddenkemper, R. Microbiologic Outcome of Interventions against *Mycobacterium avium* Complex Pulmonary Disease: A Systematic Review. *Chest* **2018**, *153*, 888–921. [CrossRef] [PubMed]

18. Koh, W.J.; Jeong, B.H.; Jeon, K.; Lee, N.Y.; Lee, K.S.; Woo, S.Y.; Shin, S.J.; Kwon, O.J. Clinical Significance of the Differentiation between *Mycobacterium avium* and *Mycobacterium intracellulare* in M avium Complex Lung Disease. *Chest* **2012**, *142*, 1482–1488. [[CrossRef](#)] [[PubMed](#)]
19. Boudehen, Y.M.; Kremer, L. *Mycobacterium abscessus*. *Trends Microbiol.* **2021**, *29*, 951–952. [[CrossRef](#)] [[PubMed](#)]
20. Victoria, L.; Gupta, A.; Gómez, J.L.; Robledo, J. *Mycobacterium abscessus* complex: A Review of Recent Developments in an Emerging Pathogen. *Front. Cell. Infect. Microbiol.* **2021**, *11*, 659997. [[CrossRef](#)]
21. Spaulding, A.B.; Lai, Y.L.; Zelazny, A.M.; Olivier, K.N.; Kadri, S.S.; Prevots, D.R.; Adjemian, J. Geographic distribution of nontuberculous mycobacterial species identified among clinical isolates in the United States, 2009–2013. *Ann. Am. Thorac. Soc.* **2017**, *14*, 1655–1661. [[CrossRef](#)]
22. Low, J.L.; Wu, M.L.; Aziz, D.B.; Laleu, B.; Dick, T. Screening of TB actives for activity against nontuberculous mycobacteria delivers high hit rates. *Front. Microbiol.* **2017**, *8*, 1539. [[CrossRef](#)]
23. Richter, A.; Strauch, A.; Chao, J.; Ko, M.; Av-Gay, Y. Screening of preselected libraries targeting *mycobacterium abscessus* for drug discovery. *Antimicrob. Agents Chemother.* **2018**, *62*, 10–1128. [[CrossRef](#)] [[PubMed](#)]
24. Ballell, L.; Bates, R.H.; Young, R.J.; Alvarez-Gomez, D.; Alvarez-Ruiz, E.; Barroso, V.; Blanco, D.; Crespo, B.; Escibano, J.; González, R.; et al. Fueling Open-Source Drug Discovery: 177 Small-Molecule Leads against Tuberculosis. *ChemMedChem* **2013**, *8*, 313–321. [[CrossRef](#)] [[PubMed](#)]
25. Lang, M.; Ganapathy, U.S.; Mann, L.; Abdelaziz, R.; Seidel, R.W.; Goddard, R.; Sequenzia, I.; Hoenke, S.; Schulze, P.; Aragaw, W.W.; et al. Synthesis and Characterization of Phenylalanine Amides Active against *Mycobacterium abscessus* and Other Mycobacteria. *J. Med. Chem.* **2023**, *66*, 5079–5098. [[CrossRef](#)] [[PubMed](#)]
26. Mann, L.; Lang, M.; Schulze, P.; Halz, J.H.; Csuk, R.; Hoenke, S.; Seidel, R.W.; Richter, A. Racemization-free synthesis of N $\alpha$ -2-thiophenyl-phenylalanine-2-morpholinoanilide enantiomers and their antimycobacterial activity. *Amino Acids* **2021**, *53*, 1187–1196. [[CrossRef](#)] [[PubMed](#)]
27. Ebright, R.H.; Ebright, Y.W.; Mandal, S.; Wilde, R.; Li, S. Preparation of N-Alpha-Aroyl-N-aryl-Phenylalaninamides as Inhibitors of Bacterial RNA Polymerase and as Antibacterials. U.S. Patent WO2015120320 A1, 13 August 2015.
28. Mann, L.; Ganapathy, U.S.; Abdelaziz, R.; Lang, M.; Zimmerman, M.D.; Dartois, V.; Dick, T.; Richter, A. In Vitro Profiling of the Synthetic RNA Polymerase Inhibitor MMV688845 against *Mycobacterium abscessus*. *Microbiol. Spectr.* **2022**, *10*, e02760-22. [[CrossRef](#)] [[PubMed](#)]
29. Lin, W.; Mandal, S.; Degen, D.; Liu, Y.; Ebright, Y.W.; Li, S.; Feng, Y.; Zhang, Y.; Mandal, S.; Jiang, Y.; et al. Structural Basis of *Mycobacterium tuberculosis* Transcription and Transcription Inhibition. *Mol. Cell* **2017**, *66*, 169–179.e8. [[CrossRef](#)] [[PubMed](#)]
30. Hashish, E.; Merwad, A.; Elgaml, S.; Amer, A.; Kamal, H.; Elsadek, A.; Marei, A.; Sitohy, M. *Mycobacterium marinum* infection in fish and man: Epidemiology, pathophysiology and management; a review. *Vet. Q.* **2018**, *38*, 35. [[CrossRef](#)]
31. Yotsu, R.R.; Suzuki, K.; Simmonds, R.E.; Bedimo, R.; Ablordey, A.; Yeboah-Manu, D.; Phillips, R.; Asiedu, K. Buruli Ulcer: A Review of the Current Knowledge. *Curr. Trop. Med. Rep.* **2018**, *5*, 247–256. [[CrossRef](#)] [[PubMed](#)]
32. Lang, M.; Ganapathy, U.S.; Mann, L.; Seidel, R.W.; Goddard, R.; Erdmann, F.; Dick, T.; Richter, A. Synthesis and in vitro Metabolic Stability of Sterically Shielded Antimycobacterial Phenylalanine Amides. *ChemMedChem* **2024**, *19*, e202300593. [[CrossRef](#)]
33. Van, N.; Degefu, Y.N.; Aldridge, B.B. *Efficient Measurement of Drug Interactions with DiaMOND (Diagonal Measurement of N-Way Drug Interactions)*; Humana: New York, NY, USA, 2021; pp. 703–713. [[CrossRef](#)]
34. Bastian, S.; Veziris, N.; Roux, A.L.; Brossier, F.; Gaillard, J.L.; Jarlier, V.; Cambau, E. Assessment of Clarithromycin Susceptibility in Strains Belonging to the *Mycobacterium abscessus* Group by erm(41) and rrl Sequencing. *Antimicrob. Agents Chemother.* **2011**, *55*, 775. [[CrossRef](#)]
35. Schildkraut, J.A.; Raaijmakers, J.; Aarnoutse, R.; Hoefsloot, W.; Wertheim, H.F.L.; van Ingen, J. The role of rifampicin within the treatment of *Mycobacterium avium* pulmonary disease. *Antimicrob. Agents Chemother.* **2023**, *67*, e00874-23. [[CrossRef](#)] [[PubMed](#)]
36. Van Ingen, J.; Boeree, M.J.; Dekhuijzen, P.N.R.; Van Soolingen, D. Clinical relevance of *Mycobacterium simiae* in pulmonary samples. *Eur. Respir. J.* **2008**, *31*, 106–109. [[CrossRef](#)] [[PubMed](#)]
37. Nasiri, M.J.; Amini, S.; Nikpor, Z.; Arefzadeh, S.; Mousavi, S.M.J.; Goudarzi, H. Drug Susceptibility Testing of *Mycobacterium simiae*: An Emerging Pathogen in Iran. *Infect. Disord. Drug Targets* **2020**, *21*, 619–622. [[CrossRef](#)] [[PubMed](#)]
38. Van Ingen, J.; Totten, S.E.; Heifets, L.B.; Boeree, M.J.; Daley, C.L. Drug susceptibility testing and pharmacokinetics question current treatment regimens in *Mycobacterium simiae* complex disease. *Int. J. Antimicrob. Agents* **2012**, *39*, 173–176. [[CrossRef](#)] [[PubMed](#)]
39. Grantham, R. Amino Acid Difference Formula to Help Explain Protein Evolution. *Science* **1974**, *185*, 862–864. [[CrossRef](#)] [[PubMed](#)]
40. Aziz, D.B.; Low, J.L.; Wu, M.L.; Gengenbacher, M.; Teo, J.W.; Dartois, V.; Dick, T. Rifabutin Is active against *Mycobacterium abscessus* complex. *Antimicrob. Agents Chemother.* **2017**, *61*, 10–1128. [[CrossRef](#)] [[PubMed](#)]
41. Matern, W.M.; Bader, J.S.; Karakousis, P.C. Genome analysis of *Mycobacterium avium* subspecies hominissuis strain 109. *Sci. Data* **2018**, *5*, 180277. [[CrossRef](#)]

42. Yee, M.; Klinzing, D.; Wei, J.R.; Gengenbacher, M.; Rubin, E.J.; Chien, J.Y.; Hsueh, P.R.; Dick, T. Draft Genome Sequence of *Mycobacterium avium* 11. *Genome Announc.* **2017**, *5*, 10–1128. [[CrossRef](#)]
43. Pettersen, E.F.; Goddard, T.D.; Huang, C.C.; Meng, E.C.; Couch, G.S.; Croll, T.I.; Morris, J.H.; Ferrin, T.E. UCSF ChimeraX: Structure visualization for researchers, educators, and developers. *Protein Sci.* **2021**, *30*, 70–82. [[CrossRef](#)]

**Disclaimer/Publisher’s Note:** The statements, opinions and data contained in all publications are solely those of the individual author(s) and contributor(s) and not of MDPI and/or the editor(s). MDPI and/or the editor(s) disclaim responsibility for any injury to people or property resulting from any ideas, methods, instructions or products referred to in the content.



## 3) Summary & Discussion

This section summarizes and discusses the key findings of the three studies that are the focus of this cumulative thesis, providing a comparative analysis of their contributions to the field. The discussion suggests future directions for research and development to enhance the potential of AAPs as mycobacterial RNAP inhibitors.

### ***3.1) Chemical Derivatization & Structure-Activity Relationship***

The chemical scaffold of AAPs contains an amino acid core - mostly phenylalanine or tyrosine - which is connected to two aromatic systems via amide bonds. This modular character, together with the well-studied field of peptide bond synthesis facilitates structural derivatization of the highly customizable AAP structure. During the course of this project, more than 100 distinct AAP molecules have been synthesized. While not all of these structures were published yet, each one of them contributed to our understanding of the chemical flexibility of AAPs in relation to their biological activity. The following paragraphs exclusively discuss the derivatives synthesized in the papers that constitute this cumulative thesis. An overview of the variety of substituents introduced is given in **Figure 11**.

We based our synthetic approaches on the crystal structure of *M. tuberculosis* RNAP with D-AAP1 as published by Lin *et al.* and the patent by Ebright *et al.* that describes the preparation of a large set of AAPs [189], [196]. The patent discloses biological activities of the synthesized compounds against *M. tuberculosis* H37Rv, *M. smegmatis* ATCC 19420 and *M. avium* ATCC 25291, which we took into account when deciding on our own structural modifications.

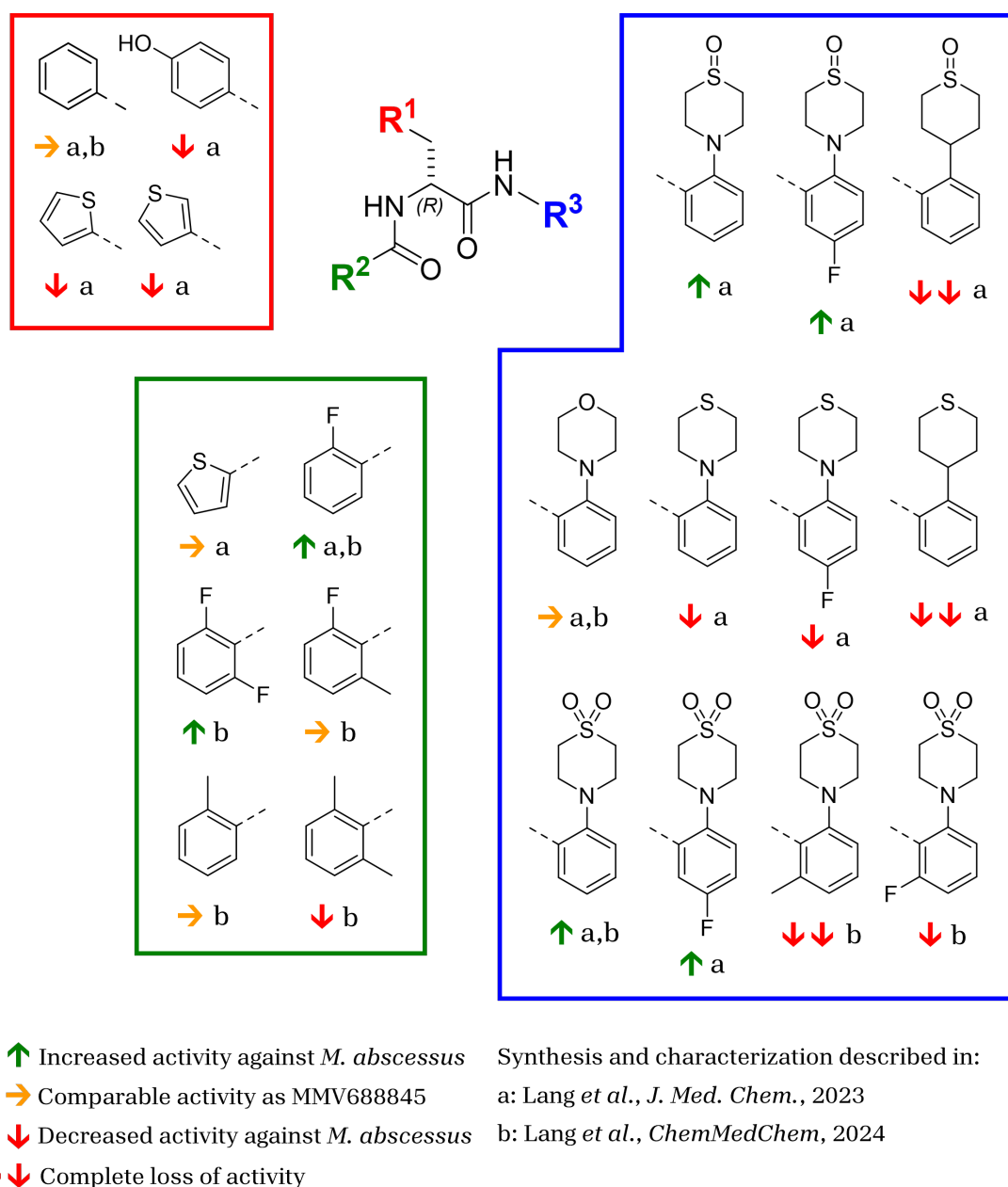


**Figure 11.** Overview of substituents that were introduced to the AAP chemical scaffold in the present publications. Arrows indicate the overall effect on biological activity. Letters indicate in which publication the respective moieties were used for derivatization.

### 3.1.1) General Synthetic Procedure

The synthesis is usually achieved by an amide coupling of the 2- substituted aniline with an *N*-protected amino acid. The coupling reagent of choice for this reaction was T3P due to the practical purification process, enabled by the polar nature of the side products, and the exceptionally high yields of usually 80% – 90%, given the relatively non-nucleophilic anilines used as reactants. Derivatives of 2-morpholinoaniline, if not commercially available, were synthesized by nucleophilic

substitution of a halogen atom, attached to a nitro-activated aromatic system and subsequent reduction of the nitro group by Pd-catalyzed reduction with hydrogen. After deprotection of the synthesized amide adduct, a second amide coupling between the amino acid nitrogen and an aromatic carboxylic acid was employed to yield the final AAP molecule. PyBOP or DEPBT were utilized as coupling reagents, depending on the polarity of the product and the reactivity of the aromatic carboxylic acid [187], [197].

### 3.1.2) Analysis of the Stereo Configuration

In the patent by Ebright *et al.*, the synthetic method was based on a racemic mixture of *N*-protected phenylalanine and preparative separation of the two resulting enantiomers with chiral column material on an HPLC system [196]. As enantiopure, protected phenylalanine is a readily available starting material and chiral preparative HPLC columns are costly, one of the key goals of establishing our synthetic pathway was to achieve the conservation of the critical (*R*) stereo configuration of the amino acid core throughout the entire sequence. Therefore, the synthetic procedures we published earlier were refined and adapted [198]. We analyzed the stereo configuration at each step of the synthetic sequence by chiral, analytical HPLC to verify conformity. The evaluation showed an enantiomeric excess of the intermediates and final products of 99% indicating a very high degree of stereo conservation [190].

### 3.1.3) Derivatization of the Amino Acid Core

The choice of an amino acid core ( $R^1$ ) other than phenylalanine is strongly restricted by the fact that the space offered by the lipophilic binding pocket of the target is already largely occupied by one phenyl group. Only tyrosine derivatives were found to exhibit biological activity comparable to the phenylalanine compounds [190], [196]. The sterically and electronically similar thiophenyl substituents [190] also demonstrated activity which suggests that other aromatic heterocycles at this position may offer interesting features. However, this area of derivatization is currently understudied.

### 3.1.4) Derivatization of the Aroyl-Moiety ( $R^2$ )

Analyzing the target crystal structure suggests that altering  $R^2$  is only promising in the *ortho*-position and not in *meta*- or *para*-position to the amide bond. This is also indicated by the patent, in which the latter substitutions mainly resulted in compounds with a loss of biological activity. Halogen atoms and methyl groups are tolerated in the *ortho*-position, while spatially more demanding groups like ethyl resulted in a loss of activity. Interestingly, a 4-indole substituent was introduced,

and the resulting compound still showed activity that is comparable to MMV6888845 against *M. tuberculosis*. The synthesis of other heteroaromatic derivatives could yield promising candidates in the future but was not part of the synthetic projects presented here.

### 3.1.5) Derivatization of Morpholinoaniline-Moiety (R<sup>3</sup>)

Both the crystal structure by Lin *et al.* and the patent by Ebright *et al.* revealed that the module exhibiting the greatest tolerance to chemical changes in regard to the resulting biological activity, is the morpholino moiety of MMV688845 or the methyl group of D-AAP1, respectively (the R<sup>3</sup> region in **Figure 11**) [189], [196]. Piperazine, quinoline, indazole, methoxy, monofluoromethoxy and difluoromethoxy groups were employed as substituents at the aromatic system, yielding compounds with similar or better *in vitro* activity against *M. tuberculosis* compared to MMV688845 [196]. The highest activity that has been reported in the patent is an MIC<sub>90</sub> of 0.39 μM (0.19 μg/mL) and belongs to a compound containing a methoxy group [196]. The highest activity against *M. avium* was reported with an MIC<sub>90</sub> of 0.43 μM (0.19 μg/mL). The highest activities reported in the presented publications were found for AAPs which contain a thiomorpholine *S*-oxide, e.g. an MIC<sub>90</sub> of 0.15 μM with a thiomorpholine sulfone containing compound against *M. tuberculosis* (compound 2 in publication II [190], for more details on biological activity see section 3.2). The introduction of these substituents into the AAP compounds generally resulted in enhanced activity in growth inhibition assays.

These compounds were synthesized by oxidation of the respective thiomorpholine precursors with different oxidizing agents. The use of an excess amount of *m*-chloroperbenzoic acid in dichloromethane resulted in the formation of the sulfone in good yields. The corresponding sulfoxides were formed by treatment with one equivalent of sodium periodate (NaIO<sub>4</sub>) in methanol/acetonitrile mixtures. Both reactions can be carried out directly after the nucleophilic substitution of thiomorpholine to an aromatic halonitroarene or after the first amide coupling with phenylalanine [190]. We also attempted to obtain sulfone products through direct nucleophilic aromatic substitution using commercially available thiomorpholine sulfone. However, this proved to be challenging due to the lower degree of nucleophilicity of thiomorpholine sulfone in comparison to thiomorpholine. A Buchwald-Hartwig amination resulted in the desired product but was not performed routinely. Substitution with thiomorpholine and subsequent oxidation proved to be more efficient as reactions are metal-free and both *S*-oxides (sulfone and sulfoxide) can be synthesized from the same precursor with good yields. Only

strongly activated aromatic systems, e.g. 1,3-difluoro-2-nitrobenzene, reacted directly with thiomorpholine sulfone directly [197].

A review of the literature of sulfoxides and sulfones reveals their importance as functional groups in modern drug design [199], [200], [201]. Several approved drugs and drugs in clinical trials contain sulfones. Sulfoxides are far less abundant as structural components in clinically used substances, with the prominent exception of proton pump inhibitory benzimidazoles. An overview of drugs with S-oxides is given in **Figure 12**. These groups can act as hydrogen bond acceptors for improved target binding, their lower lipophilicity can increase bioavailability. For example, in figoltinib, the exchange of morpholine to thiomorpholine dioxide improved metabolic stability and bioavailability and was carried through to clinical trials subsequently [202], [203]. The high electronegativity reduces the electron density in adjacent areas of the molecule, which in our case reduces the basicity of the aromatic amine. This could be beneficial for hERG toxicity profiles [199]. Sulfoxides, due to their high polarity, can give the AAPs a 10-fold increase in aqueous solubility [190].

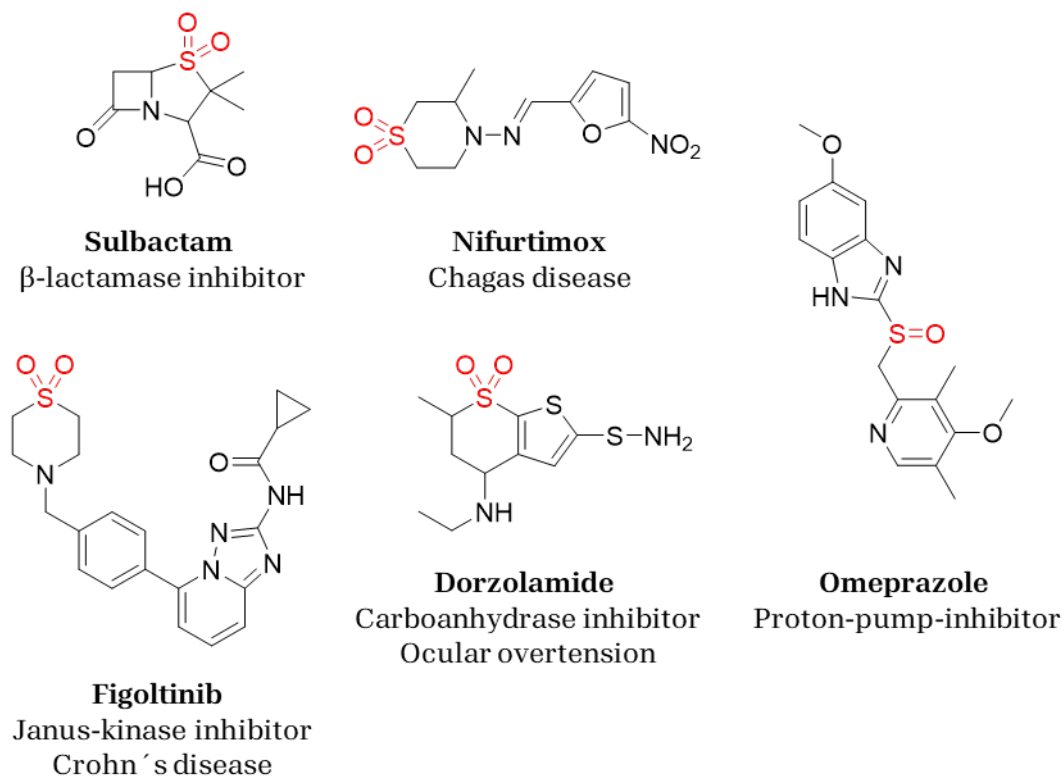


**Figure 12.** Selection of clinically used compounds with S-oxides as structural elements.

### 3.1.6) Necessity of Tertiary Nitrogen in Morpholine-like Derivatives

Another aspect that was analyzed during our structure-activity-relationship studies is the necessity of the tertiary aromatic amine that is part of the morpholino moiety [190]. The synthesis involved a carbon-carbon coupling of a tosyl hydrazone intermediate with an aromatic boronic acid [204]. The resulting derivatives demonstrated complete loss of activity, indicating the necessity of the geometry of the tertiary nitrogen rather than the tetrahedral geometry of an  $sp^3$  hybridized carbon. This phenomenon seems to be exclusive to derivatives containing a morpholine-like moiety. In contrast, AAPs with smaller substituents in the *ortho*-position to the amide bond, for example D-AAP1, have been observed to retain activity without the need for nitrogen. This can be attributed to the steric demand of the (thio)morpholine ring system, which may necessitates a distinct binding mode.

### 3.1.7) N-Methylation of Amide Bonds

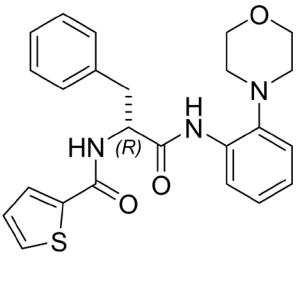
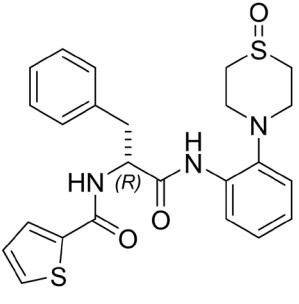
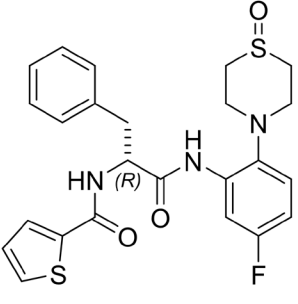
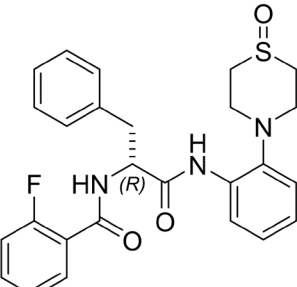
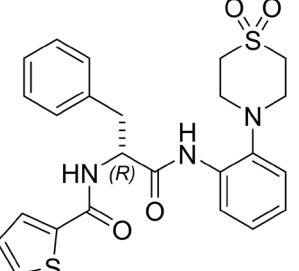
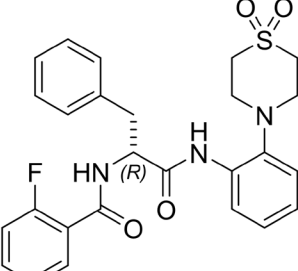
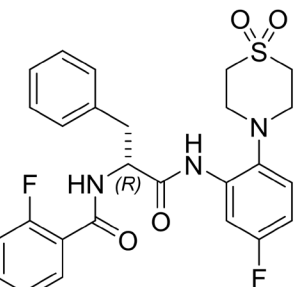
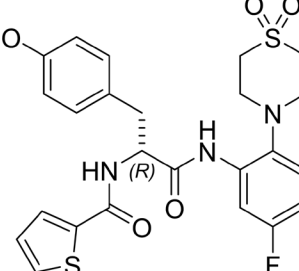
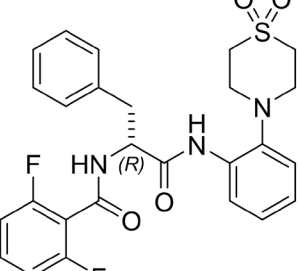
For the preparation AAP derivatives that contain methyl groups at the nitrogen of the amide bonds, either commercially available Boc-*N*-methyl-D-phenylalanine was used, or *N*-methyl-2-morpholinoaniline was synthesized by the formation of the formamide of 2-morpholinoaniline and subsequent reduction with  $LiAlH_4$ . *N*-Methylation was pursued as a method to impede hydrolysis of the amide bonds [205], yet this kind of modification can also prove beneficial when aiming to enhance membrane permeability, as it was shown for cyclopeptides [206]. When considering the inherently lipophilic mycomembrane that acts as a barrier to the target of AAPs, ensuring permeation is crucial. However, *N*-methylation of AAPs led to a complete loss of activity [197], which was probably due to the methyl group forcing the amide bonds into the energetically unfavorable *cis*-confirmation, altering the geometry of the molecule to an extent which prevents target binding [207]. Furthermore, it did not enhance microsomal stability, rendering the concept of *N*-methylation unsuitable for further consideration [197].

### 3.2) Antimycobacterial Activity of AAP Derivatives

The microbiological methods employed in the presented papers are integral to our research on AAPs, as the *in vitro* assays for the evaluation of antimycobacterial activity provide a framework for evaluation and optimization of AAP candidates. Our initial analysis of a newly synthesized compound is a microdilution assay in 96-well format against *M. abscessus*, *M. smegmatis* or *M. intracellulare*. By measurement of either optical density or RFP fluorescence of the bacterial suspensions we determine MIC<sub>90</sub> values as a first line assessment of antimycobacterial properties. With the conducted inhibition assays, we demonstrated the potential of AAPs to reach MIC<sub>90</sub> values of under 1 μM against *M. abscessus*, *M. tuberculosis* and *M. intracellulare*. A structural overview of the most active AAPs that were synthesized and characterized during the project is presented in **Table 9**. These derivatives demonstrate MIC<sub>90</sub> values that are in a comparable range to the MIC<sub>90</sub> values of antibiotics which are used against mycobacterial infections in the clinic. A selection of reported MIC<sub>90</sub> values for comparison is given in **Table 10**. It has to be noted that the presented MIC<sub>90</sub> values are defined as the concentrations that inhibit 90% of bacterial growth in comparison to uninhibited growth under the same conditions. This may differ from the way MIC<sub>90</sub> values are defined in other publications, most of which have a clinical rather than a drug development background: a compound concentration that inhibits 90% of clinical isolate strains that have been tested. Therefore, it is most necessary to carefully read the methods sections of other publications before comparing values.

Compounds that show low MIC<sub>90</sub> values are advanced to be tested in a fluorescence-based *M. abscessus* macrophage infection model [190], [208]. The ability of certain mycobacteria to invade and replicate within human immune cells – particularly macrophages - creates a unique niche for their survival. To address this, the employed model determines growth inhibition within infected macrophages under the influence of compounds. AAPs show the tendency to be around 2-4 times less active in the macrophage infection model compared to the normal *M. abscessus* inhibition assay [190]. A striking observation was the near-total loss of activity of highly polar AAPs that bear sulfoxide functional groups. We postulate that their high polarity makes it more difficult for them to pass across the two biological membranes (macrophage and bacterium).

**Table 9.** Selection of synthesized AAP derivatives with the highest activities against *M. tuberculosis* H37Rv (*Mtb*), *M. abscessus* ATCC 19977 (*Mabs*) and *M. intracellulare* ATCC 35761 (*Mintra*). **Black** compound numbering as in **Publication I**, Lang et al., *J. Med. Chem.*, 2023. **Blue** compound numbering as in **Publication II**, Lang et al., *ChemMedChem*, 2024. **Orange** compound numbering as in **Publication III**, Lang et al., *Antibiotics*, 2024.

	Compound name		
MIC <sub>90</sub>	<b>MMV688845</b>	<b>14 / 1</b>	<b>17 / 4</b>
			
<i>Mtb</i>	0.78 μM	0.4 μM	0.4 μM
<i>Mabs</i>	6.25 μM	3.13 μM	1.56 μM
<i>Mintra</i>	0.78 μM	0.1 μM	0.05 μM
	<b>18 / 2</b>	<b>20 / 3</b>	<b>24 / 2 / 7</b>
			
<i>Mtb</i>	0.78 μM	0.2 μM	0.2 μM
<i>Mabs</i>	3.13 μM	3.13 μM	0.78 μM
<i>Mintra</i>	0.2 μM	0.1 μM	0.05 μM
	<b>29</b>	<b>39 / 6</b>	<b>3 / 8</b>
			
<i>Mtb</i>	0.78 μM	0.78 μM	0.15 μM
<i>Mabs</i>	3.13 μM	6.25 μM	0.78 μM
<i>Mintra</i>	0.1 μM	0.05 μM	0.025 μM

Another important aspect of microbiological characterization is the determination of the sterilizing properties of drug candidates in the form of bactericidal assays and MBC calculation. There are not many drugs that are utilized in current anti-*M. abscessus* therapy that show low MBC<sub>90</sub> values, some of those being rifabutin, amikacin, imipenem, cefoxitin and moxifloxacin. **Table 10** displays MIC<sub>90</sub> values and MBC values from commonly used antimycobacterial antibiotics and compares them with a selection of AAP derivatives. Bedaquiline demonstrates a notable reduction of viable bacteria but with a delayed onset after around 10 days [185], [209]. The sterilizing properties of macrolides like clarithromycin show a strong dependency on the *M. abscessus* strain that is analyzed, and the results are further complicated by the inducible resistance mechanisms present in *M. abscessus*. This leads to seemingly contradictory MBCs published in the literature [92], [185], [210]. The bactericidal activity of AAP derivatives has been demonstrated in our experiments as displayed in **Table 10**. The MBC<sub>90</sub> values for a set of the most active AAP derivatives are in the range 3.13 μM to 6.25 μM, which is comparable to the reported MBC<sub>90</sub> of rifabutin of 5 μM [185]. Moxifloxacin as another highly bactericidal drug reaches MBC<sub>90</sub> values of 2 – 12 μM. Still, *in vivo* conditions cannot be simulated well enough with this type of assay. To further evaluate the potential of AAPs, it would be an appropriate next step to test them against non-replicating persisters in ex vivo caseum or caseum surrogate. It is notable that many common antibiotics lose a significant portion of their sterilizing activity in caseum [211].

**Table 10.** Comparison of MBC and MIC values of a selection of antibiotics and AAP derivatives against *M. abscessus*. Colors indicate identical compounds analyzed in different publications. ND: not determined. For structures of AAP derivatives see Table 9.

Substance	Ref.	Broth MIC <sub>90</sub> [μM]	Broth MBC <sub>90</sub> [μM]	Broth MBC <sub>99</sub> [μM]
Imipenem	[92] <sup>a</sup>	5	12.5	ND
Cefoxitin		16	25	ND
Clarithromycin		0.2	>100	ND
Moxifloxacin		2	3	ND
Moxifloxacin	[185] <sup>a</sup>	6	2	ND
Rifabutin		3	5	ND
Amikacin		25	40	ND
Bedaquiline		0.4	2 <sup>d</sup>	ND
Clarithromycin	[210] <sup>b</sup>	0.4	2	ND
Clarithromycin		2.0	>16	>16
Moxifloxacin		3	12	24
MMV688845	[190], [212]	6.25 - 12.5	12.5	50
20	[190] <sup>c</sup>	0.78	3.13	6.25
14		3.13	6.25	12.5
15		6.25	6.25	12.5
24		0.78	3.13	25 <sup>e</sup>

a MBCs determined after 5 days of incubation with *M. abscessus* Bamboo

b MBCs determined after 3 days of incubation with *M. abscessus* ATCC 19977

c MBCs determined after 4 days of incubation with *M. abscessus* ATCC 19977

d MBCs determined after 10 days of incubation instead of 5 days

e At 6.25 μM 98.6% of viable bacteria were sterilized

Assays conducted on *M. tuberculosis* were mostly performed by Uday S. Ganapathy and his coworkers in Thomas Dick's laboratory at the Center for Discovery and Innovation (Nutley, NJ, USA). Advanced AAPs show nanomolar MIC<sub>90</sub> values of down to 0.15  $\mu$ M against *M. tuberculosis* underscoring their potential beyond the group of NTM [190], [197].

During my research stay at the Center for Discovery and Innovation, we were able to generate and analyze data from testing a set of structurally diverse AAPs against a large collection of different NTM. The results are presented in the joint publication in MDPI Antibiotics, publication III [191]. The aim of this project was to find out whether certain structural features of AAPs behave different against different species and to see if any NTM species show inherent resistance or unusual susceptibility to AAPs in general. An overview that displays a comparison of MIC<sub>50</sub> values between clarithromycin, MMV688845 and compound 3, the most active compound of publication II [197], is given in **Figure 13**. We observed activity for all AAPs especially within the *M. abscessus* complex and the *M. avium* complex. For the set of NTM that are rarely seen in human disease, the results were more diverse. *M. ulcerans* was unusually susceptible to AAPs, while the growth of *M. xenopi* and *M. simiae* was notably less inhibited. Clarithromycin shows a high activity against *M. xenopi* but not against *M. simiae*. This translates into clinical manifestations of *M. simiae*, for which extreme drug resistance to most antibiotics has been described, complicating therapy [89]. *M. xenopi* could have another mechanism of resistance which makes it particularly resistant to AAPs. To see if the target sites of AAPs differ between species, we conducted a comparing alignment analysis of the RNAP primary sequences of the strains used for testing. The results showed that the target site of AAPs between the  $\beta$  and  $\beta'$  subunits is highly conserved. There are no amino acid variations that are crucial for AAP binding. This suggests that other mechanisms lead to higher resistance against AAPs in *M. simiae* and *M. xenopi*. These mechanism could be of metabolic nature, since AAPs could be susceptible to specialized enzymatic degradation processes. Morphological differences, such as cell wall composition or the presence or absence of distinct ABC transporter systems, could also contribute to the observed variations.

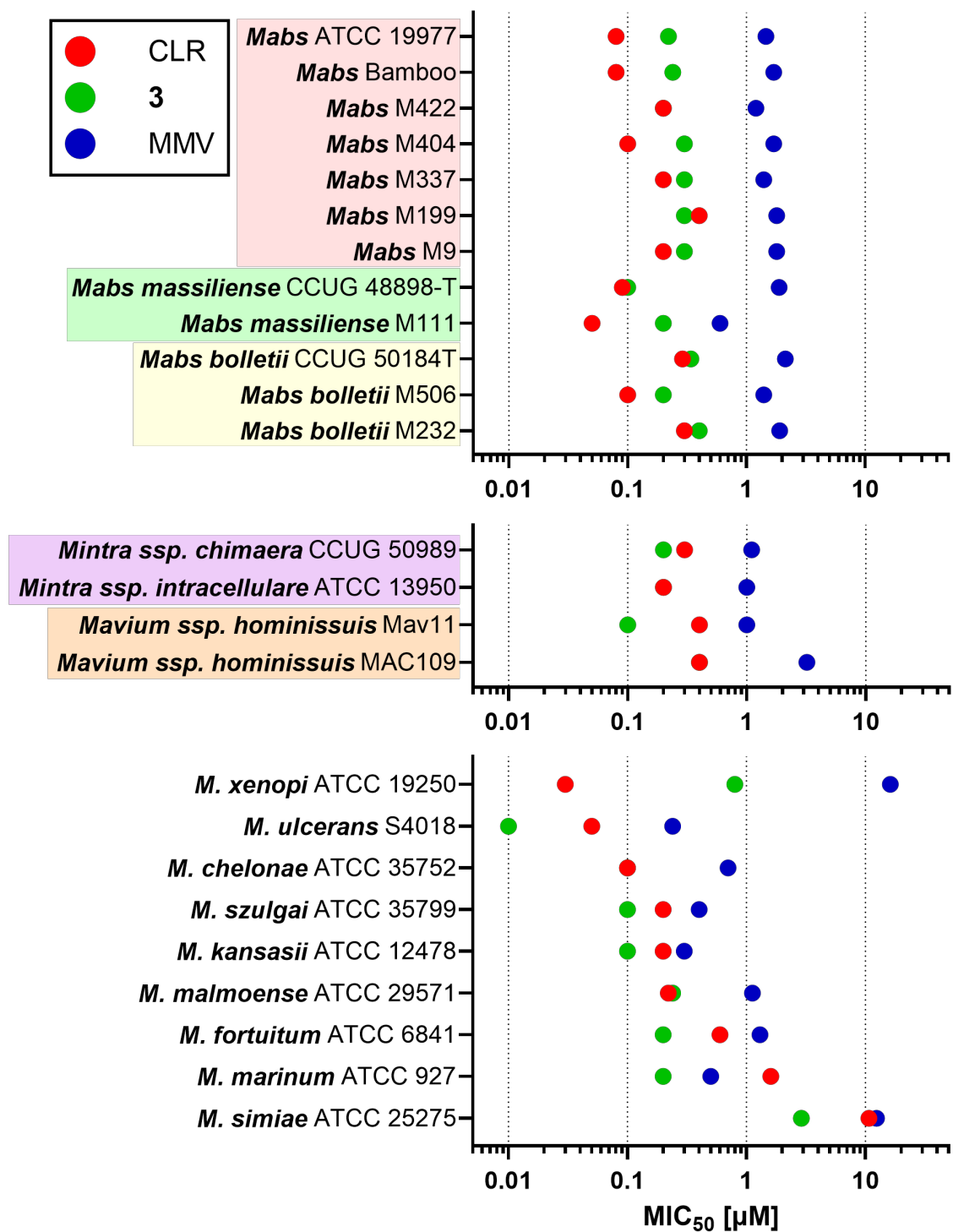


**Figure 13.** Overview of MIC<sub>50</sub> values determined against strains of the *M. abscessus* complex, the *M. avium* complex and a set of different other NTM. CLR: clarithromycin; Compound 3: Improved AAP derivative; compound 3 in publication III [197]; MMV: MMV688845.

### 3.3) *Metabolic in vitro* Stability of AAPs

Metabolic stability remains a significant challenge in the development of AAPs. The snapshot pharmacokinetic analysis conducted with female CD-1 mice indicates a very low oral bioavailability of the screening hit MMV688845 [212], which necessitates a detailed analysis of the metabolic stability of AAPs with *in vitro* testing methods.

As MMV688845 is included in the Pathogen Box<sup>®</sup> it comes with a set of various predetermined pharmacokinetic parameters. The MMV data set showed that MMV688845 is degraded in mouse plasma with 60% remaining substance after 4 h. When our research team first published *in vitro* plasma stability data we determined a value of 60% after 2 h of incubation in murine plasma [190]. The compound did not show any instability in human plasma. The synthetic derivative that was tested (Compound 24) was not degraded in murine or human plasma, indicating higher stability than the screening hit MMV688845. This was also true for the derivatives presented in our ChemMedChem publication [197]. The exchange of morpholine to thiomorpholine dioxide could be the reason for the improved stability of these derivatives for the reasons stated in section 3.1.5).

Additionally, the data set provided by MMV contained *in vitro* microsomal stability data as an indicator for hepatic metabolism and stability. The compounds were incubated in preparations of human or murine liver, which contain mainly enzymes of the p450 enzyme family that catalyze oxidative metabolic functionalization. MMV688845 was reported to have a microsomal half-life of 129 min in human microsomal suspensions and of 795 min in murine microsomal suspensions, indicating exceptional stability against hepatic enzymes. This result is contradictory to what we determined for MMV688845 [190], [197]. With half-lives of MMV688845 of only 1.7 min and 0.9 min in human and murine microsomal suspensions, the difference is striking. We did not have access to detailed protocols that MMV used for the determination. We can only suspect a methodological difference in the procedure, like the addition of NADPH to the incubated mixture. Microsomal half-lives were also determined for the set of sterically shielded AAPs that we synthesized in publication II [197]. We hypothesized that hydrolysis of amide bonds, in particular of the electron deficient anilide bond, lead to low microsomal stability. By the addition of small substituents we tried to sterically shield the amide bonds from the enzymes catalyzing hydrolysis that are present in the microsomal suspensions like carboxylesterases [213]. The derivatization in close proximity to the amide bonds indeed improved the stability of the compounds, but unfortunately at the expense of *in vitro* activity. In particular, the addition of a methyl or fluoro substituent to the anilide bond provided increased stability. In the

future, the integration of amide bond bioisosteres to the AAP scaffold could remove the hydrolytic liability.

Still, it seems that other, probably oxidative, reactions degrade AAPs, which makes a detailed identification of the formed metabolites imperative for successful improvement. We suspect that the morpholine moiety is the main source of instability as it is known that unsaturated heterocycles are often susceptible to electrophilic oxidation mediated by p450 enzymes [214]. For instance, lowering the general lipophilicity of the saturated ring or the addition of fluoro substituents improved microsomal stability [215]. The higher electron deficiency of thiomorpholine *S*-oxides in comparison to morpholine should already lead to a higher stability of the aliphatic ring system [199]. However, as these derivatives also do not show improved stability compared to MMV688845, we need more insight into the metabolism of these substances. Identification of metabolites of substances containing thiomorpholine *S*-oxides appears imperative. At this stage of research, we do not know whether the aliphatic ring system is oxidized or whether another part of the molecule, e.g. the aromatic rings, are (also) affected by microsomal enzymes. To address this lack of information, extensive metabolic experiments are currently conducted.

### 3.4) Target, Structural Insights & Binding Mode

The first time that an AAP compound was tested for activity against *M. tuberculosis* RNAP  $\sigma^A$ -holoenzyme was almost 15 years ago, when a high-throughput screen of 114,260 compounds was initiated in 2009 by Dr. Scott Diamond and Dr. Edison Lucumi at the University of Pennsylvania, as disclosed in the thesis of Soma Mandal [188]. The library was tested, and 88 hits could be confirmed. Of these, 15 compounds were found to inhibit *M. tuberculosis* in culture and one of the compounds was D-AAP1. Unfortunately, the details of this screen were never published. Lin *et al.* only state that information about the screen would be published elsewhere, which seems to have never happened [189]. It took until 2014 and 2017 when the first studies were published that employed biochemical experiments like generation and analysis of resistant mutants and different *in vitro* transcription assays validating the target. The target was verified by us with the generation of resistant mutants of *M. abscessus* under the influence of MMV688845 [212]. The resistant *M. abscessus* strains showed insusceptibility to novel AAP derivatives providing further proof of the target [190].

The actual target site of AAPs was revealed utilizing an X-ray crystal structure of *M. tuberculosis* RNAP together with D-AAP1 [188], [189]. The published structure gave us a first insight into the binding mode of AAPs. With a resolution of 4.0 Å only, the structure still contains a high degree of uncertainty on the atomic level. This problem also carries over to the homology models that we prepared based on this structure [190]. Nevertheless, this approach allowed us to verify that the RNAP target site is highly conserved in *M. abscessus*, and that target binding should not be affected by differences in tertiary structure of the protein, compared to the *M. tuberculosis* target. We also demonstrated a high degree of target homology across different mycobacterial species indicating proper target binding of AAPs, which was verified by whole cell growth inhibition assays [191].

In the future, we need a more detailed structural analysis of the target to overcome the limitations of low-resolution structures. To do so, we established a collaboration with Professor Dr. Elizabeth Campbell (The Rockefeller University, Manhattan, NY) with the goal to resolve AAP compounds together with their target structure by cryo-EM analysis. Preliminary results indicate an encouraging resolution of 2.5 Å of the target site with compound 24 (publication I, [190]) that could be depicted in its binding pocket (see **Figure 14**, unpublished). A manuscript describing the new cryo-EM structure and further findings regarding the mechanism of action of AAPs is currently under preparation.

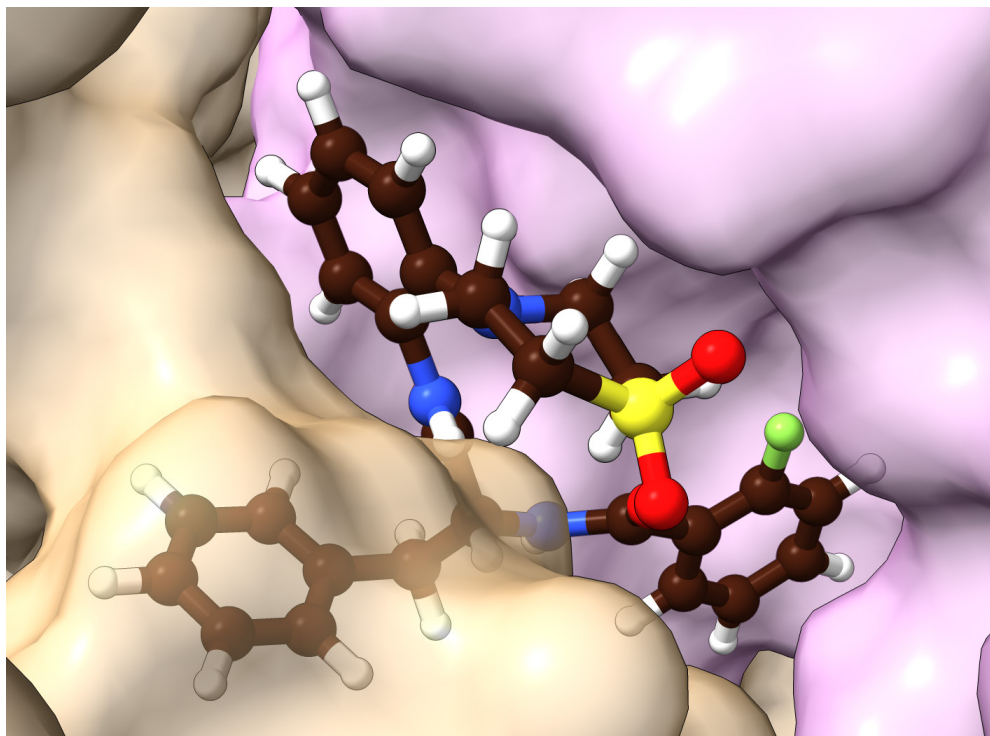


**Figure 14.** Preliminary 2.5 Å cryo-EM structure of *M. tuberculosis* RNAP together with compound 24 (Lang et. al., *J. Med. Chem.*, 2023) bound to the AAP target site (unpublished).

### **3.5) Conclusion**

In conclusion, this dissertation demonstrates the potential of AAPs to become effective antimycobacterial agents. However, it also highlights the necessity for further optimization of their pharmacokinetic properties and a deeper understanding of metabolism *in vivo*. This comprehensive investigation lays a robust foundation for future research aimed to develop AAPs with enhanced stability and efficacy, paving the way for new treatments against a broad spectrum of mycobacterial infections.



## 4) References

- [1] E. Tortoli *et al.*, “The new phylogeny of the genus *Mycobacterium*: The old and the news,” *Infection, Genetics and Evolution*, vol. 56, pp. 19–25, Dec. 2017, doi: 10.1016/J.MEEGID.2017.10.013.
- [2] World Health Organization, “Global Tuberculosis Report 2023,” 2023. Accessed: Dec. 18, 2023. [Online]. Available: <https://www.who.int/teams/global-tuberculosis-programme/tb-reports/global-tuberculosis-report-2023>
- [3] P. H. Le *et al.*, “Pathogenesis, Clinical Considerations, and Treatments: A Narrative Review on Leprosy,” *Cureus*, vol. 15, no. 12, Dec. 2023, doi: 10.7759/CUREUS.49954.
- [4] World Health Organization, “Number of New Leprosy Cases.” Accessed: Aug. 21, 2024. [Online]. Available: <https://www.who.int/data/gho/data/indicators/indicator-details/GHO/number-of-new-leprosy-cases>
- [5] M. A. Riojas, K. J. McGough, C. J. Rider-Riojas, N. Rastogi, and M. H. Hazbón, “Phylogenomic analysis of the species of the mycobacterium tuberculosis complex demonstrates that mycobacterium africanum, mycobacterium bovis, mycobacterium caprae, mycobacterium microti and mycobacterium pinnipedii are later heterotypic synonyms of mycobacterium tuberculosis,” *Int J Syst Evol Microbiol*, vol. 68, no. 1, pp. 324–332, Jan. 2018, doi: 10.1099/IJSEM.0.002507.
- [6] M. A. Forrellad *et al.*, “Virulence factors of the *Mycobacterium tuberculosis* complex,” *Virulence*, vol. 4, no. 1, pp. 3–66, Jan. 2013, doi: 10.4161/VIRU.22329.
- [7] S. T. Cole *et al.*, “Massive gene decay in the leprosy bacillus,” *Nature* 2001 409:6823, vol. 409, no. 6823, pp. 1007–1011, Feb. 2001, doi: 10.1038/35059006.
- [8] E. H. Runyon, “Anonymous *Mycobacteria* in Pulmonary Disease,” *Medical Clinics of North America*, vol. 43, no. 1, pp. 273–290, Jan. 1959, doi: 10.1016/S0025-7125(16)34193-1.
- [9] E. Tortoli, “Microbiological features and clinical relevance of new species of the genus *Mycobacterium*,” *Clin Microbiol Rev*, vol. 27, no. 4, pp. 727–752, Oct. 2014, doi: 10.1128/CMR.00035-14.
- [10] C. Y. Turenne, “Nontuberculous mycobacteria: Insights on taxonomy and evolution,” *Infection, Genetics and Evolution*, vol. 72, pp. 159–168, Aug. 2019, doi: 10.1016/J.MEEGID.2019.01.017.

- [11] R. S. Gupta, B. Lo, and J. Son, "Phylogenomics and comparative genomic studies robustly support division of the genus *Mycobacterium* into an emended genus *Mycobacterium* and four novel genera," *Front Microbiol*, vol. 9, no. FEB, p. 67, Feb. 2018, doi: 10.3389/FMICB.2018.00067.
- [12] E. Tortoli *et al.*, "Same meat, different gravy: ignore the new names of mycobacteria," *European Respiratory Journal*, vol. 54, no. 1, Jul. 2019, doi: 10.1183/13993003.00795-2019.
- [13] J. Van Ingen, C. Y. Turenne, E. Tortoli, R. J. Wallace, and B. A. Brown-Elliott, "A definition of the *Mycobacterium avium* complex for taxonomical and clinical purposes, a review," *Int J Syst Evol Microbiol*, vol. 68, no. 11, pp. 3666–3677, Nov. 2018, doi: 10.1099/IJSEM.0.003026.
- [14] V. J. Timms, G. Daskalopoulos, H. M. Mitchell, and B. A. Neilan, "The Association of *Mycobacterium avium* subsp. *paratuberculosis* with Inflammatory Bowel Disease," *PLoS One*, vol. 11, no. 2, p. e0148731, Feb. 2016, doi: 10.1371/JOURNAL.PONE.0148731.
- [15] J. E. Gross *et al.*, "Molecular Epidemiologic Investigation of *Mycobacterium intracellulare* Subspecies *chimaera* Lung Infections at an Adult Cystic Fibrosis Program," *Ann Am Thorac Soc*, vol. 20, no. 5, pp. 677–686, May 2023, doi: 10.1513/ANNALSATS.202209-779OC.
- [16] A. Togawa *et al.*, "Multiple mutations of *Mycobacterium intracellulare* subsp. *chimaera* causing false-negative reaction to the transcription-reverse transcription concerted method for pathogen detection," *International Journal of Infectious Diseases*, vol. 133, pp. 14–17, Aug. 2023, doi: 10.1016/j.ijid.2023.04.406.
- [17] N. L. Wengenack *et al.*, "This is giving me a complex: a practical attempt to streamline nontuberculous mycobacteria nomenclature for clinical purposes," *J Clin Microbiol*, vol. 62, no. 3, Mar. 2024, doi: 10.1128/JCM.01531-23.
- [18] R. C. Lopeman, J. Harrison, M. Desai, and J. A. G. Cox, "Mycobacterium abscessus: Environmental Bacterium Turned Clinical Nightmare," *Microorganisms 2019, Vol. 7, Page 90*, vol. 7, no. 3, p. 90, Mar. 2019, doi: 10.3390/MICROORGANISMS7030090.
- [19] E. Tortoli *et al.*, "Emended description of *mycobacterium abscessus mycobacterium abscessus* subsp. *Abscessus* and *mycobacterium abscessus* subsp. *bolletii* and designation of *mycobacterium abscessus* subsp. *massiliense* comb. nov.," *Int J Syst Evol Microbiol*, vol. 66, no. 11, pp. 4471–4479, Nov. 2016, doi: 10.1099/IJSEM.0.001376.
- [20] A. Koul, E. Arnoult, N. Lounis, J. Guillemont, and K. Andries, "The challenge of new drug discovery for tuberculosis," *Nature 2011 469:7331*, vol. 469, no. 7331, pp. 483–490, Jan. 2011, doi: 10.1038/nature09657.

- [21] C. L. Dulberger, E. J. Rubin, and C. C. Boutte, "The mycobacterial cell envelope — a moving target," *Nature Reviews Microbiology* 2019 18:1, vol. 18, no. 1, pp. 47–59, Nov. 2019, doi: 10.1038/s41579-019-0273-7.
- [22] L. J. Alderwick, J. Harrison, G. S. Lloyd, and H. L. Birch, "The Mycobacterial Cell Wall—Peptidoglycan and Arabinogalactan," *Cold Spring Harb Perspect Med*, vol. 5, no. 8, p. a021113, Aug. 2015, doi: 10.1101/CSHPERSPECT.A021113.
- [23] S. Mahapatra, H. Scherman, P. J. Brennan, and D. C. Crick, "N glycolylation of the nucleotide precursors of peptidoglycan biosynthesis of *Mycobacterium* spp. is altered by drug treatment," *J Bacteriol*, vol. 187, no. 7, pp. 2341–2347, Apr. 2005, doi: 10.1128/JB.187.7.2341-2347.2005.
- [24] P. J. Brennan and H. Nikaido, "The envelope of mycobacteria," *Annu Rev Biochem*, vol. 64, no. Volume 64, 1995, pp. 29–63, Jul. 1995, doi: 10.1146/ANNUREV.BI.64.070195.000333.
- [25] D. E. Minnikin *et al.*, "Pathophysiological Implications of Cell Envelope Structure in *Mycobacterium tuberculosis* and Related Taxa," *Tuberculosis - Expanding Knowledge*, Jul. 2015, doi: 10.5772/59585.
- [26] Y. Yuan, Y. Q. Zhu, D. D. Crane, and C. E. Barry, "The effect of oxygenated mycolic acid composition on cell wall function and macrophage growth in *Mycobacterium tuberculosis*," *Mol Microbiol*, vol. 29, no. 6, pp. 1449–1458, Sep. 1998, doi: 10.1046/J.1365-2958.1998.01026.X.
- [27] V. Jarlier and H. Nikaido, "Permeability barrier to hydrophilic solutes in *Mycobacterium chelonae*," *J Bacteriol*, vol. 172, no. 3, pp. 1418–1423, 1990, doi: 10.1128/JB.172.3.1418-1423.1990.
- [28] J. S. Schorey and L. Sweet, "The mycobacterial glycopeptidolipids: structure, function, and their role in pathogenesis," *Glycobiology*, vol. 18, no. 11, pp. 832–841, Nov. 2008, doi: 10.1093/GLYCOB/CWN076.
- [29] C. J. Cambier *et al.*, "Mycobacteria manipulate macrophage recruitment through coordinated use of membrane lipids," *Nature* 2013 505:7482, vol. 505, no. 7482, pp. 218–222, Dec. 2013, doi: 10.1038/nature12799.
- [30] C. J. Cambier, S. M. Banik, J. A. Buonomo, and C. R. Bertozzi, "Spreading of a mycobacterial cell surface lipid into host epithelial membranes promotes infectivity," *Elife*, vol. 9, pp. 1–68, Oct. 2020, doi: 10.7554/ELIFE.60648.
- [31] N. Zamora, J. Esteban, T. J. Kinnari, A. Celdrán, J. J. Granizo, and C. Zafra, "In-vitro evaluation of the adhesion to polypropylene sutures of non-pigmented, rapidly growing mycobacteria," *Clinical Microbiology and Infection*, vol. 13, no. 9, pp. 902–907, Sep. 2007, doi: 10.1111/J.1469-0691.2007.01769.X.

- [32] M. C. Muñoz-Egea, A. Akir, and J. Esteban, "Mycobacterium biofilms," *Biofilm*, vol. 5, Dec. 2023, doi: 10.1016/j.biofilm.2023.100107.
- [33] J. Van Ingen, H. Blaak, J. De Beer, A. M. De Roda Husman, and D. Van Soolingen, "Rapidly growing nontuberculous mycobacteria cultured from home tap and shower water," *Appl Environ Microbiol*, vol. 76, no. 17, pp. 6017–6019, Sep. 2010, doi: 10.1128/AEM.00843-10.
- [34] S. S. Branda, Å. Vik, L. Friedman, and R. Kolter, "Biofilms: The matrix revisited," *Trends Microbiol*, vol. 13, no. 1, pp. 20–26, Jan. 2005, doi: 10.1016/j.tim.2004.11.006.
- [35] J. Recht, A. Martínez, S. Torello, and R. Kolter, "Genetic analysis of sliding motility in *Mycobacterium smegmatis*," *J Bacteriol*, vol. 182, no. 15, pp. 4348–4351, Aug. 2000, doi: 10.1128/JB.182.15.4348-4351.2000.
- [36] M. M. Zambrano and R. Kolter, "Mycobacterial Biofilms: A Greasy Way to Hold It Together," *Cell*, vol. 123, no. 5, pp. 762–764, Dec. 2005, doi: 10.1016/J.CELL.2005.11.011.
- [37] A. K. Ojha *et al.*, "Growth of *Mycobacterium tuberculosis* biofilms containing free mycolic acids and harbouring drug-tolerant bacteria," *Mol Microbiol*, vol. 69, no. 1, pp. 164–174, Jul. 2008, doi: 10.1111/J.1365-2958.2008.06274.X.
- [38] T. Qvist *et al.*, "Chronic pulmonary disease with *Mycobacterium abscessus* complex is a biofilm infection," *European Respiratory Journal*, vol. 46, no. 6, pp. 1823–1826, Dec. 2015, doi: 10.1183/13993003.01102-2015.
- [39] A. Bernut *et al.*, "Insights into the smooth-to-rough transitioning in *Mycobacterium bolletii* unravels a functional Tyr residue conserved in all mycobacterial MmpL family members," *Mol Microbiol*, vol. 99, no. 5, pp. 866–883, Mar. 2016, doi: 10.1111/MMI.13283.
- [40] M. D. Johansen, J. L. Herrmann, and L. Kremer, "Non-tuberculous mycobacteria and the rise of *Mycobacterium abscessus*," *Nat Rev Microbiol*, vol. 18, no. 7, pp. 392–407, Jul. 2020, doi: 10.1038/S41579-020-0331-1.
- [41] W. Daher *et al.*, "Glycopeptidolipid glycosylation controls surface properties and pathogenicity in *Mycobacterium abscessus*," *Cell Chem Biol*, vol. 29, no. 5, pp. 910–924.e7, May 2022, doi: 10.1016/J.CHEMBIOL.2022.03.008.
- [42] C. Brambilla *et al.*, "Mycobacteria Clumping Increase Their Capacity to Damage Macrophages," *Front Microbiol*, vol. 7, no. OCT, Oct. 2016, doi: 10.3389/FMICB.2016.01562.
- [43] A. L. Roux *et al.*, "The distinct fate of smooth and rough *Mycobacterium abscessus* variants inside macrophages," *Open Biol*, vol. 6, no. 11, 2016, doi: 10.1098/RSOB.160185.

- [44] A. Bernut *et al.*, “Mycobacterium abscessus cording prevents phagocytosis and promotes abscess formation,” *Proc Natl Acad Sci U S A*, vol. 111, no. 10, pp. E943–E952, Mar. 2014, doi: 10.1073/PNAS.1321390111.
- [45] R. Pavan *et al.*, “Moles of Molecules against Mycobacterium abscessus: A Review of Current Research,” *Future Pharmacology 2023, Vol. 3, Pages 637-663*, vol. 3, no. 3, pp. 637–663, Sep. 2023, doi: 10.3390/FUTUREPHARMACOL3030041.
- [46] M. J. Colston and R. A. Cox, “Mycobacterial Growth and Dormancy,” *Mycobacteria*, pp. 198–219, Sep. 1999, doi: 10.1002/9781444311433.CH11.
- [47] J. Liu, C. E. Barry Iii, G. S. Besra, and H. Nikaido, “Mycolic Acid Structure Determines the Fluidity of the Mycobacterial Cell Wall\*,” *Journal of Biological Chemistry*, vol. 271, pp. 29545–29551, 1996, doi: 10.1074/jbc.271.47.29545.
- [48] C. Stahl, S. Kubetzko, I. Kaps, S. Seeber, H. Engelhardt, and M. Niederweis, “MspA provides the main hydrophilic pathway through the cell wall of Mycobacterium smegmatis,” *Mol Microbiol*, vol. 40, no. 2, pp. 451–464, Apr. 2001, doi: 10.1046/J.1365-2958.2001.02394.X.
- [49] S. Sharbati-Tehrani, B. Meister, B. Appel, and A. Lewin, “The porin MspA from Mycobacterium smegmatis improves growth of Mycobacterium bovis BCG,” *International Journal of Medical Microbiology*, vol. 294, no. 4, pp. 235–245, Oct. 2004, doi: 10.1016/J.IJMM.2004.02.001.
- [50] M. Braibant, P. Gilot, and J. Content, “The ATP binding cassette (ABC) transport systems of Mycobacterium tuberculosis,” *FEMS Microbiol Rev*, vol. 24, no. 4, pp. 449–467, Oct. 2000, doi: 10.1111/J.1574-6976.2000.TB00550.X.
- [51] Z. Ditse, M. H. Lamers, and D. F. Warner, “DNA Replication in Mycobacterium tuberculosis,” *Microbiol Spectr*, vol. 5, no. 2, Mar. 2017, doi: 10.1128/MICROBIOLSPEC.TBTB2-0027-2016.
- [52] A. Lewin and S. Sharbati-Tehrani, “Das langsame Wachstum von Mykobakterien. Mögliche Ursachen und Bedeutung für die Pathogenität,” *Bundesgesundheitsblatt Gesundheitsforschung Gesundheitsschutz*, vol. 48, no. 12, pp. 1390–1399, Dec. 2005, doi: 10.1007/S00103-005-1171-X.
- [53] S. Gagneux, “Host–pathogen coevolution in human tuberculosis,” *Philosophical Transactions of the Royal Society B: Biological Sciences*, vol. 367, no. 1590, pp. 850–859, 2012, doi: 10.1098/RSTB.2011.0316.
- [54] J. O. Falkinham, “Nontuberculous mycobacteria from household plumbing of patients with nontuberculous mycobacteria disease,” *Emerg Infect Dis*, vol. 17, no. 3, pp. 419–424, Mar. 2011, doi: 10.3201/EID1703.101510.

- [55] J. O. Falkinham, "Nontuberculous mycobacteria in the environment," *Clin Chest Med*, vol. 23, no. 3, pp. 529–551, Sep. 2002, doi: 10.1016/S0272-5231(02)00014-X.
- [56] E. Hashish *et al.*, "Mycobacterium marinum infection in fish and man: epidemiology, pathophysiology and management; a review," *Vet Q*, vol. 38, no. 1, p. 35, Jan. 2018, doi: 10.1080/01652176.2018.1447171.
- [57] R. R. Yotsu *et al.*, "Buruli Ulcer: a Review of the Current Knowledge," *Curr Trop Med Rep*, vol. 5, no. 4, pp. 247–256, Dec. 2018, doi: 10.1007/S40475-018-0166-2/TABLES/1.
- [58] V. Dartois, C. Sizemore, and T. Dick, "Editorial: NTM—The new uber-bugs," *Front Microbiol*, vol. 10, no. JUN, p. 1299, 2019, doi: 10.3389/FMICB.2019.01299.
- [59] A. R. Cullen, C. L. Cannon, E. J. Mark, and A. A. Colin, "Mycobacterium abscessus Infection in Cystic Fibrosis: Colonization or Infection?," *Am J Respir Crit Care Med*, vol. 161, no. 2 I, pp. 641–645, Dec. 2012, doi: 10.1164/AJRCCM.161.2.9903062.
- [60] T. M. Gonzalez-Santiago and L. A. Drage, "Nontuberculous Mycobacteria: Skin and Soft Tissue Infections," *Dermatol Clin*, vol. 33, no. 3, pp. 563–577, 2015, doi: 10.1016/J.DET.2015.03.017.
- [61] M. Kuntz *et al.*, "Risk Factors for Complicated Lymphadenitis Caused by Nontuberculous Mycobacteria in Children," *Emerg Infect Dis*, vol. 26, no. 3, pp. 579–586, 2020, doi: 10.3201/EID2603.191388.
- [62] S. M. September, V. S. Brözel, and S. N. Venter, "Diversity of Nontuberculoïd Mycobacterium Species in Biofilms of Urban and Semiurban Drinking Water Distribution Systems," *Appl Environ Microbiol*, vol. 70, no. 12, pp. 7571–7573, Dec. 2004, doi: 10.1128/AEM.70.12.7571-7573.2004.
- [63] L. M. Feazel, L. K. Baumgartner, K. L. Peterson, D. N. Frank, J. K. Harris, and N. R. Pace, "Opportunistic pathogens enriched in showerhead biofilms," *Proc Natl Acad Sci U S A*, vol. 106, no. 38, pp. 16393–16398, Sep. 2009, doi: 10.1073/PNAS.0908446106.
- [64] R. Thomson, C. Tolson, R. Carter, C. Coulter, F. Huygens, and M. Hargreaves, "Isolation of nontuberculous mycobacteria (NTM) from household water and shower aerosols in patients with pulmonary disease caused by NTM," *J Clin Microbiol*, vol. 51, no. 9, pp. 3006–3011, Sep. 2013, doi: 10.1128/JCM.00899-13.
- [65] D. R. Prevots, J. Adjemian, A. G. Fernandez, M. R. Knowles, and K. N. Olivier, "Environmental risks for nontuberculous mycobacteria: Individual exposures and climatic factors in the cystic fibrosis population," *Ann Am Thorac Soc*, vol. 11, no. 7, pp. 1032–1038, Sep. 2014, doi: 10.1513/ANNALSATS.201404-184OC.

- [66] M. A. De Groote, N. R. Pace, K. Fulton, and J. O. Falkinham, "Relationships between Mycobacterium isolates from patients with pulmonary mycobacterial infection and potting soils," *Appl Environ Microbiol*, vol. 72, no. 12, pp. 7602–7606, Dec. 2006, doi: 10.1128/AEM.00930-06.
- [67] J. M. Bryant *et al.*, "Population-level genomics identifies the emergence and global spread of a human transmissible multidrug-resistant nontuberculous mycobacterium," *Science*, vol. 354, no. 6313, p. 751, Nov. 2016, doi: 10.1126/SCIENCE.AAF8156.
- [68] N. Commins, M. R. Sullivan, K. McGowen, E. M. Koch, E. J. Rubin, and M. Farhat, "Mutation rates and adaptive variation among the clinically dominant clusters of Mycobacterium abscessus," *Proc Natl Acad Sci U S A*, vol. 120, no. 22, p. e2302033120, May 2023, doi: 10.1073/PNAS.2302033120.
- [69] I. K. Park and K. N. Olivier, "Nontuberculous mycobacteria in cystic fibrosis and non-cystic fibrosis bronchiectasis," *Semin Respir Crit Care Med*, vol. 36, no. 2, pp. 217–224, Apr. 2015, doi: 10.1055/s-0035-1546751.
- [70] T. K. Marras *et al.*, "Risk of nontuberculous mycobacterial pulmonary disease with obstructive lung disease," *European Respiratory Journal*, vol. 48, no. 3, pp. 928–931, Sep. 2016, doi: 10.1183/13993003.00033-2016.
- [71] C. Herzmann and C. Lange, "Nicht-tuberkulöse Mykobakteriosen bei der HIV-Infektion," *DMW - Deutsche Medizinische Wochenschrift*, vol. 135, no. 23, pp. 1192–1197, 2010, doi: 10.1055/S-0030-1255130.
- [72] M. K. Haas and C. L. Daley, "Mycobacterial Lung Disease Complicating HIV Infection," *Semin Respir Crit Care Med*, vol. 37, no. 2, pp. 230–242, Apr. 2016, doi: 10.1055/s-0036-1572559.
- [73] E. Henkle and K. L. Winthrop, "Nontuberculous mycobacteria infections in immunosuppressed hosts," *Clin Chest Med*, vol. 36, no. 1, pp. 91–99, Mar. 2015, doi: 10.1016/J.CCM.2014.11.002.
- [74] D. C. Gadsby, P. Vergani, and L. Csanády, "The ABC protein turned chloride channel whose failure causes cystic fibrosis," *Nature* 2006 440:7083, vol. 440, no. 7083, pp. 477–483, Mar. 2006, doi: 10.1038/nature04712.
- [75] T. Baird and S. Bell, "Cystic Fibrosis-Related Nontuberculous Mycobacterial Pulmonary Disease," *Clin Chest Med*, Aug. 2023, doi: 10.1016/j.ccm.2023.06.008.
- [76] C. J. Richards and K. N. Olivier, "Nontuberculous Mycobacteria in Cystic Fibrosis," *Semin Respir Crit Care Med*, vol. 40, no. 06, pp. 737–750, Dec. 2019, doi: 10.1055/s-0039-1693706.

- [77] C. R. Esther, D. A. Esserman, P. Gilligan, A. Kerr, and P. G. Noone, "Chronic Mycobacterium abscessus infection and lung function decline in cystic fibrosis," *Journal of Cystic Fibrosis*, vol. 9, no. 2, pp. 117–123, Mar. 2010, doi: 10.1016/J.JCF.2009.12.001.
- [78] "Reported TB in the US 2022 | Data & Statistics | TB | CDC." Accessed: Jul. 02, 2024. [Online]. Available: <https://www.cdc.gov/tb/statistics/reports/2022/default.htm>
- [79] D. R. Prevots, J. E. Marshall, D. Wagner, and K. Morimoto, "Global Epidemiology of Nontuberculous Mycobacterial Pulmonary Disease: A Review," *Clin Chest Med*, Sep. 2023, doi: 10.1016/J.CCM.2023.08.012.
- [80] Research Institute of Tuberculosis and Japan Anti-Tuberculosis Association, "Tuberculosis in Japan - Annual Report 2022," 2022. Accessed: Jul. 02, 2024. [Online]. Available: <https://jata-ekigaku.jp/english/tb-in-japan>
- [81] H. Namkoong *et al.*, "Epidemiology of Pulmonary Nontuberculous Mycobacterial Disease, Japan - Volume 22, Number 6—June 2016 - Emerging Infectious Diseases journal - CDC," *Emerg Infect Dis*, vol. 22, no. 6, pp. 1116–1117, Jun. 2016, doi: 10.3201/EID2206.151086.
- [82] R. A. Blakney *et al.*, "Incidence of Nontuberculous Mycobacterial Pulmonary Infection, by Ethnic Group, Hawaii, USA, 2005–2019 - Volume 28, Number 8—August 2022 - Emerging Infectious Diseases journal - CDC," *Emerg Infect Dis*, vol. 28, no. 8, pp. 1543–1550, Aug. 2022, doi: 10.3201/EID2808.212375.
- [83] S. Kambali *et al.*, "Pulmonary nontuberculous mycobacterial disease in Florida and association with large-scale natural disasters," *BMC Public Health*, vol. 21, no. 1, pp. 1–11, Dec. 2021, doi: 10.1186/S12889-021-12115-7.
- [84] M. Yan, S. K. Brode, and T. K. Marras, "Treatment of the Less Common Nontuberculous Mycobacterial Pulmonary Disease," *Clin Chest Med*, Aug. 2023, doi: 10.1016/j.ccm.2023.06.011.
- [85] J. Van Ingen, M. J. Boeree, W. C. M. De Lange, P. E. W. De Haas, P. N. R. Dekhuijzen, and D. Van Soolingen, "Clinical relevance of Mycobacterium szulgai in The Netherlands," *Clinical Infectious Diseases*, vol. 46, no. 8, pp. 1200–1205, Apr. 2008, doi: 10.1086/529443/2/46-8-1200-FIG002.GIF.
- [86] J. Marks, P. A. Jenkins, and M. Tsukamura, "Mycobacterium szulgai - A new pathogen," *Tubercle*, vol. 53, no. 3, pp. 210–214, 1972, doi: 10.1016/0041-3879(72)90018-9.
- [87] M. J. Nasiri, S. Amini, Z. Nikpor, S. Arefzadeh, S. M. J. Mousavi, and H. Goudarzi, "Drug Susceptibility Testing of Mycobacterium Simiae: An Emerging Pathogen in Iran," *Infect Disord Drug Targets*, vol. 21, no. 4, pp. 619–622, Jul. 2020, doi: 10.2174/1871526520999200727114148.

- [88] C. L. Daley *et al.*, “Treatment of nontuberculous mycobacterial pulmonary disease: An official ATS/ERS/ESCMID/IDSA clinical practice guideline,” *European Respiratory Journal*, vol. 71, no. 4, pp. E1–E36, Aug. 2020, doi: 10.1093/CID/CIAA241.
- [89] B. A. Brown-Elliott, K. A. Nash, and R. J. Wallace, “Antimicrobial Susceptibility Testing, Drug Resistance Mechanisms, and Therapy of Infections with Nontuberculous Mycobacteria,” *Clin Microbiol Rev*, vol. 25, no. 3, pp. 545–582, 2012, doi: 10.1128/CMR.05030-11.
- [90] C. L. Daley *et al.*, “Treatment of Nontuberculous Mycobacterial Pulmonary Disease: An Official ATS/ERS/ESCMID/IDSA Clinical Practice Guideline,” *Clinical Infectious Diseases*, vol. 71, no. 4, pp. e1–e36, Aug. 2020, doi: 10.1093/CID/CIAA241.
- [91] A. Sawka and A. Burke, “Medications and Monitoring in Treatment of Nontuberculous Mycobacteria Lung Disease,” *Clin Chest Med*, Aug. 2023, doi: 10.1016/j.ccm.2023.06.012.
- [92] Y. K. Yam, N. Alvarez, M. L. Go, and T. Dick, “Extreme Drug Tolerance of Mycobacterium abscessus ‘Persists,’” *Front Microbiol*, vol. 11, Mar. 2020, doi: 10.3389/FMICB.2020.00359.
- [93] “M24 | Susceptibility Testing of Mycobacteria, Nocardia spp., and Other Aerobic Actinomycetes, 3rd Edition.” Accessed: Jul. 16, 2024. [Online]. Available: <https://clsi.org/standards/products/microbiology/documents/m24/>
- [94] “M24S | Performance Standards for Susceptibility Testing of Mycobacteria, Nocardia spp., and Other Aerobic Actinomycetes, 2nd Edition.” Accessed: Jul. 16, 2024. [Online]. Available: <https://clsi.org/standards/products/microbiology/documents/m24s/>
- [95] E. Tanaka *et al.*, “Effect of Clarithromycin Regimen for Mycobacterium avium Complex Pulmonary Disease,” *Am J Respir Crit Care Med*, vol. 160, no. 3, pp. 866–872, Dec. 2012, doi: 10.1164/AJRCCM.160.3.9811086.
- [96] Albrecht Meier *et al.*, “Molecular Mechanisms of Clarithromycin Resistance in Mycobacterium avium: Observation of Multiple 23S rDNA Mutations in a Clonal Population on JSTOR,” *J Infect Dis*, vol. 174, no. 2, pp. 354–360, 1996, Accessed: Jul. 16, 2024. [Online]. Available: <https://www.jstor.org/stable/30131614>
- [97] H. Y. Kim *et al.*, “Mycobacterium massiliense is differentiated from Mycobacterium abscessus and Mycobacterium bolletii by erythromycin ribosome methyltransferase gene (erm) and clarithromycin susceptibility patterns,” *Microbiol Immunol*, vol. 54, no. 6, pp. 347–353, Jun. 2010, doi: 10.1111/J.1348-0421.2010.00221.X.

- [98] B. A. Brown-Elliott *et al.*, “In vitro activity of amikacin against isolates of mycobacterium avium complex with proposed MIC breakpoints and finding of a 16S rRNA gene mutation in treated isolates,” *J Clin Microbiol*, vol. 51, no. 10, pp. 3389–3394, Oct. 2013, doi: 10.1128/jcm.01612-13.
- [99] Y. C. Huang *et al.*, “Clinical outcome of Mycobacterium abscessus infection and antimicrobial susceptibility testing,” *J Microbiol Immunol Infect*, vol. 43, no. 5, pp. 401–406, Oct. 2010, doi: 10.1016/S1684-1182(10)60063-1.
- [100] J. Jarand, A. Levin, L. Zhang, G. Huitt, J. D. Mitchell, and C. L. Daley, “Clinical and Microbiologic Outcomes in Patients Receiving Treatment for Mycobacterium abscessus Pulmonary Disease,” *Clinical Infectious Diseases*, vol. 52, no. 5, pp. 565–571, Mar. 2011, doi: 10.1093/CID/CIQ237.
- [101] M. Liu and S. Douthwaite, “Activity of the Ketolide Telithromycin Is Refractory to Erm Monomethylation of Bacterial rRNA,” *Antimicrob Agents Chemother*, vol. 46, no. 6, pp. 1629–1633, 2002, doi: 10.1128/AAC.46.6.1629-1633.2002.
- [102] K. A. Nash, N. Andini, Y. Zhang, B. A. Brown-Elliott, and R. J. Wallace, “Intrinsic Macrolide Resistance in Rapidly Growing Mycobacteria,” *Antimicrob Agents Chemother*, vol. 50, no. 10, p. 3476, Oct. 2006, doi: 10.1128/AAC.00402-06.
- [103] K. A. Nash, “Intrinsic macrolide resistance in Mycobacterium smegmatis is conferred by a novel erm gene, erm(38),” *Antimicrob Agents Chemother*, vol. 47, no. 10, pp. 3053–3060, Oct. 2003, doi: 10.1128/AAC.47.10.3053-3060.2003.
- [104] B. A. Brown-Elliott *et al.*, “Emergence of Inducible Macrolide Resistance in Mycobacterium chelonae Due to Broad-Host-Range Plasmid and Chromosomal Variants of the Novel 23S rRNA Methylase Gene, erm(55),” *J Clin Microbiol*, vol. 61, no. 7, Jul. 2023, doi: 10.1128/JCM.00428-23.
- [105] K. Buriánková *et al.*, “Molecular Basis of Intrinsic Macrolide Resistance in the Mycobacterium tuberculosis Complex,” *Antimicrob Agents Chemother*, vol. 48, no. 1, pp. 143–150, 2004, doi: 10.1128/AAC.48.1.143-150.2004.
- [106] M. R. Holt and T. Baird, “Treatment Approaches to Mycobacterium abscessus Pulmonary Disease,” *Clin Chest Med*, Aug. 2023, doi: 10.1016/j.ccm.2023.06.010.
- [107] W. Nie, H. Duan, H. Huang, Y. Lu, D. Bi, and N. Chu, “Species identification of Mycobacterium abscessus subsp. abscessus and Mycobacterium abscessus subsp. bolletii using rpoB and hsp65, and susceptibility testing to eight antibiotics,” *International Journal of Infectious Diseases*, vol. 25, pp. 170–174, Aug. 2014, doi: 10.1016/J.IJID.2014.02.014.

- [108] K. To, R. Cao, A. Yegiazaryan, J. Owens, and V. Venketaraman, "General Overview of Nontuberculous Mycobacteria Opportunistic Pathogens: Mycobacterium avium and Mycobacterium abscessus," *Journal of Clinical Medicine* 2020, Vol. 9, Page 2541, vol. 9, no. 8, p. 2541, Aug. 2020, doi: 10.3390/JCM9082541.
- [109] D. B. Aziz *et al.*, "Rifabutin Is active against mycobacterium abscessus complex," *Antimicrob Agents Chemother*, vol. 61, no. 6, Jun. 2017, doi: 10.1128/AAC.00155-17.
- [110] T. Dick, S. J. Shin, W. J. Koh, V. Dartois, and M. Gengenbacher, "Rifabutin is active against mycobacterium abscessus in mice," *Antimicrob Agents Chemother*, vol. 64, no. 2, Jan. 2020, doi: 10.1128/AAC.01943-19.
- [111] F. Alcaide, G. E. Pfyffer, and A. Telenti, "Role of embB in natural and acquired resistance to ethambutol in mycobacteria," *Antimicrob Agents Chemother*, vol. 41, no. 10, pp. 2270–2273, 1997, doi: 10.1128/AAC.41.10.2270.
- [112] E. Story-Roller, E. C. Maggioncalda, K. A. Cohen, and G. Lamichhane, "Mycobacterium abscessus and  $\beta$ -lactams: Emerging insights and potential opportunities," *Front Microbiol*, vol. 9, no. SEP, p. 402937, Sep. 2018, doi: 10.3389/FMICB.2018.02273.
- [113] D. A. Negatu *et al.*, "Activity of Oral Tebipenem-Avibactam in a Mouse Model of Mycobacterium abscessus Lung Infection," *Antimicrob Agents Chemother*, vol. 67, no. 2, Feb. 2023, doi: 10.1128/aac.01459-22.
- [114] R. Nessar, E. Cambau, J. M. Reyrat, A. Murray, and B. Gicquel, "Mycobacterium abscessus: a new antibiotic nightmare," *Journal of Antimicrobial Chemotherapy*, vol. 67, no. 4, pp. 810–818, Apr. 2012, doi: 10.1093/JAC/DKR578.
- [115] M.-V. H. Nguyen and C. L. Daley, "Treatment of Mycobacterium avium Complex Pulmonary Disease: When Should I Treat and What Therapy Should I Start?," *Clin Chest Med*, Aug. 2023, doi: 10.1016/j.ccm.2023.06.009.
- [116] R. Diel *et al.*, "Microbiologic Outcome of Interventions Against Mycobacterium avium Complex Pulmonary Disease: A Systematic Review," *Chest*, vol. 153, no. 4, pp. 888–921, Apr. 2018, doi: 10.1016/J.CHEST.2018.01.024.
- [117] Y. Park, E. H. Lee, I. Jung, G. Park, and Y. A. Kang, "Clinical characteristics and treatment outcomes of patients with macrolide-resistant Mycobacterium avium complex pulmonary disease: A systematic review and meta-analysis," *Respir Res*, vol. 20, no. 1, pp. 1–10, Dec. 2019, doi: 10.1186/S12931-019-1258-9.

- [118] J. van Ingen, W. Hoefsloot, V. Dartois, and T. Dick, "Rifampicin has no role in treatment of Mycobacterium avium complex pulmonary disease and bactericidal sterilising drugs are needed: a viewpoint," *European Respiratory Journal*, vol. 63, no. 5, p. 2302210, May 2024, doi: 10.1183/13993003.02210-2023.
- [119] D. J. Horne, C. Spitters, and M. Narita, "Experience with rifabutin replacing rifampin in the treatment of tuberculosis," *International Journal of Tuberculosis and Lung Disease*, vol. 15, no. 11, pp. 1485–1489, Nov. 2011, doi: 10.5588/IJTL.11.0068.
- [120] H. Choi *et al.*, "Clinical Characteristics and Treatment Outcomes of Patients with Acquired Macrolide-Resistant Mycobacterium abscessus Lung Disease," *Antimicrob Agents Chemother*, vol. 61, no. 10, 2017, doi: 10.1128/AAC.01146-17.
- [121] W. J. Koh *et al.*, "Mycobacterial Characteristics and Treatment Outcomes in Mycobacterium abscessus Lung Disease," *Clinical Infectious Diseases*, vol. 64, no. 3, pp. 309–316, Feb. 2017, doi: 10.1093/CID/CIW724.
- [122] A. Egorova, M. Jackson, V. Gavriluk, and V. Makarov, "Pipeline of anti-Mycobacterium abscessus small molecules: Repurposable drugs and promising novel chemical entities," *Med Res Rev*, vol. 41, no. 4, p. 2350, Jul. 2021, doi: 10.1002/MED.21798.
- [123] U. S. Ganapathy, V. Dartois, and T. Dick, "Repositioning rifamycins for Mycobacterium abscessus lung disease," *Expert Opinion on Drug Discovery*, vol. 14, no. 9, pp. 867–878, Sep. 2019, doi: 10.1080/17460441.2019.1629414.
- [124] U. S. Ganapathy and T. Dick, "Why Matter Matters: Fast-Tracking Mycobacterium abscessus Drug Discovery," *Molecules 2022, Vol. 27, Page 6948*, vol. 27, no. 20, p. 6948, Oct. 2022, doi: 10.3390/MOLECULES27206948.
- [125] D. E. Griffith *et al.*, "An Official ATS/IDSA Statement: Diagnosis, Treatment, and Prevention of Nontuberculous Mycobacterial Diseases," *Am J Respir Crit Care Med*, vol. 175, no. 4, pp. 367–416, Dec. 2012, doi: 10.1164/RCCM.200604-571ST.
- [126] F. Conradie *et al.*, "Treatment of Highly Drug-Resistant Pulmonary Tuberculosis," *New England Journal of Medicine*, vol. 382, no. 10, pp. 893–902, Mar. 2020, doi: 10.1056/NEJMOA1901814.
- [127] I. Shah, V. Poojari, and H. Meshram, "Multi-Drug Resistant and Extensively-Drug Resistant Tuberculosis," *Indian J Pediatr*, vol. 87, no. 10, pp. 833–839, Oct. 2020, doi: 10.1007/S12098-020-03230-1/TABLES/2.
- [128] H. Boyaci *et al.*, "Fidaxomicin jams Mycobacterium tuberculosis RNA polymerase motions needed for initiation via RbpA contacts," *Elife*, vol. 7, Feb. 2018, doi: 10.7554/ELIFE.34823.

- [129] Q. Sun *et al.*, “In vitro activity of fidaxomicin against nontuberculosis mycobacteria,” *J Med Microbiol*, vol. 71, no. 6, p. 001549, Jun. 2022, doi: 10.1099/JMM.0.001549.
- [130] R. H. Ebright, “RNA Polymerase: Structural Similarities Between Bacterial RNA Polymerase and Eukaryotic RNA Polymerase II,” *J Mol Biol*, vol. 304, no. 5, pp. 687–698, Dec. 2000, doi: 10.1006/JMBI.2000.4309.
- [131] D. Sweetser, M. Nonet, and R. A. Young, “Prokaryotic and eukaryotic RNA polymerases have homologous core subunits.,” *Proceedings of the National Academy of Sciences*, vol. 84, no. 5, pp. 1192–1196, Mar. 1987, doi: 10.1073/PNAS.84.5.1192.
- [132] K. S. Murakami and S. A. Darst, “Bacterial RNA polymerases: The whole story,” *Curr Opin Struct Biol*, vol. 13, no. 1, pp. 31–39, Feb. 2003, doi: 10.1016/S0959-440X(02)00005-2.
- [133] K. M. Lelli, M. Slattery, and R. S. Mann, “Disentangling the Many Layers of Eukaryotic Transcriptional Regulation,” *Annu Rev Genet*, vol. 46, pp. 43–68, Nov. 2012, doi: 10.1146/ANNUREV-GENET-110711-155437.
- [134] K. S. Murakami, “Structural biology of bacterial RNA polymerase,” *Biomolecules*, vol. 5, no. 2, pp. 848–864, May 2015, doi: 10.3390/BIOM5020848.
- [135] R. G. Roeder, “50+ years of eukaryotic transcription: an expanding universe of factors and mechanisms,” *Nature Structural & Molecular Biology* 2019 26:9, vol. 26, no. 9, pp. 783–791, Aug. 2019, doi: 10.1038/s41594-019-0287-x.
- [136] C. D. Kuhn *et al.*, “Functional Architecture of RNA Polymerase I,” *Cell*, vol. 131, no. 7, pp. 1260–1272, Dec. 2007, doi: 10.1016/J.CELL.2007.10.051.
- [137] P. Cramer *et al.*, “Architecture of RNA polymerase II and implications for the transcription mechanism,” *Science (1979)*, vol. 288, no. 5466, pp. 640–649, Apr. 2000, doi: 10.1126/science.288.5466.640.
- [138] A. J. Jasiak, K. J. Armache, B. Martens, R. P. Jansen, and P. Cramer, “Structural Biology of RNA Polymerase III: Subcomplex C17/25 X-Ray Structure and 11 Subunit Enzyme Model,” *Mol Cell*, vol. 23, no. 1, pp. 71–81, Jul. 2006, doi: 10.1016/J.MOLCEL.2006.05.013.
- [139] T. Kouba, J. Pospíšil, J. Hnilicová, H. Šanderová, I. Barvík, and L. Krásný, “The core and holoenzyme forms of RNA polymerase from mycobacterium smegmatis,” *J Bacteriol*, vol. 201, no. 4, Feb. 2019, doi: 10.1128/JB.00583-18.
- [140] E. F. Pettersen *et al.*, “UCSF ChimeraX: Structure visualization for researchers, educators, and developers,” *Protein Sci*, vol. 30, no. 1, pp. 70–82, Jan. 2021, doi: 10.1002/PRO.3943.

- [141] A. Ishihama, "Role of the RNA polymerase  $\alpha$  subunit in transcription activation," *Mol Microbiol*, vol. 6, no. 22, pp. 3283–3288, Nov. 1992, doi: 10.1111/J.1365-2958.1992.TB02196.X.
- [142] H. Mosaei and J. Harbottle, "Mechanisms of antibiotics inhibiting bacterial RNA polymerase," *Biochem Soc Trans*, vol. 47, no. 1, pp. 339–350, Feb. 2019, doi: 10.1042/BST20180499.
- [143] F. Stephanie, U. S. F. Tambunan, and T. J. Siahaan, "M. tuberculosis Transcription Machinery: A Review on the Mycobacterial RNA Polymerase and Drug Discovery Efforts," *Life*, vol. 12, no. 11, Nov. 2022, doi: 10.3390/LIFE12111774.
- [144] V. Sosunov *et al.*, "The involvement of the aspartate triad of the active center in all catalytic activities of multisubunit RNA polymerase," *Nucleic Acids Res*, vol. 33, no. 13, pp. 4202–4211, Jul. 2005, doi: 10.1093/NAR/GKI688.
- [145] A. Srivastava *et al.*, "New target for inhibition of bacterial RNA polymerase: 'switch region,'" *Curr Opin Microbiol*, vol. 14, no. 5, pp. 532–543, Oct. 2011, doi: 10.1016/J.MIB.2011.07.030.
- [146] A. Mazumder, M. Lin, A. N. Kapanidis, and R. H. Ebright, "Closing and opening of the RNA polymerase trigger loop," *Proc Natl Acad Sci U S A*, vol. 117, no. 27, pp. 15642–15649, Jul. 2020, doi: 10.1073/pnas.1920427117.
- [147] Thomas Fouqueau, "Function of the trigger loop in distinct steps of the transcription cycle," Universität Regensburg, Regensburg, 2013.
- [148] N. Miropolskaya, D. Esyunina, S. Klimašauskas, V. Nikiforov, I. Artsimovitch, and A. Kulbachinskiy, "Interplay between the trigger loop and the F loop during RNA polymerase catalysis," *Nucleic Acids Res*, vol. 42, no. 1, pp. 544–552, Jan. 2014, doi: 10.1093/NAR/GKT877.
- [149] P. P. Hein and R. Landick, "The bridge helix coordinates movements of modules in RNA polymerase," *BMC Biol*, vol. 8, no. 1, pp. 1–4, Nov. 2010, doi: 10.1186/1741-7007-8-141.
- [150] G. Bar-Nahum, V. Epshtein, A. E. Ruckenstein, R. Rafikov, A. Mustaev, and E. Nudler, "A ratchet mechanism of transcription elongation and its control," *Cell*, vol. 120, no. 2, pp. 183–193, Jan. 2005, doi: 10.1016/j.cell.2004.11.045.
- [151] A. Weixlbaumer, K. Leon, R. Landick, and S. A. Darst, "Structural Basis of Transcriptional Pausing in Bacteria," *Cell*, vol. 152, no. 3, pp. 431–441, Jan. 2013, doi: 10.1016/J.CELL.2012.12.020.
- [152] R. Manganelli, "Sigma Factors: Key Molecules in Mycobacterium tuberculosis Physiology and Virulence," *Microbiol Spectr*, vol. 2, no. 1, Jan. 2014, doi: 10.1128/microbiolspec.mgm2-0007-2013.

- [153] S. Rodrigue, R. Provvedi, P. É. Jacques, L. Gaudreau, and R. Manganelli, "The  $\sigma$  factors of *Mycobacterium tuberculosis*," *FEMS Microbiol Rev*, vol. 30, no. 6, pp. 926–941, Nov. 2006, doi: 10.1111/J.1574-6976.2006.00040.X.
- [154] R. Manganelli, M. I. Voskuil, G. K. Schoolnik, E. Dubnau, M. Gomez, and I. Smith, "Role of the extracytoplasmic-function  $\sigma$  Factor  $\sigma^H$  in *Mycobacterium tuberculosis* global gene expression," *Mol Microbiol*, vol. 45, no. 2, pp. 365–374, Jul. 2002, doi: 10.1046/J.1365-2958.2002.03005.X.
- [155] M. Ando, T. Yoshimatsu, C. Ko, P. J. Converse, and W. R. Bishai, "Deletion of *Mycobacterium tuberculosis* Sigma Factor E Results in Delayed Time to Death with Bacterial Persistence in the Lungs of Aerosol-Infected Mice," *Infect Immun*, vol. 71, no. 12, pp. 7170–7172, Dec. 2003, doi: 10.1128/IAI.71.12.7170-7172.2003.
- [156] S. F. Altschul, W. Gish, W. Miller, E. W. Myers, and D. J. Lipman, "Basic local alignment search tool," *J Mol Biol*, vol. 215, no. 3, pp. 403–410, Oct. 1990, doi: 10.1016/S0022-2836(05)80360-2.
- [157] E. F. Ruff, M. T. Record, I. Artsimovitch, D. M. Hinton, and S. Wigneshweraraj, "Initial Events in Bacterial Transcription Initiation," *Biomolecules 2015, Vol. 5, Pages 1035-1062*, vol. 5, no. 2, pp. 1035–1062, May 2015, doi: 10.3390/BIOM5021035.
- [158] G. A. Belogurov and I. Artsimovitch, "Regulation of Transcript Elongation," *Annu Rev Microbiol*, vol. 69, no. 1, p. 49, Oct. 2015, doi: 10.1146/ANNUREV-MICRO-091014-104047.
- [159] S. H. Kirsch, F. P. J. Haeckl, and R. Müller, "Beyond the approved: target sites and inhibitors of bacterial RNA polymerase from bacteria and fungi," *Nat Prod Rep*, vol. 39, no. 6, pp. 1226–1263, Jun. 2022, doi: 10.1039/D1NP00067E.
- [160] J. Lee and S. Borukhov, "Bacterial RNA Polymerase-DNA Interaction—The Driving Force of Gene Expression and the Target for Drug Action," *Front Mol Biosci*, vol. 3, no. NOV, p. 73, Nov. 2016, doi: 10.3389/FMOLB.2016.00073.
- [161] A. Ray-Soni, M. J. Bellecourt, and R. Landick, "Mechanisms of Bacterial Transcription Termination: All Good Things Must End," *Annu Rev Biochem*, vol. 85, pp. 319–347, Jun. 2016, doi: 10.1146/ANNUREV-BIOCHEM-060815-014844.
- [162] J. W. Roberts, "Mechanisms of Bacterial Transcription Termination," *J Mol Biol*, vol. 431, no. 20, pp. 4030–4039, Sep. 2019, doi: 10.1016/J.JMB.2019.04.003.
- [163] P. Mitra, G. Ghosh, M. Hafeezunnisa, and R. Sen, "Rho Protein: Roles and Mechanisms," *Annu Rev Microbiol*, vol. 71, pp. 687–709, Sep. 2017, doi: 10.1146/ANNUREV-MICRO-030117-020432.

- [164] P. Sensi, "History of the Development of Rifampin," *Rev Infect Dis*, vol. 5, no. Supplement\_3, pp. S402–S406, Jul. 1983, doi: 10.1093/CLINIDS/5.SUPPLEMENT\_3.S402.
- [165] S. Bala *et al.*, "Reclassification of *Amycolatopsis mediterranei* DSM 46095 as *Amycolatopsis rifamycinica* sp. nov.," *Int J Syst Evol Microbiol*, vol. 54, no. 4, pp. 1145–1149, Jul. 2004, doi: 10.1099/IJS.0.02901-0/CITE/REFWORKS.
- [166] A. Le Breton and J. Dassin, *Rifift*, (1955). Accessed: May 30, 2024. [Online Video]. Available: [https://www.imdb.com/title/tt0048021/?ref\\_=fn\\_al\\_tt\\_2](https://www.imdb.com/title/tt0048021/?ref_=fn_al_tt_2)
- [167] M. Grobbelaar, G. E. Louw, S. L. Sampson, P. D. van Helden, P. R. Donald, and R. M. Warren, "Evolution of rifampicin treatment for tuberculosis," *Infection, Genetics and Evolution*, vol. 74, p. 103937, Oct. 2019, doi: 10.1016/J.MEEGID.2019.103937.
- [168] W. E. Bullock, "Rifampin in the Treatment of Leprosy," *Rev Infect Dis*, vol. 5, no. Supplement\_3, pp. S606–S613, Jul. 1983, doi: 10.1093/clinids/5.Supplement\_3.S606.
- [169] J. O. Pinho, M. Ferreira, M. Coelho, S. N. Pinto, S. I. Aguiar, and M. M. Gaspar, "Liposomal Rifabutin—A Promising Antibiotic Repurposing Strategy against Methicillin-Resistant *Staphylococcus aureus* Infections," *Pharmaceuticals*, vol. 17, no. 4, p. 470, Apr. 2024, doi: 10.3390/PH17040470/S1.
- [170] G. N. Forrest and K. Tamura, "Rifampin Combination Therapy for Nonmycobacterial Infections," *Clin Microbiol Rev*, vol. 23, no. 1, pp. 14–34, Jan. 2010, doi: 10.1128/CMR.00034-09.
- [171] K. Bujnowski, L. Synoradzki, R. C. Darłak, T. A. Zevaco, and E. Dinjus, "Semi-synthetic zwitterionic rifamycins: a promising class of antibiotics; survey of their chemistry and biological activities," *RSC Adv*, vol. 6, no. 115, pp. 114758–114772, Dec. 2016, doi: 10.1039/C6RA22880A.
- [172] J. Peek *et al.*, "Rifamycin congeners kanglemycins are active against rifampicin-resistant bacteria via a distinct mechanism," *Nature Communications 2018 9:1*, vol. 9, no. 1, pp. 1–15, Oct. 2018, doi: 10.1038/s41467-018-06587-2.
- [173] T. Lan *et al.*, "Redesign of Rifamycin Antibiotics to Overcome ADP-Ribosylation-Mediated Resistance," *Angewandte Chemie*, vol. 134, no. 45, p. e202211498, Nov. 2022, doi: 10.1002/ANGE.202211498.
- [174] C. Calvori, L. Frontali, L. Leoni, and G. Tecce, "Effect of Rifamycin on Protein Synthesis," *Nature 1965 207:4995*, vol. 207, no. 4995, pp. 417–418, 1965, doi: 10.1038/207417a0.

- [175] W. R. McClure and C. L. Cech, "On the mechanism of rifampicin inhibition of RNA synthesis.," *Journal of Biological Chemistry*, vol. 253, no. 24, pp. 8949–8956, Dec. 1978, doi: 10.1016/S0021-9258(17)34269-2.
- [176] E. A. Campbell *et al.*, "Structural Mechanism for Rifampicin Inhibition of Bacterial RNA Polymerase," *Cell*, vol. 104, no. 6, pp. 901–912, Mar. 2001, doi: 10.1016/S0092-8674(01)00286-0.
- [177] I. Artsimovitch and D. G. Vassylyev, "Is It Easy to Stop RNA Polymerase?," *Cell Cycle*, vol. 5, no. 4, pp. 399–404, Feb. 2006, doi: 10.4161/CC.5.4.2466.
- [178] R. A. Adams *et al.*, "Rifamycin antibiotics and the mechanisms of their failure," *The Journal of Antibiotics 2021 74:11*, vol. 74, no. 11, pp. 786–798, Aug. 2021, doi: 10.1038/s41429-021-00462-x.
- [179] G. D. Boorgula, L. U. M. R. Jakkula, T. Gumbo, B. Jung, and S. Srivastava, "Comparison of Rifamycins for Efficacy Against Mycobacterium avium Complex and Resistance Emergence in the Hollow Fiber Model System," *Front Pharmacol*, vol. 12, Apr. 2021, doi: 10.3389/FPHAR.2021.645264.
- [180] J. A. Schildkraut, J. Raaijmakers, R. Aarnoutse, W. Hoefsloot, H. F. L. Wertheim, and J. van Ingen, "The role of rifampicin within the treatment of Mycobacterium avium pulmonary disease," *Antimicrob Agents Chemother*, vol. 67, no. 11, Nov. 2023, doi: 10.1128/aac.00874-23.
- [181] A. Rominski, A. Roditscheff, P. Selchow, E. C. Böttger, and P. Sander, "Intrinsic rifamycin resistance of Mycobacterium abscessus is mediated by ADP-ribosyltransferase MAB\_0591," *Journal of Antimicrobial Chemotherapy*, vol. 72, no. 2, pp. 376–384, Feb. 2017, doi: 10.1093/JAC/DKW466.
- [182] V. Molodtsov, N. T. Scharf, M. A. Stefan, G. A. Garcia, and K. S. Murakami, "Structural basis for rifamycin resistance of bacterial RNA polymerase by the three most clinically important RpoB mutations found in Mycobacterium tuberculosis," *Mol Microbiol*, vol. 103, no. 6, pp. 1034–1045, Mar. 2017, doi: 10.1111/MMI.13606.
- [183] J. Baysarowich *et al.*, "Rifamycin antibiotic resistance by ADP-ribosylation: Structure and diversity of Arr," *Proc Natl Acad Sci U S A*, vol. 105, no. 12, pp. 4886–4891, Mar. 2008, doi: 10.1073/pnas.0711939105.
- [184] U. S. Ganapathy, T. Lan, V. Dartois, C. C. Aldrich, and T. Dick, "Blocking ADP-ribosylation expands the anti-mycobacterial spectrum of rifamycins," *Microbiol Spectr*, vol. 11, no. 5, Oct. 2023, doi: 10.1128/spectrum.01900-23.
- [185] M. Xie *et al.*, "ADP-ribosylation-resistant rifabutin analogs show improved bactericidal activity against drug-tolerant M. abscessus in caseum surrogate," *Antimicrob Agents Chemother*, vol. 67, no. 9, Sep. 2023, doi: 10.1128/AAC.00381-23.

- [186] U. S. Ganapathy *et al.*, “Blocking bacterial naphthohydroquinone oxidation and adpribosylation improves activity of rifamycins against mycobacterium abscessus,” *Antimicrob Agents Chemother*, vol. 65, no. 9, Sep. 2021, doi: 10.1128/AAC.00978-21.
- [187] R. W. Seidel, R. Goddard, M. Lang, and A. Richter, “N $\alpha$ -aroyl-N-aryl-phenylalanine amides: a promising class of antimycobacterial agents targeting the RNA polymerase,” *Chem Biodivers*, vol. 21, no. 6, p. e202400267, Apr. 2024, doi: 10.1002/CBDV.202400267.
- [188] S. Mandal, “Novel small-molecule inhibitors of mycobacterial RNAP ‘AAPS,’” Dissertation, Graduate School-New Brunswick Rutgers, The State University of New Jersey, 2014. doi: 10.7282/T3Q52MQZ.
- [189] W. Lin *et al.*, “Structural Basis of Mycobacterium tuberculosis Transcription and Transcription Inhibition,” *Mol Cell*, vol. 66, no. 2, pp. 169-179.e8, 2017, doi: 10.1016/j.molcel.2017.03.001.
- [190] M. Lang *et al.*, “Synthesis and Characterization of Phenylalanine Amides Active against Mycobacterium abscessus and Other Mycobacteria,” *J Med Chem*, vol. 66, no. 7, pp. 5079–5098, Mar. 2023, doi: 10.1021/ACS.JMEDCHEM.3C00009.
- [191] M. Lang, U. S. Ganapathy, R. Abdelaziz, T. Dick, and A. Richter, “Broad-Spectrum In Vitro Activity of N $\alpha$ -aroyl-N-aryl-Phenylalanine Amides against Non-Tuberculous Mycobacteria and comparative Analysis of RNA Polymerases,” *Antibiotics*, vol. 13, no. 5, p. 404, Apr. 2024, doi: 10.3390/ANTIBIOTICS13050404.
- [192] I. Artsimovitch, C. Chu, A. S. Lynch, and R. Landick, “A new class of bacterial RNA polymerase inhibitor affects nucleotide addition,” *Science*, vol. 302, no. 5645, pp. 650–654, Oct. 2003, doi: 10.1126/SCIENCE.1087526.
- [193] Y. Feng *et al.*, “Structural Basis of Transcription Inhibition by CBR Hydroxamidines and CBR Pyrazoles,” *Structure*, vol. 23, no. 8, pp. 1470–1481, Aug. 2015, doi: 10.1016/j.str.2015.06.009.
- [194] A. M. Malinen *et al.*, “CBR antimicrobials alter coupling between the bridge helix and the  $\beta$  subunit in RNA polymerase,” *Nature Communications 2014 5:1*, vol. 5, no. 1, pp. 1–9, Mar. 2014, doi: 10.1038/ncomms4408.
- [195] B. Bae, D. Nayak, A. Ray, A. Mustaev, R. Landick, and S. A. Darst, “CBR antimicrobials inhibit RNA polymerase via at least two bridge-helix cap-mediated effects on nucleotide addition,” *Proc Natl Acad Sci U S A*, vol. 112, no. 31, pp. E4178–E4187, Aug. 2015, doi: 10.1073/pnas.1502368112.
- [196] R. H. Ebright, Y. W. Ebright, S. Mandal, R. Wilde, and S. Li, “Preparation of N-alpha-aroyl-N-aryl-phenylalaninamides as inhibitors of bacterial RNA polymerase and as antibacterials,” WO2015120320 A1 2015-08-13, 2015

- [197] M. Lang *et al.*, “Synthesis and in vitro Metabolic Stability of Sterically Shielded Antimycobacterial Phenylalanine Amides,” *ChemMedChem*, vol. 19, no. 6, p. e202300593, Feb. 2024, doi: 10.1002/CMDC.202300593.
- [198] L. Mann *et al.*, “Racemization-free synthesis of Na-2-thiophenoyl-phenylalanine-2-morpholinoanilide enantiomers and their antimycobacterial activity,” *Amino Acids*, vol. 53, no. 8, pp. 1187–1196, Aug. 2021, doi: 10.1007/S00726-021-03044-1.
- [199] A. Regueiro-Ren, “Cyclic sulfoxides and sulfones in drug design,” *Adv Heterocycl Chem*, vol. 134, pp. 1–30, Jan. 2021, doi: 10.1016/BS.AIHCH.2020.10.003.
- [200] M. Feng, B. Tang, S. H. Liang, and X. Jiang, “Sulfur Containing Scaffolds in Drugs: Synthesis and Application in Medicinal Chemistry,” *Curr Top Med Chem*, vol. 16, no. 11, p. 1200, Mar. 2016, doi: 10.2174/1568026615666150915111741.
- [201] D. Lowe, “Sulfoxides: A Sneaking Affection | Science | AAAS.” Accessed: Jul. 24, 2024. [Online]. Available: <https://www.science.org/content/blog-post/sulfoxides-sneaking-affection>
- [202] F. Namour, K. Anderson, C. Nelson, and C. Tasset, “Filgotinib: A Clinical Pharmacology Review,” *Clin Pharmacokinet*, vol. 61, no. 6, pp. 819–832, Jun. 2022, doi: 10.1007/S40262-022-01129-Y.
- [203] C. J. Menet *et al.*, “Triazolopyridines as selective JAK1 inhibitors: From hit identification to GLPG0634,” *J Med Chem*, vol. 57, no. 22, pp. 9323–9342, Nov. 2014, doi: 10.1021/JM501262Q.
- [204] J. Barluenga, M. Tomás-Gamasa, F. Aznar, and C. Valdés, “Metal-free carbon–carbon bond-forming reductive coupling between boronic acids and tosylhydrazones,” *Nature Chemistry* 2009 1:6, vol. 1, no. 6, pp. 494–499, Aug. 2009, doi: 10.1038/nchem.328.
- [205] F. Haviv *et al.*, “Effect of N-Methyl Substitution of the Peptide Bonds in Luteinizing Hormone-Releasing Hormone Agonists,” *J Med Chem*, vol. 36, no. 3, pp. 363–369, 1993, doi: 10.1021/JM00055A007.
- [206] A. F. B. Räder, F. Reichart, M. Weinmüller, and H. Kessler, “Improving oral bioavailability of cyclic peptides by N-methylation,” *Bioorg Med Chem*, vol. 26, no. 10, pp. 2766–2773, Jun. 2018, doi: 10.1016/J.BMC.2017.08.031.
- [207] J. Chatterjee, F. Rechenmacher, and H. Kessler, “N-Methylation of Peptides and Proteins: An Important Element for Modulating Biological Functions,” *Angewandte Chemie International Edition*, vol. 52, no. 1, pp. 254–269, Jan. 2013, doi: 10.1002/ANIE.201205674.

- [208] A. Richter, T. Shapira, and Y. Av-Gay, "THP-1 and Dictyostelium Infection Models for Screening and Characterization of Anti-Mycobacterium abscessus Hit Compounds," *Antimicrob Agents Chemother*, vol. 64, no. 1, Oct. 2020, doi: 10.1128/AAC.01601-19.
- [209] A. Koul *et al.*, "Diarylquinolines Are Bactericidal for Dormant Mycobacteria as a Result of Disturbed ATP Homeostasis," *Journal of Biological Chemistry*, vol. 283, no. 37, pp. 25273–25280, Sep. 2008, doi: 10.1074/JBC.M803899200.
- [210] D. A. Negatu *et al.*, "Piperidine-4-carboxamides target DNA gyrase in mycobacterium abscessus," *Antimicrob Agents Chemother*, vol. 65, no. 8, Aug. 2021, doi: 10.1128/AAC.00676-21.
- [211] J. P. Sarathy *et al.*, "A Novel Tool to Identify Bactericidal Compounds against Vulnerable Targets in Drug-Tolerant M. tuberculosis found in Caseum," *mBio*, vol. 14, no. 2, Mar. 2023, doi: 10.1128/MBIO.00598-23.
- [212] L. Mann *et al.*, "In Vitro Profiling of the Synthetic RNA Polymerase Inhibitor MMV688845 against Mycobacterium abscessus," *Microbiol Spectr*, vol. 10, no. 6, p. e02760, Nov. 2022, doi: 10.1128/SPECTRUM.02760-22.
- [213] L. Di, "The Impact of Carboxylesterases in Drug Metabolism and Pharmacokinetics," *Curr Drug Metab*, vol. 20, no. 2, pp. 91–102, Aug. 2018, doi: 10.2174/1389200219666180821094502.
- [214] D. J. St. Jean and C. Fotsch, "Mitigating heterocycle metabolism in drug discovery," *J Med Chem*, vol. 55, no. 13, pp. 6002–6020, Jul. 2012, doi: 10.1021/JM300343M.
- [215] Z. K. Wan *et al.*, "Efficacious 11 $\beta$ -hydroxysteroid dehydrogenase type I inhibitors in the diet-induced obesity mouse model," *J Med Chem*, vol. 52, no. 17, pp. 5449–5461, Sep. 2009, doi: 10.1021/JM900639U.

## 5) Appendices

### *5.1) Comment on Provided Supplementary Information*

The appended Supplementary Information provides additional methodologies and experimental data of the presented publications. The chemical documentation of intermediates and final products, including their written purity, NMR and MS documentation, and chemical procedures, is presented here. This document contains the published Supplementary Information documents that are accessible online, abbreviated by HPLC traces used for purity determination and NMR spectra. This decision was made in order to keep this thesis in a compact format. The excluded documentation can be found in the online versions of the documents.



## **5.2) Supplementary Information Publication I**

# **Synthesis and Characterization of Phenylalanine Amides Active against *Mycobacterium abscessus* and Other Mycobacteria**

Markus Lang, Uday S. Ganapathy, Lea Mann, Rana Abdelaziz, Rüdiger W. Seidel, Richard Goddard, Ilaria Sequenzia, Sophie Hoenke, Philipp Schulze, Wassihun Wedajo Aragaw, René Csuk, Thomas Dick, Adrian Richter

**American Chemical Society Publishing**  
**Journal of Medicinal Chemistry**

*J. Med. Chem.* 2023, 66, 7, 5079–5098

Publication Date: March 31, 2023

DOI: 10.1002/cmdc.202300593

# Supplementary Information

## **Synthesis and characterization of phenylalanine amides active against *Mycobacterium abscessus* and other mycobacteria**

Markus Lang<sup>a</sup>, Uday S. Ganapathy<sup>b</sup>, Lea Mann<sup>a</sup>, Rana Abdelaziz<sup>a</sup>, Rüdiger W. Seidel<sup>a</sup>, Richard Goddard<sup>c</sup>, Ilaria Sequenzia<sup>a</sup>, Sophie Hoenke<sup>f</sup>, Philipp Schulze<sup>c</sup>, Wassihun Wedajo Aragaw<sup>b</sup>, René Csuk, Thomas Dick<sup>b,d,e</sup>, Adrian Richter<sup>a\*</sup>

<sup>a</sup>Institut für Pharmazie, Martin-Luther-Universität Halle-Wittenberg, Wolfgang-Langenbeck-Str. 4, 06120 Halle (Saale), Germany

<sup>b</sup>Center for Discovery and Innovation, Hackensack Meridian Health, 111 Ideation Way, 07110 Nutley, New Jersey, USA

<sup>c</sup>Max-Planck-Institut für Kohlenforschung, Kaiser-Wilhelm-Platz 1, 45470 Mülheim an der Ruhr, Germany

<sup>d</sup>Department of Medical Sciences, Hackensack Meridian School of Medicine, 123 Metro Blvd, 07110 Nutley, New Jersey, USA

<sup>e</sup>Department of Microbiology and Immunology, Georgetown University, 3900 Reservoir Road, N.W., 20007 Washington DC, USA

<sup>f</sup>Institut für Chemie, Martin-Luther-Universität Halle-Wittenberg, Kurt-Mothes-Str. 2, 06120 Halle (Saale), Germany

\*Corresponding author:

Dr. Adrian Richter

Wolfgang-Langenbeck-Str. 4

06120 Halle (Saale)

Germany

adrian.richter@pharmazie.uni-halle.de

## Table of Contents

- 1. Molecular docking studies**
  - a. Methodology
  - b. Figure S1
  - c. Figure S2
  - d. Table S1
- 2. X-ray crystallography**
  - a. Methodology
  - b. Table S2
  - c. Table S3
  - d. Figure S3
  - e. Literature
- 3. Antimycobacterial activity of MMV688845 derivatives, additional data**
  - a. Table S4
- 4. Structures and synthetic protocols**
- 5. NMR spectra and HPLC-purity chromatograms**

## 1. Molecular docking studies

### a. Methodology

The crystal structure of the *Mycobacterium tuberculosis* transcription initiation complex obtained from the protein databank (PDB: 5UHE), was used for docking. The protein preparation wizard with Schrödinger software (Schrödinger Suite 2022-3, Schrödinger, New York, USA, NY, 2021) was used to prepare the protein for modelling. First, missing hydrogen atoms were added, and the ionization and tautomeric states of the ligand were adjusted. Then, the hydrogen bond networks and the amino acid residues protonation states were optimized using PROPKA. Finally, the resulting structure was refined through an energy minimization step using OPLS4 force field (default).

The receptor grid was generated using the receptor grid generator panel without any constraints, assigning the co-crystallized ligand (D-AAP1) as the center of the grid. Ligands were prepared using the LigPrep (LigPrep, Schrödinger, LLC, New York, NY, 2021.) using default settings. The protonation states were generated using Epik (Epik, Schrödinger, LLC, New York, NY, 2021). Following this step, bioactive conformers (maximum of 20) of the prepared ligands were generated using ConfGen panel (ConfGen, Schrödinger, LLC, New York, NY, 2021). Glide (Glide, Schrödinger, LLC, New York, NY, 2021.) was used for docking: the precision mode was set to standard precision (SP) and no constraints were applied.

Visualizations have been created with **Schrödinger Release 2022-3: Maestro**, Schrödinger, LLC, New York, NY, 2021.

#### *References:*

##### ConfGen

- Watts, K.S.; Dalal, P.; Murphy, R.B.; Sherman, W.; Friesner, R.A.; Shelley, J.C., "ConfGen: A Conformational Search Method for Efficient Generation of Bioactive Conformers," *J.Chem. Inf. Model.*, **2010**, *50*, 534-546

**Schrödinger Release 2022-3: ConfGen**, Schrödinger, LLC, New York, NY, 2021.

##### Epik

- Greenwood, J. R.; Calkins, D.; Sullivan, A. P.; Shelley, J. C., "Towards the comprehensive, rapid, and accurate prediction of the favorable tautomeric states of drug-like molecules in aqueous solution," *J. Comput. Aided Mol. Des.*, **2010**, *24*, 591-604
- Shelley, J.C.; Cholleti, A.; Frye, L; Greenwood, J.R.; Timlin, M.R.; Uchimaya, M., "Epik: a software program for  $pK_a$  prediction and protonation state generation for drug-like molecules," *J. Comp.-Aided Mol. Design*, **2007**, *21*, 681-691

**Schrödinger Release 2022-3: Epik**, Schrödinger, LLC, New York, NY, 2021.

##### Glide

- Friesner, R. A.; Murphy, R. B.; Repasky, M. P.; Frye, L. L.; Greenwood, J. R.; Halgren, T. A.; Sanschagrin, P. C.; Mainz, D. T., "Extra Precision Glide: Docking and Scoring Incorporating a Model of Hydrophobic Enclosure for Protein-Ligand Complexes," *J. Med. Chem.*, **2006**, *49*, 6177-6196

- Halgren, T. A.; Murphy, R. B.; Friesner, R. A.; Beard, H. S.; Frye, L. L.; Pollard, W. T.; Banks, J. L., "Glide: A New Approach for Rapid, Accurate Docking and Scoring. 2. Enrichment Factors in Database Screening," *J. Med. Chem.*, **2004**, *47*, 1750–1759
- Friesner, R. A.; Banks, J. L.; Murphy, R. B.; Halgren, T. A.; Klicic, J. J.; Mainz, D. T.; Repasky, M. P.; Knoll, E. H.; Shaw, D. E.; Shelley, M.; Perry, J. K.; Francis, P.; Shenkin, P. S., "Glide: A New Approach for Rapid, Accurate Docking and Scoring. 1. Method and Assessment of Docking Accuracy," *J. Med. Chem.*, **2004**, *47*, 1739–1749

Schrödinger Release 2022-3: Glide, Schrödinger, LLC, New York, NY, 2021.

#### LigPrep

Schrödinger Release 2022-3: LigPrep, Schrödinger, LLC, New York, NY, 2021.

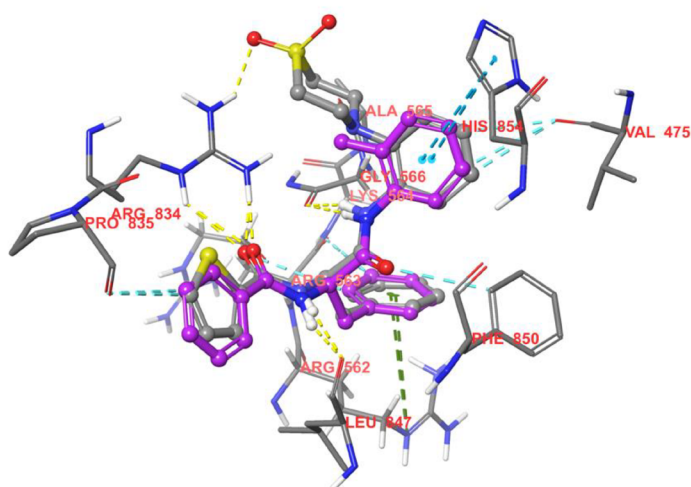


**Figure S1** Superposition of D-AAP1 and substance **20** is to showed a similar target interaction. **20** (a sulfone) exhibits an analogous binding mode to RNAP subunit  $\beta'$  as the formerly co-crystallized D-AAP1 indicating an on-target mode of action. **20**, additionally, exhibits a hydrogen bond to ARG834 which could lead to stronger target interaction. Visualization generated with Maestro graphical interface (Schrödinger Release 2022-3: Maestro, Schrödinger, LLC, New York, NY, 2021).

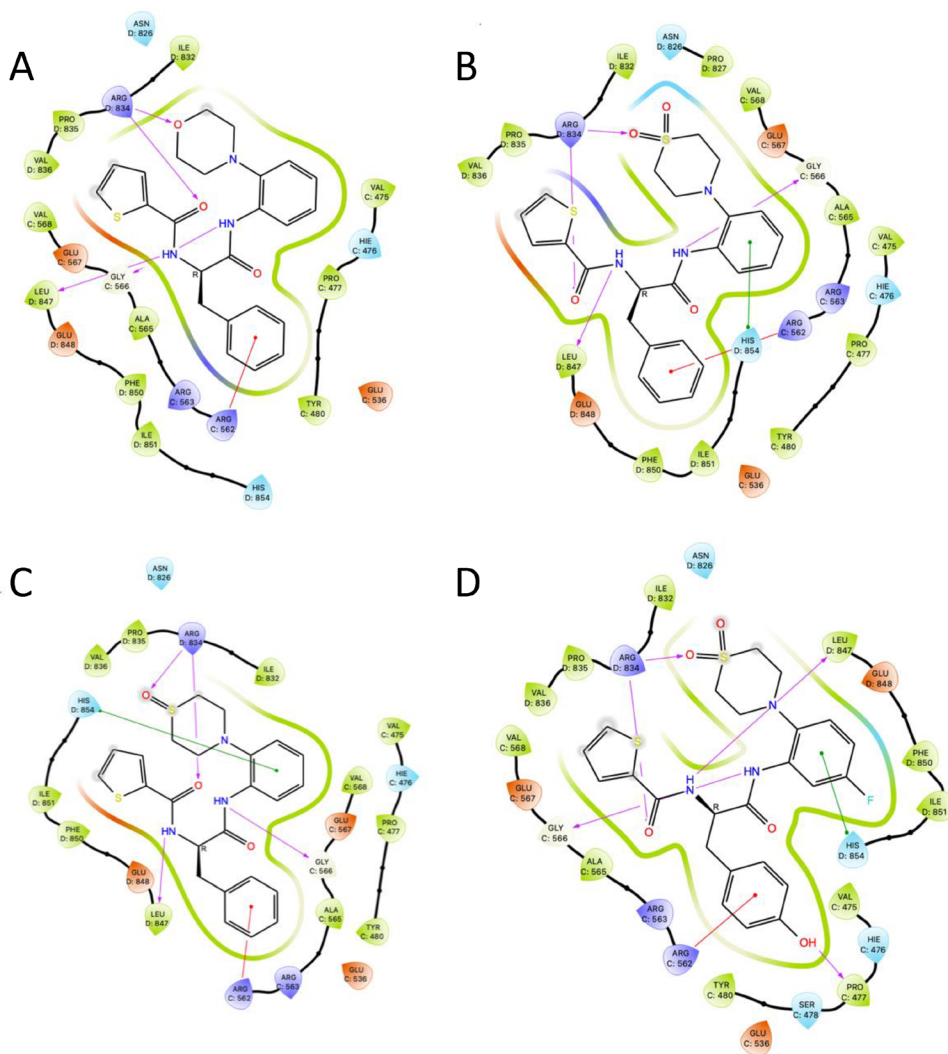


**Figure S2** 2D visualization of the proposed binding modes of the hit compound MMV688845 and derivatives to the target protein RNAP<sub>Mtb</sub>. 2D views originate from the same docking study as the 3D presentations in Figure 1. The drug-target interactions are presented in 2D views for clarity. Hydrogen bonds are displayed as yellow dashed lines. A: Molecular docking of MMV688845 shows a hydrogen bond between the oxygen atom of the morpholine moiety and R834 of the beta' subunit of RNAP. B&C: Sulfone and sulfoxide groups of the substances **20** and **14** are able to form hydrogen bonds with R834 without clashes with the target protein. D: Exchanging benzyl for p-hydroxy benzyl shows an additional hydrogen bond between the p-hydroxy group and P477. Visualization generated with Schrödinger Release 2022-3: Maestro, Schrödinger, LLC, New York, NY, 2021.

**Table S1** List of amino acids that showed drug-target interaction between MMV688845 derivatived and *Mtb*  $\beta$  and  $\beta'$  RNAP subunits together with their BLAST aligned counterparts in *Mabs*  $\beta$  and  $\beta'$  RNAP subunits. *Mtb* protein sequence was extracted from PDB (Code 5UHE) and *Mabs* protein sequence was extracted from UniProt (*M. abscessus* ATCC 19977 RNAP  $\beta$  subunit: B1MH62; *M. abscessus* ATCC 19977 RNAP  $\beta'$  subunit: B1MH61)

	<i>Mtb</i>		<i>Mabs</i>	
	Position	Amino acid	Position	Amino acid
$\beta$ subunit	475	Valine	422	Valine
	477	Proline	424	Proline
	562	Arginine	509	Arginine
	565	Alanine	512	Glycine
	566	Glycine	513	Glycine
	567	Glutamic acid	514	Glutamic acid
$\beta'$ subunit	834	Arginine	833	Arginine
	835	Proline	834	Proline
	847	Leucine	846	Leucine
	850	Phenylalanine	849	Phenylalanine
	854	Histidine	853	Histidine

## 2. X-ray crystallography

### a. Methodology

The X-ray intensity data collections were carried out at 100 K on a Bruker AXS Kappa Mach3 APEX II diffractometer, using Mo-K $\alpha$  radiation ( $\lambda = 0.71073$  Å) from an Incoatec  $\mu$ S microfocus X-ray source with Helios mirrors. The crystal was mounted on a MiTeGen cryo loop using perfluoropolyether PFO-XR75. The programs APEX3 [1] and SAINT [2] were used to control the data collections and to process the raw diffraction data. Scaling and absorption corrections based on indexed crystal faces (Gaussian method) were performed with SADABS [3].

The crystal structures were solved with SHELXT[4] and refined with SHELXL-2018/3 [5]. Minor positional disorder of the thiophene rings in **6** and **20** was modelled with appropriate geometric restraints and constraints on anisotropic atomic displacement parameters (see supplementary crystallographic information). The ratios of occupancies were refined by means of free variables to give 0.936(3) / 0.064(3) (unique molecule 1) and 0.932(3) / 0.068(3) (unique molecule 2) for **6**, and 0.8883(19) / 0.1117(19) (unique molecule 1) and 0.9462(17) / 0.0538(17) (unique molecule 2) for **20**. In **6** and **20**, carbon-bound hydrogen atoms were placed in geometrically calculated positions and refined using a riding model with  $U_{\text{iso}}(\text{H}) = 1.2 U_{\text{eq}}(\text{C})$ . Nitrogen-bound hydrogen atoms were located in difference Fourier maps and the positions were subsequently refined with the N–H distances restrained to a target value of 0.88(2) Å, and with  $U_{\text{iso}}(\text{H}) = 1.2 U_{\text{eq}}(\text{N})$ . The final structure refinement of **14** · **1.5 H<sub>2</sub>O** was carried by Hirshfeld atom refinement with aspherical scattering factors using NoSpherA2 [6, 7] partitioning in Olex2 1.5 [8] based on electron density from iterative single determinant SCF single point DFT calculations using ORCA v.4.1.1 [9] with a B3LYP functional [10, 11] and a def2-TZVPP basis set. Positions and  $U_{\text{iso}}$  values of all hydrogen atoms were refined freely. The R configuration at the  $\alpha$ -carbon atom (C2) in **6**, **20** and **14** · **1.5 H<sub>2</sub>O** was inferred from the known absolute

configuration of the starting material and the absolute structures were confirmed by Flack  $x$  parameters [12] and Hooft  $y$  parameters [13] close to zero (see **Table S1** in the supporting information).

Displacement ellipsoid plots were drawn with Diamond 3.2k4 [14]. Crystal data and refinement details are listed in **Table S1**. Selected hydrogen bond parameters in **6**, **20**, **14 · 1.5 H<sub>2</sub>O** and *rac*-MMV688845 [15] are given in **Table S2**. **Figure S1** shows a structure overlay plot of the *pseudo* centrosymmetric hydrogen-bonded dimer of **6** and the centrosymmetric hydrogen-bonded dimer of the racemic morpholino analogue MMV688845.

**b. Table S2** Crystal data and refinement details for **6**, **20** and **14 · 1.5 H<sub>2</sub>O**.

	<b>6</b>	<b>20</b>	<b>14 · 1.5 H<sub>2</sub>O</b>
Empirical formula	C <sub>24</sub> H <sub>25</sub> N <sub>3</sub> O <sub>2</sub> S <sub>2</sub>	C <sub>24</sub> H <sub>25</sub> N <sub>3</sub> O <sub>4</sub> S <sub>2</sub>	C <sub>24</sub> H <sub>28</sub> N <sub>3</sub> O <sub>4.5</sub> S <sub>2</sub>
$M_r$	451.59	483.59	494.62
Crystal system, space group	Triclinic, <i>P1</i>	Triclinic, <i>P1</i>	Monoclinic, <i>I2</i>
$a$ (Å)	9.1619(5)	9.0832(5)	12.4647(10)
$b$ (Å)	9.8922(6)	10.2796(5)	7.3964(6)
$c$ (Å)	13.1151(8)	13.1078(7)	26.030(2)
$\alpha$ (°)	77.928(2)	78.029(2)	90
$\beta$ (°)	71.907(2)	72.009(2)	98.749(3)
$\gamma$ (°)	82.156(2)	79.983(2)	90
$V$ (Å <sup>3</sup> )	1101.60(11)	1130.77(10)	2371.9(3)
$Z$ , $\rho_{\text{calc}}$ (mg m <sup>-3</sup> )	2, 1.361	2, 1.420	4, 1.385
$\mu$ (mm <sup>-1</sup> )	0.269	0.273	0.264
$F(000)$	476	508	1044
Crystal size (mm)	0.070 × 0.057 × 0.023	0.123 × 0.104 × 0.020	0.234 × 0.129 × 0.079
$\theta$ range (°)	1.660 - 29.997	1.656 - 40.363	1.58 - 31.05
Reflections collected / unique	43786 / 12610	144443 / 26964	40189 / 7575
$R_{\text{int}}$	0.0307	0.0267	0.0191
Completeness to $\theta_{\text{full}}$ (%)	99.9	100.0	100.0
Data / restraints / parameters	12610 / 31 / 597	26964 / 31 / 633	7575 / 1 / 415
Observed data [ $I > 2\sigma(I)$ ]	11482	24554	7359
Goodness-of-fit on $F^2$	1.016	1.036	1.0523
$R1$ [ $I > 2\sigma(I)$ ]	0.0343	0.0342	0.0151
$wR2$ (all data)	0.0820	0.0891	0.0319
Flack $x$ parameter	-0.030(18) <sup>a</sup>	0.000(8) <sup>a</sup>	0.022(9) <sup>b</sup>
Hooft $y$ parameter	-0.027(15) <sup>b</sup>	0.009(7) <sup>b</sup>	0.016(9) <sup>c</sup>
$\Delta\rho_{\text{max}}$ , $\Delta\rho_{\text{min}}$ (e Å <sup>-3</sup> )	0.377, -0.219	0.635, -0.292	0.222, -0.102
CCDC No.	2231845	2231846	2231847

<sup>a</sup> Calculated with SHELXL-2018/3.

<sup>b</sup> Calculated with PLATON [16].

<sup>c</sup> Calculated with Olex2.

**Table S3** Selected hydrogen bond parameters in **6**, *rac*-MMV688845, **20** and **14** · 1.5 H<sub>2</sub>O.<sup>a</sup>

<i>D</i> –H... <i>A</i>	<i>d</i> ( <i>D</i> –H) (Å)	<i>d</i> (H... <i>A</i> ) (Å)	<i>d</i> ( <i>D</i> ... <i>A</i> ) (Å)	<(DHA) (°)
<b>6</b>				
N2_1–H2_1...O1_2	0.88(2)	2.03(2)	2.897(2)	169(3)
N2_2–H2_2...O1_1	0.88(2)	1.95(2)	2.796(2)	163(3)
<i>rac</i> -MMV688845 <sup>b</sup>				
N2–H2...O1 <sup>c</sup>	0.82(2)	2.11(3)	2.925(2)	174(2)
<b>20</b>				
N2_1–H2_1...O1_2	0.855(17)	2.082(17)	2.9222(12)	167.5(19)
N2_2–H2_2...O1_1	0.842(17)	2.004(18)	2.7870(12)	154(2)
<b>14</b> · 1.5 H <sub>2</sub> O				
N2–H2...O1 <sup>c</sup>	0.971(8)	2.032(9)	2.9560(7)	158.4(8)

<sup>a</sup> The number after the underscore indicates crystallographically unique molecules.

<sup>b</sup> Data taken from CSD entry BALNUB [15].

<sup>c</sup> Symmetry-related atoms.

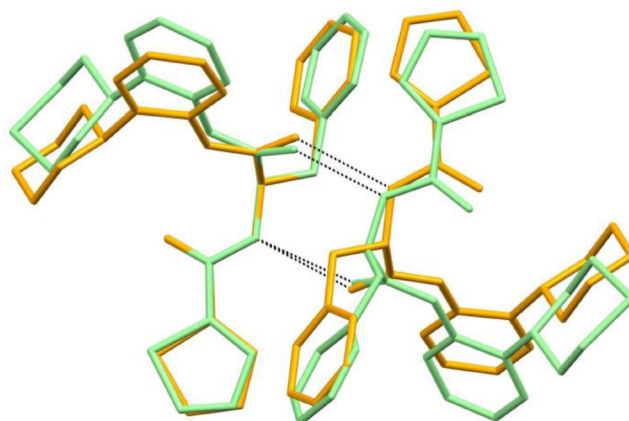


**Figure S3** Structure overlay plot of one chirality centre ( $\alpha$ -carbon atom) of the pseudo centrosymmetric hydrogen-bonded dimer of **6** (green) and the corresponding chirality centre of the centrosymmetric hydrogen-bonded dimer of *rac*-MMV688845 [15] (CSD refcode: BALNUB, orange). Hydrogen atoms are omitted for clarity. The dashed lines illustrate N–H...O hydrogen bonds between the phenylalanine amide groups. The picture was generated with Mercury.[17]

#### Literature

1. APEX3. 2018, Bruker AXS Inc., Madison, Wisconsin, USA.
2. SAINT. 2012, Bruker AXS Inc.: Madison, Wisconsin, USA.
3. SADABS. 2012, Bruker AXS Inc.: Madison, Wisconsin, USA.
4. Sheldrick, G.M., *SHELXT - integrated space-group and crystal-structure determination*. Acta Crystallogr A Found Adv, 2015. **71**(Pt 1): p. 3-8.
5. Sheldrick, G.M., *Crystal structure refinement with SHELXL*. Acta Crystallogr C Struct Chem, 2015. **71**(Pt 1): p. 3-8.
6. Kleemiss, F., et al., *Accurate crystal structures and chemical properties from NoSpherA2*. Chemical Science, 2021. **12**(5): p. 1675-1692.

7. Midgley, L., et al., *Vanishing of the atomic form factor derivatives in non-spherical structural refinement - a key approximation scrutinized in the case of Hirshfeld atom refinement*. Acta Crystallogr A Found Adv, 2021. **77**(Pt 6): p. 519-533.
8. Dolomanov, O.V., et al., *OLEX2: a complete structure solution, refinement and analysis program*. Journal of Applied Crystallography, 2009. **42**(2): p. 339-341.
9. Neese, F., et al., *The ORCA quantum chemistry program package*. J Chem Phys, 2020. **152**(22): p. 224108.
10. Becke, A.D., *Density-functional thermochemistry. III. The role of exact exchange*. The Journal of Chemical Physics, 1993. **98**(7): p. 5648-5652.
11. Lee, C., W. Yang, and R.G. Parr, *Development of the Colle-Salvetti correlation-energy formula into a functional of the electron density*. Physical Review B, 1988. **37**(2): p. 785-789.
12. Parsons, S., H.D. Flack, and T. Wagner, *Use of intensity quotients and differences in absolute structure refinement*. Acta Crystallogr B Struct Sci Cryst Eng Mater, 2013. **69**(Pt 3): p. 249-59.
13. Hooft, R.W.W., L.H. Straver, and A.L. Spek, *Using the t-distribution to improve the absolute structure assignment with likelihood calculations*. Journal of Applied Crystallography, 2010. **43**(4): p. 665-668.
14. Brandenburg, K. 2018, Crystal Impact GbR: Bonn, Germany.
15. Mann, L., et al., *Racemization-free synthesis of Nalpha-2-thiophenoyl-phenylalanine-2-morpholinoanilide enantiomers and their antimycobacterial activity*. Amino Acids, 2021. **53**(8): p. 1187-1196.
16. Spek, A.L., *Structure validation in chemical crystallography*. Acta Crystallogr D Biol Crystallogr, 2009. **65**(Pt 2): p. 148-55.
17. Macrae, C.F., et al., *Mercury 4.0: from visualization to analysis, design and prediction*. J Appl Crystallogr, 2020. **53**(Pt 1): p. 226-235.

### 3. Antimycobacterial activity of MMV688845 derivatives, additional data

**Table S4** Antimycobacterial activity of MMV688845 derivatives<sup>A</sup>, OD measurements

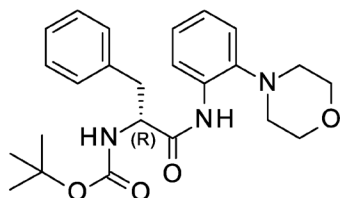
	R <sup>1</sup>	R <sup>2</sup>	X, Y	R <sup>3</sup>	MIC <sub>90</sub>			
					<i>Msmeg</i> m <sup>c</sup> 155 <sup>B</sup>	<i>Mabs</i> ATCC19977 <sup>B</sup>	<i>Mabs</i> ATCC19977 <sup>B</sup>	<i>Mintra</i> ATCC 35761 <sup>B</sup>
					7H9	7H9	MHII	7H9
					OD	OD	OD	OD
<b>MMV845</b>	Phenyl	H	O, N	2-Thiophenoyl	0.78	6.25	12.5	0.39
<b>6</b>	Phenyl	H	S, N	2-Thiophenoyl	3.13	6.25	> 100	0.39
<b>7</b>	Phenyl	H	S, N	2-F-Benzoyl	3.13	6.25	> 100	0.78
<b>11</b>	Phenyl	F	S, N	2-Thiophenoyl	3.13	25	> 100	1.56
<b>12</b>	Phenyl	F	S, N	2-F-Benzoyl	3.13	25	> 100	1.56
<b>14</b>	Phenyl	H	S=O, N	2-Thiophenoyl	1.56	3.13	6.25	0.1
<b>15</b>	Phenyl	H	S=O, N	2-F-Benzoyl	0.7	6.25	6.25	0.1
<b>17</b>	Phenyl	F	S=O, N	2-Thiophenoyl	1.56	1.56	6.25	0.2
<b>18</b>	Phenyl	F	S=O, N	2-F-Benzoyl	1.56	3.13	3.13	0.39
<b>20</b>	Phenyl	H	O=S=O, N	2-Thiophenoyl	1.56	1.56	3.13	0.1
<b>24</b>	Phenyl	H	O=S=O, N	2-F-Benzoyl	0.78	0.78	1.56	0.1
<b>28</b>	Phenyl	F	O=S=O, N	2-Thiophenoyl	1.56	3.13	1.56	0.1
<b>29</b>	Phenyl	F	O=S=O, N	2-F-Benzoyl	1.56	3.13	1.56	0.2
<b>32</b>	Phenyl	H	S, CH	2-Thiophenoyl	6.25	50	100	12.5
<b>34</b>	Phenyl	H	S=O, CH	2-Thiophenoyl	3.13	25	25	3.13
<b>36</b>	p-Hydroxyphenyl	F	S, N	2-Thiophenoyl	12.5	25	25	0.2
<b>37</b>	p-Hydroxyphenyl	F	S, N	2-F-Benzoyl	6.25	25	50	0.39
<b>39</b>	p-Hydroxyphenyl	F	O=S=O, N	2-Thiophenoyl	6.25	12.5	3.13	0.05
<b>40</b>	p-Hydroxyphenyl	F	O=S=O, N	2-F-Benzoyl	6.25	6.25	6.25	0.2
<b>42</b>	3-Thiophenyl	H	O, N	2-Thiophenoyl	1.56	12.5	25	1.56
<b>43</b>	3-Thiophenyl	H	O, N	2-F-Benzoyl	1.56	6.25	12.5	1.56
<b>45</b>	2-Thiophenyl	H	O, N	2-Thiophenoyl	1.56	12.5	25	1.56
<b>46</b>	2-Thiophenyl	H	O, N	2-F-Benzoyl	1.56	12.5	12.5	1.56
<b>50</b>	3-Thiophenyl	H	S=O, N	2-Thiophenoyl	1.56	6.25	12.5	0.39
<b>51</b>	3-Thiophenyl	H	S=O, N	2-F-Benzoyl	1.56	6.25	12.5	0.39
<b>53</b>	2-Thiophenyl	H	S=O, N	2-Thiophenoyl	3.13	6.25	25	0.39
<b>54</b>	2-Thiophenyl	H	S=O, N	2-F-Benzoyl	1.56	6.25	12.5	0.39

<sup>A</sup>For detailed information on the methodology of the assays see supporting information. <sup>B</sup>Incubated for three days at 37 °C (*M. smegmatis* and *M. abscessus*) or five days (*M. intracellulare*). Performed in duplicate, results were averaged. Data was obtained via OD measurements.

#### 4. Structures and synthetic protocols

##### 1-(R)

tert-butyl N-[(1R)-1-[[2-(morpholin-4-yl)phenyl]carbonyl]-2-phenylethyl]carbamate



##### Synthesis:

Synthesis was carried out according to **general procedure A**.

**Quantities:** Pyridine (5 mL); EtOAc (10 mL); **2-morpholinoaniline** (244 mg, 1.37 mmol, 1 eq., BLD-Pharm); **N-Boc-D-phenylalanine** (400 mg, 1.51 mmol, 1.1 eq., TCI); **T3P 50 % m/v in EtOAc** (1630  $\mu$ L, 2.74 mmol, 2 eq., Aldrich)

##### Purification:

Flash chromatography ethyl acetate/heptane gradient 85 % heptane to 60 % over 8 CV over 90 g normal phase silica gel 0.63 – 0.2  $\mu$ m particle size. Yield: 511 mg, 88 %

##### Analytcs:

$R_f$  value: 0.55 ethyl acetate/heptane 1:1

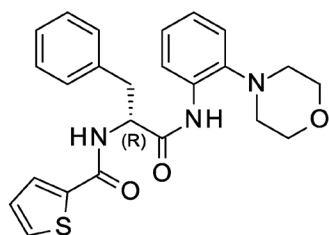
$^1\text{H}$  NMR (Figure S4) (400 MHz, Chloroform-*d*)  $\delta$  8.92 (s, 1H), 8.41 (d,  $J$  = 8.0 Hz, 1H), 7.29 – 7.01 (m, 8H), 5.11 (s, 1H), 4.50 (s, 1H), 3.76 – 3.59 (m, 4H), 3.23 – 3.11 (m, 2H), 2.71 – 2.53 (m, 4H), 1.41 (s, 9H).

Mass: Calculated  $m/z$  for  $\text{C}_{24}\text{H}_{32}\text{N}_3\text{O}_4^+$   $[\text{M}+\text{H}]^+ = 426.2388$ ; found APCI:  $[\text{M}+\text{H}]^+ 426.4$

Specific optical rotation: Starting material N-Boc-D-phenylalanine (**Boc-Phe-D**)  $[\alpha]^{23.5}_D -12.14$  (c 0.3065, methanol); After anilide formation (**1-D**)  $[\alpha]^{22.7}_D 21.65$  (c 0.145, methanol)

##### 2B-(R)

(2R)-N-[2-(morpholin-4-yl)phenyl]-3-phenyl-2-[(thiophen-2-yl)formamido]propenamide



**Synthesis:**

Synthesis was carried out according to **general procedure B**.

**Quantities:** DCM (10 mL); TFA (10 mL); **1-R** (511 mg, 1.20 mmol) Boc-protected crude product isolation: 331 mg; Used for next step: 311 mg (0.96 mmol, 1 eq.); THF, dry (15 ml); **2-carboxythiophene** (135 mg, 1.06 mmol, 1.1 eq., Alfa Aesar); **DEPBT** (862 mg, 2.88 mmol, 3 eq., BLD-Pharm); **DIPEA** (490  $\mu$ L, 2.88 mmol, 3 eq., Aldrich)

**Purification:**

Flash chromatography ethyl acetate/heptane gradient 90 % heptane to 60 % over 12 CV on 45 g. Yield: 176 mg; 39 %

**Analytics:**

$R_f$  value: 0.35 ethyl acetate/heptane 1:1

$^1\text{H}$  NMR (*Figure S5*) (400 MHz, Chloroform-*d*)  $\delta$  8.83 (s, 1H), 8.40 (dd,  $J = 8.0, 1.5$  Hz, 1H), 7.52 (dd,  $J = 3.7, 1.2$  Hz, 1H), 7.47 (dd,  $J = 5.0, 1.1$  Hz, 1H), 7.32 – 7.25 (m, 4H), 7.23 – 7.17 (m, 1H), 7.16 – 7.05 (m, 3H), 7.03 (dd,  $J = 5.0, 3.7$  Hz, 1H), 6.95 (d,  $J = 7.8$  Hz, 1H), 4.95 (td,  $J = 8.0, 5.6$  Hz, 1H), 3.68 – 3.53 (m, 4H), 3.39 (dd,  $J = 13.6, 5.6$  Hz, 1H), 3.25 (dd,  $J = 13.6, 8.1$  Hz, 1H), 2.69 – 2.50 (m, 4H).

$^{13}\text{C}$  NMR APT (*Figure S6*) (101 MHz, Chloroform-*d*)  $\delta$  168.77, 161.56, 141.19, 137.97, 136.50, 132.91, 130.75, 129.38, 128.86, 128.66, 127.81, 127.12, 125.69, 124.33, 120.80, 119.52, 67.25, 56.19, 52.46, 38.47.

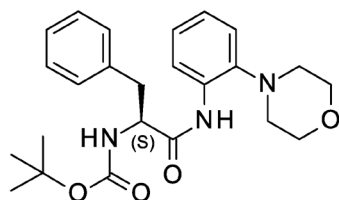
Mass: Calculated  $m/z$  for  $\text{C}_{24}\text{H}_{26}\text{N}_3\text{O}_3\text{S}^+$   $[\text{M}+\text{H}]^+ = 436.1689$ ;  $\text{C}_{24}\text{H}_{25}\text{N}_3\text{O}_3\text{SNa}^+$   $[\text{M}+\text{Na}]^+ = 458.1509$ ; found APCI: 436.1; found HRMS:  $[\text{M}+\text{H}]^+ 436.1691$ ;  $[\text{M}+\text{Na}]^+ 458.1506$

HPLC purity: 98.9 %  $t_R = 4.526$  min (*Figure S7*); 50 mm Eclipse Plus C18 1.8  $\mu\text{m}$ , 4.6 mm, acetonitrile/water 45:55,  $v = 1.0$  mL/min,  $\lambda = 220$  nm

Specific optical rotation: Boc-protected intermediate (**2-D**)  $[\alpha]^{22.7}_D 46.01$  (c 0.119, methanol); final compound (**3-D**)  $[\alpha]^{22.7}_D 56.74$  (c 0.1375, methanol)

**1-(S)**

tert-butyl N-[(1S)-1-[[2-(morpholin-4-yl)phenyl]carbamoyl]-2-phenylethyl]carbamate

**Synthesis:**

Synthesis was carried out according to general procedure A.

**Quantities:** Pyridine (5 mL); EtOAc (10 mL); **2-morpholinoaniline** (244 mg, 1.37 mmol, 1 eq., BLD-Pharm); **N-Boc-L-phenylalanine** (400 mg, 1.51 mmol, 1.1 eq., TCI); **T3P 50 % m/v in EtOAc** (1630  $\mu$ L, 2.74 mmol, 2 eq., Aldrich)

**Purification:**

Flash chromatography ethyl acetate/heptane gradient 85 % heptane to 60 % over 10 CV over 45 g normal phase silica gel 0.63 – 0.2  $\mu$ m particle size. Followed by flash chromatography ethyl acetate/heptane gradient 90 % heptane to 65 % + 1 % formic acid over 10 CV over 90 g normal phase silica gel 0.63 – 0.2  $\mu$ m particle size Yield: 376 mg, 65 %

**Analytics:**

$R_F$  value: 0.50 ethyl acetate/heptane 1:1

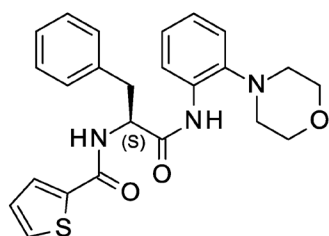
$^1\text{H NMR}$  (Figure S8) (400 MHz, Chloroform- $d$ )  $\delta$  8.93 (s, 1H), 8.42 (d,  $J$  = 8.0 Hz, 1H), 7.30 – 6.99 (m, 8H), 5.12 (s, 1H), 4.60 – 4.39 (m, 1H), 3.76 – 3.57 (m, 4H), 3.17 (d,  $J$  = 6.6 Hz, 2H), 2.72 – 2.52 (m, 4H), 1.41 (s, 9H).

Mass: Calculated  $m/z$  for  $\text{C}_{24}\text{H}_{32}\text{N}_3\text{O}_4^+$   $[\text{M}+\text{H}]^+ = 426.2388$ ; found APCI:  $[\text{M}+\text{H}]^+ 426.4$

Specific optical rotation: Starting material N-Boc-D-phenylalanine (**Boc-Phe-L**)  $[\alpha]^{23.8}_D 10.10$  ( $c$  0.215, methanol); After anilide formation (**1-L**)  $[\alpha]^{24.6}_D -20.19$  ( $c$  0.103, methanol)

**2B-(S)**

(2S)-N-[2-(morpholin-4-yl)phenyl]-3-phenyl-2-[(thiophen-2-yl)formamido]propanamide



**Synthesis:**

Synthesis was carried out according to **general procedure B**.

**Quantities:** DCM (10 mL); TFA (10 mL); **1-S** (356 mg, 0.84 mmol) Boc-protected crude product isolation: 280 mg; Used for next step: 249 mg (0.77 mmol, 1 eq.); THF, dry (10 ml); **2-carboxythiophene** (108 mg, 0.84 mmol, 1.1 eq., Alfa Aesar); **DEPBT** (687 mg, 2.30 mmol, 3 eq., BLD-Pharm); **DIPEA** (391  $\mu$ L, 2.30 mmol, 3 eq., Aldrich)

**Purification:**

Flash chromatography ethyl acetate/heptane gradient 85 % heptane to 50 % over 10 CV over 45 g normal phase silica gel 0.63 – 0.2  $\mu$ m particle size. Followed by flash chromatography ethyl acetate/heptane gradient 70 % heptane to 6 % over 6 CV over 45 g normal phase silica gel 0.63 – 0.2  $\mu$ m particle size. Yield: 238 mg, 71 %

Analytcs:

$R_f$  value: 0.40 ethyl acetate/heptane 1:1

$^1\text{H}$  NMR (*Figure S9*)(400 MHz, Chloroform-*d*)  $\delta$  8.82 (s, 1H), 8.40 (dd,  $J = 8.1, 1.5$  Hz, 1H), 7.52 (dd,  $J = 3.8, 1.1$  Hz, 1H), 7.48 (dd,  $J = 5.0, 1.3$  Hz, 1H), 7.34 – 7.24 (m, 4H), 7.23 – 7.17 (m, 1H), 7.17 – 7.01 (m, 4H), 6.93 (t,  $J = 7.5$  Hz, 1H), 4.95 (td,  $J = 7.9, 5.5$  Hz, 1H), 3.69 – 3.52 (m, 4H), 3.39 (dd,  $J = 13.6, 5.5$  Hz, 1H), 3.25 (dd,  $J = 13.6, 8.1$  Hz, 1H), 2.70 – 2.48 (m, 4H).

$^{13}\text{C}$  NMR APT (*Figure S10*) (101 MHz, Chloroform-*d*)  $\delta$  168.75, 161.55, 141.18, 137.97, 136.48, 132.91, 130.74, 129.38, 128.86, 128.66, 127.81, 127.13, 125.69, 124.33, 120.80, 119.52, 67.25, 56.18, 52.46, 38.48.

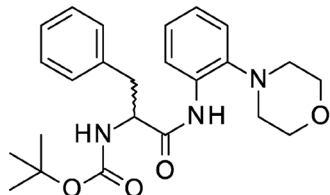
Mass: Calculated  $m/z$  for  $\text{C}_{24}\text{H}_{26}\text{N}_3\text{O}_3\text{S}^+$   $[\text{M}+\text{H}]^+ = 436.1689$ ;  $\text{C}_{24}\text{H}_{25}\text{N}_3\text{O}_3\text{SNa}^+$   $[\text{M}+\text{Na}]^+ = 458.1509$ ; found APCI: 435.9; found HRMS:  $[\text{M}+\text{H}]^+ 436.1689$ ;  $[\text{M}+\text{Na}]^+ 458.1509$

HPLC purity: 98.3 %  $t_R = 4.523$  min (*Figure S11*); 50 mm Eclipse Plus C18 1.8  $\mu\text{m}$ , 4.6 mm, acetonitrile/water 45:55,  $v = 1.0$  mL/min,  $\lambda = 220$  nm

Specific optical rotation: Boc-protected intermediate (**2-L**)  $[\alpha]^{23.5}_D -54.70$  (c 0.107, methanol); final compound (**3-L**)  $[\alpha]^{23.7}_D -57.75$  (c 0.1235, methanol)

**1-(rac)**

tert-butyl N-(1-([2-(morpholin-4-yl)phenyl]carbonyl)-2-phenylethyl)carbamate

Synthesis:

Synthesis was carried out according to **general procedure A**.

*Quantities:* **Pyridine** (5 mL); **EtOAc** (10 mL); **2-morpholinoaniline** (244 mg, 1.37 mmol, 1 eq., BLD-Pharm); **N-Boc-D/L-phenylalanine** (400 mg, 1.51 mmol, 1.1 eq., BLD-Pharm); **T3P 50 % m/v in EtOAc** (1630  $\mu\text{L}$ , 2.74 mmol, 2 eq., Aldrich)

Purification:

Flash chromatography ethyl acetate/heptane gradient 85 % heptane to 60 % over 10 CV over 90 g normal phase silica gel 0.63 – 0.2  $\mu\text{m}$  particle size. Yield: 464 mg; 80 %

Analytcs:

$R_f$  value: 0.50 ethyl acetate/heptane 1:1

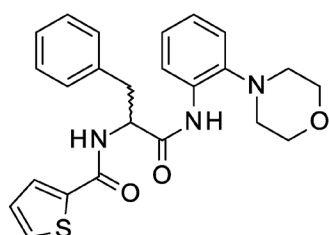
$^1\text{H}$  NMR (Figure S12) (400 MHz, Chloroform-*d*)  $\delta$  8.94 (s, 1H), 8.41 (d,  $J$  = 8.0 Hz, 1H), 7.31 – 6.95 (m, 8H), 5.33 – 4.98 (m, 1H), 4.62 – 4.38 (m, 1H), 3.79 – 3.61 (m, 4H), 3.17 (d,  $J$  = 6.7 Hz, 2H), 2.73 – 2.49 (m, 4H), 1.40 (s, 9H).

Mass: Calculated  $m/z$  for  $\text{C}_{24}\text{H}_{32}\text{N}_3\text{O}_4^+$   $[\text{M}+\text{H}]^+ = 426.2388$ ; found APCI:  $[\text{M}+\text{H}]^+ 426.4$

Specific optical rotation: Starting material N-Boc-D-phenylalanine (**Boc-Phe-D/L**)  $[\alpha]^{24.8}_{\text{D}} 0.25$  ( $c$  0.190, methanol); After anilide formation (**1-D/L**)  $[\alpha]^{23.9}_{\text{D}} -0.49$  ( $c$  0.137, methanol)

## 2B-(rac)

N-[2-(morpholin-4-yl)phenyl]-3-phenyl-2-[(thiophen-2-yl)formamido]propenamamide



### Synthesis:

Synthesis was carried out according to **general procedure B**.

**Quantities:** DCM (10 mL); TFA (10 mL); **1-R/S** (464 mg, 1.09 mmol) Boc-protected crude product isolation: 283 mg; Used for next step: 252 mg (0.78 mmol, 1 eq.); THF, dry (15 ml); **2-carboxythiophene** (110 mg, 0.86 mmol, 1.1 eq., Alfa Aesar); **DEPBT** (700 mg, 2.34 mmol, 3 eq., BLD-Pharm); **DIPEA** (399  $\mu\text{L}$ , 2.34 mmol, 3 eq., Aldrich)

### Purification:

Flash chromatography ethyl acetate/heptane gradient 85 % heptane to 60 % over 10 CV over 45 g normal phase silica gel 0.63 – 0.2  $\mu\text{m}$  particle size. Yield: 118 mg, 35 %

### Analytcs:

$R_f$  value: 0.50 ethyl acetate/heptane 1:1

$^1\text{H}$  NMR (Figure S13) (400 MHz, Chloroform-*d*)  $\delta$  8.80 (s, 1H), 8.41 (dd,  $J$  = 8.1, 1.4 Hz, 1H), 7.57 – 7.48 (m, 2H), 7.32 – 7.24 (m, 4H), 7.25 – 7.04 (m, 5H), 6.77 (d,  $J$  = 7.7 Hz, 1H), 4.94 (td,  $J$  = 8.0, 5.3 Hz, 1H), 3.67 – 3.53 (m, 4H), 3.38 (dd,  $J$  = 13.5, 5.3 Hz, 1H), 3.21 (dd,  $J$  = 13.5, 8.1 Hz, 1H), 2.69 – 2.48 (m, 4H).

$^{13}\text{C}$  NMR (Figure S14)(101 MHz, Chloroform-*d*)  $\delta$  168.56, 161.47, 141.13, 137.93, 136.40, 132.91, 130.75, 129.39, 128.87, 128.65, 127.84, 127.15, 125.74, 124.32, 120.82, 119.47, 67.26, 56.07, 52.46, 38.55.

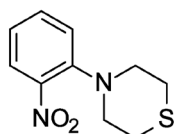
Mass: Calculated  $m/z$  for  $\text{C}_{24}\text{H}_{26}\text{N}_3\text{O}_3\text{S}^+$   $[\text{M}+\text{H}]^+ = 436.1689$ ;  $\text{C}_{24}\text{H}_{25}\text{N}_3\text{O}_3\text{SNa}^+$   $[\text{M}+\text{Na}]^+ = 458.1509$ ; found APCI: 435.9; found HRMS:  $[\text{M}+\text{H}]^+ 436.1687$ ;  $[\text{M}+\text{Na}]^+ 458.1509$

HPLC purity: 98.5 %  $t_R=4.523$  min (Figure S15); 50 mm Eclipse Plus C18 1.8  $\mu\text{m}$ , 4.6 mm, acetonitrile/water 45:55,  $v=1.0$  mL/min 10 min,  $\lambda=220$  nm

Specific optical rotation: Boc-protected intermediate (**2-D/L**)  $[\alpha]^{23.6}_D -1.38$  (c 0.166, methanol); final compound (**3-D/L**)  $[\alpha]^{23.8}_D -0.47$  (c 0.154, methanol)

### 3

4-(2-nitrophenyl)thiomorpholine



#### Synthesis:

Synthesis was carried out according to **general procedure C**.

**Quantities:** **Thiomorpholine** (3065 mg; 2976  $\mu$ l; 29.70 mmol; 3 eq.; TCI); **1-bromo-2-nitro-benzene** (2000 mg; 1 eq.; Alfa Aesar)

#### Purification:

Flash chromatography ethyl acetate/heptane gradient 90 % heptane to 50 % over 8 CV over 90 g normal phase silica gel 0.63 – 0.2  $\mu$ m particle size. Yield: 2063 mg, 93 %

#### Analytics:

$R_f$  value: 0.65 ethyl acetate/heptane 1:1

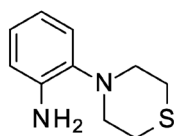
<sup>1</sup>H NMR (*Figure S16*) (500 MHz, Chloroform-*d*)  $\delta$  7.74 (dd,  $J = 8.1, 1.6$  Hz, 1H), 7.49 (ddd,  $J = 8.3, 7.3, 1.6$  Hz, 1H), 7.17 (dd,  $J = 8.2, 1.3$  Hz, 1H), 7.10 (ddd,  $J = 8.4, 7.4, 1.3$  Hz, 1H), 3.39 – 3.23 (m, 4H), 2.88 – 2.68 (m, 4H).

<sup>13</sup>C NMR (*Figure S17*) (126 MHz, Chloroform-*d*)  $\delta$  146.91, 144.46, 133.32, 125.51, 122.80, 122.46, 54.68, 27.92.

Mass: Calculated  $m/z$  for C<sub>10</sub>H<sub>13</sub>N<sub>2</sub>O<sub>2</sub>S<sup>+</sup> [M+H]<sup>+</sup> = 225.0692; found APCI: 225.0

### 4

2-thiomorpholinoaniline



#### Synthesis:

Synthesis was carried out according to **general procedure D**.

**Quantities:** **Ethanol** (30 mL); **3** (1196 mg; 5.33 mmol; 1 eq.); **Hydrazine 50 % m/v in water** (855 mg; 831  $\mu$ l; 2.5 eq.; Aldrich); **Pd/C 10 % m/m** (2400 mg (2x m 3))

Before reflux, addition of another 1.25 eq. of hydrazine solution.

**Purification:**

Flash chromatography ethyl acetate/heptane gradient 80 % heptane to 55 % over 8 CV over 90 g normal phase silica gel 0.63 – 0.2  $\mu\text{m}$  particle size. Yield: 724 mg, 70 %

**Analytics:**

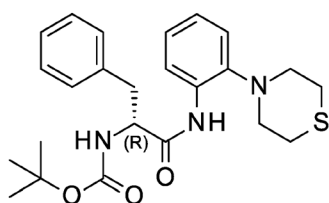
$R_f$  value: 0.55 ethyl acetate/heptane 1:1

$^1\text{H}$  NMR (*Figure S18*) (400 MHz, Chloroform-*d*)  $\delta$  7.04 – 6.87 (m, 2H), 6.79 – 6.70 (m, 2H), 4.07 (s, 1H), 3.26 – 3.06 (m, 4H), 2.92 – 2.70 (m, 4H).

Mass: Calculated  $m/z$  for  $\text{C}_{10}\text{H}_{15}\text{N}_2\text{S}^+$   $[\text{M}+\text{H}]^+= 195.0950$ ; found APCI: 195.3

**5**

tert-butyl N-[(1R)-1-benzyl-2-oxo-2-(2-thiomorpholino)ethyl]carbamate



**Synthesis:**

Synthesis was carried out according to **general procedure A**.

*Quantities:* **Pyridine** (5 mL); **EtOAc** (10 mL); **4** (715 mg, 3.68 mmol, 1 eq.); **N-Boc-D-phenylalanine** (1074 mg, 4.05 mmol, 1.1 eq., TCI); **T3P 50 % m/v in EtOAc** (4381  $\mu\text{L}$ , 7.36 mmol, 2 eq., Aldrich)

Instead of washing with 0.25 M  $\text{KH}_2\text{PO}_4$  solution three times the mixture was washed with 0.5 N HCl one time.

**Purification:**

Flash chromatography ethyl acetate/heptane 80 % heptane + 1 % formic acid over 90 g normal phase silica gel 0.63 – 0.2  $\mu\text{m}$  particle size. Increased amount of ethyl acetate after 6 CV. Yield: 1613 mg, 99 %

**Analytics:**

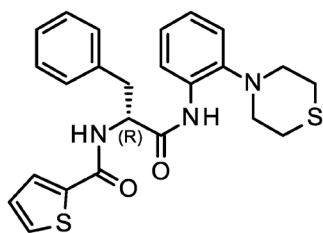
$R_f$  value: 0.55 ethyl acetate/heptane 1:1

$^1\text{H}$  NMR (*Figure S19*) (400 MHz, Chloroform-*d*)  $\delta$  8.98 (s, 1H), 8.42 (d,  $J = 8.1$  Hz, 1H), 7.34 – 6.98 (m, 8H), 4.97 (s, 1H), 4.53 (s, 1H), 3.19 (dd,  $J = 6.5, 1.8$  Hz, 2H), 3.01 – 2.80 (m, 4H), 2.75 – 2.50 (m, 4H), 1.42 (s, 9H).

Mass: Calculated  $m/z$  for  $\text{C}_{24}\text{H}_{32}\text{N}_3\text{O}_3\text{S}^+$   $[\text{M}+\text{H}]^+= 442.2159$ ; found APCI: 442.7

## 6

N-[(1R)-1-benzyl-2-oxo-2-(2-thiomorpholinoanilino)ethyl]thiophene-2-carboxamide

Synthesis:

Synthesis was carried out according to **general procedure B**.

**Quantities:** DCM (5 mL); TFA (5 mL); **5** (300 mg, 0.68 mmol) **Boc-protected crude product isolation:** 245 mg; Used for next step: 88 mg (0.26 mmol, 1 eq.); THF, dry (5 ml); **2-carboxythiophene** (33 mg, 0.26 mmol, 1.0 eq., Alfa Aesar); **DEPBT** (154 mg, 0.52 mmol, 2 eq., BLD-Pharm); **DIPEA** (88  $\mu$ L, 0.52 mmol, 2 eq., Aldrich)

After 2 h addition of another 0.5 eq. 2-carboxythiophene, 1 eq. DEPBT, and 1 eq. DIPEA. Instead of washing with 0.25 M  $\text{KH}_2\text{PO}_4$  solution the washing step was performed with 0.5 N HCl instead.

Purification:

Flash chromatography dichloromethane 100 % over 45 g normal phase silica gel 0.63 – 0.2  $\mu\text{m}$  particle size. Added 10 % v/v of methanol after 15 CV to increase elution power. Afterwards second flash chromatography ethyl acetate/heptane 85 % heptane to 70 % over 45 g normal phase silica gel 0.63 – 0.2  $\mu\text{m}$  particle size. Yield: 71 mg; 61 %

Analytics:

$R_f$  value: 0.45 ethyl acetate/heptane 1:1

$^1\text{H}$  NMR (*Figure S20*) (500 MHz, Chloroform-*d*)  $\delta$  8.77 (s, 1H), 8.41 (dd,  $J = 8.1, 1.5$  Hz, 1H), 7.54 – 7.50 (m, 2H), 7.33 – 7.27 (m, 4H), 7.25 – 7.20 (m, 1H), 7.16 (ddd,  $J = 8.4, 7.1, 1.8$  Hz, 1H), 7.12 – 7.08 (m, 2H), 7.05 (ddd,  $J = 7.9, 7.1, 1.5$  Hz, 1H), 6.61 (d,  $J = 7.7$  Hz, 1H), 4.94 (td,  $J = 7.9, 5.2$  Hz, 1H), 3.41 (dd,  $J = 13.6, 5.1$  Hz, 1H), 3.20 (dd,  $J = 13.6, 8.0$  Hz, 1H), 2.91 – 2.76 (m, 4H), 2.58 – 2.46 (m, 4H).

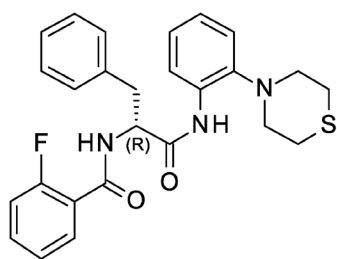
$^{13}\text{C}$  NMR (*Figure S21*) (126 MHz, Chloroform-*d*)  $\delta$  168.45, 161.38, 142.22, 137.84, 136.30, 132.81, 130.77, 129.42, 128.90, 128.69, 127.89, 127.24, 125.88, 124.21, 121.41, 119.31, 55.85, 54.48, 38.52, 28.54.

Mass: Calculated  $m/z$  for  $\text{C}_{24}\text{H}_{26}\text{N}_3\text{O}_2\text{S}_2^+$   $[\text{M}+\text{H}]^+ = 452.1461$ ;  $\text{C}_{24}\text{H}_{25}\text{N}_3\text{O}_2\text{S}_2\text{Na}^+$   $[\text{M}+\text{Na}]^+ = 474.1280$ ; found APCI: 452.4; found HRMS:  $[\text{M}+\text{H}]^+ 452.1464$ ;  $[\text{M}+\text{Na}]^+ 474.1283$

HPLC purity: 100.0 %  $t_R = 10.4$  min (*Figure S22*)

## 7

N-[(1R)-1-benzyl-2-oxo-2-(2-thiomorpholinoanilino)ethyl]-2-fluoro-benzamide



### Synthesis:

Synthesis was carried out according to **general procedure B**. The crude product of Boc-deprotection of **6** was used for the further steps.

**Quantities:** Boc-protected crude product of **6**: 80 mg (0.23 mmol, 1 eq.); THF, dry (5 ml); 2-fluorobenzoic acid (36 mg, 0.25 mmol, 1.1 eq., Alfa Aesar); DEPBT (210 mg, 0.70 mmol, 3 eq., BLD-Pharm); DIPEA (119  $\mu$ L, 0.7 mmol, 3 eq., Aldrich)

Instead of washing with 0.25 M  $\text{KH}_2\text{PO}_4$  solution the washing step was performed with 0.5 N HCl instead.

### Purification:

Flash chromatography ethyl acetate/heptane 85 % heptane to 60 % over 45 g normal phase silica gel 0.63 – 0.2  $\mu\text{m}$  particle size. Yield: 81 mg; 74 %

### Analytics:

$R_f$  value: 0.55 ethyl acetate/heptane 1:1

$^1\text{H}$  NMR (Figure S23) (400 MHz, Chloroform-*d*)  $\delta$  8.84 (s, 1H), 8.44 (d,  $J = 7.7$  Hz, 1H), 8.11 (td,  $J = 7.9$ , 1.9 Hz, 1H), 7.55 – 7.47 (m, 1H), 7.41 (dd,  $J = 13.7$ , 7.3 Hz, 1H), 7.33 – 6.99 (m, 10H), 5.03 (tdd,  $J = 7.4$ , 5.5, 2.1 Hz, 1H), 3.42 (dd,  $J = 13.7$ , 5.5 Hz, 1H), 3.23 (dd,  $J = 13.7$ , 7.3 Hz, 1H), 2.91 – 2.71 (m, 4H), 2.57 – 2.30 (m, 4H).

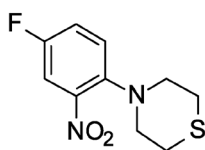
$^{13}\text{C}$  NMR (Figure S24) (101 MHz, Chloroform-*d*)  $\delta$  168.48, 163.01 (d,  $J = 3.2$  Hz), 160.82 (d,  $J = 247.9$  Hz), 142.17, 136.30, 134.01 (d,  $J = 9.5$  Hz), 132.90, 132.06 (d,  $J = 1.9$  Hz), 129.42, 128.83, 127.18, 125.90, 125.00 (d,  $J = 3.2$  Hz), 124.10, 121.33, 119.99 (d,  $J = 10.9$  Hz), 119.39, 116.26 (d,  $J = 24.8$  Hz), 56.34, 54.47, 38.28, 28.42.

Mass: Calculated  $m/z$  for  $\text{C}_{26}\text{H}_{27}\text{FN}_3\text{O}_2\text{S}^+$   $[\text{M}+\text{H}]^+ = 464.1803$ ;  $\text{C}_{26}\text{H}_{26}\text{FN}_3\text{O}_2\text{S Na}^+$   $[\text{M}+\text{Na}]^+ = 486.1622$ ; found APCI: 464.4; found HRMS:  $[\text{M}+\text{H}]^+ 464.1802$ ;  $[\text{M}+\text{Na}]^+ 486.1623$

HPLC purity: 99.8 %;  $t_R = 15.1$  min (Figure S25)

## 8

4-(4-fluoro-2-nitro-phenyl)thiomorpholine

**Synthesis:**

Synthesis was carried out according to **general procedure C**.

**Quantities:** **Thiomorpholine** (4220 mg; 4098  $\mu$ l; 44.56 mmol; 3 eq.; TCI); **1-bromo-4-fluoro-2-nitrobenzene** (3000 mg; 12.56 mmol; 1 eq.; abcr)

110 °C instead of 120 °C

**Purification:**

Flash chromatography dichloromethane/heptane gradient 95 % heptane to 85 % over 90 g normal phase silica gel 0.63 – 0.2  $\mu$ m particle size. Yield: 1822 mg, 55 %

**Analytics:**

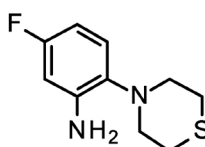
$R_f$  value: 0.75 dichloromethane

$^1\text{H}$  NMR (*Figure S26*) (400 MHz, Chloroform-*d*)  $\delta$  7.45 (dd,  $J = 7.9, 2.8$  Hz, 1H), 7.27 – 7.16 (m, 2H), 3.68 – 3.56 (m, 0H), 3.40 (d,  $J = 3.0$  Hz, 0H), 3.27 – 3.18 (m, 4H), 2.79 – 2.71 (m, 4H).

Mass: Calculated  $m/z$  for  $\text{C}_{10}\text{H}_{12}\text{FN}_2\text{O}_2\text{S}^+$   $[\text{M}+\text{H}]^+ = 243.0598$ ; found APCI: 243.0

**9**

5-fluoro-2-thiomorpholinoaniline

**Synthesis:**

Synthesis was carried out according to **general procedure D**.

**Quantities:** **Ethanol** (15 mL); **8** (514 mg; 2.12 mmol; 1 eq.); **Hydrazine 50 % m/v in water** (340 mg; 330  $\mu$ L; 2.5 eq.; Aldrich); **Pd/C 10 % m/m** (463 mg (90 % m **8**))

**Purification:**

Flash chromatography dichloromethane/heptane gradient 95 % heptane to 60 % + 1 % v/v HCOOH over 12 CV over 45 g normal phase silica gel 0.63 – 0.2  $\mu$ m particle size. Yield: 365 mg, 81 %

**Analytics:**

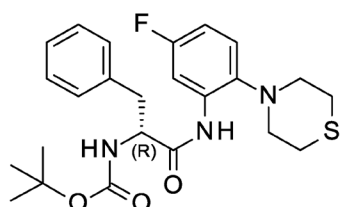
$R_f$  value: 0.55 ethyl acetate/heptane 1:1

$^1\text{H}$  NMR (400 MHz, Chloroform-*d*)  $\delta$  6.91 (dd,  $J$  = 8.5, 5.8 Hz, 1H), 6.47 – 6.34 (m, 2H), 4.11 (s, 2H), 3.07 (s, 4H), 2.78 (s, 4H).

Mass: Calculated  $m/z$  for  $\text{C}_{10}\text{H}_{14}\text{FN}_2\text{S}^+$   $[\text{M}+\text{H}]^+ = 213.0856$ ; found APCI: 213.3

## 10

tert-butyl N-[(1R)-1-[[5-fluoro-2-(thiomorpholin-4-yl)phenyl]carbamoyl]-2-phenylethyl]carbamate



### Synthesis:

Synthesis was carried out according to **general procedure A**.

**Quantities:** Pyridine (10 mL); EtOAc (20 mL); **9** (217 mg, 1.02 mmol, 1 eq.); **N-Boc-D-phenylalanine** (298 mg, 1.12 mmol, 1.1 eq., TCI); **T3P 50 % m/v in EtOAc** (1217  $\mu\text{L}$ , 2.04 mmol, 2 eq., Aldrich)

### Purification:

Flash chromatography ethyl acetate/heptane gradient 80 % heptane to 65 % over 45 g normal phase silica gel 0.63 – 0.2  $\mu\text{m}$  particle size. Increased amount of ethyl acetate after 6 CV. Afterwards second flash chromatography ethyl acetate/heptane 90 % heptane to 70 % over 45 g normal phase silica gel 0.63 – 0.2  $\mu\text{m}$  particle size. Yield: 425 mg; 91 %

### Analytcs:

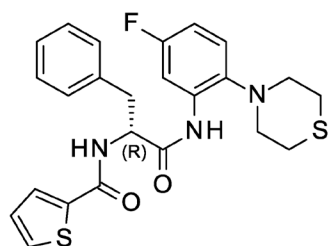
$R_f$  value: 0.70 ethyl acetate/heptane 1:1

$^1\text{H}$  NMR (Figure S28) (400 MHz, Chloroform-*d*)  $\delta$  9.09 (s, 1H), 8.24 (dd,  $J$  = 10.8, 2.9 Hz, 1H), 7.33 – 7.16 (m, 5H), 7.04 (dd,  $J$  = 8.8, 5.6 Hz, 1H), 6.72 (td,  $J$  = 8.3, 3.0 Hz, 1H), 4.98 (s, 1H), 4.52 (s, 1H), 3.18 (d,  $J$  = 6.5 Hz, 2H), 2.91 – 2.41 (m, 8H), 1.41 (s, 9H).

Mass: Calculated  $m/z$  for  $\text{C}_{24}\text{H}_{31}\text{FN}_3\text{O}_3\text{S}^+$   $[\text{M}+\text{H}]^+ = 460.2065$ ; found APCI: 460.7

## 11

N-[(1R)-1-benzyl-2-(5-fluoro-2-thiomorpholino-anilino)-2-oxo-ethyl]thiophene-2-carboxamide



**Synthesis:**

Synthesis was carried out according to **general procedure B**.

**Quantities:** DCM (5 mL); TFA (5 mL); **10** (150 mg, 0.33 mmol) Boc-protected crude product isolation: 121 mg; Used for next step: 67 mg (0.19 mmol, 1 eq.); THF, dry (5 ml); **2-carboxythiophene** (29 mg, 0.22 mmol, 1.2 eq., Alfa Aesar); **DEPBT** (61 mg, 0.21 mmol, 1.1 eq., BLD-Pharm); **DIPEA** (63  $\mu$ L, 0.37 mmol, 2 eq., Aldrich)

After the reaction time the crude reaction mixture was directly evaporated on silica gel without previous washing.

**Purification:**

Flash chromatography ethyl acetate/heptane 85 % heptane to 65 % over 45 g normal phase silica gel 0.63 – 0.2  $\mu$ m particle size. Afterwards second flash chromatography ethyl dichloromethane/ethyl acetate 97 % dichloromethane to 93 % over 45 g normal phase silica gel 0.63 – 0.2  $\mu$ m particle size. Yield: 52 mg; 58 %

**Analytics:**

$R_f$  value: 0.65 ethyl acetate/heptane 1:1

$^1\text{H}$  NMR (*Figure S29*) (400 MHz, Chloroform-*d*)  $\delta$  8.94 (s, 1H), 8.22 (dd,  $J$  = 10.8, 3.0 Hz, 1H), 7.55 – 7.48 (m, 2H), 7.33 – 7.19 (m, 5H), 7.11 – 6.97 (m, 2H), 6.78 – 6.65 (m, 2H), 4.94 (td,  $J$  = 7.8, 5.5 Hz, 1H), 3.39 (dd,  $J$  = 13.6, 5.5 Hz, 1H), 3.22 (dd,  $J$  = 13.6, 7.8 Hz, 1H), 2.79 (dtd,  $J$  = 16.5, 11.8, 4.8 Hz, 4H), 2.65 – 2.41 (m, 4H).

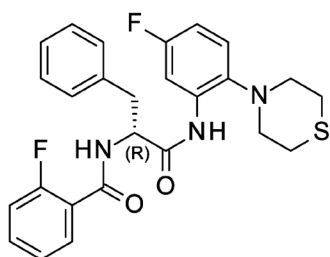
$^{13}\text{C}$  NMR (*Figure S30*) (101 MHz, Chloroform-*d*)  $\delta$  168.93, 161.55, 160.15 (d,  $J$  = 242.7 Hz), 138.07 (d,  $J$  = 3.1 Hz), 137.69, 136.21, 134.17 (d,  $J$  = 12.2 Hz), 130.92, 129.35, 128.92, 128.79, 127.92, 127.27, 122.67 (d,  $J$  = 9.6 Hz), 110.34 (d,  $J$  = 22.7 Hz), 106.82 (d,  $J$  = 28.8 Hz), 55.90, 54.71, 38.20, 28.54.

Mass: Calculated  $m/z$  for  $\text{C}_{24}\text{H}_{25}\text{FN}_3\text{O}_2\text{S}_2^+$   $[\text{M}+\text{H}]^+$  = 470.1367;  $\text{C}_{24}\text{H}_{24}\text{FN}_3\text{O}_2\text{S}_2\text{Na}^+$   $[\text{M}+\text{Na}]^+$  = 492.1186; found APCI: 470.6; found HRMS:  $[\text{M}+\text{H}]^+$  464.1802;  $[\text{M}+\text{Na}]^+$  492.1183

HPLC purity: 97.3 %;  $t_R$  = 14.5 min (*Figure S31*)

**12**

N-[(1R)-1-benzyl-2-(5-fluoro-2-thiomorpholino-anilino)-2-oxo-ethyl]-2-fluoro-benzamide



Synthesis:

Synthesis was carried out according to **general procedure B**. The crude product of Boc-deprotection of **11** was used for the further steps.

**Quantities:** **Boc-deprotected crude product of 11** (63 mg, 0.18 mmol, 1 eq.); **THF**, dry (5 ml); **2-fluorobenzoic acid** (29 mg, 0.21 mmol, 1.2 eq., Alfa Aesar); **DEPBT** (58 mg, 0.19 mmol, 1.1 eq., BLD-Pharm); **DIPEA** (60  $\mu$ L, 0.35 mmol, 2 eq., Aldrich)

After the reaction time the crude reaction mixture was directly evaporated on silica gel without previous washing.

Purification:

Flash chromatography ethyl acetate/heptane 85 % heptane to 65 % over 45 g over 8 CV normal phase silica gel 0.63 – 0.2  $\mu$ m particle size. Yield: 52 mg; 58 %

Analytics:

$R_f$  value: 0.65 ethyl acetate/heptane 1:1

$^1\text{H}$  NMR (*Figure S32*) (500 MHz, Chloroform-*d*)  $\delta$  8.96 (s, 1H), 8.26 (dd,  $J$  = 10.8, 3.0 Hz, 1H), 8.11 (td,  $J$  = 7.9, 1.9 Hz, 1H), 7.51 (dddd,  $J$  = 8.3, 7.2, 5.2, 1.9 Hz, 1H), 7.39 (dd,  $J$  = 13.9, 7.2 Hz, 1H), 7.32 – 7.25 (m, 5H), 7.24 – 7.20 (m, 1H), 7.17 (ddd,  $J$  = 12.3, 8.3, 1.1 Hz, 1H), 7.02 (dd,  $J$  = 8.7, 5.6 Hz, 1H), 6.72 (ddd,  $J$  = 8.8, 8.0, 3.0 Hz, 1H), 5.01 (tdd,  $J$  = 7.4, 5.6, 2.1 Hz, 1H), 3.41 (dd,  $J$  = 13.8, 5.6 Hz, 1H), 3.22 (dd,  $J$  = 13.7, 7.2 Hz, 1H), 2.86 – 2.70 (m, 4H), 2.58 – 2.30 (m, 4H).

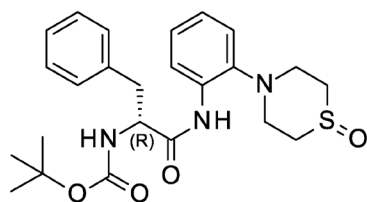
$^{13}\text{C}$  NMR (*Figure S33*) (126 MHz, Chloroform-*d*)  $\delta$  168.76, 163.08 (d,  $J$  = 3.3 Hz), 160.84 (d,  $J$  = 247.9 Hz), 160.21 (d,  $J$  = 243.2 Hz), 137.99 (d,  $J$  = 2.9 Hz), 136.14, 134.24 (d,  $J$  = 12.3 Hz), 134.13 (d,  $J$  = 9.5 Hz), 132.07 (d,  $J$  = 1.9 Hz), 129.37, 128.86, 127.23, 125.05 (d,  $J$  = 3.3 Hz), 122.56 (d,  $J$  = 9.8 Hz), 119.80 (d,  $J$  = 10.9 Hz), 116.28 (d,  $J$  = 24.8 Hz), 110.22 (d,  $J$  = 22.7 Hz), 106.85 (d,  $J$  = 28.7 Hz), 56.31, 54.67, 38.10, 28.43.

Mass: Calculated  $m/z$  for  $\text{C}_{26}\text{H}_{26}\text{F}_2\text{N}_3\text{O}_2\text{S}^+$   $[\text{M}+\text{H}]^+$  = 482.1709;  $\text{C}_{26}\text{H}_{25}\text{F}_2\text{N}_3\text{O}_2\text{SNa}^+$   $[\text{M}+\text{Na}]^+$  = 504.1528; found APCI: 482.6; found HRMS:  $[\text{M}+\text{H}]^+$  482.1708;  $[\text{M}+\text{Na}]^+$  504.1526

HPLC purity: 98.5 %;  $t_R$  = 15.1 min (*Figure S34*)

**13**

tert-butyl N-[(1R)-1-benzyl-2-oxo-2-[2-(1-oxo-1,4-thiazinan-4-yl)anilino]ethyl]carbamate



Synthesis:

Synthesis was carried out according to **general procedure E**.

**Quantities:** **Sodiumperiodate** (76 mg; 0.36 mmol; 1.05 eq.); **Water** (5 mL); **5** (150 mg, 0.34 mmol, 1 eq.); **methanol** (5 ml); **Acetonitrile** (5 mL)

Purification:

Flash chromatography chloroform/methanol 100 % chloroform to 95 % over 90 g over 8 CV normal phase silica gel 0.63 – 0.2 µm particle size. Yield: 107 mg; 69 %

Analytics:

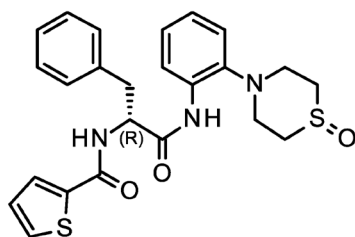
$R_f$  value: 0.75 chloroform/methanol 1:10

$^1\text{H}$  NMR (*Figure S35*) (400 MHz, Chloroform-*d*)  $\delta$  8.88 (s, 1H), 8.40 (s, 1H), 7.32 – 7.15 (m, 7H), 7.12 – 7.04 (m, 1H), 5.17 (s, 1H), 4.46 (q,  $J = 7.2$  Hz, 1H), 3.69 – 3.37 (m, 2H), 3.31 – 3.04 (m, 2H), 3.00 – 2.54 (m, 6H), 1.38 (s, 9H).

Mass: Calculated  $m/z$  for  $\text{C}_{24}\text{H}_{32}\text{N}_3\text{O}_4\text{S}^+$   $[\text{M}+\text{H}]^+ = 458.2108$ ; found APCI: 458.3

**14**

N-[(1R)-1-benzyl-2-oxo-2-[2-(1-oxo-1,4-thiazinan-4-yl)anilino]ethyl]thiophene-2-carboxamide

Synthesis:

Synthesis was carried out according to **general procedure B**.

**Quantities:** **DCM** (2.5 mL); **TFA** (2.5 mL); **13** (107 mg, 0.24 mmol) **Boc-protected crude product isolation:** 65 mg; Used for next step: 33 mg (0.09 mmol, 1 eq.); **THF**, dry (2.5 ml); **2-carboxythiophene** (13 mg, 0.10 mmol, 1.1 eq., Alfa Aesar); **DEPBT** (83 mg, 0.28 mmol, 3 eq., BLD-Pharm); **DIPEA** (47 µL, 0.37 mmol, 3 eq., Aldrich)

Purification:

Flash chromatography ethyl acetate/methanol 100 % ethyl acetate to 90 % over 45 g normal phase silica gel 0.63 – 0.2 µm particle size. Yield: 42 mg; 91 %

Analytics:

$R_f$  value: 0.30 ethyl acetate

$^1\text{H}$  NMR (Figure S36) (400 MHz, Chloroform-*d*)  $\delta$  9.10 (s, 1H), 8.39 (dd,  $J = 8.2, 1.5$  Hz, 1H), 7.54 – 7.44 (m, 2H), 7.36 – 7.12 (m, 7H), 7.11 – 7.02 (m, 2H), 6.88 (d,  $J = 8.0$  Hz, 1H), 4.95 (q, 1H), 3.63 – 3.47 (m, 2H), 3.41 – 3.27 (m, 2H), 2.98 – 2.78 (m, 4H), 2.74 – 2.59 (m, 2H).

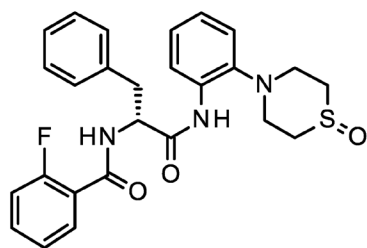
$^{13}\text{C}$  NMR (Figure S37) (101 MHz, Chloroform-*d*)  $\delta$  168.79, 161.85, 141.29, 137.63, 136.59, 133.20, 131.07, 129.36, 128.86, 128.76, 128.00, 127.16, 126.37, 124.40, 121.62, 119.65, 55.66, 46.20, 43.47, 43.16, 37.17.

Mass: Calculated  $m/z$  for  $\text{C}_{24}\text{H}_{26}\text{N}_3\text{O}_3\text{S}_2^+$   $[\text{M}+\text{H}]^+ = 468.1410$ ;  $\text{C}_{24}\text{H}_{25}\text{N}_3\text{O}_3\text{S}_2\text{Na}^+$   $[\text{M}+\text{Na}]^+ = 490.1230$ ;  
found APCI: 468.0; found HRMS:  $[\text{M}+\text{H}]^+ 468.1412$ ;  $[\text{M}+\text{Na}]^+ 490.1231$

HPLC purity: 100 %;  $t_{\text{R}} = 12.5$  min (Figure S38)

## 15

N-[(1R)-1-benzyl-2-oxo-2-[2-(1-oxo-1,4-thiazinan-4-yl)anilino]ethyl]-2-fluoro-benzamide



### Synthesis:

Synthesis was carried out according to **general procedure B**. The crude product of Boc-deprotection of **14** was used for the further steps.

**Quantities:** **Boc-deprotected crude product of 14** (32 mg, 0.09 mmol, 1 eq.); **THF**, dry (2.5 ml); **2-fluorobenzoic acid** (14 mg, 0.10 mmol, 1.1 eq., Alfa Aesar); **DEPBT** (80 mg, 0.27 mmol, 3 eq., BLD-Pharm); **DIPEA** (46  $\mu\text{L}$ , 0.27 mmol, 3 eq., Aldrich)

### Purification:

Flash chromatography ethyl acetate/methanol 100 % ethyl acetate to 90 % over 45 g normal phase silica gel 0.63 – 0.2  $\mu\text{m}$  particle size. Yield: 36 mg; 84 %

### Analytics:

$R_{\text{F}}$  value: 0.30 ethyl acetate

$^1\text{H}$  NMR (Figure S39) (400 MHz, Chloroform-*d*)  $\delta$  8.99 (s, 1H), 8.48 – 8.39 (m, 1H), 8.03 (td,  $J = 7.9, 1.9$  Hz, 1H), 7.56 – 7.46 (m, 1H), 7.41 – 7.03 (m, 11H), 5.02 (qd,  $J = 7.3, 6.3, 2.2$  Hz, 1H), 3.59 – 3.46 (m, 2H), 3.33 (qd,  $J = 13.9, 6.7$  Hz, 2H), 2.89 – 2.59 (m, 6H).

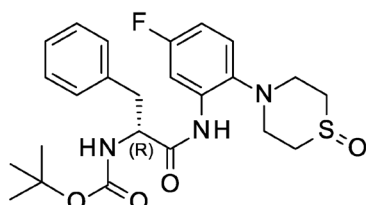
$^{13}\text{C}$  NMR (Figure S40) (101 MHz, Chloroform-*d*)  $\delta$  168.47, 163.28 (d,  $J = 3.1$  Hz), 160.75 (d,  $J = 248.3$  Hz), 141.18, 136.45, 134.21 (d,  $J = 9.5$  Hz), 133.10, 131.83 (d,  $J = 1.9$  Hz), 129.39, 128.84, 127.17, 126.40, 125.12 (d,  $J = 3.4$  Hz), 124.33, 121.44, 119.79 (d,  $J = 10.9$  Hz), 119.70, 116.35 (d,  $J = 24.7$  Hz), 56.13, 46.45, 43.43, 37.45.

Mass: Calculated  $m/z$  for  $C_{26}H_{27}FN_3O_3S^+$   $[M+H]^+$  = 480.1752;  $C_{26}H_{26}FN_3O_3SNa^+$   $[M+Na]^+$  = 502.1571; found APCI: 480.4; found HRMS:  $[M+H]^+$  480.1755;  $[M+Na]^+$  502.1573

HPLC purity: 99.9 %;  $t_R$  = 13.0 min (Figure S41)

## 16

tert-butyl N-[(1R)-1-benzyl-2-[5-fluoro-2-(1-oxo-1,4-thiazinan-4-yl)anilino]-2-oxo-ethyl]carbamate



### Synthesis:

Synthesis was carried out according to **general procedure E**.

**Quantities:** **Sodiumperiodate** (137 mg; 0.64 mmol; 1.05 eq.); **Water** (5 mL); **5** (280 mg, 0.61 mmol, 1 eq.); **methanol** (1 ml); **Acetonitrile** (45 mL)

After 1 d another 1.05 eq. of sodiumperiodate in 5 mL were added. After 2 d another 1.05 eq. of sodiumperiodate in 5 mL were added.

### Purification:

Flash chromatography dichloromethane/methanol 100 % dichloromethane to 95 % over 45 g over 8 CV normal phase silica gel 0.63 – 0.2  $\mu$ m particle size. Afterwards second flash chromatography dichloromethane/heptane 30 % heptane to 0 % over 8 CV on 45 g normal phase silica gel 0.63 – 0.2  $\mu$ m particle size. Yield: 260 mg; 90 %

### Analytics:

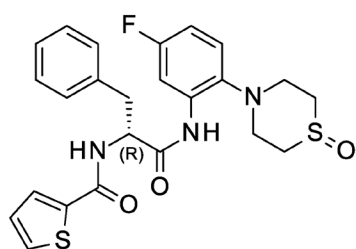
$R_f$  value: 0.50 ethyl acetate

$^1H$  NMR (Figure S42) (400 MHz, Methanol- $d_4$ )  $\delta$  8.11 (d,  $J$  = 10.9 Hz, 1H), 7.37 – 7.12 (m, 5H), 6.81 (td,  $J$  = 8.5, 3.0 Hz, 1H), 4.48 (d,  $J$  = 7.9 Hz, 1H), 3.52 – 3.39 (m, 2H), 3.35 – 3.27 (m, 1H), 3.16 (d,  $J$  = 11.6 Hz, 1H), 3.08 – 2.76 (m, 6H), 2.71 (dt,  $J$  = 13.9, 4.1 Hz, 1H), 1.33 (s, 9H).

Mass: Calculated  $m/z$  for  $C_{24}H_{31}FN_3O_4S^+$   $[M+H]^+$  = 476.2014; found APCI: 476.7

## 17

N-[(1R)-1-benzyl-2-[5-fluoro-2-(1-oxo-1,4-thiazinan-4-yl)anilino]-2-oxo-ethyl]thiophene-2-carboxamide



### Synthesis:

Synthesis was carried out according to **general procedure B**.

**Quantities:** **DCM** (7.5 mL); **TFA** (7.5 mL); **16** (260 mg, 0.55 mmol) Boc-protected crude product isolation: 153 mg; Used for next step: 82 mg (0.22 mmol, 1 eq.); **THF**, dry (5 ml); **2-carboxythiophene** (34 mg, 0.26 mmol, 1.2 eq., Alfa Aesar); **DEPBT** (72 mg, 0.24 mmol, 1.1 eq., BLD-Pharm); **DIPEA** (56  $\mu$ L, 0.44 mmol, 2 eq., Aldrich)

After the reaction time the crude reaction mixture was directly evaporated on silica gel without previous washing.

### Purification:

Flash chromatography ethyl acetate/heptane 85 % ethyl acetate to 100 % over 7 CV on 45 g normal phase silica gel 0.63 – 0.2  $\mu$ m particle size. Yield: 99 mg; 93 %

### Analytcs:

$R_f$  value: 0.30 ethyl acetate

$^1\text{H}$  NMR (*Figure S43*) (400 MHz, Chloroform-*d*)  $\delta$  9.31 (s, 1H), 8.21 (dd,  $J$  = 10.9, 2.8 Hz, 1H), 7.50 (ddt,  $J$  = 4.6, 2.6, 1.2 Hz, 2H), 7.34 – 7.19 (m, 5H), 7.15 (ddd,  $J$  = 9.0, 5.6, 1.2 Hz, 1H), 7.05 (ddd,  $J$  = 5.3, 3.7, 1.3 Hz, 2H), 6.77 – 6.70 (m, 1H), 4.95 (q,  $J$  = 7.3 Hz, 1H), 3.60 – 3.45 (m, 2H), 3.38 – 3.26 (m, 2H), 3.01 – 2.80 (m, 4H), 2.62 (dq,  $J$  = 12.5, 4.0 Hz, 2H).

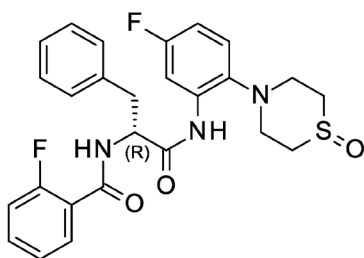
$^{13}\text{C}$  NMR (*Figure S44*) (101 MHz, Chloroform-*d*)  $\delta$  169.14, 162.06, 160.41 (d,  $J$  = 243.5 Hz), 137.56, 137.14 (d,  $J$  = 3.0 Hz), 136.54 (d,  $J$  = 1.1 Hz), 134.77 (d,  $J$  = 12.2 Hz), 131.19, 129.31, 128.86, 128.04, 127.15, 122.96 (d,  $J$  = 9.8 Hz), 110.48 (d,  $J$  = 22.8 Hz), 107.00 (d,  $J$  = 28.9 Hz), 55.65, 46.08, 43.64, 43.29, 36.70.

Mass: Calculated  $m/z$  for  $\text{C}_{24}\text{H}_{25}\text{FN}_3\text{O}_3\text{S}_2^+$   $[\text{M}+\text{H}]^+$  = 486.1316;  $\text{C}_{24}\text{H}_{24}\text{FN}_3\text{O}_3\text{S}_2\text{Na}^+$   $[\text{M}+\text{Na}]^+$  = 508.1135; found APCI: 486.3; found HRMS:  $[\text{M}+\text{H}]^+$  486.1314;  $[\text{M}+\text{Na}]^+$  508.1133

HPLC purity: 100 %;  $t_R$  = 12.7 min (*Figure S45*)

## 18

N-[(1R)-1-benzyl-2-[5-fluoro-2-(1-oxo-1,4-thiazinan-4-yl)anilino]-2-oxo-ethyl]-2-fluoro-benzamide



### Synthesis:

Synthesis was carried out according to **general procedure B**. The crude product of Boc-deprotection of **17** was used for the further steps.

**Quantities:** **Boc-deprotected crude product of 17** (79 mg, 0.21 mmol, 1 eq.); **THF**, dry (5 mL); **2-fluorobenzoic acid** (35 mg, 0.25 mmol, 1.2 eq., Alfa Aesar); **DEPBT** (69 mg, 0.23 mmol, 1.1 eq., BLD-Pharm); **DIPEA** (72  $\mu$ L, 0.42 mmol, 2 eq., Aldrich)

After the reaction time the crude reaction mixture was directly evaporated on silica gel without previous washing.

### Purification:

Flash chromatography ethyl acetate/heptane 95 % ethyl acetate to 100 % over 1 CV on 45 g normal phase silica gel 0.63 – 0.2  $\mu$ m particle size. Yield: 80 mg; 76 %

### Analytics:

$R_f$  value: 0.30 ethyl acetate

$^1\text{H}$  NMR (*Figure S46*) (400 MHz, Chloroform-*d*)  $\delta$  9.31 (s, 1H), 8.21 (dd,  $J = 10.9, 2.8$  Hz, 1H), 7.50 (ddt,  $J = 4.6, 2.6, 1.2$  Hz, 2H), 7.34 – 7.19 (m, 5H), 7.15 (ddd,  $J = 9.0, 5.6, 1.2$  Hz, 1H), 7.05 (ddd,  $J = 5.3, 3.7, 1.3$  Hz, 2H), 6.77 – 6.70 (m, 1H), 4.95 (q,  $J = 7.3$  Hz, 1H), 3.60 – 3.45 (m, 2H), 3.38 – 3.26 (m, 2H), 3.01 – 2.80 (m, 4H), 2.62 (dq,  $J = 12.5, 4.0$  Hz, 2H).

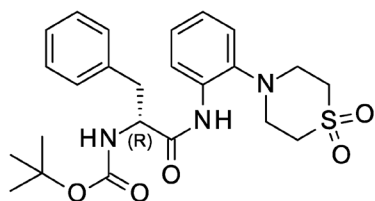
$^{13}\text{C}$  NMR (*Figure S47*) (126 MHz, Chloroform-*d*)  $\delta$  168.74, 163.45 (d,  $J = 3.2$  Hz), 160.74 (d,  $J = 248.4$  Hz), 160.47 (d,  $J = 243.6$  Hz), 136.99 (d,  $J = 3.3$  Hz), 136.31, 134.57 (d,  $J = 12.2$  Hz), 134.29 (d,  $J = 9.4$  Hz), 131.75 (d,  $J = 1.8$  Hz), 129.35, 128.85, 127.19, 125.14 (d,  $J = 3.3$  Hz), 122.77 (d,  $J = 9.8$  Hz), 119.70 (d,  $J = 10.9$  Hz), 116.38 (d,  $J = 24.8$  Hz), 110.48 (d,  $J = 22.7$  Hz), 107.13 (d,  $J = 28.9$  Hz), 56.06, 46.32, 43.56, 37.17.

Mass: Calculated  $m/z$  for  $\text{C}_{26}\text{H}_{26}\text{F}_2\text{N}_3\text{O}_3\text{S}^+$   $[\text{M}+\text{H}]^+ = 498.1657$ ;  $\text{C}_{26}\text{H}_{25}\text{F}_2\text{N}_3\text{O}_3\text{SNa}^+$   $[\text{M}+\text{Na}]^+ = 520.1477$ ; found APCI: 498.3; found HRMS:  $[\text{M}+\text{H}]^+ 498.1652$ ;  $[\text{M}+\text{Na}]^+ 520.1473$

HPLC purity: 99.6 %;  $t_R = 13.3$  min (*Figure S48*)

## 19

tert-butyl N-[(1R)-1-benzyl-2-[2-(1,1-dioxo-1,4-thiazinan-4-yl)anilino]-2-oxo-ethyl]carbamate

**Synthesis:**

Synthesis was carried out according to **general procedure F**.

**Quantities:** **5** (150 mg; 0.34 mmol; 1 eq.); **DCM** (for thiomorpholine; 5 mL); **m-CPBA 77 %** (176 mg, 0.82 mmol, 2.4 eq.); **DCM** (for m-CPBA; 5 ml)

**Purification:**

Flash chromatography ethyl acetate/heptane 90 % heptane to 60 % over 45 g normal phase silica gel 0.63 – 0.2  $\mu$ m particle size. Yield: 46 mg; 29 %

**Analytics:**

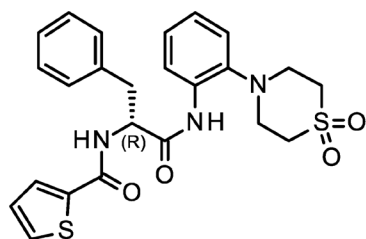
$R_F$  value: 0.30 ethyl acetate/heptane 1:1

$^1\text{H NMR}$  (Figure S49) (400 MHz, Chloroform-*d*)  $\delta$  8.84 (s, 1H), 8.40 (d,  $J = 8.2$  Hz, 1H), 7.33 – 7.13 (m, 7H), 7.08 (td,  $J = 7.7, 1.5$  Hz, 1H), 4.98 (d,  $J = 7.8$  Hz, 1H), 4.46 (q,  $J = 7.1$  Hz, 1H), 3.35 – 2.98 (m, 10H), 1.40 (s, 9H).

Mass: Calculated  $m/z$  for  $\text{C}_{24}\text{H}_{32}\text{N}_3\text{O}_5\text{S}^+$   $[\text{M}+\text{H}]^+ = 474.2057$ ; found APCI: 474.4

**20**

N-[(1R)-1-benzyl-2-[2-(1,1-dioxo-1,4-thiazinan-4-yl)anilino]-2-oxo-ethyl]thiophene-2-carboxamide

**Synthesis:**

Synthesis was carried out according to general procedure B.

**Quantities:** **DCM** (2.5 mL); **TFA** (2.5 mL); **19** (46 mg, 0.10 mmol) **Boc-protected crude product isolation:** 34 mg; Used for next step: 34 mg (0.09 mmol, 1 eq.); **THF**, dry (2.5 ml); **2-carboxythiophene** (13 mg, 0.10 mmol, 1.1 eq., Alfa Aesar); **DEPBT** (82 mg, 0.27 mmol, 3 eq., BLD-Pharm); **DIPEA** (47  $\mu$ L, 0.27 mmol, 3 eq., Aldrich)

**Purification:**

Flash chromatography dichloromethane/methanol 100 % dichloromethane to 95 % over 2 CV on 45 g normal phase silica gel 0.63 – 0.2  $\mu\text{m}$  particle size. Afterwards second flash chromatography ethyl acetate/heptane 85 % heptane to 50 % over 45 g normal phase silica gel 0.63 – 0.2  $\mu\text{m}$  particle size. Yield: 35 mg; 80 %

**Analytcs:**

$R_f$  value: 0.30 ethyl acetate/heptane 1:1

$^1\text{H}$  NMR (*Figure S50*) (400 MHz, Chloroform-*d*)  $\delta$  9.23 (s, 1H), 8.40 (dd,  $J = 8.6, 1.5$  Hz, 1H), 7.53 – 7.46 (m, 2H), 7.36 – 7.28 (m, 4H), 7.28 – 7.21 (m, 1H), 7.21 – 7.13 (m, 2H), 7.11 – 7.02 (m, 2H), 6.67 (d,  $J = 7.5$  Hz, 1H), 4.96 (q,  $J = 7.2$  Hz, 1H), 3.35 (d,  $J = 7.0$  Hz, 2H), 3.22 (s, 8H).

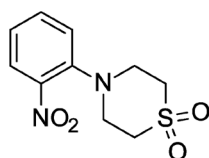
$^{13}\text{C}$  NMR (*Figure S52*) (101 MHz, Chloroform-*d*)  $\delta$  168.93, 162.12, 140.05, 137.18, 136.45, 133.16, 131.21, 129.37, 129.10, 128.94, 128.12, 127.23, 126.79, 124.32, 121.65, 119.97, 55.72, 51.86, 51.32, 36.77.

Mass: Calculated  $m/z$  for  $\text{C}_{24}\text{H}_{26}\text{N}_3\text{O}_4\text{S}_2^+$   $[\text{M}+\text{H}]^+ = 484.1359$ ;  $\text{C}_{24}\text{H}_{25}\text{N}_3\text{O}_4\text{S}_2\text{Na}^+$   $[\text{M}+\text{Na}]^+ = 506.1179$ ; found APCI: 484.3; found HRMS:  $[\text{M}+\text{H}]^+ 484.1362$ ;  $[\text{M}+\text{Na}]^+ 506.1180$

HPLC purity: 100 %;  $t_R = 12.5$  min (*Figure S51*)

**21**

4-(2-nitrophenyl)-1,4-thiazinane 1,1-dioxide

**Synthesis:**

Synthesis was carried out according to general procedure G.

*Quantities:* Dioxane (15 mL); 1-bromo-2-nitro-benzene (1019 mg; 5.04 mmol; 1 eq.; Alfa Aesar); Thiomorpholine-1,1-dioxide (681 mg; 5.04 mmol; 1 eq.; TCI);  $\text{Cs}_2\text{CO}_3$  (5000 mg; 15.12 mmol; 3 eq.; Aldrich);  $\text{Pd}(\text{OAc})_2$  (113 mg, 0.50 mmol, 0.1 eq.; Aldrich); ( $\pm$ )-BINAP (314 mg; 0.50 mmol; 0.1 eq.; Carbolution)

**Purification:**

Flash chromatography ethyl acetate/heptane 85 % heptane to 60 % over 90 g normal phase silica gel 0.63 – 0.2  $\mu\text{m}$  particle size. Yield: 408 mg; 32 %

**Analytcs:**

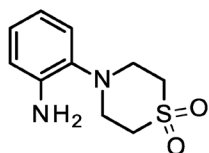
$R_f$  value: 0.25 ethyl acetate/heptane 1:1

$^1\text{H}$  NMR (Figure S53) (400 MHz, Chloroform-*d*)  $\delta$  7.83 (dd,  $J = 8.1, 1.6$  Hz, 1H), 7.62 – 7.51 (m, 1H), 7.37 – 7.19 (m, 2H), 3.68 – 3.52 (m, 4H), 3.25 – 3.07 (m, 4H).

Mass: Calculated  $m/z$  for  $\text{C}_{10}\text{H}_{13}\text{N}_2\text{O}_4\text{S}^+$   $[\text{M}+\text{H}]^+ = 257.0591$ ; found APCI: 256.9

## 22

2-(1,1-dioxo-1,4-thiazinan-4-yl)aniline



### Synthesis:

Synthesis was carried out according to **general procedure D**.

**Quantities:** Ethanol (35 mL); **21** (408 mg; 1.59 mmol; 1 eq.); Hydrazine 50 % m/v in water (255mg; 248  $\mu\text{L}$ ; 2.5 eq.; Aldrich); Pd/C 10 % m/m (367 mg (90 % m **21**))

### Purification:

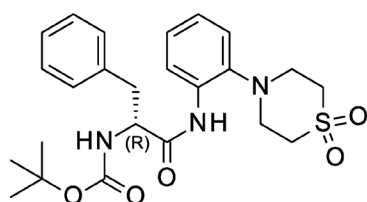
Used without further purification. Yield: 153 mg, 43 %

### Analytcs:

$R_f$  value: 0.55 ethyl acetate/heptane 1:1

## 23

tert-butyl N-[(1R)-1-benzyl-2-[2-(1,1-dioxo-1,4-thiazinan-4-yl)anilino]-2-oxo-ethyl]carbamate



### Synthesis:

Synthesis was carried out according to **general procedure A**.

**Quantities:** Pyridine (8 mL); EtOAc (16 mL); **22** (153 mg, 0.68 mmol, 1 eq.); N-Boc-D-phenylalanine (198 mg, 0.75 mmol, 1.1 eq., TCI); T3P 50 % m/v in EtOAc (865  $\mu\text{L}$ , 1.36 mmol, 2 eq., Aldrich)

### Purification:

Flash chromatography dichloromethane/ethyl acetate gradient 85 % dichloromethane to 40 % over 10 CV on 45 g normal phase silica gel 0.63 – 0.2  $\mu\text{m}$  particle size. Yield: 277 mg; 86 %

Analytics:

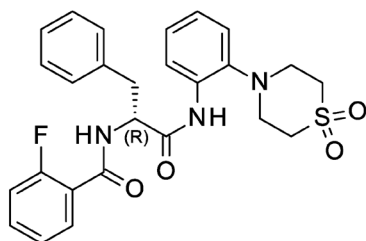
$R_f$  value: 0.30 ethyl acetate/heptane 1:1

$^1\text{H}$  NMR (Figure S54) (400 MHz, Chloroform-*d*)  $\delta$  8.89 (s, 1H), 8.38 (d,  $J = 8.1$  Hz, 1H), 7.31 – 7.11 (m, 7H), 7.08 – 7.01 (m, 1H), 5.40 – 5.13 (m, 1H), 4.47 (q,  $J = 7.3$  Hz, 1H), 3.33 – 3.00 (m, 10H), 1.37 (s, 9H).

Mass: Calculated  $m/z$  for  $\text{C}_{24}\text{H}_{32}\text{N}_3\text{O}_5\text{S}^+$   $[\text{M}+\text{H}]^+ = 474.2057$ ; found APCI: 474.2

**24**

N-[(1R)-1-benzyl-2-[2-(1,1-dioxo-1,4-thiazinan-4-yl)anilino]-2-oxo-ethyl]-2-fluoro-benzamide

Synthesis:

Boc-deprotection was carried out according to **general procedure B**. The amide coupling though was carried out with another coupling reagent, PyBOP. The deprotected **23**, 2-fluorobenzoic acid and DIPEA are dissolved in DCM. The mixture is put under light protection and argon before the addition of PyBOP. The reaction is stirred over night.

**Quantities:** DCM (5 mL); TFA (5 mL); **23** (277 mg, 0.58 mmol) Boc-deprotected crude product isolation: 151 mg; Used for next step: 76 mg (0.20 mmol, 1 eq.); DCM (5 ml); **2-fluorobenzoic acid** (28 mg, 0.20 mmol, 1 eq., Alfa Aesar); **PyBOP** (114 mg, 0.22 mmol, 1.1 eq., Aldrich); **DIPEA** (104  $\mu\text{L}$ , 0.60 mmol, 3 eq., Aldrich)

After the reaction time the crude reaction mixture was directly evaporated on silica gel without previous washing.

Purification:

Flash chromatography dichloromethane/ethyl acetate gradient 100 % dichloromethane to 45 % over 10 CV on 45 g normal phase silica gel 0.63 – 0.2  $\mu\text{m}$  particle size. Yield: 89 mg; 90 %

Analytics:

$R_f$  value: 0.30 ethyl acetate

$^1\text{H}$  NMR (Figure S55) (500 MHz, Chloroform-*d*)  $\delta$  9.16 (s, 1H), 8.44 (dd,  $J = 8.2, 1.4$  Hz, 1H), 8.08 (td,  $J = 7.9, 1.9$  Hz, 1H), 7.52 (dddd,  $J = 8.3, 7.2, 5.3, 1.9$  Hz, 1H), 7.36 – 7.22 (m, 7H), 7.20 (ddd,  $J = 8.4, 7.5, 1.5$  Hz, 1H), 7.18 – 7.13 (m, 2H), 7.06 (td,  $J = 7.7, 1.5$  Hz, 1H), 5.04 (qd,  $J = 6.9, 2.2$  Hz, 1H), 3.40 – 3.30 (m, 2H), 3.21 (t,  $J = 5.3$  Hz, 4H), 3.12 (t,  $J = 5.1$  Hz, 4H).

$^{13}\text{C}$  NMR (Figure S56) (126 MHz, Chloroform-*d*)  $\delta$  168.70, 163.62 (d,  $J = 3.3$  Hz), 160.82 (d,  $J = 248.0$  Hz), 139.97, 136.41, 134.36 (d,  $J = 9.5$  Hz), 133.12, 131.91 (d,  $J = 1.8$  Hz), 129.41, 128.89, 127.19, 126.84, 125.29 (d,  $J = 3.2$  Hz), 124.25, 121.51, 120.06, 119.43 (d,  $J = 10.8$  Hz), 116.47 (d,  $J = 24.7$  Hz), 56.07, 51.92, 51.27, 36.92.

Mass: Calculated  $m/z$  for  $\text{C}_{26}\text{H}_{27}\text{FN}_3\text{O}_4\text{S}^+$   $[\text{M}+\text{H}]^+ = 496.1701$ ;  $\text{C}_{26}\text{H}_{26}\text{FN}_3\text{O}_4\text{SNa}^+$   $[\text{M}+\text{Na}]^+ = 518.1520$ ; found APCI: 496.1; found HRMS:  $[\text{M}+\text{H}]^+ 496.1696$ ;  $[\text{M}+\text{Na}]^+ 518.1515$

HPLC purity: 99.7 %;  $t_{\text{R}} = 12.9$  min (Figure S57)

## 25

4-(4-fluoro-2-nitro-phenyl)-1,4-thiazinane 1,1-dioxide



### Synthesis:

Synthesis was carried out according to **general procedure F**.

**Quantities:** **8** (474 mg; 1.96 mmol; 1 eq.); **DCM** (for thiomorpholine; 10 mL); **m-CPBA 77 % m/m** (810 mg, 4.70 mmol, 2.4 eq.); **DCM** (for m-CPBA; 10 ml)

Added additional 2.4 eq. of m-CPBA in 10 mL DCM over 20 min after 1 h at room temperature.

### Purification:

Flash chromatography ethyl acetate/heptane 60 % heptane to 30 % over 45 g normal phase silica gel 0.63 – 0.2  $\mu\text{m}$  particle size. Afterwards second flash chromatography ethyl acetate/heptane 1:1 + 2 %  $\text{NH}_3$  (25 % v/v  $\text{NH}_3$  in aqueous solution) over 45 g normal phase silica gel 0.63 – 0.2  $\mu\text{m}$  particle size. Yield: 403 mg; 75 %

### Analytcs:

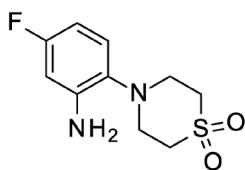
$R_{\text{F}}$  value: 0.35 ethyl acetate/heptane 1:1

$^1\text{H}$  NMR (Figure S58) (400 MHz, Chloroform-*d*)  $\delta$  7.58 – 7.52 (m, 1H), 7.35 – 7.27 (m, 2H), 3.58 – 3.46 (m, 4H), 3.27 – 3.14 (m, 4H).

Mass: Calculated  $m/z$  for  $\text{C}_{10}\text{H}_{12}\text{FN}_2\text{O}_4\text{S}^+$   $[\text{M}+\text{H}]^+ = 275.0496$ ; found APCI: 275.0

## 26

2-(1,1-dioxo-1,4-thiazinan-4-yl)-5-fluoro-aniline

**Synthesis:**

Synthesis was carried out according to **general procedure D**.

**Quantities:** Ethanol (15 mL); **25** (403 mg; 1.47 mmol; 1 eq.); Hydrazine 50 % m/v in water (236 mg; 229  $\mu$ L; 2.5 eq.; Aldrich); Pd/C 10 % m/m (360 mg (90 % m **25**))

**Purification:**

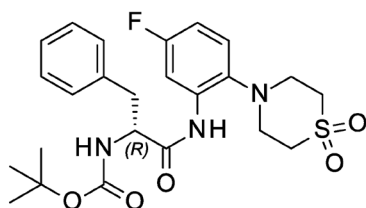
Used without further purification as a crude product.

**Analytics:**

$R_f$  value of 0.10 in ethyl acetate/heptane 1:1 and strong brown colour with iodine detection on TLC.

**27**

tert-butyl N-[(1R)-1-benzyl-2-[2-(1,1-dioxo-1,4-thiazinan-4-yl)-5-fluoro-anilino]-2-oxo-ethyl]carbamate

**Synthesis:**

Synthesis was carried out according to general procedure A.

**Quantities:** Pyridine (5 mL); EtOAc (10 mL); **26** (192 mg, 0.79 mmol, 1 eq.); N-Boc-D-phenylalanine (229 mg, 0.87 mmol, 1.1 eq., TCI); T3P 50 % m/v in EtOAc (936  $\mu$ L, 1.57 mmol, 2 eq., Aldrich)

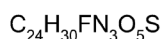
**Purification:**

Flash chromatography ethyl acetate/heptane gradient 60 % heptane to 30 % over 45 g normal phase silica gel 0.63 – 0.2  $\mu$ m particle size. Yield: 244 mg; 63 %

**Analytics:**

$R_f$  value: 0.45 ethyl acetate/heptane 1:1

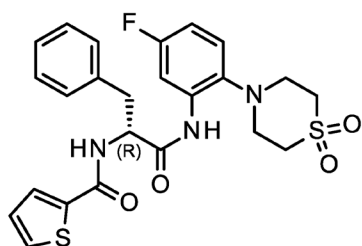
$^1\text{H}$  NMR (Figure S59) (400 MHz, Chloroform- $d$ )  $\delta$  9.01 (s, 1H), 8.22 (dd,  $J$  = 10.8, 2.9 Hz, 1H), 7.32 – 7.17 (m, 5H), 7.11 (dd,  $J$  = 8.8, 5.5 Hz, 1H), 6.73 (ddd,  $J$  = 8.8, 7.8, 3.0 Hz, 1H), 5.16 (d, 1H), 4.45 (q,  $J$  = 7.1 Hz, 1H), 3.41 – 2.89 (m, 10H), 1.38 (s, 9H).



Mass: Calculated m/z for  $\text{C}_{24}\text{H}_{30}\text{FN}_3\text{O}_5\text{S}^+$   $[\text{M}+\text{H}]^+= 492.1963$ ; found APCI: 492.1

## 28

N-[(1R)-1-benzyl-2-[2-(1,1-dioxo-1,4-thiazinan-4-yl)-5-fluoro-anilino]-2-oxo-ethyl]thiophene-2-carboxamide



### Synthesis:

Synthesis was carried out according to **general procedure B**.

**Quantities:** DCM (5 mL); TFA (5 mL); **27** (244 mg, 0.50 mmol) Boc-deprotected crude product isolation: 184 mg; Used for next step: 89 mg (0.23 mmol, 1 eq.); THF, dry (5 ml); **2-carboxythiophene** (32 mg, 0.25 mmol, 1.1 eq., Alfa Aesar); **DEPBT** (204 mg, 0.68 mmol, 3 eq., BLD-Pharm); **DIPEA** (116  $\mu\text{L}$ , 0.68 mmol, 3 eq., Aldrich)

### Purification:

Flash chromatography dichloromethane/ethyl acetate 100 % DCM to 90 % over 6 CV on 45 g normal phase silica gel 0.63 – 0.2  $\mu\text{m}$  particle size. Afterwards second flash chromatography ethyl acetate/heptane 60 % heptane to 30 % over 45 g normal phase silica gel 0.63 – 0.2  $\mu\text{m}$  particle size. Yield: 64 mg; 57 %

### Analytatics:

$R_f$  value: 0.40 ethyl acetate/heptane 1:1

$^1\text{H}$  NMR (*Figure S60*) (400 MHz, Chloroform-*d*)  $\delta$  9.47 (s, 1H), 8.22 (dd,  $J = 10.9, 3.0$  Hz, 1H), 7.50 (d,  $J = 4.4$  Hz, 2H), 7.35 – 7.20 (m, 5H), 7.14 (dd,  $J = 8.8, 5.5$  Hz, 1H), 7.05 (t,  $J = 4.4$  Hz, 1H), 6.80 – 6.69 (m, 2H), 4.95 (q,  $J = 7.2$  Hz, 1H), 3.45 – 3.10 (m, 10H).

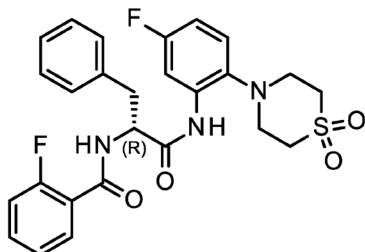
$^{13}\text{C}$  NMR (*Figure S61*) (101 MHz, Chloroform-*d*)  $\delta$  169.27, 162.33, 160.64 (d,  $J = 244.1$  Hz), 137.11, 136.38, 135.84 (d,  $J = 3.3$  Hz), 134.74 (d,  $J = 12.2$  Hz), 131.36, 129.33, 129.17, 128.92, 128.15, 127.22, 122.97 (d,  $J = 9.8$  Hz), 110.49 (d,  $J = 22.9$  Hz), 107.33 (d,  $J = 28.9$  Hz), 55.77, 51.82, 51.58, 36.42.

Mass: Calculated m/z for  $\text{C}_{24}\text{H}_{25}\text{FN}_3\text{O}_4\text{S}_2^+$   $[\text{M}+\text{H}]^+= 502.1265$ ;  $\text{C}_{24}\text{H}_{24}\text{FN}_3\text{O}_4\text{S}_2\text{Na}^+$   $[\text{M}+\text{Na}]^+= 524.1085$ ; found APCI: 502.2; found HRMS:  $[\text{M}+\text{H}]^+ 502.1269$ ;  $[\text{M}+\text{Na}]^+ 524.1086$

HPLC purity: 99.159 %;  $t_R=12.8$  min (*Figure S62*)

**29**

N-[(1R)-1-benzyl-2-[2-(1,1-dioxo-1,4-thiazinan-4-yl)-5-fluoro-anilino]-2-oxo-ethyl]-2-fluoro-benzamide

**Synthesis:**

Synthesis was carried out according to **general procedure B**. The crude product of Boc-deprotection of **28** was used for the further steps.

**Quantities:** **Boc-deprotected crude product of 28** (86 mg, 0.22 mmol, 1 eq.); **THF**, dry (5 mL); **2-fluorobenzoic acid** (34 mg, 0.24 mmol, 1.1 eq., Alfa Aesar); **DEPBT** (197 mg, 0.66 mmol, 3 eq., BLD-Pharm); **DIPEA** (112  $\mu$ L, 0.66 mmol, 3 eq., Aldrich)

**Purification:**

Flash chromatography dichloromethane + 4 %  $\text{NH}_3$  (25 % v/v  $\text{NH}_3$  in aqueous solution)/ethyl acetate 100 % DCM to 90 % over 7 CV on 45 g normal phase silica gel 0.63 – 0.2  $\mu\text{m}$  particle size. Afterwards second flash chromatography ethyl acetate/heptane 1:1 over 45 g normal phase silica gel 0.63 – 0.2  $\mu\text{m}$  particle size. Yield: 87 mg; 77 %

**Analytics:**

$R_f$  value: 0.40 ethyl acetate/heptane 1:1

$^1\text{H}$  NMR (*Figure S63*) (400 MHz, Chloroform-*d*)  $\delta$  9.36 (s, 1H), 8.25 (dd,  $J = 10.9, 3.0$  Hz, 1H), 8.05 (td,  $J = 7.9, 1.8$  Hz, 1H), 7.52 (dddd,  $J = 8.2, 7.2, 5.2, 1.8$  Hz, 1H), 7.38 – 7.07 (m, 9H), 6.73 (ddd,  $J = 8.6, 7.8, 3.0$  Hz, 1H), 5.03 (qd,  $J = 6.9, 2.2$  Hz, 1H), 3.33 (d,  $J = 6.8$  Hz, 2H), 3.26 – 2.92 (m, 8H).

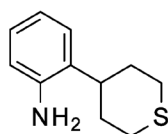
$^{13}\text{C}$  NMR (*Figure S64*) (101 MHz, Chloroform-*d*)  $\delta$  168.94, 163.78 (d,  $J = 3.3$  Hz), 160.81 (d,  $J = 248.0$  Hz), 160.70 (d,  $J = 244.1$  Hz), 136.28, 135.73 (d,  $J = 3.1$  Hz), 134.66 (d,  $J = 12.2$  Hz), 134.44 (d,  $J = 9.5$  Hz), 131.83 (d,  $J = 1.6$  Hz), 129.47 – 129.27 (m), 128.88, 127.21, 125.30 (d,  $J = 3.1$  Hz), 122.81 (d,  $J = 9.8$  Hz), 119.34 (d,  $J = 10.7$  Hz), 116.49 (d,  $J = 24.6$  Hz), 110.43 (d,  $J = 23.0$  Hz), 107.42 (d,  $J = 28.9$  Hz), 56.03, 51.87, 51.52, 36.65.

Mass: Calculated  $m/z$  for  $\text{C}_{26}\text{H}_{26}\text{F}_2\text{N}_3\text{O}_4\text{S}^+$   $[\text{M}+\text{H}]^+ = 514.1607$ ;  $\text{C}_{26}\text{H}_{25}\text{F}_2\text{N}_3\text{O}_4\text{SNa}^+$   $[\text{M}+\text{Na}]^+ = 536.1426$ ; found APCI: 514.2; found HRMS:  $[\text{M}+\text{H}]^+ 514.1607$ ;  $[\text{M}+\text{Na}]^+ 536.1429$

HPLC purity: 99.398 %;  $t_R = 13.3$  min (*Figure S65*)

**30**

2-tetrahydrothiopyran-4-ylaniline

**Synthesis:**

Synthesis was carried out according to **general procedure H**.

**Quantities:**

**Methanol** (20 mL); **4-Oxothiane** (500 mg; 4.30 mmol, 1 eq., abcr); **p-Toluenesulfonylhydrazide** (802 mg, 4.30 mmol, 1 eq., abcr)

**Crude product used for next step:** 297 mg (1.04 mmol, 1 eq.); **Dioxane** (8 mL); **Boc-2-aminophenylboronic acid pinacol ester** (500 mg, 1.57 mmol, 1.5 eq., BLD-Pharm); **Caesium carbonate** (510 mg, 1.57 mmol, 1.5 eq., Aldrich)

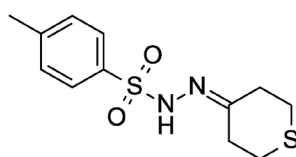
**DCM** (5 mL); **TFA** (5 mL); **23** (277 mg, 0.58 mmol)

**Purification:**

Flash chromatography has been performed with the Boc-protected C-C coupled intermediate tert-butyl N-(2-tetrahydrothiopyran-4-ylphenyl)carbamate

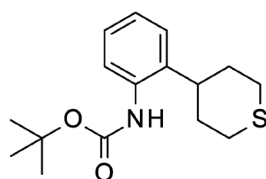
Flash chromatography heptane/ethyl acetate 85 % heptane to 60 % over 8 CV on 45 g normal phase silica gel 0.63 – 0.2  $\mu\text{m}$  particle size. Yield: 190 mg; 62 %

Crude product after Boc-deprotection: 99 mg

**Analytcs:****Analytcs for 4-methyl-N-(tetrahydrothiopyran-4-ylideneamino)benzenesulfonamide:**

$R_F$  value: 0.50 ethyl acetate/heptane 1:1

Mass: Calculated  $m/z$  for  $\text{C}_{12}\text{H}_{17}\text{N}_2\text{O}_2\text{S}_2^+$   $[\text{M}+\text{H}]^+$  = 285.0726; found APCI: 285.4

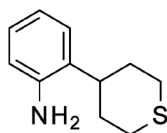
**Analytcs for tert-butyl N-(2-tetrahydrothiopyran-4-ylphenyl)carbamate:**

$R_F$  value: 0.70 ethyl acetate/heptane 1:1

$^1\text{H}$  NMR (400 MHz, Chloroform-*d*)  $\delta$  7.48 (d,  $J$  = 7.4 Hz, 1H), 7.27 – 7.10 (m, 3H), 6.27 (s, 1H), 2.90 – 2.79 (m, 2H), 2.73 – 2.61 (m, 3H), 2.07 (dq,  $J$  = 13.8, 3.2 Hz, 2H), 1.84 (qd,  $J$  = 12.3, 3.2 Hz, 2H), 1.51 (s, 9H).

Mass: Calculated for  $\text{C}_{16}\text{H}_{24}\text{NO}_2\text{S}^+$   $[\text{M}+\text{H}]^+$  = 294.1522; found APCI: 294.6

Analytics for 2-tetrahydrothiopyran-4-ylaniline:

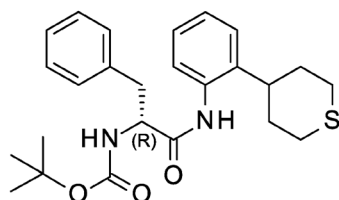


$R_f$  value: 0.45 ethyl acetate/heptane 1:1

Mass: Calculated for  $\text{C}_{11}\text{H}_{16}\text{NS}^+$   $[\text{M}+\text{H}]^+$  = 194.0998; found APCI: 194.2

### 31

tert-butyl N-[(1R)-1-benzyl-2-oxo-2-(2-tetrahydrothiopyran-4-ylanilino)ethyl]carbamate



Synthesis:

Synthesis was carried out according to **general procedure A**.

**Quantities:** Pyridine (5 mL); EtOAc (10 mL); **30** (99 mg, 0.51 mmol, 1 eq.); **N-Boc-D-phenylalanine** (150 mg, 0.56 mmol, 1.1 eq., TCI); **T3P 50 % m/v in EtOAc** (610  $\mu\text{L}$ , 1.02 mmol, 2 eq., Aldrich)

Purification:

Flash chromatography ethyl acetate/heptane gradient 80 % heptane to 65 % over 7 CV on 45 g normal phase silica gel 0.63 – 0.2  $\mu\text{m}$  particle size. Yield: 202 mg; 90 %

Analytics:

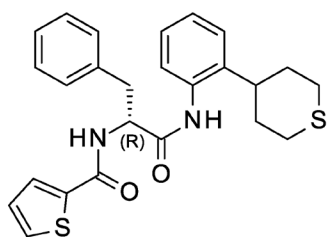
$R_f$  value: 0.60 ethyl acetate/heptane 1:1

$^1\text{H}$  NMR (*Figure S66*) (400 MHz, Chloroform-*d*)  $\delta$  7.81 (s, 1H), 7.44 (d,  $J$  = 8.8 Hz, 1H), 7.35 – 7.10 (m, 8H), 5.25 (dd,  $J$  = 8.3, 3.5 Hz, 1H), 4.51 (q,  $J$  = 7.3 Hz, 1H), 3.26 – 3.05 (m, 2H), 2.83 – 2.70 (m, 2H), 2.60 (dq,  $J$  = 11.7, 3.9, 3.1 Hz, 2H), 2.45 (tt,  $J$  = 12.1, 3.2 Hz, 1H), 1.99 – 1.88 (m, 2H), 1.82 – 1.67 (m, 2H), 1.44 (s, 9H).

Mass: Calculated for  $\text{C}_{25}\text{H}_{33}\text{N}_2\text{O}_3\text{S}^+$   $[\text{M}+\text{H}]^+$  = 441.2206; found APCI: 441.7

### 32

N-[(1R)-1-benzyl-2-oxo-2-(2-tetrahydrothiopyran-4-ylanilino)ethyl]thiophene-2-carboxamide



### Synthesis:

Synthesis was carried out according to **general procedure B**.

**Quantities:** DCM (5 mL); TFA (5 mL); **31** (79 mg, 0.18 mmol) Boc-protected crude product isolation: 54 mg; Used for next step: 54 mg (0.16 mmol, 1 eq.); THF, dry (10 ml); **2-carboxythiophene** (24 mg, 0.19 mmol, 1.2 eq., Alfa Aesar); **DEPBT** (52 mg, 0.17 mmol, 1.1 eq., BLD-Pharm); **DIPEA** (54  $\mu$ L, 0.32 mmol, 2 eq., Aldrich)

### Purification:

Flash chromatography ethyl acetate/heptane 80 % heptane to 60 % over 8 CV on 45 g normal phase silica gel 0.63 – 0.2  $\mu$ m particle size. Afterwards second flash chromatography ethyl acetate/heptane 80 % heptane to 65 % over 8 CV on 45 g normal phase silica gel 0.63 – 0.2  $\mu$ m particle size. Yield: 39 mg; 54 %

### Analytics:

$R_f$  value: 0.50 ethyl acetate/heptane 1:1

$^1\text{H}$  NMR (*Figure S67*) (400 MHz, Chloroform-*d*)  $\delta$  8.19 (s, 1H), 7.50 (dq,  $J$  = 3.8, 1.1 Hz, 2H), 7.44 (dd,  $J$  = 7.6, 1.7 Hz, 1H), 7.37 – 7.23 (m, 5H), 7.22 – 7.08 (m, 3H), 7.07 – 7.00 (m, 2H), 5.01 (q,  $J$  = 7.4 Hz, 1H), 3.34 (qd, 2H), 2.80 (ddd,  $J$  = 13.4, 12.3, 2.6 Hz, 1H), 2.65 (ddd,  $J$  = 14.6, 12.3, 2.6 Hz, 1H), 2.60 – 2.45 (m, 3H), 1.96 – 1.81 (m, 2H), 1.80 – 1.63 (m, 2H).

$^{13}\text{C}$  NMR (*Figure S68*) (101 MHz, Chloroform-*d*)  $\delta$  169.72, 162.42, 139.32, 137.59, 136.46, 133.32, 131.12, 129.35, 128.89, 127.94, 127.25, 126.59, 126.45, 124.85, 55.65, 37.68, 37.24, 34.34, 34.27, 29.10, 29.05.

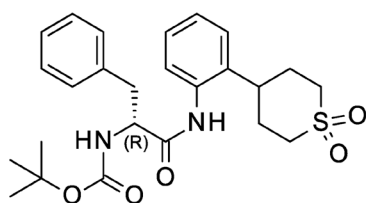
Two carbon nuclei signals are superimposed in the APT spectrum. Additional spectral data is provided with gHSQC data for the respective area (*Figure S69*)

Mass: Calculated  $m/z$  for  $\text{C}_{25}\text{H}_{27}\text{N}_2\text{O}_2\text{S}_2^+$   $[\text{M}+\text{H}]^+$  = 451.1508;  $\text{C}_{25}\text{H}_{26}\text{N}_2\text{O}_2\text{S}_2\text{Na}^+$   $[\text{M}+\text{Na}]^+$  = 473.1328; found APCI: 451.4; found HRMS:  $[\text{M}+\text{H}]^+$  451.1509;  $[\text{M}+\text{Na}]^+$  473.1325

HPLC purity: 98.602 %;  $t_R$  = 14.0 min (*Figure S70*)

## 33

tert-butyl N-[(1R)-1-benzyl-2-[2-(1,1-dioxothian-4-yl)anilino]-2-oxo-ethyl]carbamate

**Synthesis:**

Synthesis was carried out according to **general procedure F**.

**Quantities:** **31** (103 mg; 0.23 mmol; 1 eq.); **DCM** (for thiomorpholine; 5 mL); **m-CPBA 77 %** (126 mg, 0.56 mmol, 2.4 eq.); **DCM** (for m-CPBA; 5 ml)

**Purification:**

Flash chromatography ethyl acetate/heptane 50 % heptane to 30 % over 45 g normal phase silica gel 0.63 – 0.2  $\mu\text{m}$  particle size. Yield: 97 mg; 87 %

**Analytics:**

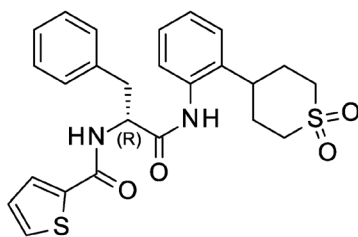
$R_f$  value: 0.20 ethyl acetate/heptane 1:1

$^1\text{H}$  NMR (*Figure S71*) (400 MHz, Chloroform-*d*)  $\delta$  7.84 (d,  $J = 5.4$  Hz, 1H), 7.44 – 7.13 (m, 8H), 7.08 (d,  $J = 8.3$  Hz, 1H), 5.25 (t,  $J = 5.9$  Hz, 1H), 4.47 (q,  $J = 7.2$  Hz, 1H), 3.24 – 2.92 (m, 6H), 2.79 (tt,  $J = 12.2, 3.1$  Hz, 1H), 2.30 – 2.13 (m, 2H), 2.08 – 1.94 (m, 2H), 1.43 (s, 9H).

Mass: Calculated for  $\text{C}_{25}\text{H}_{33}\text{N}_2\text{O}_5\text{S}^+$   $[\text{M}+\text{H}]^+ = 473.2105$ ;  $\text{C}_{25}\text{H}_{32}\text{N}_2\text{O}_5\text{SNa}^+$   $[\text{M}+\text{Na}]^+ = 495.1924$ ; found APCI: 473.4; found ESI-MS:  $[\text{M}+\text{Na}]^+ 495.0$

**34**

N-[(1R)-1-benzyl-2-[2-(1,1-dioxothian-4-yl)anilino]-2-oxo-ethyl]thiophene-2-carboxamide

**Synthesis:**

Synthesis was carried out according to **general procedure B**.

**Quantities:** **DCM** (5 mL); **TFA** (5 mL); **33** (97 mg, 0.21 mmol) Boc-protected crude product isolation: 46 mg; Used for next step: 46 mg (0.12 mmol, 1 eq.); **THF**, dry (10 ml); **2-carboxythiophene** (19 mg, 0.15 mmol, 1.2 eq., Alfa Aesar); **DEPBT** (41 mg, 0.14 mmol, 1.1 eq., BLD-Pharm); **DIPEA** (42  $\mu\text{L}$ , 0.25 mmol, 2 eq., Aldrich)

**Purification:**

Flash chromatography ethyl acetate/heptane 50 % heptane to 30 % over 8 CV on 45 g normal phase silica gel 0.63 – 0.2  $\mu\text{m}$  particle size. Afterwards reversed phase preparative HPLC water/methanol gradient. Yield: 27 mg; 47 %

**Analytcs:**

$R_F$  value: 0.20 ethyl acetate/heptane 1:1

$^1\text{H}$  NMR (Figure S72) (400 MHz, Chloroform-*d*)  $\delta$  8.26 (d,  $J$  = 6.2 Hz, 1H), 7.54 (dt,  $J$  = 4.6, 1.1 Hz, 1H), 7.50 (dd,  $J$  = 3.8, 1.1 Hz, 1H), 7.40 – 7.11 (m, 9H), 7.10 – 7.02 (m, 1H), 6.92 (q,  $J$  = 7.2, 6.7 Hz, 1H), 4.91 (q,  $J$  = 7.4 Hz, 1H), 3.37 (dd,  $J$  = 13.8, 8.0 Hz, 1H), 3.28 (dd,  $J$  = 13.8, 6.9 Hz, 1H), 3.21 (dt,  $J$  = 13.8, 3.2 Hz, 1H), 3.06 – 2.79 (m, 4H), 2.32 – 2.10 (m, 2H), 2.01 (dq,  $J$  = 13.8, 3.1 Hz, 1H), 1.90 (dq,  $J$  = 14.3, 3.4 Hz, 1H).

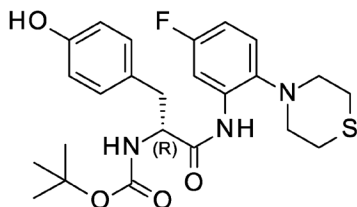
$^{13}\text{C}$  NMR (Figure S73) (101 MHz, Chloroform-*d*)  $\delta$  169.97, 162.86, 137.47, 137.18, 136.18, 133.53, 131.59, 129.28, 129.04, 129.00, 128.18, 127.45, 127.41, 127.04, 126.18, 125.57, 55.98, 51.55, 51.48, 36.77, 35.67, 30.79, 30.54.

Mass: Calculated  $m/z$  for  $\text{C}_{25}\text{H}_{27}\text{N}_2\text{O}_4\text{S}_2^+$   $[\text{M}+\text{H}]^+$  = 483.1407;  $\text{C}_{25}\text{H}_{26}\text{N}_2\text{O}_4\text{S}_2\text{Na}^+$   $[\text{M}+\text{Na}]^+$  = 505.1226; found APCI: 483.5; found HRMS:  $[\text{M}+\text{H}]^+$  483.1402;  $[\text{M}+\text{Na}]^+$  505.1220

HPLC purity: 99.6 %;  $t_R$ =11.8 min (Figure S74)

**35**

tert-butyl N-[(1R)-2-(5-fluoro-2-thiomorpholino-anilino)-1-[(4-hydroxyphenyl)methyl]-2-oxo-ethyl]carbamate

**Synthesis:**

Synthesis was carried out according to **general procedure A**.

**Quantities:** Pyridine (10 mL); EtOAc (20 mL); **9** (71 mg, 0.33 mmol, 1 eq.); **N-Boc-D-tyrosine** (104 mg, 0.37 mmol, 1.1 eq., TCI); **T3P 50 % m/v in EtOAc** (398  $\mu\text{L}$ , 0.67 mmol, 2 eq., Aldrich)

**Purification:**

Flash chromatography ethyl acetate/heptane gradient 85 % heptane to 70 % over 45 g normal phase silica gel 0.63 – 0.2  $\mu\text{m}$  particle size. Yield: 115 mg; 73 %

**Analytcs:**

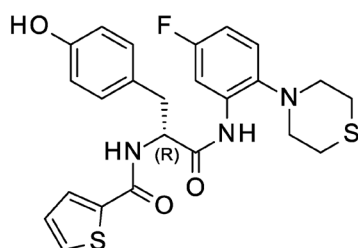
$R_F$  value: 0.50 ethyl acetate/heptane 1:1

$^1\text{H}$  NMR (*Figure S75*) (400 MHz, Chloroform-*d*)  $\delta$  9.03 (s, 1H), 8.21 (d,  $J = 10.5$  Hz, 1H), 7.11 – 6.91 (m, 3H), 6.83 – 6.68 (m, 3H), 6.36 (s, 1H), 5.07 (s, 1H), 4.42 (s, 1H), 3.07 (qd,  $J = 14.0, 6.5$  Hz, 2H), 2.94 – 2.73 (m, 4H), 2.62 (s, 4H), 1.42 (s, 9H).

Mass: Calculated for  $\text{C}_{24}\text{H}_{31}\text{FN}_3\text{O}_4\text{S}^+$   $[\text{M}+\text{H}]^+ = 476.2014$ ; found APCI: 476.6

### 36

N-[(1R)-2-(5-fluoro-2-thiomorpholino-anilino)-1-[(4-hydroxyphenyl)methyl]-2-oxo-ethyl]thiophene-2-carboxamide



#### Synthesis:

Synthesis was carried out according to **general procedure B**.

**Quantities:** DCM (5 mL); TFA (5 mL); **35** (110 mg, 0.23 mmol) Boc-protected crude product isolation: 93 mg; Used for next step: 35 mg (0.09 mmol, 1 eq.); THF, dry (5 ml); **2-carboxythiophene** (14 mg, 0.11 mmol, 1.2 eq., Alfa Aesar); **DEPBT** (31 mg, 0.10 mmol, 1.1 eq., BLD-Pharm); **DIPEA** (32  $\mu\text{L}$ , 0.19 mmol, 2 eq., Aldrich)

#### Purification:

Flash chromatography ethyl acetate/heptane 75 % heptane to 55 % over 8 CV on 45 g normal phase silica gel 0.63 – 0.2  $\mu\text{m}$  particle size. Afterwards flash chromatography ethyl acetate/heptane 65 % heptane to 45 % over 15 CV on 8 g normal phase silica gel 0.63 – 0.2  $\mu\text{m}$  particle size. Yield: 33 mg; 75 %.

After the reaction time the crude reaction mixture was directly evaporated on silica gel without previous washing.

#### Analytcs:

$R_f$  value: 0.45 ethyl acetate/heptane 1:1

$^1\text{H}$  NMR (*Figure S76*) (400 MHz, Methanol-*d*<sub>4</sub>)  $\delta$  8.14 (dd,  $J = 11.1, 3.0$  Hz, 1H), 7.77 (dd,  $J = 3.8, 1.1$  Hz, 1H), 7.68 (d,  $J = 5.1$  Hz, 1H), 7.21 – 7.16 (m, 1H), 7.15 – 7.08 (m, 3H), 6.77 (td,  $J = 8.5, 3.0$  Hz, 1H), 6.70 – 6.63 (m, 2H), 4.79 (dd,  $J = 8.7, 6.2$  Hz, 1H), 3.34 (dd, 1H), 3.06 (dd,  $J = 14.0, 8.7$  Hz, 1H), 2.87 – 2.80 (m, 4H), 2.55 – 2.47 (m, 4H).

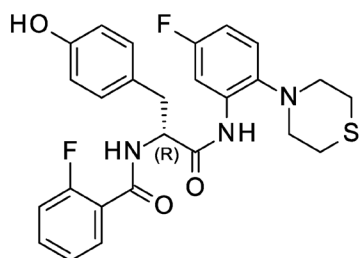
$^{13}\text{C}$  NMR (*Figure S77*) (101 MHz, Methanol-*d*<sub>4</sub>)  $\delta$  170.13, 163.07, 159.99 (d,  $J = 241.0$  Hz), 155.95, 138.73 (d,  $J = 3.1$  Hz), 137.74, 134.33 (d,  $J = 12.2$  Hz), 131.34, 129.85, 129.08, 127.81, 127.64, 123.02 (d,  $J = 9.6$  Hz), 115.00, 109.77 (d,  $J = 22.8$  Hz), 105.93 (d,  $J = 29.0$  Hz), 56.91, 54.59, 35.68, 27.93.

Mass: Calculated  $m/z$  for  $C_{24}H_{25}FN_3O_3S_2^+$   $[M+H]^+$  = 486.1316;  $C_{24}H_{24}FN_3O_3S_2Na^+$   $[M+Na]^+$  = 508.1135; found APCI: 486.6; found HRMS:  $[M+H]^+$  486.1311;  $[M+Na]^+$  508.1131

HPLC purity: 98.5 %;  $t_R$  = 13.3 min (*Figure S78*)

### 37

2-fluoro-N-[(1R)-2-(5-fluoro-2-thiomorpholino-anilino)-1-[(4-hydroxyphenyl)methyl]-2-oxoethyl]benzamide



#### Synthesis:

Synthesis was carried out according to **general procedure B**. The crude product of Boc-deprotection of **36** was used for the further steps.

**Quantities:** Boc-protected crude product of **36** (39 mg, 0.10 mmol, 1 eq.); THF, dry (5 ml); 2-fluorobenzoic acid (17 mg, 0.12 mmol, 1.2 eq., Alfa Aesar); DEPBT (34 mg, 0.10 mmol, 1.1 eq., BLD-Pharm); DIPEA (35  $\mu$ L, 0.19 mmol, 2 eq., Aldrich)

#### Purification:

After the reaction time the crude reaction mixture was directly evaporated on silica gel without previous washing.

Flash chromatography ethyl acetate/heptane 80 % heptane to 60 % over 8 CV on 45 g normal phase silica gel 0.63 – 0.2  $\mu$ m particle size. Afterwards flash chromatography ethyl acetate/heptane 60 % heptane to 40 % over 8 CV on 45 g normal phase silica gel 0.63 – 0.2  $\mu$ m particle size. Yield: 39 mg; 78 %

#### Analytics:

$R_F$  value: 0.50 ethyl acetate/heptane 1:1

$^1H$  NMR (*Figure S79*) (400 MHz, Chloroform-*d*)  $\delta$  8.90 (s, 1H), 8.24 (dd,  $J$  = 10.8, 3.0 Hz, 1H), 8.09 (td,  $J$  = 7.9, 1.9 Hz, 1H), 7.56 – 7.41 (m, 2H), 7.32 – 7.23 (m, 1H), 7.17 (ddd,  $J$  = 12.3, 8.4, 1.1 Hz, 1H), 7.11 (d,  $J$  = 8.4 Hz, 2H), 7.02 (dd,  $J$  = 8.8, 5.6 Hz, 1H), 6.80 – 6.67 (m, 3H), 6.09 (s, 1H), 4.93 (tdd,  $J$  = 7.4, 5.4, 2.1 Hz, 1H), 3.31 (dd,  $J$  = 13.8, 5.4 Hz, 1H), 3.12 (dd,  $J$  = 13.9, 7.4 Hz, 1H), 2.86 – 2.70 (m, 4H), 2.60 – 2.35 (m, 4H).

$^{13}C$  NMR (*Figure S80*) (126 MHz, Chloroform-*d*)  $\delta$  168.98, 163.33 (d,  $J$  = 3.1 Hz), 160.85 (d,  $J$  = 248.1 Hz), 160.18 (d,  $J$  = 243.1 Hz), 155.32, 138.06 (d,  $J$  = 3.1 Hz), 134.23 (d,  $J$  = 9.5 Hz), 134.07 (d,  $J$  = 12.1 Hz), 131.97 (d,  $J$  = 1.8 Hz), 130.53, 127.58, 125.10 (d,  $J$  = 3.2 Hz), 122.63 (d,  $J$  = 9.6 Hz), 119.72 (d,  $J$  = 10.8

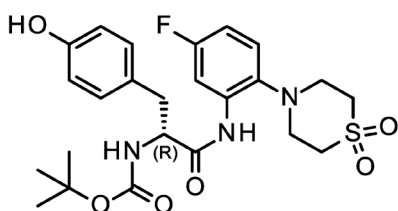
Hz), 116.33 (d,  $J = 24.7$  Hz), 115.78, 110.36 (d,  $J = 22.7$  Hz), 106.87 (d,  $J = 28.8$  Hz), 56.70, 54.70, 37.51, 28.41.

Mass: Calculated  $m/z$  for  $C_{26}H_{26}F_2N_3O_3S^+$   $[M+H]^+ = 498.1657$ ;  $C_{26}H_{25}F_2N_3O_3SNa^+$   $[M+Na]^+ = 520.1477$ ; found APCI: 498.8; found HRMS:  $[M+H]^+ 498.1659$ ;  $[M+Na]^+ 520.1476$

HPLC purity: 95.1 %;  $t_R = 13.8$  min (Figure S81)

### 38

tert-butyl N-[(1R)-2-[2-(1,1-dioxo-1,4-thiazinan-4-yl)-5-fluoro-anilino]-1-[(4-hydroxyphenyl)methyl]-2-oxo-ethyl]carbamate



#### Synthesis:

Synthesis was carried out according to general procedure A.

*Quantities:* **Pyridine** (5 mL); **EtOAc** (10 mL); **26** (187 mg, 0.77 mmol, 1 eq.); **N-Boc-D-tyrosine** (237 mg, 0.84 mmol, 1.1 eq., TCI); **T3P 50 % m/v in EtOAc** (911  $\mu$ L, 1.53 mmol, 2 eq., Aldrich)

#### Purification:

Flash chromatography dichloromethane/ethyl acetate gradient 80 % dichloromethane to 50 % over 45 g normal phase silica gel 0.63 – 0.2  $\mu$ m particle size. Yield: 357 mg; 91 %

#### Analytics:

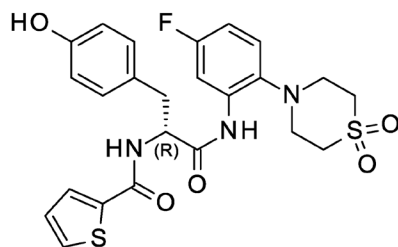
$R_f$  value: 0.30 ethyl acetate/heptane 1:1

$^1H$  NMR (400 MHz, Chloroform-*d*)  $\delta$  8.75 (s, 1H), 8.19 (d,  $J = 10.6$  Hz, 1H), 7.23 – 6.88 (m, 7H), 6.78 – 6.68 (m, 3H), 5.41 (s, 1H), 4.35 (q,  $J = 7.1$  Hz, 1H), 3.21 – 2.93 (m, 10H), 1.38 (s, 9H).

Mass: Calculated for  $C_{24}H_{31}FN_3O_6S^+$   $[M+H]^+ = 508.1912$ ; found APCI: 508.5

### 39

N-[(1R)-2-[2-(1,1-dioxo-1,4-thiazinan-4-yl)-5-fluoro-anilino]-1-[(4-hydroxyphenyl)methyl]-2-oxo-ethyl]thiophene-2-carboxamide



### Synthesis:

Synthesis was carried out according to **general procedure B**.

**Quantities:** DCM (5 mL); TFA (5 mL); **38** (357 mg, 0.70 mmol) Boc-protected crude product isolation: 227 mg; Used for next step: 127 mg (0.31 mmol, 1 eq.); THF, dry (5 ml); **2-carboxythiophene** (44 mg, 0.34 mmol, 1.1 eq., Alfa Aesar); **DEPBT** (280 mg, 0.94 mmol, 3 eq., BLD-Pharm); **DIPEA** (159  $\mu$ L, 0.94 mmol, 3 eq., Aldrich)

### Purification:

Flash chromatography dichloromethane/ethyl acetate 100 % heptane to 45 % over 14 CV on 45 g normal phase silica gel 0.63 – 0.2  $\mu$ m particle size. Afterwards flash chromatography ethyl acetate/heptane 80 % heptane to 35 % over 12 CV on 45 g normal phase silica gel 0.63 – 0.2  $\mu$ m particle size. Yield: 73 mg; 45 %

### Analytcs:

$R_f$  value: 0.10 ethyl acetate/heptane 1:1

$^1\text{H}$  NMR (*Figure S83*) (400 MHz, Methanol- $d_4$ )  $\delta$  8.10 (dd,  $J = 11.0, 3.0$  Hz, 1H), 7.72 (dd,  $J = 3.7, 1.1$  Hz, 1H), 7.60 (d,  $J = 5.0, 1.2$  Hz, 1H), 7.26 – 7.18 (m, 1H), 7.16 – 7.03 (m, 3H), 6.75 (td,  $J = 8.4, 2.9$  Hz, 1H), 6.71 – 6.63 (m, 2H), 5.11 – 4.52 (m, 1H), 3.38 – 2.97 (m, 10H).

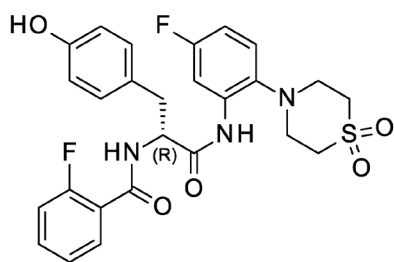
$^{13}\text{C}$  NMR (*Figure S84*) (101 MHz, Methanol- $d_4$ )  $\delta$  170.52, 163.10, 160.31 (d,  $J = 242.1$  Hz), 155.87, 137.65, 136.65, 134.39 (d,  $J = 12.1$  Hz), 131.25, 130.02, 129.12, 127.86, 127.77, 123.08 (d,  $J = 9.9$  Hz), 115.07, 110.09 (d,  $J = 22.8$  Hz), 106.88 (d,  $J = 29.0$  Hz), 56.75, 51.51, 51.19, 35.35.

Mass: Calculated  $m/z$  for  $\text{C}_{24}\text{H}_{25}\text{FN}_3\text{O}_5\text{S}_2^+$   $[\text{M}+\text{H}]^+ = 518.1214$ ;  $\text{C}_{24}\text{H}_{24}\text{FN}_3\text{O}_5\text{S}_2\text{Na}^+$   $[\text{M}+\text{Na}]^+ = 540.1034$ ; found APCI: 518.2; found HRMS:  $[\text{M}+\text{Na}]^+ 540.1036$

HPLC purity: 100.0 %;  $t_R = 11.5$  min (*Figure S85*)

## 40

N-[(1R)-2-[2-(1,1-dioxo-1,4-thiazinan-4-yl)-5-fluoro-anilino]-1-[(4-hydroxyphenyl)methyl]-2-oxo-ethyl]-2-fluoro-benzamide



### Synthesis:

Synthesis was carried out according to **general procedure B**. The crude product of Boc-deprotection of **39** was used for the further steps.

**Quantities:** **Boc-deprotected crude product of 36** (130 mg, 0.32 mmol, 1 eq.); **THF**, dry (5 ml); **2-fluorobenzoic acid** (49 mg, 0.35 mmol, 1.1 eq., Alfa Aesar); **DEPBT** (286 mg, 0.96 mmol, 3 eq., BLD-Pharm); **DIPEA** (163  $\mu$ L, 0.94 mmol, 3 eq., Aldrich)

### Purification:

Flash chromatography dichloromethane/ethyl acetate + 4 % v/v  $\text{NH}_3$  in  $\text{H}_2\text{O}$  100 % dichloromethane to 35 % over 10 CV on 45 g normal phase silica gel 0.63 – 0.2  $\mu\text{m}$  particle size. Afterwards flash chromatography ethyl acetate/heptane 60 % heptane to 30 % over 15 CV on 45 g normal phase silica gel 0.63 – 0.2  $\mu\text{m}$  particle size. Yield: 73 mg; 45 %

### Analytics:

$R_f$  value: 0.20 ethyl acetate/heptane 1:1

$^1\text{H}$  NMR (*Figure S86*) (400 MHz, Chloroform-*d*)  $\delta$  8.89 (s, 1H), 8.23 (dd,  $J = 10.8, 3.0$  Hz, 1H), 8.02 (td,  $J = 7.9, 1.9$  Hz, 1H), 7.60 – 7.45 (m, 2H), 7.27 (td,  $J = 7.6, 1.1$  Hz, 1H), 7.20 – 7.06 (m, 4H), 7.04 – 6.95 (m, 1H), 6.82 – 6.69 (m, 3H), 4.96 (tdd,  $J = 7.6, 6.0, 2.0$  Hz, 1H), 3.34 – 3.01 (m, 10H).

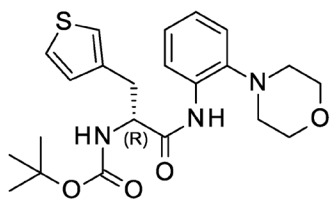
$^{13}\text{C}$  NMR (*Figure S87*) (101 MHz, Chloroform-*d*)  $\delta$  169.18, 163.88 (d,  $J = 3.2$  Hz), 160.79 (d,  $J = 248.7$  Hz), 160.64 (d,  $J = 244.3$  Hz), 155.56, 135.74 (d,  $J = 3.1$  Hz), 134.43 (d,  $J = 9.5$  Hz), 134.10 (d,  $J = 12.2$  Hz), 131.65 (d,  $J = 1.6$  Hz), 130.62, 127.61, 125.25 (d,  $J = 3.3$  Hz), 122.74 (d,  $J = 9.6$  Hz), 119.54 (d,  $J = 10.8$  Hz), 116.53 (d,  $J = 24.5$  Hz), 115.83, 110.72 (d,  $J = 22.9$  Hz), 107.59 (d,  $J = 28.9$  Hz), 56.77, 51.89, 51.47, 37.14.

Mass: Calculated  $m/z$  for  $\text{C}_{26}\text{H}_{26}\text{F}_2\text{N}_3\text{O}_5\text{S}^+$   $[\text{M}+\text{H}]^+ = 530.1556$ ;  $\text{C}_{26}\text{H}_{25}\text{F}_2\text{N}_3\text{O}_5\text{SNa}^+$   $[\text{M}+\text{Na}]^+ = 552.1375$ ; found APCI: : 530.2; found HRMS:  $[\text{M}+\text{Na}]^+ 552.1379$

HPLC purity: 99.8 %;  $t_R = 12.2$  min (*Figure S88*)

## 41

tert-butyl N-[(1R)-2-(2-morpholinoanilino)-2-oxo-1-(3-thienylmethyl)ethyl]carbamate

**Synthesis:**

Synthesis was carried out according to **general procedure A**.

**Quantities:** Pyridine (5 mL); EtOAc (10 mL); **2-morpholinoaniline** (279 mg, 1.57 mmol, 1 eq.); **N-Boc-D-3-thienylalanine** (467 mg, 1.72 mmol, 1.1 eq., TCI); **T3P 50 % m/v in EtOAc** (1862  $\mu$ L, 3.12 mmol, 2 eq., Aldrich)

**Purification:**

Flash chromatography ethyl acetate/heptane gradient 75 % heptane to 40 % over 45 g normal phase silica gel 0.63 – 0.2  $\mu$ m particle size. Yield: 448 mg; 66 %

**Analytcs:**

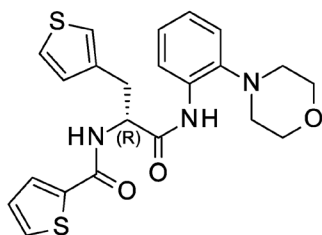
$R_f$  value: 0.50 ethyl acetate/heptane 1:1

$^1\text{H}$  NMR (*Figure S89*) (500 MHz, Chloroform-*d*)  $\delta$  9.06 (s, 1H), 8.40 (d,  $J = 8.0$  Hz, 1H), 7.21 (dd,  $J = 4.9, 2.9$  Hz, 1H), 7.17 – 7.09 (m, 2H), 7.09 – 7.04 (m, 2H), 6.95 (d,  $J = 4.9$  Hz, 1H), 5.08 (s, 1H), 4.52 (s, 1H), 3.80 – 3.67 (m, 4H), 3.26 (dd,  $J = 14.3, 6.1$  Hz, 1H), 3.18 (dd,  $J = 14.3, 6.5$  Hz, 1H), 2.77 – 2.62 (m, 4H), 1.42 (s, 9H).

Mass: Calculated for  $\text{C}_{22}\text{H}_{30}\text{N}_3\text{O}_4\text{S}^+$   $[\text{M}+\text{H}]^+ = 432.1952$ ; found APCI: 432.2

**42**

N-[(1R)-2-(2-morpholinoanilino)-2-oxo-1-(3-thienylmethyl)ethyl]thiophene-2-carboxamide

**Synthesis:**

Synthesis was carried out according to **general procedure B**.

**Quantities:** DCM (5 mL); TFA (5 mL); **41** (448 mg, 1.04 mmol) Boc-deprotected crude product isolation: 320 mg; Used for next step: 151 mg (0.46 mmol, 1 eq.); THF, dry (10 ml); **2-carboxythiophene** (70 mg, 0.55 mmol, 1.2 eq., Alfa Aesar); **DEPBT** (150 mg, 0.50 mmol, 1.1 eq., BLD-Pharm); **DIPEA** (155  $\mu$ L, 0.91 mmol, 2 eq., Aldrich)

**Purification:**

Flash chromatography ethyl acetate/heptane 85 % heptane to 60 % on 45 g normal phase silica gel 0.63 – 0.2  $\mu\text{m}$  particle size. Afterwards second flash chromatography tert-butyl methyl ether/methanol 100 % tert-butyl methyl ether to 90 % over 8 g normal phase silica gel 0.63 – 0.2  $\mu\text{m}$  particle size. Yield: 139 mg; 69 %

**Analytcs:**

$R_f$  value: 0.30 ethyl acetate/heptane 1:1

$^1\text{H}$  NMR (*Figure S90*) (400 MHz, Chloroform-*d*)  $\delta$  8.96 (s, 1H), 8.39 (d,  $J = 6.9$  Hz, 1H), 7.52 (dd,  $J = 3.8, 1.1$  Hz, 1H), 7.49 (dt,  $J = 5.0, 1.4$  Hz, 1H), 7.27 – 7.23 (m, 1H), 7.17 – 7.01 (m, 6H), 6.90 – 6.82 (m, 1H), 4.96 (td,  $J = 7.6, 5.5$  Hz, 1H), 3.73 – 3.60 (m, 4H), 3.43 (dd,  $J = 14.2, 5.5$  Hz, 1H), 3.29 (dd,  $J = 14.2, 7.5$  Hz, 1H), 2.74 – 2.59 (m, 4H).

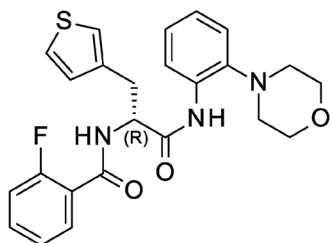
$^{13}\text{C}$  NMR (*Figure S91*) (101 MHz, Chloroform-*d*)  $\delta$  168.75, 161.62, 141.26, 137.86, 136.58, 132.96, 130.86, 128.74, 128.50, 127.87, 126.46, 125.71, 124.38, 123.06, 120.85, 119.55, 67.25, 55.22, 52.57, 32.59.

Mass: Calculated  $m/z$  for  $\text{C}_{22}\text{H}_{24}\text{N}_3\text{O}_3\text{S}_2^+$   $[\text{M}+\text{H}]^+ = 442.1254$ ;  $\text{C}_{22}\text{H}_{23}\text{N}_3\text{O}_3\text{S}_2\text{Na}^+$   $[\text{M}+\text{Na}]^+ = 464.1073$ ; found APCI: 442.4; found HRMS:  $[\text{M}+\text{H}]^+ 442.1249$ ;  $[\text{M}+\text{Na}]^+ 464.1072$

HPLC purity: 99.1 %;  $t_R = 12.8$  min (*Figure S92*)

**43**

2-fluoro-N-[(1R)-2-(2-morpholinoanilino)-2-oxo-1-(3-thienylmethyl)ethyl]benzamide

**Synthesis:**

Synthesis was carried out according to **general procedure B**. The crude product of Boc-deprotection of **42** was used for the further steps.

**Quantities:** Boc-protected crude product of **42** (175 mg, 0.53 mmol, 1 eq.); THF, dry (10 mL); 2-fluorobenzoic acid (89 mg, 0.63 mmol, 1.2 eq., Alfa Aesar); DEPBT (174 mg, 0.58 mmol, 1.1 eq., BLD-Pharm); DIPEA (180  $\mu\text{L}$ , 1.06 mmol, 2 eq., Aldrich)

**Purification:**

Flash chromatography ethyl acetate/heptane 85 % DCM to 60 % on 45 g normal phase silica gel 0.63 – 0.2  $\mu\text{m}$  particle size. Yield: 189 mg; 79 %

Analytics:

$R_F$  value: 0.25 ethyl acetate/heptane 1:1

$^1\text{H}$  NMR (Figure S93) (400 MHz, Chloroform-*d*)  $\delta$  8.96 (s, 1H), 8.43 (dd,  $J = 8.1, 1.4$  Hz, 1H), 8.11 (td,  $J = 7.9, 1.9$  Hz, 1H), 7.52 (dddd,  $J = 8.4, 7.3, 5.2, 1.9$  Hz, 1H), 7.38 (dd,  $J = 13.6, 7.4$  Hz, 1H), 7.32 – 7.23 (m, 2H), 7.20 – 7.00 (m, 6H), 5.03 (tdd,  $J = 7.3, 5.3, 2.2$  Hz, 1H), 3.57 (qt,  $J = 11.4, 4.7$  Hz, 4H), 3.48 (dd,  $J = 14.3, 5.4$  Hz, 1H), 3.27 (dd,  $J = 14.2, 7.0$  Hz, 1H), 2.71 – 2.57 (m, 4H).

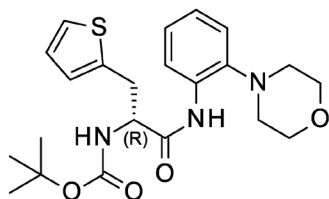
$^{13}\text{C}$  NMR (Figure S94) (101 MHz, Chloroform-*d*)  $\delta$  168.47, 163.10 (d,  $J = 3.2$  Hz), 160.80 (d,  $J = 247.9$  Hz), 141.11, 136.41, 134.09 (d,  $J = 9.4$  Hz), 133.01, 132.08 (d,  $J = 2.0$  Hz), 128.50, 126.38, 125.77, 125.05 (d,  $J = 3.3$  Hz), 124.23, 123.18, 120.74, 120.01 (d,  $J = 11.0$  Hz), 119.54, 116.24 (d,  $J = 24.7$  Hz), 67.20, 55.56, 52.52, 32.55.

Mass: Calculated  $m/z$  for  $\text{C}_{24}\text{H}_{25}\text{FN}_3\text{O}_3\text{S}^+$   $[\text{M}+\text{H}]^+ = 454.1595$ ;  $\text{C}_{24}\text{H}_{24}\text{FN}_3\text{O}_3\text{SNa}^+$   $[\text{M}+\text{Na}]^+ = 476.1415$ ; found APCI: 454.3; found HRMS:  $[\text{M}+\text{H}]^+ 454.1590$ ;  $[\text{M}+\text{Na}]^+ 476.1413$

HPLC purity: 99.0 %;  $t_R = 13.5$  min (Figure S95)

**44**

tert-butyl N-[(1R)-2-(2-morpholinoanilino)-2-oxo-1-(2-thienylmethyl)ethyl]carbamate

Synthesis:

Synthesis was carried out according to **general procedure A**.

**Quantities:** Pyridine (5 mL); EtOAc (10 mL); **2-morpholinoaniline** (245 mg, 1.37 mmol, 1 eq.); **N-Boc-D-2-thienylalanine** (410 mg, 1.51 mmol, 1.1 eq., TCI); **T3P 50 % m/v in EtOAc** (1800  $\mu\text{L}$ , 3.02 mmol, 2 eq., Aldrich)

Purification:

Flash chromatography ethyl acetate/heptane gradient 80 % heptane to 50 % over 7 CV on 45 g normal phase silica gel 0.63 – 0.2  $\mu\text{m}$  particle size. Yield: 587 mg; 99 %

Analytics:

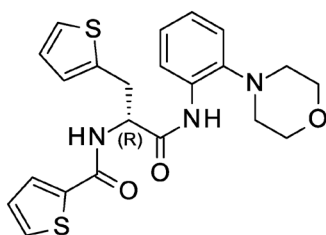
$R_F$  value: 0.50 ethyl acetate/heptane 1:1

$^1\text{H}$  NMR (Figure S96) (400 MHz, Chloroform-*d*)  $\delta$  9.12 (s, 1H), 8.39 (d,  $J = 7.9$  Hz, 1H), 7.17 – 6.99 (m, 4H), 6.91 – 6.82 (m, 2H), 5.28 (s, 1H), 4.54 (s, 1H), 3.82 – 3.68 (m, 4H), 3.48 – 3.31 (m, 2H), 2.75 – 2.58 (m, 4H), 1.43 (s, 9H).

Mass: Calculated for  $\text{C}_{22}\text{H}_{30}\text{N}_3\text{O}_4\text{S}^+$   $[\text{M}+\text{H}]^+ = 432.1952$ ; found APCI: 432.8

## 45

N-[(1R)-2-(2-morpholinoanilino)-2-oxo-1-(2-thienylmethyl)ethyl]thiophene-2-carboxamide

Synthesis:

Synthesis was carried out according to **general procedure B**.

**Quantities:** DCM (5 mL); TFA (5 mL); **44** (587 mg, 1.36 mmol) Boc-protected crude product isolation: 387 mg; Used for next step: 199 mg (0.60 mmol, 1 eq.); THF, dry (15 ml); **2-carboxythiophene** (92 mg, 0.72 mmol, 1.2 eq., Alfa Aesar); **DEPBT** (198 mg, 0.66 mmol, 1.1 eq., BLD-Pharm); **DIPEA** (204  $\mu$ L, 1.20 mmol, 2 eq., Aldrich)

Purification:

Flash chromatography ethyl acetate/heptane 75 % heptane to 55 % over 7 CV on 45 g normal phase silica gel 0.63 – 0.2  $\mu$ m particle size. Yield: 260 mg; 95 %

Analytics:

$R_f$  value: 0.45 ethyl acetate/heptane 1:1

$^1\text{H}$  NMR (*Figure S97*) (500 MHz, Chloroform-*d*)  $\delta$  9.07 (s, 1H), 8.38 (dd,  $J$  = 7.9, 1.6 Hz, 1H), 7.56 (dd,  $J$  = 3.8, 1.2 Hz, 1H), 7.48 (dd,  $J$  = 5.0, 1.2 Hz, 1H), 7.17 – 7.00 (m, 6H), 6.96 – 6.88 (m, 2H), 5.01 (td,  $J$  = 7.2, 5.7 Hz, 1H), 3.72 – 3.65 (m, 4H), 3.62 (dd,  $J$  = 14.9, 5.8 Hz, 1H), 3.49 (dd,  $J$  = 14.8, 7.0 Hz, 1H), 2.68 (dd,  $J$  = 5.9, 3.4 Hz, 4H).

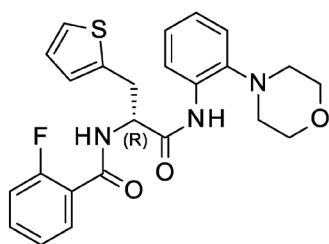
$^{13}\text{C}$  NMR (*Figure S98*) (126 MHz, Chloroform-*d*)  $\delta$  168.42, 161.72, 141.32, 138.03, 137.86, 133.00, 130.98, 128.84, 127.87, 127.29, 126.97, 125.69, 124.97, 124.39, 120.85, 119.65, 67.22, 55.63, 52.58, 32.05.

Mass: Calculated  $m/z$  for  $\text{C}_{22}\text{H}_{24}\text{N}_3\text{O}_3\text{S}_2^+$   $[\text{M}+\text{H}]^+$  = 442.1254;  $\text{C}_{22}\text{H}_{23}\text{N}_3\text{O}_3\text{S}_2\text{Na}^+$   $[\text{M}+\text{Na}]^+$  = 464.1073; found APCI: 442.7; found HRMS:  $[\text{M}+\text{H}]^+$  442.1255;  $[\text{M}+\text{Na}]^+$  464.1071

HPLC purity: 99.1 %;  $t_R$  = 13.0 min (*Figure S99*)

## 46

2-fluoro-N-[(1R)-2-(2-morpholinoanilino)-2-oxo-1-(2-thienylmethyl)ethyl]benzamide



### Synthesis:

Synthesis was carried out according to **general procedure B**. The crude product of Boc-deprotection of **42** was used for the further steps.

**Quantities:** **Boc-deprotected crude product of 45** (173 mg, 0.52 mmol, 1 eq.); **THF**, dry (15 mL); **2-fluorobenzoic acid** (88 mg, 0.63 mmol, 1.2 eq., Alfa Aesar); **DEPBT** (172 mg, 0.57 mmol, 1.1 eq., BLD-Pharm); **DIPEA** (178  $\mu$ L, 1.04 mmol, 2 eq., Aldrich)

### Purification:

Flash chromatography ethyl acetate/heptane 80 % heptane to 60 % over 12 CV on 45 g normal phase silica gel 0.63 – 0.2  $\mu$ m particle size. Yield: 208 mg; 85 %

### Analytcs:

$R_F$  value: 0.45 ethyl acetate/heptane 1:1

$^1\text{H}$  NMR (*Figure S100*) (500 MHz, Chloroform-*d*)  $\delta$  9.03 (s, 1H), 8.43 (dd,  $J = 8.2, 1.4$  Hz, 1H), 8.11 (td,  $J = 7.9, 1.8$  Hz, 1H), 7.55 – 7.40 (m, 2H), 7.27 (t,  $J = 7.6$  Hz, 1H), 7.19 – 7.09 (m, 4H), 7.06 (td,  $J = 7.6, 1.5$  Hz, 1H), 6.96 – 6.88 (m, 2H), 5.08 (tdd,  $J = 7.3, 5.4, 2.2$  Hz, 1H), 3.65 (dd,  $J = 14.8, 5.4$  Hz, 1H), 3.62 – 3.53 (m, 4H), 3.46 (dd,  $J = 14.9, 6.7$  Hz, 1H), 2.73 – 2.57 (m, 4H).

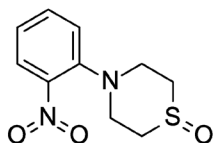
$^{13}\text{C}$  NMR (*Figure S101*) (126 MHz, Chloroform-*d*)  $\delta$  168.08, 163.20 (d,  $J = 3.2$  Hz), 160.80 (d,  $J = 248.3$  Hz), 141.18, 137.88, 134.10 (d,  $J = 9.3$  Hz), 133.04, 132.06 (d,  $J = 1.9$  Hz), 127.19, 127.04, 125.75, 125.06, 125.03 (d,  $J = 3.3$  Hz), 124.27, 120.75, 120.03 (d,  $J = 10.9$  Hz), 119.65, 116.25 (d,  $J = 24.6$  Hz), 67.19, 55.99, 52.54, 32.14.

Mass: Calculated  $m/z$  for  $\text{C}_{24}\text{H}_{25}\text{FN}_3\text{O}_3\text{S}^+$   $[\text{M}+\text{H}]^+ = 454.1595$ ;  $\text{C}_{24}\text{H}_{24}\text{FN}_3\text{O}_3\text{SNa}^+$   $[\text{M}+\text{Na}]^+ = 476.1415$ ; found APCI: 454.7; found HRMS:  $[\text{M}+\text{H}]^+ 454.1590$ ;  $[\text{M}+\text{Na}]^+ 476.1408$

HPLC purity: 98.9 %;  $t_R = 13.6$  min (*Figure S102*)

## 47

4-(2-nitrophenyl)-1,4-thiazinane 1-oxide



Synthesis:

Synthesis was carried out according to **general procedure E**.

**Quantities:** **Sodiumperiodate** (1016 mg; 4.75 mmol; 1.05 eq.); **Water** (15 mL); **3** (1015 mg, 4.53 mmol, 1 eq.); **methanol** (4 ml); **Acetonitrile** (20 mL)

Purification:

Flash chromatography ethyl acetate 100 % over 90 g normal phase silica gel 0.63 – 0.2  $\mu\text{m}$  particle size.  
Yield: 968 mg; 89 %

Analytics:

$R_f$  value: 0.20 ethyl acetate

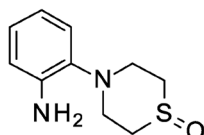
$^1\text{H}$  NMR (*Figure S103*) (400 MHz, Chloroform-*d*)  $\delta$  7.80 (dd,  $J = 8.1, 1.6$  Hz, 1H), 7.54 (ddd,  $J = 8.8, 7.5, 1.6$  Hz, 1H), 7.29 (dd,  $J = 8.2, 1.2$  Hz, 1H), 7.18 (ddd,  $J = 8.3, 7.4, 1.3$  Hz, 1H), 3.82 (ddd,  $J = 13.3, 7.5, 5.6$  Hz, 2H), 3.25 – 3.11 (m, 2H), 3.05 – 2.91 (m, 4H).

$^{13}\text{C}$  NMR (101 MHz, Chloroform-*d*)  $\delta$  146.17, 144.82, 133.77, 125.63, 124.05, 122.63, 46.17, 43.52.

Mass: Calculated for  $\text{C}_{10}\text{H}_{13}\text{N}_2\text{O}_3\text{S}^+$   $[\text{M}+\text{H}]^+ = 241.0641$ ; found APCI: 241.1

**48**

2-(1-oxo-1,4-thiazinan-4-yl)aniline

Synthesis:

Synthesis was carried out according to **general procedure D**.

**Quantities:** **Ethanol** (25 mL); **47** (423 mg; 1.76 mmol; 1 eq.); **Hydrazine 50 % m/v in water** (282 mg; 274  $\mu\text{L}$ ; 2.5 eq.; Aldrich); **Pd/C 10 % m/m** (381 mg (90 % m **47**))

1/3 of the whole amount of catalyst was enough for total conversion.

Purification:

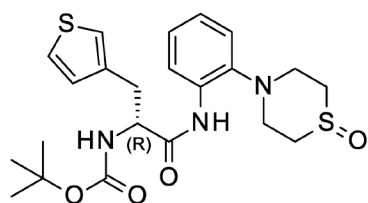
Used without further purification. Yield: 348 mg, 94 %

Analytics:

$R_f$  value: 0.10 ethyl acetate

**49**

tert-butyl N-[(1R)-2-oxo-2-[2-(1-oxo-1,4-thiazinan-4-yl)anilino]-1-(3-thienylmethyl)ethyl]carbamate

**Synthesis:**

Synthesis was carried out according to **general procedure A**.

**Quantities:** Pyridine (5 mL); EtOAc (10 mL); **48** (168 mg, 0.80 mmol, 1 eq.); **N-Boc-D-3-thienylalanine** (238 mg, 0.88 mmol, 1.1 eq., TCI); **T3P 50 % m/v in EtOAc** (951  $\mu$ L, 1.60 mmol, 2 eq., Aldrich)

**Purification:**

Flash chromatography ethyl acetate/methanol 100 % ethyl acetate to 97 % over 7 CV on 45 g normal phase silica gel 0.63 – 0.2  $\mu$ m particle size. Yield: 314 mg; 85 %

**Analytics:**

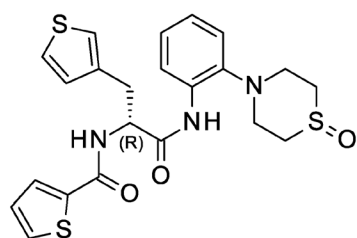
$R_f$  value: 0.25 ethyl acetate

$^1\text{H NMR}$  (Figure S105) (400 MHz, Chloroform-*d*)  $\delta$  8.99 (s, 1H), 8.40 (d,  $J = 7.7$  Hz, 1H), 7.25 – 7.14 (m, 3H), 7.12 – 7.03 (m, 2H), 6.95 (d,  $J = 4.9$  Hz, 1H), 5.10 (s, 1H), 4.45 (d,  $J = 7.9$  Hz, 1H), 3.71 – 3.48 (m, 2H), 3.21 (d,  $J = 6.3$  Hz, 2H), 3.01 – 2.63 (m, 6H), 1.39 (s, 9H).

Mass: Calculated for  $\text{C}_{22}\text{H}_{30}\text{N}_3\text{O}_4\text{S}_2^+$   $[\text{M}+\text{H}]^+ = 464.1672$ ; found APCI: 464.3

**50**

N-[(1R)-2-oxo-2-[2-(1-oxo-1,4-thiazinan-4-yl)anilino]-1-(3-thienylmethyl)ethyl]thiophene-2-carboxamide

**Synthesis:**

Synthesis was carried out according to **general procedure B**.

**Quantities:** DCM (5 mL); TFA (5 mL); **49** (314 mg, 0.68 mmol) Boc-deprotected crude product isolation: 234 mg; Used for next step: 109 mg (0.30 mmol, 1 eq.); THF, dry (10 ml); **2-carboxythiophene** (46 mg, 0.36 mmol, 1.2 eq., Alfa Aesar); **DEPBT** (99 mg, 0.33 mmol, 1.1 eq., BLD-Pharm); **DIPEA** (102  $\mu$ L, 0.60 mmol, 2 eq., Aldrich)

After Boc-deprotection the residue was reconstituted in DCM (not ethyl acetate). The watery phase was extracted with DCM 2x.

#### Purification:

Flash chromatography ethyl acetate/methanol 100 % ethyl acetate to 97 % on 45 g normal phase silica gel 0.63 – 0.2  $\mu\text{m}$  particle size. Afterwards second flash chromatography tert-butyl methyl ether/methanol 100 % heptane to 90 % over 20 CV on 8 g normal phase silica gel 0.63 – 0.2  $\mu\text{m}$  particle size. Yield: 96 mg; 68 %

After the reaction time the crude reaction mixture was directly evaporated on silica gel without previous washing.

#### Analytics:

$R_f$  value: 0.25 ethyl acetate

$^1\text{H}$  NMR (*Figure S106*) (400 MHz, Chloroform-*d*)  $\delta$  9.26 (s, 1H), 8.36 (dt,  $J = 8.2, 1.8$  Hz, 1H), 7.56 – 7.52 (m, 1H), 7.51 – 7.47 (m, 1H), 7.32 – 7.08 (m, 5H), 7.08 – 6.99 (m, 3H), 4.97 (q,  $J = 7.1$  Hz, 1H), 3.63 – 3.48 (m, 2H), 3.44 – 3.30 (m, 2H), 3.02 (ddd,  $J = 14.7, 11.3, 3.6$  Hz, 1H), 2.97 – 2.79 (m, 3H), 2.76 – 2.63 (m, 2H).

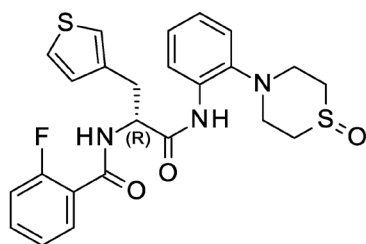
$^{13}\text{C}$  NMR (*Figure S107*) (101 MHz, Chloroform-*d*)  $\delta$  169.00, 162.05, 141.41, 137.75, 136.90, 133.37, 131.17, 128.88, 128.51, 128.03, 126.32, 126.29, 124.35, 122.86, 121.67, 119.60, 54.90, 46.15, 46.10, 43.59, 43.13, 31.23.

Mass: Calculated  $m/z$  for  $\text{C}_{22}\text{H}_{24}\text{N}_3\text{O}_3\text{S}_3^+$   $[\text{M}+\text{H}]^+ = 474.0974$ ;  $\text{C}_{22}\text{H}_{23}\text{N}_3\text{O}_3\text{S}_3\text{Na}^+$   $[\text{M}+\text{Na}]^+ = 496.0794$ ; found APCI: 474.2; found HRMS:  $[\text{M}+\text{H}]^+ 474.0969$ ;  $[\text{M}+\text{Na}]^+ 496.0789$

HPLC purity: 99.5 %;  $t_R = 11.9$  min (*Figure S108*)

## 51

2-fluoro-N-[(1R)-2-oxo-2-[2-(1-oxo-1,4-thiazinan-4-yl)anilino]-1-(3-thienylmethyl)ethyl]benzamide



#### Synthesis:

Synthesis was carried out according to **general procedure B**. The crude product of Boc-deprotection of **50** was used for the further steps.

**Quantities:** **Boc-deprotected crude product of 50** (112 mg, 0.31 mmol, 1 eq.); **THF**, dry (10 mL); **2-fluorobenzoic acid** (52 mg, 0.37 mmol, 1.2 eq., Alfa Aesar); **DEPBT** (101 mg, 0.34 mmol, 1.1 eq., BLD-Pharm); **DIPEA** (105  $\mu\text{L}$ , 0.62 mmol, 2 eq., Aldrich)

**Purification:**

Flash chromatography ethyl acetate/methanol 100 % ethyl acetate to 97 % on 45 g normal phase silica gel 0.63 – 0.2  $\mu\text{m}$  particle size. Afterwards second flash chromatography 100 % tert-butyl methyl ether over 8 g normal phase silica gel 0.63 – 0.2  $\mu\text{m}$  particle size. Yield: 81 mg; 54 %

After the reaction time the crude reaction mixture was directly evaporated on silica gel without previous washing.

**Analytatics:**

$R_f$  value: 0.20 ethyl acetate

$^1\text{H}$  NMR (*Figure S109*) (400 MHz, Chloroform-*d*)  $\delta$  9.11 (s, 1H), 8.41 (dd,  $J = 8.2, 1.6$  Hz, 1H), 8.02 (td,  $J = 7.9, 2.2$  Hz, 1H), 7.51 (td,  $J = 7.5, 5.4$  Hz, 1H), 7.40 – 7.23 (m, 3H), 7.23 – 7.01 (m, 6H), 5.03 (td,  $J = 8.4, 7.4, 5.5$  Hz, 1H), 3.60 – 3.49 (m, 2H), 3.44 (dd,  $J = 14.4, 6.0$  Hz, 1H), 3.30 (dd,  $J = 14.4, 6.7$  Hz, 1H), 2.91 – 2.65 (m, 6H).

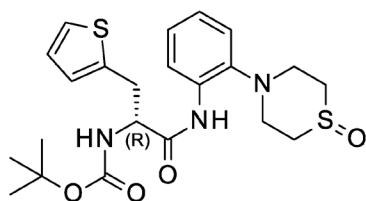
$^{13}\text{C}$  NMR (*Figure S110*) (101 MHz, Chloroform-*d*)  $\delta$  168.50, 163.39 (d,  $J = 3.3$  Hz), 160.72 (d,  $J = 248.3$  Hz), 141.27, 136.53, 134.28 (d,  $J = 9.4$  Hz), 133.19, 131.80 (d,  $J = 1.7$  Hz), 128.53, 126.38, 125.17 (d,  $J = 3.3$  Hz), 124.34, 123.14, 121.50, 119.80 (d,  $J = 10.9$  Hz), 119.69, 116.38 (d,  $J = 24.5$  Hz), 55.23, 46.42, 43.57, 43.41, 31.64.

Mass: Calculated  $m/z$  for  $\text{C}_{24}\text{H}_{25}\text{FN}_3\text{O}_3\text{S}_2^+$   $[\text{M}+\text{H}]^+ = 486.1316$ ;  $\text{C}_{24}\text{H}_{24}\text{FN}_3\text{O}_3\text{S}_2\text{Na}^+$   $[\text{M}+\text{Na}]^+ = 508.1135$ ; found APCI: 486.2; found HRMS:  $[\text{M}+\text{H}]^+ 486.1314$ ;  $[\text{M}+\text{Na}]^+ 508.1132$

HPLC purity: 99.5 %;  $t_R = 12.5$  min (*Figure S111*)

**52**

tert-butyl N-[(1R)-2-oxo-2-[2-(1-oxo-1,4-thiazinan-4-yl)anilino]-1-(2-thienylmethyl)ethyl]carbamate

**Synthesis:**

Synthesis was carried out according to **general procedure A**.

**Quantities:** Pyridine (5 mL); EtOAc (10 mL); **48** (175 mg, 0.83 mmol, 1 eq.); **N-Boc-D-2-thienylalanine** (248 mg, 0.92 mmol, 1.1 eq., TCI); **T3P 50 % m/v in EtOAc** (991  $\mu\text{L}$ , 1.66 mmol, 2 eq., Aldrich)

**Purification:**

Flash chromatography ethyl acetate/methanol 100 % ethyl acetate to 97 % over 8 CV on 45 g normal phase silica gel 0.63 – 0.2  $\mu\text{m}$  particle size. Yield: 345 mg; 90 %

Analytcs:

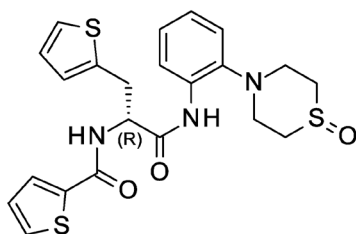
$R_f$  value: 0.25 ethyl acetate

$^1\text{H}$  NMR (400 MHz, Chloroform-*d*)  $\delta$  9.28 – 8.90 (m, 1H), 8.36 (d,  $J$  = 8.1 Hz, 1H), 7.20 – 7.07 (m, 3H), 7.03 (td,  $J$  = 7.6, 1.6 Hz, 1H), 6.90 – 6.82 (m, 2H), 5.55 – 5.37 (m, 1H), 4.47 (d,  $J$  = 7.8 Hz, 1H), 3.64 – 3.47 (m, 2H), 3.46 – 3.30 (m, 2H), 3.00 – 2.82 (m, 4H), 2.72 (dt,  $J$  = 13.2, 4.0 Hz, 2H), 1.37 (s, 9H).

Mass: Calculated for  $\text{C}_{22}\text{H}_{30}\text{N}_3\text{O}_4\text{S}_2^+$   $[\text{M}+\text{H}]^+=$  464.1672; found APCI: 464.3

**53**

N-[(1R)-2-oxo-2-[2-(1-oxo-1,4-thiazinan-4-yl)anilino]-1-(2-thienylmethyl)ethyl]thiophene-2-carboxamide

Synthesis:

Synthesis was carried out according to **general procedure B**.

**Quantities:** DCM (7.5 mL); TFA (7.5 mL); **52** (345 mg, 0.74 mmol) Boc-protected crude product isolation: 256 mg; Used for next step: 126 mg (0.35 mmol, 1 eq.); THF, dry (10 ml); **2-carboxythiophene** (53 mg, 0.42 mmol, 1.2 eq., Alfa Aesar); **DEPBT** (114 mg, 0.38 mmol, 1.1 eq., BLD-Pharm); **DIPEA** (118  $\mu\text{L}$ , 0.69 mmol, 2 eq., Aldrich)

After Boc-deprotection the residue was reconstituted in DCM (not ethyl acetate). The watery phase was extracted with DCM 1x.

Purification:

Flash chromatography tert-butyl methyl ether/methanol 100 % tert-butyl methyl ether to 93 % on 45 g normal phase silica gel 0.63 – 0.2  $\mu\text{m}$  particle size. Yield: 119 mg; 72 %

After the reaction time the crude reaction mixture was directly evaporated on silica gel without previous washing.

Analytcs:

$R_f$  value: 0.25 ethyl acetate

$^1\text{H}$  NMR (*Figure S113*) (400 MHz, Chloroform-*d*)  $\delta$  9.32 (s, 1H), 8.37 (dd,  $J$  = 8.1, 1.5 Hz, 1H), 7.59 (dd,  $J$  = 3.8, 1.1 Hz, 1H), 7.50 (dd,  $J$  = 5.0, 1.1 Hz, 1H), 7.42 – 7.30 (m, 1H), 7.19 – 7.14 (m, 2H), 7.13 – 7.08 (m, 1H), 7.07 – 7.00 (m, 2H), 6.98 – 6.94 (m, 1H), 6.92 (dd,  $J$  = 5.0, 3.5 Hz, 1H), 5.00 (dt,  $J$  = 8.2, 6.7 Hz, 1H),

3.65 – 3.47 (m, 4H), 3.06 (ddd,  $J = 14.9, 11.6, 3.7$  Hz, 1H), 2.98 – 2.80 (m, 3H), 2.70 (ddt,  $J = 23.7, 13.0, 3.8$  Hz, 2H).

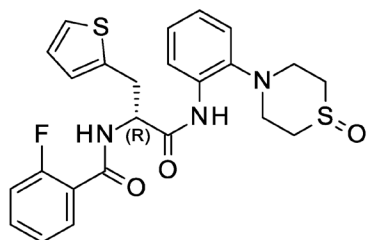
$^{13}\text{C}$  NMR (Figure S114) (101 MHz, Chloroform- $d$ )  $\delta$  168.63, 162.13, 141.43, 138.48, 137.73, 133.39, 131.26, 128.99, 128.05, 127.19, 126.84, 126.30, 124.91, 124.36, 121.68, 119.62, 55.35, 46.09, 46.03, 43.62, 43.01, 30.88.

Mass: Calculated  $m/z$  for  $\text{C}_{22}\text{H}_{24}\text{N}_3\text{O}_3\text{S}_3^+$   $[\text{M}+\text{H}]^+ = 474.0974$ ;  $\text{C}_{22}\text{H}_{23}\text{N}_3\text{O}_3\text{S}_3\text{Na}^+$   $[\text{M}+\text{Na}]^+ = 496.0794$ ; found APCI: 473.9; found HRMS:  $[\text{M}+\text{Na}]^+ 496.0793$

HPLC purity: 98.8 %;  $t_R = 12.0$  min (Figure S115)

## 54

2-fluoro-N-[(1R)-2-oxo-2-[2-(1-oxo-1,4-thiazinan-4-yl)anilino]-1-(2-thienylmethyl)ethyl]benzamide



### Synthesis:

Synthesis was carried out according to **general procedure B**. The crude product of Boc-deprotection of **53** was used for the further steps.

**Quantities:** **Boc-deprotected crude product of 53** (123 mg, 0.34 mmol, 1 eq.); **THF**, dry (10 mL); **2-fluorobenzoic acid** (57 mg, 0.41 mmol, 1.2 eq., Alfa Aesar); **DEPBT** (111 mg, 0.37 mmol, 1.1 eq., BLD-Pharm); **DIPEA** (115  $\mu\text{L}$ , 0.68 mmol, 2 eq., Aldrich)

### Purification:

Flash chromatography tert-butyl methyl ether/methanol 98 % tert-butyl methyl ether to 90 % on 45 g normal phase silica gel 0.63 – 0.2  $\mu\text{m}$  particle size. Yield: 125 mg; 76 %

After the reaction time the crude reaction mixture was directly evaporated on silica gel without previous washing.

### Analytcs:

$R_f$  value: 0.15 ethyl acetate

$^1\text{H}$  NMR (Figure S116) (400 MHz, Chloroform- $d$ )  $\delta$  9.18 (s, 1H), 8.40 (d,  $J = 8.2, 1.5$  Hz, 1H), 8.15 – 7.88 (m, 1H), 7.55 – 7.47 (m, 1H), 7.42 (dd,  $J = 13.2, 7.6$  Hz, 1H), 7.31 – 7.24 (m, 1H), 7.22 – 7.01 (m, 5H), 6.98 – 6.89 (m, 2H), 5.06 (tdd,  $J = 8.0, 5.4, 1.7$  Hz, 1H), 3.82 – 3.30 (m, 4H), 2.96 – 2.61 (m, 6H).

$^{13}\text{C}$  NMR (Figure S117) (101 MHz, Chloroform- $d$ )  $\delta$  168.18, 163.53 (d,  $J = 3.1$  Hz), 160.73 (d,  $J = 248.4$  Hz), 141.32, 138.08, 134.28 (d,  $J = 9.5$  Hz), 133.21, 131.77, 127.17, 127.07, 126.36, 125.14, 125.11, 124.37, 121.50, 119.88, 119.78, 116.39 (d,  $J = 24.5$  Hz), 55.69, 46.37, 43.62, 43.28, 31.32.

Mass: Calculated m/z for  $C_{24}H_{25}FN_3O_3S_2^+$   $[M+H]^+$  = 486.1316;  $C_{24}H_{24}FN_3O_3S_2Na^+$   $[M+Na]^+$  = 508.1135;  
found APCI: 486.3; found HRMS:  $[M+H]^+$  486.1314;  $[M+Na]^+$  508.1132

HPLC purity: 97.2 %;  $t_R$ =12.5 min (*Figure S118*)



**5.3) Supplementary Information Publication II**

**Synthesis and *in vitro* Metabolic Stability of Sterically Shielded Antimycobacterial Phenylalanine Amides**

Markus Lang, Uday S. Ganapathy, Lea Mann, Rüdiger W. Seidel, Richard Goddard, Frank Erdmann, Thomas Dick, Adrian Richter

**European Chemical Society Publishing  
ChemMedChem**

*ChemMedChem*, 19(6), e202300593.

Publication Date: 08.02.2024

DOI: 10.1002/cmdc.202300593

# ChemMedChem

## Supporting Information

### **Synthesis and *in vitro* Metabolic Stability of Sterically Shielded Antimycobacterial Phenylalanine Amides**

Markus Lang, Uday S. Ganapathy, Lea Mann, Rüdiger W. Seidel, Richard Goddard, Frank Erdmann, Thomas Dick, and Adrian Richter\*

## ***Supplementary Information***

# **Synthesis and *in vitro* Metabolic Stability of Sterically Shielded Antimycobacterial Phenylalanine Amides**

Markus Lang<sup>[a]</sup>, Uday S. Ganapathy<sup>[b]</sup>, Lea Mann<sup>[a]</sup>, Rüdiger W. Seidel<sup>[a]</sup>, Richard Goddard<sup>[c]</sup>, Frank Erdmann<sup>[a]</sup>, Thomas Dick<sup>[b],[d],[e]</sup>, Adrian Richter<sup>[a]\*</sup>

---

- [a] M. Lang, L. Mann, Dr. R. W. Seidel, Dr. F. Erdmann, Dr. A. Richter  
Institut für Pharmazie, Martin-Luther-Universität Halle-Wittenberg  
Wolfgang-Langenbeck-Str. 4, 06120 Halle (Saale), Germany
- [b] Dr. U. S. Ganapathy, Prof. Dr. T. Dick  
Center for Discovery and Innovation, Hackensack Meridian Health  
111 Ideation Way, 07110 Nutley, New Jersey, USA
- [c] Dr. R. Goddard  
Max-Planck-Institut für Kohlenforschung  
Kaiser-Wilhelm-Platz 1, 45470 Mülheim an der Ruhr, Germany
- [d] Prof. Dr. T. Dick  
Department of Medical Sciences, Hackensack Meridian School of Medicine  
123 Metro Blvd, 07110 Nutley, New Jersey, USA
- [e] Prof. Dr. T. Dick  
Department of Microbiology and Immunology, Georgetown University  
3900 Reservoir Road, N.W., 20007 Washington DC, USA

## 1. Table of contents

<b>1. Table of contents</b> .....	<b>2</b>
<b>2. Methods &amp; Materials</b> .....	<b>4</b>
General .....	4
X-ray crystallography .....	4
Plasma stability .....	7
Microsomal stability .....	7
HPLC .....	8
Microbiological assays .....	8
<b>3. Structures and synthetic protocols</b> .....	<b>11</b>
MMV .....	11
1 .....	11
2 .....	12
3 .....	13
4 .....	14
5 .....	15
6 .....	16
7 .....	17
8 .....	18
9 .....	18
10 .....	19
11 .....	20
12 .....	21
13 .....	22
14 .....	23
15 .....	23
16 .....	24
17 .....	25
18 .....	25
19 .....	26
20 .....	27
21 .....	28
22 .....	29
23 .....	30
24 .....	31
25 .....	32
	S2

26.....	33
27.....	34
28.....	35
29.....	36
<b>4. NMR spectra and HPLC traces .....</b>	<b>38</b>

## 2. Methods & Materials

### General

The purchased starting materials were used as received without further purification. Solvents used for either synthetical or purification purposes were distilled and stored over 4 Å-molecular sieves. Glassware was oven-dried at 110 °C prior to use. For the determination of  $R_f$  values and other analytical purposes such as qualitative chromatography Merck TLC silica gel 60 on aluminium sheets with fluorescent indicator F254 were used. Flash chromatography was performed with a puriFlash® 430 instrument (Interchim, Montluçon, France). Columns were packed in either 8 g ( $v=10$  mL/min), 45 g ( $v=30$  mL/min) or 90 g ( $v=40$  mL/min) cartridges with 40 - 63  $\mu\text{m}$  normal phase silica gel produced by Carl Roth. Column loading was performed with the dry load method. NMR spectra were recorded on an Agilent Technologies VNMR5 400 MHz spectrometer. Chemical shifts are reported relative to the residual solvent signal ( $\text{CDCl}_3$ :  $\delta_{\text{H}} = 7.26$  ppm;  $\delta_{\text{C}} = 77.36$  ppm;  $\text{CD}_3\text{OD}$   $\delta_{\text{H}} = 3.31$  ppm).  $^{13}\text{C}$  NMR spectral data were determined as attached-proton-test spectra (APT) and plain  $^{13}\text{C}$  spectra. Spectra have been cut, baseline and phase corrected and analyzed utilizing MestreNova 11.0 software (Mestrelab Research, S.L., Spain). APCI-MS (atmospheric pressure chemical ionization) was performed using an expression CMS mass spectrometer (Advion Inc., Ithaca, NY, USA), with both ASAP (atmospheric solids analysis probe) sampling and with the help of the Plate Express TLC-plate extractor. ESI measurements have been conducted on the same expression CMS mass spectrometer with an ESI ionization module and direct injection sampling. HRMS was carried out using a LTQ Orbitrap XL mass spectrometer (Thermo Fisher Scientific Inc., Waltham, MA, USA).

### X-ray crystallography

Crystals of **2** suitable for single-crystal X-ray diffraction were obtained by slow evaporation from a solution in ethanol. The X-ray intensity data collection was carried out at 100 K on a Bruker AXS D8 Venture diffractometer, using Mo- $K_{\alpha}$  radiation from an Incoatec  $1\mu\text{S}$  Diamond microfocus X-ray source with Montel multilayer optics. A crystal was mounted on a MiTeGen cryo loop using perfluoropolyether PFO-XR75. The programs APEX4<sup>[30]</sup> and SAINT<sup>[31]</sup> were used to control the data collection and to process the raw diffraction data. Scaling and an absorption corrections based on indexed crystal faces was performed with APEX5<sup>[32]</sup>. The crystal structure was solved with SHELXT<sup>[33]</sup> and initially refined with SHELXL-2019/3<sup>[34]</sup>. The final structure refinement was carried out by Hirshfeld atom refinement with aspherical scattering factors using NoSpherA2<sup>[23]</sup> partitioning in Olex2 1.5<sup>[35]</sup> based on electron density from iterative single determinant SCF single point DFT calculations using ORCA v.4.1.1<sup>[36]</sup> with a B3LYP functional<sup>[37]</sup> and a def2-TZVPP basis set. Positions and  $U_{\text{iso}}$  values of all hydrogen atoms were refined freely. The  $R$  configuration at the  $\alpha$ -carbon atoms was inferred from the known absolute configuration of the starting material and the absolute structure was confirmed by a Flack  $x$  parameter<sup>[38]</sup> and a Hooft  $y$  parameter<sup>[39]</sup> close to zero (**Table S1**). Structure pictures were drawn with Mercury<sup>[40]</sup>. Crystal data and refinement details are given in **Table S1**. **Figure S1** shows a displacement ellipsoid plot and **Table S2** lists the corresponding hydrogen bond parameters. CCDC 2293688 contains the supplementary crystallographic data for this paper. These data can be obtained free of charge from the Cambridge Crystallographic Data Centre and Fachinformationszentrum Karlsruhe via [www.ccdc.cam.ac.uk/structures](http://www.ccdc.cam.ac.uk/structures).

**Table S1** Crystal data and refinement details for **2**.

Empirical formula	C <sub>26</sub> H <sub>26</sub> FN <sub>3</sub> O <sub>4</sub> S
$M_r$	495.578
$T$ (K)	100(2)
$\lambda$ (Å)	0.71073
Crystal system, space group	Triclinic, $P1$
$a$ (Å)	9.5510(8)
$b$ (Å)	10.4458(9)
$c$ (Å)	12.6068(10)
$\alpha$ (°)	73.785(4)
$\beta$ (°)	78.752(4)
$\gamma$ (°)	85.654(4)
$V$ (Å <sup>3</sup> )	1184.22(17)
$Z$ , $\rho_{\text{calc}}$ (mg m <sup>-3</sup> )	2,
$\mu$ (mm <sup>-1</sup> )	0.184
$F(000)$	520.570
Crystal size (mm)	0.197 × 0.165 × 0.118
$\theta$ range (°)	2.03 - 36.38
Reflections collected / unique	551394
$R_{\text{int}}$	0.062
Completeness to $\theta_{\text{full}}$ (%)	99.67
Data / restraints / parameters	23006 / 3 / 839
Observed data [ $I > 2\sigma(I)$ ]	21992
Goodness-of-fit on $F^2$	1.2264
$R1$ [ $I > 2\sigma(I)$ ]	0.0179
$wR2$ (all data)	0.0374
Flack $x$ parameter	-0.002(6) <sup>a</sup>
Hoof $y$ parameter	-0.009(6) <sup>b</sup>
$\Delta\rho_{\text{max}}$ , $\Delta\rho_{\text{min}}$ (e Å <sup>-3</sup> )	0.24, -0.11
CCDC No.	2293688

<sup>a</sup> Calculated with Olex2.<sup>b</sup> Calculated with PLATON<sup>[41]</sup>.

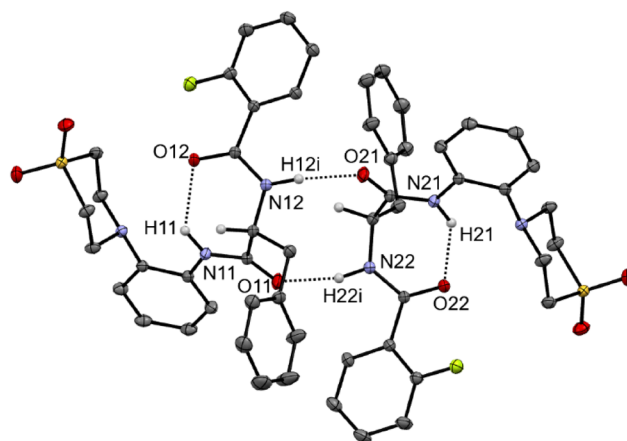


**Figure S1** Asymmetric unit of **2**. Displacement ellipsoids are drawn at the 50 % probability level. Nitrogen-bound hydrogen atoms and the carbon-bound hydrogen atoms attached to centres of chirality are represented by small spheres of arbitrary radius, otherwise omitted for clarity. Colour scheme: C, grey; H, white; N, blue; O, red; F, light green; S, yellow.

**Table S2** Hydrogen bond parameters in **2**.

D–H...A	$d(D-H)$ (Å)	$d(H...A)$ (Å)	$d(D...A)$ (Å)	$\angle(DHA)$ (°)
N11 H11 O12	1.006(7)	2.287(7)	3.0836(6)	135.2(6)
N12 H12i O21	0.988(7)	1.913(7)	2.8929(5)	170.9(6)
N21 H21 O22	0.991(8)	2.134(8)	2.9709(6)	141.1(6)
N22 H22i O11	0.984(8)	1.843(8)	2.7998(5)	163.3(6)

- [23] a) L. Midgley, L. J. Bourhis, O. V. Dolomanov, S. Grabowsky, F. Kleemiss, H. Puschmann, N. Peyerimhoff, *Acta Crystallogr., Sect. A: Found. Crystallogr.* **2021**, 77, 519–533. b) F. Kleemiss, O. V. Dolomanov, M. Bodensteiner, N. Peyerimhoff, L. Midgley, L. J. Bourhis, A. Genoni, L. A. Malaspina, D. Jayatilaka, J. L. Spencer, F. White, B. Grundkötter-Stock, S. Steinhauer, D. Lentz, H. Puschmann, S. Grabowsky, *Chem. Sci.* **2021**, 12, 1675–1692.
- [30] *APEX4 v2022.10-0*. **2019**, Bruker AXS Inc., Madison, Wisconsin, USA.
- [31] *SAINT V8.40B*. **2019**, Bruker AXS Inc.: Madison, Wisconsin, USA.
- [32] L. Krause, et al., *J. Appl. Crystallogr.* **2015**, 48(1): p. 3-10.
- [33] G. M. Sheldrick, *Acta Crystallogr., Sect. A: Found. Crystallogr.* **2015**, 71: p. 3-8.
- [34] G. M. Sheldrick, *Acta Crystallogr., Sect. C: Cryst. Struct. Commun.* **2015**, 71: p. 3-8.
- [35] O. V. Dolomanov, et al., *J. Appl. Crystallogr.* **2009**, 42: p. 339-341.
- [36] F. Neese, et al., *J. Chem. Phys.* **2020**, 152: p. 224108.
- [37] a) A. D. Becke, *J. Chem. Phys.* **1993**, p. 5648-5652. b) C. Lee, W. Yang, and R.G. Parr, *Phys. Rev. B: Condens. Matter* **1988**, 37: p. 785-789.
- [38] H. Flack, *Acta Crystallogr., Sect. A: Found. Crystallogr.* **1983**, 39(6): p. 876-881.
- [39] R. W. W. Hooft, L.H. Straver, and A.L. Spek, *J. Appl. Crystallogr.* **2010**, 43(4): p. 665-668.
- [40] C. F. Macrae, et al., *J. Appl. Crystallogr.* **2020**, 53: p. 226-235.
- [41] A. L. Spek, *Acta Crystallogr., Sect. D: Biol. Crystallogr.* **2009**, 65: p. 148-155.

### Plasma stability

Plasma stability in human and murine plasma was determined at five different time points over 120 min using HPLC-MS/MS analysis. Pooled human plasma, anti-coagulated with trisodium citrate, and non-sterile murine plasma, anti-coagulated with Li-heparin (Bienta/Enamine Ltd., batch #M190406), were used. The human plasma was used by a third-party lab and the authors were not involved in the extraction and preparation of the samples. The source of the samples was the Kyiv city blood center, Kiev, Ukraine. The plasma stability is given as the percentage of substance remaining in plasma over time. All measurements were performed using the Shimadzu Prominence HPLC system including vacuum degasser, gradient pumps, reverse phase column (ZORBAX Extend-C18 column, 2.1x50 mm, 5  $\mu$ m), column oven and autosampler. The HPLC system was coupled with tandem mass API 3000 (AB Sciex). Both positive and negative ion modes of the TurbolonSpray ion source were used. Acquisition and analysis of the data were performed using Analyst 1.6.3 software (PE Sciex).

Incubations of every compound + references (Verapamil and Propranolol) were carried out in 5 aliquots of 60  $\mu$ L each (one for each time point), in duplicates. Plasma was spiked with test compounds from a 10 mM DMSO stock solution to yield a test concentration of 1  $\mu$ M, final DMSO concentration 1%. The aliquots were incubated at 37 °C with shaking at 100 rpm. Five time points over 120 min have been analyzed. The reactions were stopped by adding 300  $\mu$ L of methanol containing internal standard with subsequent plasma proteins sedimentation by centrifuging at 6000 rpm for 4 minutes. Supernatants were analyzed by the HPLC system that was coupled with a tandem mass spectrometer. The percentage of the test compounds remaining after incubation were calculated.

### Microsomal stability

Microsomal stability in human and murine microsomal suspensions was determined at five different time points over 40 min using HPLC-MS/MS analytic. The microsomes were purchased commercially from Xenotech: human liver microsomes (pooled, mixed gender, H0630/lot N#1210097) and mouse liver microsomes (pooled, male BALB/c, M3000/lot #2010026). All measurements were performed using the Shimadzu Prominence HPLC system including vacuum degasser, gradient pumps, reverse phase column (Phenomenex Luna<sup>®</sup>-C18 column, 2.1x50 mm, 5  $\mu$ m), column oven and autosampler. The HPLC system was coupled with tandem mass API 3000 (AB Sciex). Both positive and negative ion modes of the TurbolonSpray ion source were used. Acquisition and analysis of the data were performed using Analyst 1.6.3 software (PE Sciex).

Incubations of every compound + references (Diclofenac and Propranolol for human microsomes, Propranolol and Imipramin for murine microsomes) were carried out in 5 aliquots of 30  $\mu$ L each (one for each time point), in duplicates. Liver microsomal incubation medium contained 0.42 mg of liver microsomal protein as well as phosphate buffer (100 mM, pH 7.4), MgCl<sub>2</sub> (3.3 mM), NADPH (3 mM), glucose-6-phosphate (5.3 mM) and glucose-6-phosphate dehydrogenase (0.67 units/ml). In the control reactions, the NADPH-cofactor system was substituted with phosphate buffer. Microsomal suspensions were spiked with test compounds from a 10 mM DMSO stock solution to yield a test concentration of 2  $\mu$ M, final DMSO concentration 1.6 %. The aliquots were incubated at 37 °C with

shaking at 100 rpm. Five time points over 40 min have been analyzed. The reactions were stopped by adding 5 volumes of 90 % acetonitrile containing internal standard with subsequent protein sedimentation by centrifuging at 5500 rpm for 5 minutes. Supernatants were analyzed by the HPLC system that was coupled with a tandem mass spectrometer. The percentage of the test compounds remaining after incubation were calculated. The elimination constants ( $k_{el}$ ) and half-lives ( $t_{1/2}$ ) of the compounds were determined in a plot of  $\ln(\text{AUC})$  versus time, using linear regression analysis:

$$k_{el} = -\text{slope}$$

$$t_{1/2} = \frac{0.693}{k_{el}}$$

## HPLC

### Analytical HPLC

All described final compounds described were confirmed to be of >95 % purity. The used Shimadzu HPLC system (Shimadzu, Kyoto, Japan) consists of a CBM-40 control unit, a DGU-403 degassing unit, two LC-40D chromatography pumps, a SIL-40C autosampler unit, a CTO-40C column oven and an SPD-M40 PDA UV detector. The standard method for purity determination utilized an Agilent Poroshell 120, EC-C18, 3,0x50mm, 2,7  $\mu\text{m}$  analytical column at a flow rate of 1.2 mL/min at room temperature. The 6 min gradient started at 15 % and increased to 85 % acetonitrile in water and was used in all cases. All solvents used are HPLC grade purity. UV absorbance at 254 nm was measured and the purity was derived from the integrated intensity signal.

### Preparative HPLC

If necessary, final compounds were purified by preparative HPLC. The Shimadzu HPLC system (Shimadzu, Kyoto, Japan) used consists of a CBM-40 control unit, two LC-20AP chromatography pumps, a SIL-40C autosampler unit, a CTO-40C column oven, an SPD-M40 PDA UV detector and an FRC-10A fraction collector. A preparative column manufactured by Agilent (Polaris C18-A, 5  $\mu\text{m}$ , 250 X 21.2mm) was used at a flow rate of 15 mL/min with a standard gradient of 50 % to 95% acetonitrile in water over 20 min at room temperature.

## Microbiological assays

### MIC determination against *M. intracellulare* ATCC 35761 pTEC27 and *M. abscessus* ATCC 19977 pTEC27

*M. intracellulare* ATCC 35761 pTEC27 and *M. abscessus* ATCC 19977 pTEC27 expressing tomato RFP were used for the activity assays. Cryo-stocks of the bacteria grown in 7H9 broth supplemented with 10 % ADS and 0.05 % Tween 80 were stored with approximately 15 % glycerol at  $-80^{\circ}\text{C}$ . Using an inoculation loop, bacteria were streaked on 7H10 plates supplemented with 0.5 % glycerol, 10 % ADS containing and 400  $\mu\text{g}/\text{mL}$  hygromycin and grown for 5 days in an incubator at  $37^{\circ}\text{C}$ . A single colony was picked from the 7H10 plates and the liquid culture was grown in 7H9 broth supplemented with 10 % ADS, 0.05 % Tween 80 and 400  $\mu\text{g}/\text{mL}$  hygromycin. The culture volume was 10 mL in a 50 mL Falcon tube. The tubes were shaken in an incubator at  $37^{\circ}\text{C}$ .

MIC values were determined by the broth microdilution method. 96-well flat bottom tissue culture plates (Sarstedt, 83.3924.500) were used<sup>[12a]</sup>. In the third well of each row two times the desired highest concentration of each compound was added in 7H9 medium supplemented with 10 % ADS and 0.05 % Tween 80. Each compound was diluted twofold in a nine-point serial dilution in 50 µL medium. (All drugs were prepared as 10 mM stocks in dimethyl sulfoxide (DMSO).)

The starting inoculum was diluted from a liquid culture described above at the mid-log phase (OD<sub>600</sub> 0.3 to 0.7) and an OD<sub>600</sub> of 0.1 was correlated to 1 x 10<sup>8</sup> CFU/mL. A starting inoculum of 5 x 10<sup>5</sup> cells/mL was used and 50 µl were added to each well. The plates were sealed with parafilm, placed in a container with moist tissue and incubated for three days at 37 °C (*M. abscessus*) or five days (*M. intracellulare*). After incubation the plates were monitored by OD measurement at 550 nm (BMG labtech Fluostar Optima) and by measurement of fluorescence (λ<sub>ex</sub> = 544 nm λ<sub>em</sub> = 590 nm). The assay was performed in duplicate, and the results were averaged.

Data analysis:

Every assay plate contained eight wells with dimethyl sulfoxide (1 %) as negative control, which corresponds to 100 % bacterial growth and eight wells with amikacin (100 µM) as positive control in which 100 % inhibition of bacterial growth was reached. Controls were used to monitor the assay quality through determination of the Z' score. The Z' factor was calculated as follows:

$$Z' = 1 - \frac{3(SD_{\text{amikacin}} + SD_{\text{DMSO}})}{M_{\text{amikacin}} - M_{\text{DMSO}}}$$

(SD = standard deviation, M = mean)

The percentage of growth inhibition was calculated by the equation:

$$\% \text{ growth inhibition} = 100 \% \times \frac{\text{signal(DMSO)} - \text{signal(sample)}}{\text{signal(DMSO)} - \text{signal(amikacin)}}$$

#### MIC determination against *M. avium ssp. hominissuis* strain 109 (MAC109)

MIC value determination by optical density at 600 nm [OD<sub>600</sub>] was carried out in 96-well plate format. 96-well plates were initially set up with 100 µl of 7H9 per well. For each compound, a 10-point twofold dilution series starting at twice the desired highest concentration was dispensed onto the 96-well plates using a Tecan D300e Digital Dispenser, with the DMSO concentration normalized to 2 % v/v. A bacteria culture grown to mid-log-phase (OD<sub>600</sub> 0.4 to 0.6) was diluted to OD<sub>600</sub> = 0.1 (1\*10<sup>7</sup> CFU/mL). 100 µl of the resulting bacteria suspension was dispensed onto the 96-well plates containing the sample compounds to give a final volume of 200 µl per well with an initial OD<sub>600</sub> = 0.05 (5\*10<sup>6</sup> CFU/mL) and a final DMSO concentration of 1 % v/v. Final compound concentration ranges were typically 50 to 0.098 µM or 6.25 to 0.012 µM. Untreated control wells, which contained bacteria suspension and 1 % v/v DMSO, were included on each plate. Plates were sealed with parafilm, stored in boxes with wet paper towels, and incubated at 37°C with shaking (110 rpm) and were incubated for 5 days.

To determine growth, OD<sub>600</sub> was measured using a Tecan Infinite M200 plate reader on day 0 and day 3. Two biological replicates were performed. Clarithromycin was included in each experiment as a positive control. For each well on the 96-well plate, bacterial growth was calculated by subtracting the day 0 OD<sub>600</sub> value from the day 3 OD<sub>600</sub> value. For each compound series, the bacterial growth values for the untreated control wells were averaged to give the average drug-free bacterial growth. For compound-containing wells, percentage growth was calculated by dividing their growth values by the average drug-free bacterial growth for the compound series and multiplying by 100. For each compound series, we plotted percentage growth versus compound concentration. By visual inspection of the dose-response curve, we determined the MIC of a compound as the compound concentrations that would result in 90 % growth inhibition. The MIC determination was performed two times with different starter cultures. The MIC values shown in the script are the averaged results of biological duplicates.

#### MIC determination against *M. tuberculosis* H37Rv

MICs against Mtb H47Rv were determined as described in<sup>[42]</sup>; Yang, X.; Wedajo, W.; Yamada, Y.; Dahlroth, S. L.; Neo, J. J. L.; Dick, T.; Chui, W. K. 1,3,5-Triazaspiro[5.5]Undeca-2,4-Dienes as Selective Mycobacterium Tuberculosis Dihydrofolate Reductase Inhibitors with Potent Whole Cell Activity. *Eur J Med Chem* **2018**, *144*, 262–276. <https://doi.org/10.1016/J.EJMECH.2017.12.017>. Briefly, compounds were serially diluted in flat-bottom 96-well plates, and a mid-log-phase culture was mixed with the compound-containing broth (final OD<sub>600</sub> = 0.05). Plates were sealed with Breathe-Easy sealing membrane (Sigma), placed in humidified plastic boxes and incubated at 37°C for 7 days, shaking at 80 rpm. Growth was monitored by measuring turbidity at 600 nm using a Tecan Infinite 200 Pro microplate reader (Tecan). MIC<sub>90</sub> values were deduced from the generated dose-response curves. The MIC values shown in the script are the averaged results of the two biological replicates.

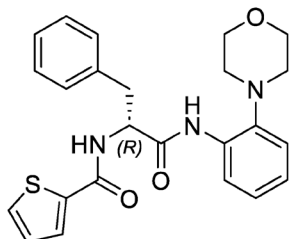
#### Cytotoxicity against immortalized human kidney epithelial

For evaluation of possible cytotoxic effects on mammalian cells, 20.000 HEK293 cells (immortalized human kidney epithelial cells; DSMZ, Braunschweig, Germany) were seeded out per well of a 96-well plate (Sarstedt, Germany) in DMEM supplemented with 10% FCS (both Gibco) and cultured in a humidified incubator at 37°C and 5% CO<sub>2</sub>. After 4 hours and attaching cells to the bottom, all compounds in DMSO were added to a final concentration of 50 µM. A sample containing only 0.5% DMSO was used as control. Cells were incubated for 24 h under the above-described conditions before AlamarBlue reagent (Thermo Fisher Scientific, Germany) was added. Samples were incubated again for 4 h before measurement was performed. The plates were analyzed in a microtiter plate reader (BMG, Germany) and the forming resorufin was quantified in fluorescence channel with Ex:550/Em:590 nm. The data are means of triplicates with standard deviation.

### 3. Structures and synthetic protocols

#### MMV

(2R)-N-[2-(morpholin-4-yl)phenyl]-3-phenyl-2-[(thiophen-2-yl)formamido]propenamide



#### Synthesis & Purification:

Described as compound **2B-(R)** in [18]: Lang, M., Ganapathy, U. S., Mann, L., Abdelaziz, R., Seidel, R. W., Goddard, R., Sequenzia, I., Hoenke, S., Schulze, P., Aragaw, W. W., Csuk, R., Dick, T., & Richter, A. (2023). Synthesis and Characterization of Phenylalanine Amides Active against Mycobacterium abscessus and Other Mycobacteria. *Journal of Medicinal Chemistry*. <https://doi.org/10.1021/ACS.JMEDCHEM.3C00009>

#### Analyses:

$R_f$  value: 0.37 ethyl acetate/heptane 1:1

$^1\text{H}$  NMR (**Spectrum 1**) (400 MHz, Chloroform-*d*)  $\delta$  8.83 (s, 1H), 8.40 (dd,  $J = 8.0, 1.5$  Hz, 1H), 7.52 (dd,  $J = 3.7, 1.2$  Hz, 1H), 7.47 (dd,  $J = 5.0, 1.1$  Hz, 1H), 7.32 – 7.25 (m, 4H), 7.23 – 7.17 (m, 1H), 7.16 – 7.05 (m, 3H), 7.03 (dd,  $J = 5.0, 3.7$  Hz, 1H), 6.95 (d,  $J = 7.8$  Hz, 1H), 4.95 (td,  $J = 8.0, 5.6$  Hz, 1H), 3.68 – 3.53 (m, 4H), 3.39 (dd,  $J = 13.6, 5.6$  Hz, 1H), 3.25 (dd,  $J = 13.6, 8.1$  Hz, 1H), 2.69 – 2.50 (m, 4H).

$^{13}\text{C}$  NMR APT (**Spectrum 2**) (101 MHz, Chloroform-*d*)  $\delta$  168.77, 161.56, 141.19, 137.97, 136.50, 132.91, 130.75, 129.38, 128.86, 128.66, 127.81, 127.12, 125.69, 124.33, 120.80, 119.52, 67.25, 56.19, 52.46, 38.47.

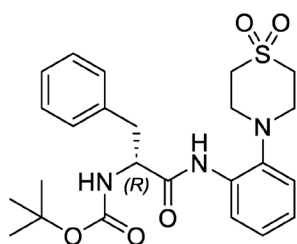
Mass: Calculated  $m/z$  for  $\text{C}_{24}\text{H}_{26}\text{N}_3\text{O}_3\text{S}^+$   $[\text{M}+\text{H}]^+ = 436.1689$ ;  $\text{C}_{24}\text{H}_{25}\text{N}_3\text{O}_3\text{SNa}^+$   $[\text{M}+\text{Na}]^+ = 458.1509$ ; found APCI: 436.1; found HRMS:  $[\text{M}+\text{H}]^+ 436.1691$ ;  $[\text{M}+\text{Na}]^+ 458.1506$

HPLC purity: 98.9 %  $t_R = 4.526$  min (**HPLC-Trace 1**); (50 mm Eclipse Plus C18 1.8  $\mu\text{m}$ , 4.6 mm, acetonitrile/ water 45:55,  $v = 1.0$  mL/min,  $\lambda = 220$  nm)

Specific optical rotation: Boc-protected intermediate (**2-D**)  $[\alpha]^{22.7}_D 46.01$  ( $c$  0.119, MeOH); final compound (**3-D**)  $[\alpha]^{22.7}_D 56.74$  ( $c$  0.1375, MeOH)

#### 1

tert-butyl N-[(1R)-1-benzyl-2-[2-(1,1-dioxo-1,4-thiazinan-4-yl)anilino]-2-oxo-ethyl]carbamate



### Synthesis & Purification:

Described as compound **23** in: Lang, M., Ganapathy, U. S., Mann, L., Abdelaziz, R., Seidel, R. W., Goddard, R., Sequenzia, I., Hoenke, S., Schulze, P., Aragaw, W. W., Csuk, R., Dick, T., & Richter, A. (2023). Synthesis and Characterization of Phenylalanine Amides Active against Mycobacterium abscessus and Other Mycobacteria. *Journal of Medicinal Chemistry*. <https://doi.org/10.1021/ACS.JMEDCHEM.3C00009>

### Analyses:

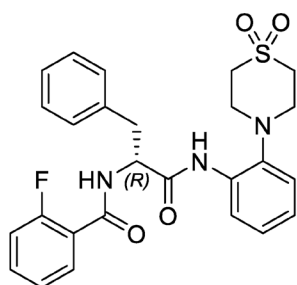
$R_f$  value: 0.31 ethyl acetate/heptane 1:1

$^1\text{H}$  NMR ( $\delta$ ) (400 MHz, Chloroform- $d$ ) 8.89 (s, 1H), 8.38 (d,  $J$  = 8.1 Hz, 1H), 7.31 – 7.11 (m, 7H), 7.08 – 7.01 (m, 1H), 5.40 – 5.13 (m, 1H), 4.47 (q,  $J$  = 7.3 Hz, 1H), 3.33 – 3.00 (m, 10H), 1.37 (s, 9H).

Mass: Calculated  $m/z$  for  $\text{C}_{24}\text{H}_{32}\text{N}_3\text{O}_5\text{S}^+$   $[\text{M}+\text{H}]^+ = 474.2057$ ; found APCI: 474.2

## 2

(2R)-2-[(2-fluorophenyl)formamido]-N-[2-(1,1-dioxo-1λ<sup>6</sup>-thiomorpholin-4-yl)phenyl]-3-phenylpropanamide



### Synthesis & Purification:

Described as compound **24** in: Lang, M., Ganapathy, U. S., Mann, L., Abdelaziz, R., Seidel, R. W., Goddard, R., Sequenzia, I., Hoenke, S., Schulze, P., Aragaw, W. W., Csuk, R., Dick, T., & Richter, A. (2023). Synthesis and Characterization of Phenylalanine Amides Active against Mycobacterium abscessus and Other Mycobacteria. *Journal of Medicinal Chemistry*. <https://doi.org/10.1021/ACS.JMEDCHEM.3C00009>

### Analyses:

$R_f$  value: 0.30 ethyl acetate

$^1\text{H}$  NMR (**Spectrum 4**) (500 MHz, Chloroform-*d*)  $\delta$  9.16 (s, 1H), 8.44 (dd,  $J = 8.2, 1.4$  Hz, 1H), 8.08 (td,  $J = 7.9, 1.9$  Hz, 1H), 7.52 (dddd,  $J = 8.3, 7.2, 5.3, 1.9$  Hz, 1H), 7.36 – 7.22 (m, 7H), 7.20 (ddd,  $J = 8.4, 7.5, 1.5$  Hz, 1H), 7.18 – 7.13 (m, 2H), 7.06 (td,  $J = 7.7, 1.5$  Hz, 1H), 5.04 (qd,  $J = 6.9, 2.2$  Hz, 1H), 3.40 – 3.30 (m, 2H), 3.21 (t,  $J = 5.3$  Hz, 4H), 3.12 (t,  $J = 5.1$  Hz, 4H).

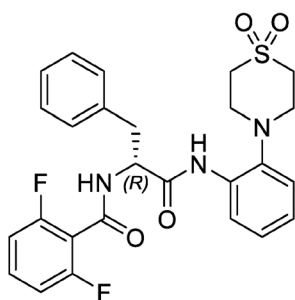
$^{13}\text{C}$  NMR (**Spectrum 5**) (126 MHz, Chloroform-*d*)  $\delta$  168.70, 163.62 (d,  $J = 3.3$  Hz), 160.82 (d,  $J = 248.0$  Hz), 139.97, 136.41, 134.36 (d,  $J = 9.5$  Hz), 133.12, 131.91 (d,  $J = 1.8$  Hz), 129.41, 128.89, 127.19, 126.84, 125.29 (d,  $J = 3.2$  Hz), 124.25, 121.51, 120.06, 119.43 (d,  $J = 10.8$  Hz), 116.47 (d,  $J = 24.7$  Hz), 56.07, 51.92, 51.27, 36.92.

Mass: Calculated  $m/z$  for  $\text{C}_{26}\text{H}_{27}\text{FN}_3\text{O}_4\text{S}^+$   $[\text{M}+\text{H}]^+ = 496.1701$ ; found APCI: 496.6; found HRMS:  $[\text{M}+\text{H}]^+ 496.1698$

HPLC purity: 98.86 %;  $t_{\text{R}} = 3.0$  min (**HPLC-Trace 2**); (Agilent Poroshell 120, EC-C18, 3,0x50 mm, 2,7  $\mu\text{m}$ , acetonitrile/ water 15:85, 6 min,  $v = 1.2$  mL/min,  $\lambda = 254$  nm)

### 3

(2R)-2-[(2,6-difluorophenyl)formamido]-N-[2-(1,1-dioxo-1 $\lambda^6$ -thiomorpholin-4-yl)phenyl]-3-phenylpropanamide



#### Synthesis:

**Quantities:** Boc-protected crude product from **2**: 156 mg (0.42 mmol, 1 eq.); **THF** (10 ml); **2,6-difluorobenzoic acid** (80 mg, 0.50 mmol, 1.2 eq., BLDpharm); **PyBOP** (328 mg, 0.63 mmol, 1.5 eq., Carbolution); **DIPEA** (214  $\mu\text{L}$ , 0.60 mmol, 3 eq., Aldrich)

**Procedure:** Boc-protected crude product from **2**, **2,6-difluorobenzoic acid** and **PyBOP** were dissolved in **THF**. Subsequently, **DIPEA** was added, and the mixture was stirred at room temperature overnight.

After the reaction time the crude reaction mixture was directly evaporated on silica gel without previous washing.

#### Purification:

Flash chromatography heptane/ethyl acetate gradient 80 % heptane to 20 % over 10 CV on 45 g normal phase silica gel 0.63 – 0.2  $\mu\text{m}$  particle size. Yield: 194 mg; 90 %

#### Analyses:

$R_{\text{F}}$  value: 0.30 ethyl acetate/heptane 1:1

$^1\text{H}$  NMR (**Spectrum 6**) (500 MHz, Chloroform-*d*)  $\delta$  9.07 (s, 1H), 8.35 (d,  $J = 8.2$  Hz, 1H), 7.40 – 7.29 (m, 5H), 7.27 – 7.22 (m, 1H), 7.21 – 7.14 (m, 2H), 7.08 (td,  $J = 7.7, 1.4$  Hz, 1H), 6.91 (tt,  $J = 8.5, 2.1$  Hz, 3H), 5.03 (q,  $J = 7.4$  Hz, 1H), 3.40 – 3.11 (m, 10H).

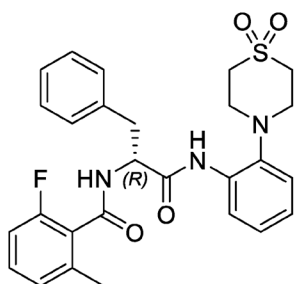
$^{13}\text{C}$  NMR (**Spectrum 7**) (126 MHz, Chloroform-*d*)  $\delta$  168.61, 160.78, 160.01 (d,  $J = 253.2$  Hz), 159.96 (d,  $J = 252.7$  Hz), 140.24, 136.32, 132.99, 132.40 (t,  $J = 10.2$  Hz), 129.41, 128.79, 127.13, 126.68, 124.44, 121.57, 120.20, 112.93 (d,  $J = 18.7$  Hz), 112.25 (d,  $J = 4.3$  Hz), 112.09 (d,  $J = 4.1$  Hz), 56.10, 51.87, 51.27, 37.08.

Mass: Calculated  $m/z$  for  $\text{C}_{26}\text{H}_{26}\text{F}_2\text{N}_3\text{O}_4\text{S}^+$   $[\text{M}+\text{H}]^+ = 514.1607$ ; found APCI: 514.6; found HRMS:  $[\text{M}+\text{H}]^+ 514.1602$

HPLC purity: 98.8 %;  $t_{\text{R}} = 4.7$  min (**HPLC-Trace 3**); (Agilent Poroshell 120, EC-C18, 3,0x50 mm, 2,7  $\mu\text{m}$ , acetonitrile/ water 15:85, 10 min,  $v = 1.2$  mL/min,  $\lambda = 254$  nm)

#### 4

(2R)-N-[2-(1,1-dioxo-1 $\lambda^6$ -thiomorpholin-4-yl)phenyl]-2-[(2-fluoro-6-methylphenyl)formamido]-3-phenylpropanamide



#### Synthesis:

*Quantities:* Boc-protected crude product from **2**: 183 mg (0.49 mmol, 1 eq.); **THF** (10 ml); **2-fluoro-6-methylbenzoic acid** (91 mg, 0.59 mmol, 1.2 eq., BLDpharm); **PyBOP** (382 mg, 0.74 mmol, 1.5 eq., Carbolution); **DIPEA** (250  $\mu\text{L}$ , 1.47 mmol, 3 eq., Aldrich)

*Procedure:* Boc-protected crude product from **2**, **2-fluoro-6-methylbenzoic acid** and **PyBOP** were dissolved in **THF**. Subsequently, **DIPEA** was added, and the mixture was stirred at room temperature overnight.

After the reaction time the crude reaction mixture was directly evaporated on silica gel without previous washing.

#### Purification:

Flash chromatography heptane/ethyl acetate gradient 75 % heptane to 25 % over 10 CV on 45 g normal phase silica gel 0.63 – 0.2  $\mu\text{m}$  particle size. Preparative HPLC afterwards. Yield: 203 mg; 81 %

#### Analyses:

$R_{\text{F}}$  value: 0.31 ethyl acetate/heptane 1:1

$^1\text{H}$  NMR (**Spectrum 8**) (400 MHz, Chloroform-*d*)  $\delta$  9.15 (s, 1H), 8.35 (dd,  $J = 8.2, 1.5$  Hz, 1H), 7.32 – 7.13 (m, 8H), 7.07 (td,  $J = 7.7, 1.5$  Hz, 1H), 6.93 (d,  $J = 7.6$  Hz, 1H), 6.84 (t,  $J = 8.9$  Hz, 1H), 6.68 – 6.59 (m, 1H), 5.07 (q,  $J = 7.8$  Hz, 1H), 3.35 (dd,  $J = 14.2, 6.9$  Hz, 1H), 3.31 – 3.12 (m, 9H), 2.06 (s, 3H).

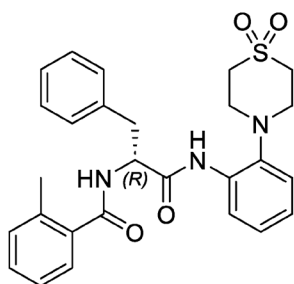
$^{13}\text{C}$  NMR (**Spectrum 9**) (101 MHz, Chloroform-*d*)  $\delta$  168.88, 165.77, 159.04 (d,  $J = 246.0$  Hz), 140.19, 138.37 (d,  $J = 2.8$  Hz), 136.52, 133.07, 130.91 (d,  $J = 8.9$  Hz), 129.29, 128.82, 127.11, 126.72, 126.34 (d,  $J = 2.9$  Hz), 124.40, 123.71 (d,  $J = 17.0$  Hz), 121.58, 120.27, 112.90 (d,  $J = 21.8$  Hz), 55.66, 51.76, 51.29, 36.82, 18.84.

Mass: Calculated  $m/z$  for  $\text{C}_{27}\text{H}_{29}\text{FN}_3\text{O}_4\text{S}^+$   $[\text{M}+\text{H}]^+ = 510.1858$ ; found APCI: 510.3; found HRMS:  $[\text{M}+\text{H}]^+ 510.1852$

HPLC purity: 98.8 %;  $t_{\text{R}} = 3.0$  min (**HPLC-Trace 4**); (Agilent Poroshell 120, EC-C18, 3,0x50 mm, 2,7  $\mu\text{m}$ , acetonitrile/ water 15:85, 6 min,  $v = 1.2$  mL/min,  $\lambda = 254$  nm)

## 5

(2R)-N-[2-(1,1-dioxo-1 $\lambda^6$ -thiomorpholin-4-yl)phenyl]-2-[(2-methylphenyl)formamido]-3-phenylpropanamide



### Synthesis:

**Quantities:** Boc-protected crude product from **2**: 42 mg (0.11 mmol, 1 eq.); **THF** (5 ml); **2-methylbenzoic acid** (18 mg, 0.13 mmol, 1.2 eq., TCI); **PyBOP** (88 mg, 0.17 mmol, 1.5 eq., Carbolution); **DIPEA** (44  $\mu\text{L}$ , 0.34 mmol, 3 eq., Aldrich)

**Procedure:** Boc-protected crude product from **2**, **2-methylbenzoic acid** and **PyBOP** were dissolved in **THF**. Subsequently, **DIPEA** was added, and the mixture was stirred at room temperature overnight.

After the reaction time the crude reaction mixture was directly evaporated on silica gel without previous washing.

### Purification:

Flash chromatography heptane/ethyl acetate gradient 75 % heptane to 25 % over 10 CV on 8 g normal phase silica gel 0.63 – 0.2  $\mu\text{m}$  particle size. Afterwards preparative HPLC. Yield: 29 mg; 54 %

### Analyses:

$R_{\text{F}}$  value: 0.42 ethyl acetate/heptane 1:1

$^1\text{H}$  NMR (**Spectrum 10**) (400 MHz, Chloroform-*d*)  $\delta$  9.18 (s, 1H), 8.39 (d,  $J = 8.6, 1.5$  Hz, 1H), 7.32 (d,  $J = 4.3$  Hz, 4H), 7.30 (dd,  $J = 7.3, 1.7$  Hz, 1H), 7.28 – 7.23 (m, 1H), 7.22 – 7.17 (m, 4H), 7.14 (td,  $J = 7.4,$

1.2 Hz, 1H), 7.11 – 7.05 (m, 1H), 6.39 (d,  $J = 7.7$  Hz, 1H), 4.96 (q,  $J = 7.5$  Hz, 1H), 3.35 (dd,  $J = 14.1, 7.4$  Hz, 1H), 3.31 – 3.14 (m, 9H), 2.30 (s, 3H).

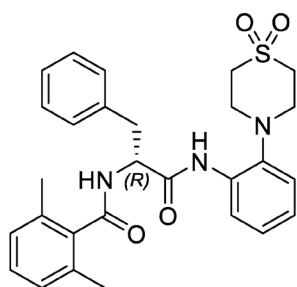
$^{13}\text{C}$  NMR (**Spectrum 11**) (101 MHz, Chloroform- $d$ )  $\delta$  170.23, 169.04, 140.01, 136.52, 136.43, 134.69, 133.09, 131.33, 130.56, 129.27, 128.88, 127.17, 126.80, 126.63, 125.86, 124.36, 121.53, 120.17, 55.92, 51.86, 51.30, 36.97, 19.79.

Mass: Calculated  $m/z$  for  $\text{C}_{27}\text{H}_{29}\text{FN}_3\text{O}_4\text{S}^+$   $[\text{M}+\text{H}]^+ = 492.1952$ ;  $[\text{M}+\text{Na}]^+ = 514.1771$ ; found APCI: 492.2; found HRMS:  $[\text{M}+\text{H}]^+ 492.1956$ ;  $[\text{M}+\text{Na}]^+ 514.1775$

HPLC purity: 97.2 %;  $t_R = 3.0$  min (**HPLC-Trace 5**); (Agilent Poroshell 120, EC-C18, 3,0x50 mm, 2,7  $\mu\text{m}$ , acetonitrile/ water 15:85, 6 min,  $v = 1.2$  mL/min,  $\lambda = 254$  nm)

## 6

(2R)-N-[2-(1,1-dioxo-1 $\lambda^6$ -thiomorpholin-4-yl)phenyl]-2-[(2,6-dimethylphenyl)formamido]-3-phenylpropanamide



### Synthesis:

*Quantities:* Boc-protected crude product from **2**: 42 mg (0.11 mmol, 1 eq.); **DMF** (10 ml); **2,6-dimethylbenzoic acid** (21 mg, 0.14 mmol, 1.2 eq., TCI); **PyBOP** (117 mg, 0.23 mmol, 2 eq., Carbolution); **DIPEA** (56  $\mu\text{L}$ , 0.33 mmol, 3 eq., Aldrich)

*Procedure:* Boc-protected crude product from **2**, **2,6-dimethylbenzoic acid** and **PyBOP** were dissolved in **THF**. Subsequently, **DIPEA** was added, and the mixture was stirred at room temperature for two days.

After the reaction time the crude reaction mixture was directly evaporated on silica gel without previous washing.

### Purification:

Flash chromatography heptane/ethyl acetate gradient 80 % heptane to 30 % over 10 CV on 8 g normal phase silica gel 0.63 – 0.2  $\mu\text{m}$  particle size. Afterwards preparative HPLC. Yield: 21 mg; 38 %

### Analyses:

$R_f$  value: 0.39 ethyl acetate/heptane 1:1

$^1\text{H}$  NMR (**Spectrum 12**) (400 MHz, Chloroform- $d$ )  $\delta$  9.30 (s, 1H), 8.40 (dd,  $J = 8.6, 1.5$  Hz, 1H), 7.35 – 7.28 (m, 4H), 7.28 – 7.19 (m, 3H), 7.13 (t,  $J = 7.6$  Hz, 1H), 7.12 – 7.07 (m, 1H), 6.94 (d,  $J = 7.6$  Hz, 2H),

6.16 (d,  $J = 7.8$  Hz, 1H), 4.99 (ddd,  $J = 8.8, 7.8, 6.8$  Hz, 1H), 3.44 – 3.19 (m, 9H), 3.13 (dd,  $J = 14.2, 8.8$  Hz, 1H), 2.00 (s, 6H).

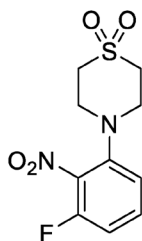
$^{13}\text{C}$  NMR (**Spectrum 13**) (101 MHz, Chloroform- $d$ )  $\delta$  170.84, 168.91, 139.99, 136.42, 136.22, 134.09, 133.11, 129.23, 129.09, 128.92, 127.51, 127.21, 126.86, 124.34, 121.55, 120.14, 55.55, 51.88, 51.39, 36.60, 18.68.

Mass: Calculated  $m/z$  for  $\text{C}_{28}\text{H}_{31}\text{N}_3\text{O}_4\text{S}^+$   $[\text{M}+\text{H}]^+ = 506.2108$ ; found APCI: 506.4; found HRMS:  $[\text{M}+\text{H}]^+ 506.2101$

HPLC purity: 99.0 %;  $t_{\text{R}} = 3.1$  min (**HPLC-Trace 6**); (Agilent Poroshell 120, EC-C18, 3,0x50 mm, 2,7  $\mu\text{m}$ , acetonitrile/ water 15:85, 6 min,  $v = 1.2$  mL/min,  $\lambda = 254$  nm)

## 7

4-(3-fluoro-2-nitrophenyl)-1 $\lambda^6$ -thiomorpholine-1,1-dioxide



### Synthesis:

**Quantities:** **1,3-Difluoro-2-nitrobenzene** (1114 mg, 7 mmol, 1 eq., BLDpharm); **Thiomorpholinedioxide** (946 mg, 7 mmol, 1 eq., BLDpharm); **DIPEA** (2382  $\mu\text{L}$ , 14 mmol, 2 eq., Aldrich)

**Procedure:** **1,3-Difluoro-2-nitrobenzene** and **thiomorpholinedioxide** were dissolved in **DIPEA** and stirred at 50  $^{\circ}\text{C}$  for 3 days.

After the reaction time the crude reaction mixture was directly evaporated on silica gel without previous washing.

### Purification:

Flash chromatography heptane/chloroform gradient 40 % heptane to 0 % over 10 CV on 90 g normal phase silica gel 0.63 – 0.2  $\mu\text{m}$  particle size. Yield: 1261 mg; 95 %

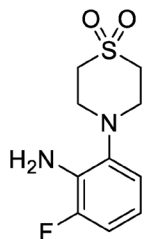
### Analyses:

$R_{\text{F}}$  value: 0.76 dichloromethane/ethyl acetate 1:1

$^1\text{H}$  NMR (**Spectrum 14**) (400 MHz, Chloroform- $d$ )  $\delta$  7.47 (td,  $J = 8.4, 6.0$  Hz, 1H), 7.15 – 7.02 (m, 2H), 3.65 – 3.43 (m, 4H), 3.27 – 3.03 (m, 4H).

Mass: Calculated  $m/z$  for  $\text{C}_{10}\text{H}_{12}\text{FN}_2\text{O}_4\text{S}^+$   $[\text{M}+\text{H}]^+ = 275.0497$ ; found APCI: 275.0

## 8

4-(2-amino-3-fluorophenyl)-1 $\lambda^6$ -thiomorpholine-1,1-dioxideSynthesis:

**Quantities:** **7** (1261 mg, 4.60 mmol, 1 eq.); **H<sub>2</sub>** (Balloon); **Pd(OH)<sub>2</sub>/C 20 %** (252 mg, 20 m %, Aldrich); **EtOH 96 % v/v** (90 mL)

**Procedure:** **7** was dissolved in **EtOH**, add catalyst; close the flask with a septum and purge the mixture with hydrogen for 30 min under stirring; add a hydrogen balloon; check for full conversion with TLC; after completion remove the catalyst with paper filter and wash the filter thoroughly with ethyl acetate; evaporate the solvents under reduced pressure

Purification:

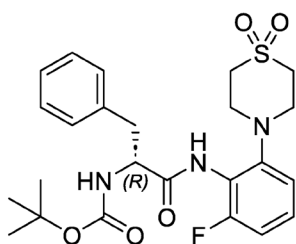
Product was used without further purification. Yield: 955 mg; 85 %

Analyses:

*R<sub>f</sub>* value: 0.25 ethyl acetate/heptane 1:1

Mass: Calculated *m/z* for C<sub>10</sub>H<sub>14</sub>FN<sub>2</sub>O<sub>2</sub>S<sup>+</sup> [M+H]<sup>+</sup> = 245.0755; found APCI: 245.2

## 9

tert-butyl N-[(1R)-1-[[2-(1,1-dioxo-1 $\lambda^6$ -thiomorpholin-4-yl)-6-fluorophenyl]carbamoyl]-2-phenylethyl]carbamateSynthesis:

**Quantities:** **Pyridine** (20 mL); **EtOAc** (40 mL); **8** (955 mg, 3.91 mmol, 1 eq.); **N-Boc-(R)-phenylalanine** (1141 mg, 4.30 mmol, 1.1 eq., TCI); **T3P 50 % m/V in EtOAc** (4655  $\mu$ L, 7.82 mmol, 2 eq., Aldrich)

**Procedure:** **8** and **N-Boc-(R)-phenylalanine** were dissolved in a 1:2 mixture of distilled **pyridine** and **EtOAc**. The mixture was cooled to -20 °C with an isopropanol dry-ice bath before **T3P 50 % m/V in EtOAc** was added. After the addition, the cooling bath was removed, and the mixture was stirred for

20 h at room temperature. Afterwards the mixture was washed with 0.25 M  $\text{KH}_2\text{PO}_4$  solution three times before the organic phase was evaporated on silica gel under reduced pressure for purification.

**Purification:**

Flash chromatography heptane/methyl tert-butyl ether gradient 50 % heptane to 0 % over 10 CV on 90 g normal phase silica gel 0.63 – 0.2  $\mu\text{m}$  particle size. Yield: 1769 mg; 92 %

**Analyses:**

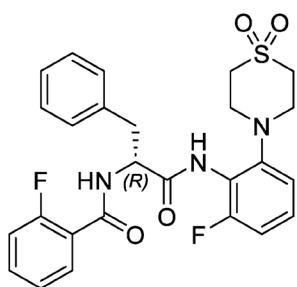
$R_F$  value: 0.42 heptane/ethyl acetate 1:1

$^1\text{H}$  NMR (**Spectrum 15****Spectrum 14**) (400 MHz,  $\text{cdCl}_3$ )  $\delta$  7.78 (s, 1H), 7.34 – 7.21 (m, 5H), 7.17 (td,  $J = 8.2, 5.9$  Hz, 1H), 6.92 – 6.81 (m, 2H), 5.15 (d,  $J = 7.6$  Hz, 1H), 4.54 (q,  $J = 7.2$  Hz, 1H), 3.45 – 3.00 (m, 10H), 1.39 (s, 9H).

Mass: Calculated  $m/z$  for  $\text{C}_{10}\text{H}_{12}\text{FN}_2\text{O}_4\text{S}^+$   $[\text{M}+\text{H}]^+ = 492.1963$ ; found APCI: 492.6

**10**

((2R)-N-[2-(1,1-dioxo-1 $\lambda^6$ -thiomorpholin-4-yl)-6-fluorophenyl]-2-[(2-fluorophenyl)formamido]-3-phenylpropanamide



**Synthesis:**

**Quantities:** DCM (10 mL); TFA (10 mL); **9** (1769 mg, 3.60 mmol) Boc-protected crude product isolation: 1019 mg; Used for next step: 201 mg (0.51 mmol, 1 eq.); THF (10 ml); **2-fluorobenzoic acid** (86 mg, 0.62 mmol, 1.2 eq., TCI); **DEPBT** (169 mg, 0.57 mmol, 1.1 eq., BLDpharm); **DIPEA** (174  $\mu\text{L}$ , 1.02 mmol, 2 eq., Aldrich)

After the reaction time the crude reaction mixture was directly evaporated on silica gel without previous washing.

**Purification:**

Flash chromatography heptane/ethyl acetate gradient 70 % heptane to 20 % over 10 CV on 45 g normal phase silica gel 0.63 – 0.2  $\mu\text{m}$  particle size. Yield: 238 mg; 91 %

**Analyses:**

$R_F$  value: 0.15 ethyl acetate/heptane 1:1

$^1\text{H}$  NMR (**Spectrum 16**) (400 MHz, Chloroform-*d*)  $\delta$  8.08 (s, 1H), 7.97 (t,  $J = 7.8$  Hz, 1H), 7.50 – 7.43 (m, 1H), 7.36 – 7.20 (m, 7H), 7.16 (td,  $J = 8.2, 5.8$  Hz, 1H), 7.09 (dd,  $J = 12.1, 8.3$  Hz, 1H), 6.94 – 6.83 (m, 2H), 5.07 (qd,  $J = 6.9, 1.7$  Hz, 1H), 3.42 – 3.23 (m, 6H), 3.23 – 3.02 (m, 4H).

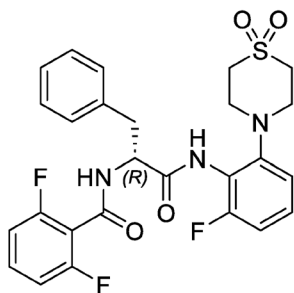
$^{13}\text{C}$  NMR (**Spectrum 17**) (101 MHz, Chloroform-*d*)  $\delta$  169.65, 163.93 (d,  $J = 3.0$  Hz), 160.73 (d,  $J = 248.7$  Hz), 157.63 (d,  $J = 252.4$  Hz), 147.82, 136.03, 134.12 (d,  $J = 9.3$  Hz), 131.77 (d,  $J = 1.8$  Hz), 129.44, 128.83, 127.72 (d,  $J = 9.3$  Hz), 127.29, 125.06 (d,  $J = 3.2$  Hz), 119.81 (d,  $J = 10.7$  Hz), 119.47 (d,  $J = 13.5$  Hz), 116.36 (d,  $J = 3.4$  Hz), 116.26 (d,  $J = 24.4$  Hz), 112.90 (d,  $J = 20.7$  Hz), 55.62, 51.96, 50.66, 37.36.

Mass: Calculated  $m/z$  for  $\text{C}_{26}\text{H}_{26}\text{F}_2\text{N}_3\text{O}_4\text{S}^+$   $[\text{M}+\text{H}]^+ = 514.1607$ ; found APCI: 514.5; found HRMS:  $[\text{M}+\text{H}]^+ 514.1601$

HPLC purity: 97.6 %;  $t_{\text{R}} = 2.7$  min (**HPLC-Trace 7**); (Agilent Poroshell 120, EC-C18, 3,0x50 mm, 2,7  $\mu\text{m}$ , acetonitrile/ water 15:85, 6 min,  $v = 1.2$  mL/min,  $\lambda = 254$  nm)

## 11

(2R)-2-[(2,6-difluorophenyl)formamido]-N-[2-(1,1-dioxo-1 $\lambda^6$ -thiomorpholin-4-yl)-6-fluorophenyl]-3-phenylpropanamide



### Synthesis:

*Quantities:* Boc-protected crude product of **10** (184 mg, 0.47 mmol, 1 eq.); THF (10 ml); **2,6-difluorobenzoic acid** (89 mg, 0.56 mmol, 1.2 eq., TCI); **DEPBT** (295 mg, 0.99 mmol, 2.1 eq., BLDpharm); **DIPEA** (160  $\mu\text{L}$ , 1.41 mmol, 3 eq., Aldrich)

After the reaction time the crude reaction mixture was directly evaporated on silica gel without previous washing.

### Purification:

Flash chromatography heptane/ethyl acetate gradient 70 % heptane to 25 % over 10 CV on 45 g normal phase silica gel 0.63 – 0.2  $\mu\text{m}$  particle size. Afterwards preparative HPLC. Yield: 170 mg; 68 %

### Analyses:

$R_{\text{F}}$  value: 0.75 ethyl acetate

$^1\text{H}$  NMR (**Spectrum 18**) (400 MHz, Acetone-*d*<sub>6</sub>)  $\delta$  8.85 (s, 1H), 8.31 (d,  $J = 8.3$  Hz, 1H), 7.52 – 7.37 (m, 3H), 7.36 – 7.21 (m, 4H), 7.09 – 6.91 (m, 4H), 5.19 (q,  $J = 8.3$  Hz, 1H), 3.50 – 3.23 (m, 7H), 3.22 – 3.10 (m, 3H).

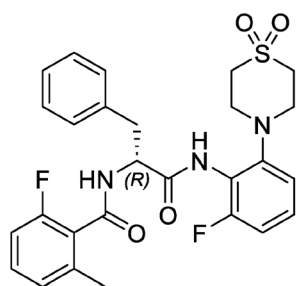
$^{13}\text{C}$  NMR (**Spectrum 19**) (101 MHz, Acetone- $d_6$ )  $\delta$  169.76 (d,  $J = 8.5$  Hz), 160.34 (d,  $J = 8.2$  Hz), 159.63 (d,  $J = 250.2$  Hz), 159.56 (d,  $J = 250.3$  Hz), 158.16 (d,  $J = 250.0$  Hz), 149.09, 137.28, 131.76 (t,  $J = 10.0$  Hz), 129.35, 128.29, 127.71 (d,  $J = 9.5$  Hz), 126.64, 119.99 – 119.35 (m), 116.33 (d,  $J = 3.0$  Hz), 115.25 – 114.38 (m), 111.82 – 111.41 (m), 55.35, 52.00, 50.39, 37.74.

Mass: Calculated  $m/z$  for  $\text{C}_{26}\text{H}_{25}\text{F}_3\text{N}_3\text{O}_4\text{S}^+$   $[\text{M}+\text{H}]^+ = 532.1513$ ; found APCI: 532.5; found HRMS:  $[\text{M}+\text{H}]^+ 532.1507$

HPLC purity: 98.9 %;  $t_{\text{R}} = 2.6$  min (**HPLC-Trace 8**); (Agilent Poroshell 120, EC-C18, 3,0x50 mm, 2,7  $\mu\text{m}$ , acetonitrile/ water 15:85, 6 min,  $v = 1.2$  mL/min,  $\lambda = 254$  nm)

## 12

(2R)-N-[2-(1,1-dioxo--thiomorpholin-4-yl)-6-fluorophenyl]-2-[(2-fluoro-6-methylphenyl)formamido]-3-phenylpropanamide



### Synthesis:

**Quantities:** Boc-protected crude product of **10** (193 mg, 0.49 mmol, 1 eq.); **THF** (10 ml); **2-fluoro-6-methylbenzoic acid** (91 mg, 0.59 mmol, 1.2 eq., TCl); **DEPBT** (308 mg, 1.03 mmol, 2.1 eq., BLDpharm); **DIPEA** (251  $\mu\text{L}$ , 1.47 mmol, 3 eq., Aldrich)

After the reaction time the crude reaction mixture was directly evaporated on silica gel without previous washing.

### Purification:

Flash chromatography heptane/ethyl acetate gradient 70 % heptane to 25 % over 10 CV on 45 g normal phase silica gel 0.63 – 0.2  $\mu\text{m}$  particle size. Yield: 245 mg; 95 %

### Analyses:

$R_{\text{F}}$  value: 0.25 heptane/ethyl acetate 1:1

$^1\text{H}$  NMR (**Spectrum 20**) (400 MHz, Chloroform- $d$ )  $\delta$  8.09 (d,  $J = 10.3$  Hz, 1H), 7.37 – 7.22 (m, 5H), 7.22 – 7.12 (m, 2H), 6.93 – 6.79 (m, 4H), 6.70 (q,  $J = 7.9$  Hz, 1H), 5.16 (tdd,  $J = 8.0, 6.9, 6.4, 2.6$  Hz, 1H), 3.45 – 3.23 (m, 5H), 3.20 – 3.03 (m, 5H), 2.08 (s, 3H).

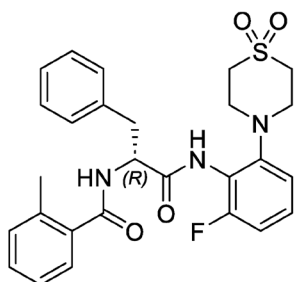
$^{13}\text{C}$  NMR (**Spectrum 21**) (101 MHz, Chloroform- $d$ )  $\delta$  169.61, 165.82, 159.08 (d,  $J = 245.5$  Hz), 157.78 (d,  $J = 251.1$  Hz), 148.01, 138.83 – 137.77 (m), 136.13, 130.84 (d,  $J = 8.8$  Hz), 129.37, 128.81, 127.91 (d,  $J = 9.7$  Hz), 127.25, 126.27 (d,  $J = 2.6$  Hz), 123.77 (d,  $J = 16.6$  Hz), 119.17 (d,  $J = 13.4$  Hz), 116.25 (d,  $J = 3.0$  Hz), 112.86 (d,  $J = 21.7$  Hz), 112.70 (d,  $J = 20.4$  Hz), 54.93, 51.84, 50.54, 37.40, 18.79.

Mass: Calculated  $m/z$  for  $C_{27}H_{28}F_2N_3O_4S^+$   $[M+H]^+$  = 528.1763; found APCI: 528.5; found HRMS:  $[M+H]^+$  528.1758

HPLC purity: 99.3 %;  $t_R$ =2.7 min (**HPLC-Trace 9**); (Agilent Poroshell 120, EC-C18, 3,0x50 mm, 2,7  $\mu$ m, acetonitrile/ water 15:85, 6 min,  $v$ =1.2 mL/min,  $\lambda$ =254 nm)

### 13

(2R)-N-[2-(1,1-dioxo-1 $\lambda^6$ -thiomorpholin-4-yl)-6-fluorophenyl]-2-[(2-methylphenyl)formamido]-3-phenylpropanamide



#### Synthesis:

*Quantities:* Boc-protected crude product of **10** (306 mg, 0.82 mmol, 1 eq.); **DMF** (10 ml); **2-methylbenzoic acid** (134 mg, 0.98 mmol, 1.2 eq., TCI); **PyBOP** (640 mg, 1.23 mmol, 1.5 eq., BLDpharm); **DIPEA** (418  $\mu$ L, 2.46 mmol, 3 eq., Aldrich)

After the reaction time the crude reaction mixture was directly evaporated on silica gel without previous washing.

#### Purification:

Flash chromatography heptane/ethyl acetate gradient 70 % heptane to 30 % over 10 CV on 8 g normal phase silica gel 0.63 – 0.2  $\mu$ m particle size. Afterwards preparative HPLC. Yield: 311 mg; 74 %

#### Analyses:

$R_f$  value: 0.20 heptane/ethyl acetate 1:1

$^1H$  NMR (**Spectrum 22**) (400 MHz, Chloroform-*d*)  $\delta$  8.11 (s, 1H), 7.41 – 7.24 (m, 6H), 7.22 – 7.09 (m, 4H), 6.93 – 6.81 (m, 2H), 6.48 (d,  $J$  = 7.6 Hz, 1H), 5.05 (q,  $J$  = 7.4 Hz, 1H), 3.46 – 3.23 (m, 5H), 3.18 (dd,  $J$  = 13.8, 7.2 Hz, 1H), 3.13 – 3.02 (m, 4H), 2.29 (s, 3H).

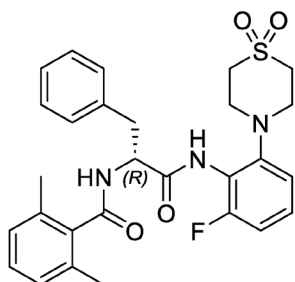
$^{13}C$  NMR (**Spectrum 23**) (101 MHz, Chloroform-*d*)  $\delta$  170.66, 169.92, 157.74 (d,  $J$  = 251.5 Hz), 147.83, 136.37, 136.20, 134.69, 131.21, 130.54, 129.39, 128.89, 127.85 (d,  $J$  = 9.4 Hz), 127.35, 126.84, 125.86, 119.25 (d,  $J$  = 13.4 Hz), 116.20 (d,  $J$  = 2.7 Hz), 112.76 (d,  $J$  = 20.7 Hz), 55.25, 51.96, 50.58, 37.19, 19.72.

Mass: Calculated  $m/z$  for  $C_{27}H_{29}FN_3O_4S^+$   $[M+H]^+$  = 510.1858<sup>+</sup>;  $[M+Na]^+$  = 532.1677; found APCI: 528.5; found HRMS:  $[M+H]^+$  510.1864;  $[M+Na]^+$  532.1679

HPLC purity: 99.5 %;  $t_R$ =2.7 min (**HPLC-Trace 10**); (Agilent Poroshell 120, EC-C18, 3,0x50 mm, 2,7  $\mu$ m, acetonitrile/ water 15:85, 6 min,  $v$ =1.2 mL/min,  $\lambda$ =254 nm)

**14**

(2R)-2-[(2,6-dimethylphenyl)formamido]-N-[2-(1,1-dioxo-1 $\lambda^6$ -thiomorpholin-4-yl)-6-fluorophenyl]-3-phenylpropanamide

**Synthesis:**

**Quantities:** Boc-protected crude product from **10**: 195 mg (0.50 mmol, 1 eq.); **THF** (10 ml); **2,6-dimethylbenzoic acid** (90 mg, 0.60 mmol, 1.2 eq., TCI); **PyBOP** (313 mg, 1.05 mmol, 2.1 eq., Carbolution); **DIPEA** (255  $\mu$ L, 1.5 mmol, 3 eq., Aldrich)

After the reaction time the crude reaction mixture was directly evaporated on silica gel without previous washing.

**Purification:**

Flash chromatography heptane/ethyl acetate gradient 60 % heptane to 15 % over 10 CV on 8 g normal phase silica gel 0.63 – 0.2  $\mu$ m particle size. Afterwards preparative HPLC. Yield: 99 mg; 38 %

**Analyses:**

$R_F$  value: 0.25 ethyl acetate/heptane 1:1

$^1\text{H}$  NMR (**Spectrum 24**) (500 MHz, Chloroform-*d*)  $\delta$  8.25 – 8.15 (m, 1H), 7.32 (dd,  $J = 23.3, 4.4$  Hz, 5H), 7.24 – 7.16 (m, 1H), 7.12 (t,  $J = 7.6$  Hz, 1H), 6.94 (d,  $J = 7.7$  Hz, 2H), 6.89 (dd,  $J = 12.0, 8.3$  Hz, 2H), 6.33 (d,  $J = 7.9$  Hz, 1H), 5.17 (q,  $J = 7.2, 6.2$  Hz, 1H), 3.45 – 3.27 (m, 5H), 3.16 – 3.03 (m, 5H), 2.07 (s, 6H).

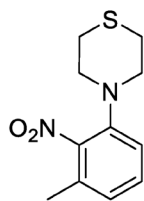
$^{13}\text{C}$  NMR (**Spectrum 25**) (126 MHz, Chloroform-*d*)  $\delta$  171.19, 169.73, 157.72 (d,  $J = 251.8$  Hz), 147.79, 136.19, 136.15, 134.32, 129.31, 129.13, 128.93, 127.83 (d,  $J = 9.9$  Hz), 127.53, 127.38, 119.14 (d,  $J = 14.3$  Hz), 116.14, 112.83 (d,  $J = 20.6$  Hz), 54.80, 52.01, 50.57, 37.37, 18.76.

Mass: Calculated  $m/z$  for  $\text{C}_{28}\text{H}_{31}\text{FN}_3\text{O}_4\text{S}^+$   $[\text{M}+\text{H}]^+ = 524.2014$ ; found APCI: 524.5; found HRMS:  $[\text{M}+\text{H}]^+ 524.2010$

HPLC purity: 98.4 %;  $t_R = 2.9$  min (**HPLC-Trace 11**); (Agilent Poroshell 120, EC-C18, 3,0x50 mm, 2,7  $\mu$ m, acetonitrile/ water 15:85, 6 min,  $v = 1.2$  mL/min,  $\lambda = 254$  nm)

**15**

4-(3-methyl-2-nitrophenyl)thiomorpholine

**Synthesis:**

**Quantities:** **1-Fluoro-3-methyl-2-nitrobenzene** (1000 mg, 6.45 mmol, 1 eq., BLDpharm); **thiomorpholine** (731 mg, 7.09 mmol, 1.1 eq., abcr GmbH); **DIPEA** (2194  $\mu$ L, 12.90 mmol, 2 eq., Aldrich)

**Procedure:** Mix **1-fluoro-3-methyl-2-nitrobenzene** and **thiomorpholine**; add **DIPEA**; stir for 24 h at 50 °C.

After the reaction time the crude reaction mixture was directly evaporated on silica gel.

**Purification:**

Flash chromatography heptane/dichloromethane gradient 95 % heptane to 50 % over 10 CV on 90 g normal phase silica gel 0.63 – 0.2  $\mu$ m particle size. Yield: 313 mg; 18 %

**Analyses:**

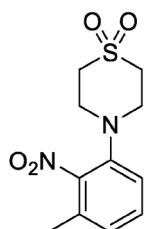
$R_f$  value: 0.30 dichloromethane/heptane 1:1

$^1\text{H}$  NMR (**Spectrum 26**) (400 MHz, Chloroform-*d*)  $\delta$  7.30 (t,  $J$  = 7.9 Hz, 1H), 7.09 (dd,  $J$  = 8.0, 1.2 Hz, 1H), 7.03 (dt,  $J$  = 7.6, 1.0 Hz, 1H), 3.20 – 3.13 (m, 4H), 2.74 – 2.65 (m, 4H), 2.25 (s, 3H).

Mass: Calculated  $m/z$  for  $\text{C}_7\text{H}_7\text{FNO}_2^+$   $[\text{M}+\text{H}]^+$  = 239.0849; found APCI: 239.1

**16**

4-(3-methyl-2-nitrophenyl)--thiomorpholine-1,1-dioxide

**Synthesis:**

**Quantities:** **15** (331 mg, 1.39 mmol, 1 eq.); **mCPBA 77 % m/m** (747 mg, 3.33 mmol, 2.4 eq., Aldrich); **DCM** (15 + 15 mL)

**Procedure:** Dissolve **15** in 15 mL **DCM**; cool the solution to -20 °C (iso-propanol bath); dissolve mCPBA in 15 mL **DCM** and add it to the **15** solution over 30 min; stir for 4 h at 0 °C; wash the mixture with saturated  $\text{NaHCO}_3$  solution; concentrate under reduced pressure

**Purification:**

Was used without further purification. Crude product yield: 376 mg; 100 %

Analyses:

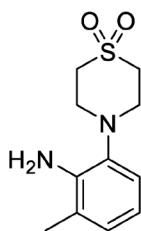
$R_F$  value: 0.7 ethyl acetate

$^1\text{H}$  NMR (**Spectrum 27**) (400 MHz, Chloroform-*d*)  $\delta$  7.36 (t,  $J = 7.9$  Hz, 1H), 7.17 (d,  $J = 8.0$  Hz, 1H), 7.13 (d,  $J = 7.7$  Hz, 1H), 3.49 – 3.41 (m, 4H), 3.16 – 3.07 (m, 4H), 2.28 (s, 3H).

Mass: Calculated  $m/z$  for  $\text{C}_{11}\text{H}_{15}\text{N}_2\text{O}_4\text{S}^+$   $[\text{M}+\text{H}]^+ = 271.3103$ ; found APCI: 271.2

**17**

4-(2-amino-3-methylphenyl)-1 $\lambda^6$ -thiomorpholine-1,1-dioxide

Synthesis:

**Quantities:** **16** (376 mg, 1.39 mmol, 1 eq.); PdOH/C 20 % m/m (75 mg (20 % m of **16**), Aldrich); **methanol** (40 mL)

**Procedure:** Dissolve **15** in 40 mL **methanol**; add catalyst; close the flask with a septum and purge the mixture with hydrogen for 30 min under stirring; add a hydrogen balloon; check for full conversion with TLC; after completion remove the catalyst with paper filter and wash the filter thoroughly with ethyl acetate; evaporate the solvents under reduced pressure

Purification:

Was used without further purification. Crude product yield: 196 mg; 58 %

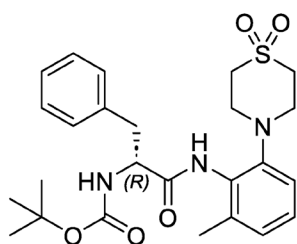
Analyses:

$R_F$  value: 0.25 ethyl acetate/heptane 1:1

Mass: Calculated  $m/z$  for  $\text{C}_{11}\text{H}_{15}\text{N}_2\text{O}_4\text{S}^+$   $[\text{M}+\text{H}]^+ = 241.1005$ ; found APCI: 241.1

**18**

tert-butyl-N-[(1R)-1-[[2-(1,1-dioxo-1 $\lambda^6$ -thiomorpholin-4-yl)-6-methylphenyl]carbamoyl]-2-phenylethyl]carbamate

**Synthesis:**

*Quantities:* **Pyridine** (15 mL); **EtOAc** (30 mL); **17** (196 mg, 0.82 mmol, 1 eq.); **N-Boc-D-phenylalanine** (238 mg, 0.90 mmol, 1.1 eq., TCI); **T3P 50 % m/V in EtOAc** (976  $\mu$ L, 1.64 mmol, 2 eq., Aldrich)

*Procedure:* Dissolve **17** and **(N)-Boc-(R)-phenylalanine** in **pyridine** and **ethyl acetate**; cool the mixture to  $-20\text{ }^{\circ}\text{C}$  before adding **T3P**; keep the temperature at  $0\text{ }^{\circ}\text{C}$  for 20 h; wash with 0.25 M  $\text{KH}_2\text{PO}_4$  solution 3x; evaporate the solvents under reduced pressure

**Purification:**

Flash chromatography heptane/methyl tert-butyl ether gradient 50 % heptane to 10 % over 8 CV on 90 g normal phase silica gel 0.63 – 0.2  $\mu\text{m}$  particle size. Yield: 222 mg; 56 %

**Analyses:**

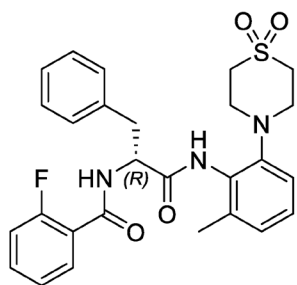
$R_f$  value: 0.35 ethyl acetate/heptane 1:1

$^1\text{H}$  NMR (**Spectrum 28**) (400 MHz, Chloroform- $d$ )  $\delta$  7.88 (s, 1H), 7.35 – 7.23 (m, 5H), 7.14 (t,  $J = 7.8$  Hz, 1H), 7.01 (d,  $J = 7.6$  Hz, 1H), 6.94 (d,  $J = 7.8$  Hz, 1H), 5.23 – 5.10 (m, 1H), 4.58 (q,  $J = 7.5$  Hz, 1H), 3.34 – 3.17 (m, 5H), 3.15 – 3.00 (m, 5H), 2.09 (s, 3H), 1.41 (s, 9H).

Mass: Calculated  $m/z$  for  $\text{C}_{25}\text{H}_{34}\text{N}_3\text{O}_5\text{S}^+$   $[\text{M}+\text{H}]^+ = 488.2214$ ; found APCI: 488.2

**19**

(2R)-N-[2-(1,1-dioxo-1 $\lambda^6$ -thiomorpholin-4-yl)-6-methylphenyl]-2-[(2-fluorophenyl)formamido]-3-phenylpropanamide

**Synthesis:**

*Quantities:* **DCM** (10 mL); **TFA** (10 mL); **18** (222 mg, 0.46 mmol) Boc-protected crude product isolation: 145 mg; Used for next step: 59 mg (0.15 mmol, 1 eq.); **THF** (10 ml); **2-fluorobenzoic acid** (26 mg, 0.18 mmol, 1.2 eq., TCI); **DEPBT** (68 mg, 0.23 mmol, 1.5 eq., BLDpharm); **DIPEA** (78  $\mu$ L, 0.47 mmol, 3 eq., Aldrich)

*Procedure:* Dissolve **18** in 10 mL **DCM** and add 10 mL **TFA** under stirring; stir for 1 h and check for full conversion by TLC; after conversion evaporate the solvents under reduced pressure; resuspend the residue in ethyl acetate and wash with saturated NaHCO<sub>3</sub> 3x; dry the organic phase with NaSO<sub>4</sub> and concentrate under reduced pressure; dissolve the Boc-protected reactant, the **2-fluorobenzoic acid** and **DEPBT** in 10 mL **THF**; add **DIPEA**; stir over night

After the reaction time the crude reaction mixture was directly evaporated on silica gel without previous washing.

#### Purification:

Flash chromatography heptane/ethyl acetate gradient 80 % heptane to 40 % over 10 CV on 45 g normal phase silica gel 0.63 – 0.2 µm particle size. Preparative HPLC afterwards. Yield: 48 mg; 62 %

#### Analyses:

R<sub>F</sub> value: 0.30 ethyl acetate/heptane 1:1

<sup>1</sup>H NMR (**Spectrum 29**) (400 MHz, Chloroform-*d*) δ 8.10 (s, 1H), 8.05 (td, *J* = 7.9, 1.9 Hz, 1H), 7.55 – 7.47 (m, 1H), 7.40 – 7.24 (m, 7H), 7.17 – 7.10 (m, 2H), 7.02 (d, *J* = 7.5 Hz, 1H), 6.96 (dd, *J* = 7.9, 1.4 Hz, 1H), 5.14 (qd, *J* = 7.1, 2.0 Hz, 1H), 3.39 (dd, *J* = 13.8, 7.0 Hz, 1H), 3.34 – 3.19 (m, 5H), 3.18 – 3.01 (m, 4H), 2.10 (s, 3H).

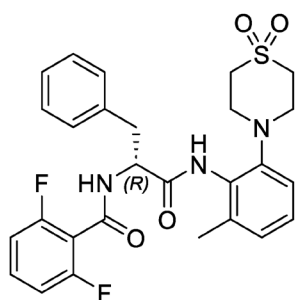
<sup>13</sup>C NMR (**Spectrum 30**) (101 MHz, Chloroform-*d*) δ 169.15, 163.77 (d, *J* = 3.3 Hz), 160.76 (d, *J* = 248.3 Hz), 146.54, 136.36, 136.20, 134.21 (d, *J* = 9.5 Hz), 131.99, 129.97, 129.50, 128.92, 127.82, 127.37, 127.28, 125.17 (d, *J* = 3.2 Hz), 119.68 (d, *J* = 11.0 Hz), 118.46, 116.27 (d, *J* = 24.7 Hz), 55.67, 52.00, 51.07, 37.30, 18.98.

Mass: Calculated m/z for C<sub>27</sub>H<sub>29</sub>FN<sub>3</sub>O<sub>4</sub>S<sup>+</sup> [M+H]<sup>+</sup> = 510.1858; found APCI: 510.3; found HRMS: [M+H]<sup>+</sup> 510.1852

HPLC purity: 98.6 %; t<sub>R</sub>=2.8 min (**HPLC-Trace 12**); (Agilent Poroshell 120, EC-C18, 3,0x50 mm, 2,7 µm, acetonitrile/water 15:85, 6 min, v=1.2 mL/min, λ=254 nm)

## **20**

(2R)-2-[(2,6-difluorophenyl)formamido]-N-[2-(1,1-dioxo-1λ<sup>6</sup>-thiomorpholin-4-yl)-6-methylphenyl]-3-phenylpropanamide



### Synthesis:

**Quantities:** Boc-protected crude product of **19** (61 mg, 0.16 mmol, 1 eq.); **THF** (10 ml); **2,6-difluorobenzoic acid** (30 mg, 0.19 mmol, 1.2 eq., TCl); **DEPBT** (71 mg, 0.24 mmol, 1.5 eq., BLDpharm); **DIPEA** (80  $\mu$ L, 0.47 mmol, 3 eq., Aldrich)

**Procedure:** Dissolve the Boc-protected reactant of **19**, the **2,6-difluorobenzoic acid** and **DEPBT** in 10 mL **THF**; add **DIPEA**; stir over night

After the reaction time the crude reaction mixture was directly evaporated on silica gel without previous washing.

### Purification:

Flash chromatography heptane/ethyl acetate gradient 70 % heptane to 30 % over 10 CV on 45 g normal phase silica gel 0.63 – 0.2  $\mu$ m particle size. Preparative HPLC afterwards. Yield: 67 mg; 81 %

### Analyses:

$R_f$  value: 0.50 heptane/ethyl acetate 1:1

$^1\text{H}$  NMR (**Spectrum 31**) (400 MHz, Chloroform-*d*)  $\delta$  8.01 (s, 1H), 7.40 – 7.23 (m, 6H), 7.14 (t,  $J = 7.8$  Hz, 1H), 7.00 (d,  $J = 7.6$  Hz, 1H), 6.95 (d,  $J = 7.9$  Hz, 1H), 6.90 (t,  $J = 8.2$  Hz, 2H), 6.81 (d,  $J = 8.0$  Hz, 1H), 5.15 (q,  $J = 7.4$  Hz, 1H), 3.36 (dd,  $J = 13.9, 7.4$  Hz, 1H), 3.32 – 3.18 (m, 5H), 3.14 – 3.03 (m, 4H), 2.07 (s, 3H).

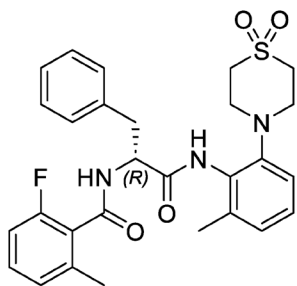
$^{13}\text{C}$  NMR (**Spectrum 32**) (101 MHz, Chloroform-*d*)  $\delta$  168.88, 160.79, 159.94 (d,  $J = 252.9$  Hz), 159.87 (d,  $J = 252.8$  Hz), 146.72, 136.52, 135.98, 132.33 (t,  $J = 10.4$  Hz), 129.71, 129.50, 128.88, 127.62, 127.44, 127.38, 118.40, 113.12 (t,  $J = 19.6$  Hz), 112.35 – 111.90 (m), 55.32, 51.92, 50.95, 37.48, 18.82.

Mass: Calculated  $m/z$  for  $\text{C}_{27}\text{H}_{28}\text{F}_2\text{N}_3\text{O}_4\text{S}^+$   $[\text{M}+\text{H}]^+ = 528.1763$ ; found APCI: 528.3; found HRMS:  $[\text{M}+\text{H}]^+ 528.1760$

HPLC purity: 99.0 %;  $t_R = 2.7$  min (**HPLC-Trace 13**); (Agilent Poroshell 120, EC-C18, 3,0x50 mm, 2,7  $\mu$ m, acetonitrile/ water 15:85, 6 min,  $v = 1.2$  mL/min,  $\lambda = 254$  nm)

## 21

(2R)-N-[2-(1,1-dioxo-1 $\lambda^6$ -thiomorpholin-4-yl)-6-methylphenyl]-2-[(2-fluoro-6-methylphenyl)formamido]-3-phenylpropanamide



### Synthesis:

**Quantities:** Boc-protected crude product of **19** (64 mg, 0.17 mmol, 1 eq.); **THF** (10 mL); **2-fluoro-6-methylbenzoic acid** (31 mg, 0.20 mmol, 1.2 eq., TCI); **DEPBT** (74 mg, 0.25 mmol, 1.5 eq., BLDpharm); **DIPEA** (84  $\mu$ L, 0.50 mmol, 3 eq., Aldrich)

**Procedure:** Dissolve the Boc-protected reactant of **19**, the **2-fluoro-6-methylbenzoic acid** and **DEPBT** in 10 mL **THF**; add **DIPEA**; stir over night

After the reaction time the crude reaction mixture was directly evaporated on silica gel without previous washing.

### Purification:

Flash chromatography heptane/ethyl acetate gradient 60 % heptane to 20 % over 10 CV on 45 g normal phase silica gel 0.63 – 0.2  $\mu$ m particle size. Preparative HPLC afterwards. Yield: 50 mg; 58 %

### Analyses:

$R_f$  value: 0.55 heptane/ethyl acetate 1:1

$^1\text{H}$  NMR (**Spectrum 33**) (400 MHz, Chloroform-*d*)  $\delta$  8.10 (s, 1H), 7.36 – 7.12 (m, 7H), 7.03 (d,  $J = 7.7$  Hz, 1H), 6.95 (dd,  $J = 16.5, 7.8$  Hz, 2H), 6.86 (t,  $J = 9.0$  Hz, 1H), 6.57 (t,  $J = 9.4$  Hz, 1H), 5.18 (td,  $J = 8.4, 6.3$  Hz, 1H), 3.44 (dd,  $J = 14.1, 6.2$  Hz, 1H), 3.29 (q,  $J = 6.1, 5.1$  Hz, 4H), 3.14 (tdd,  $J = 15.4, 10.6, 5.3$  Hz, 5H), 2.14 (s, 3H), 2.09 (s, 3H).

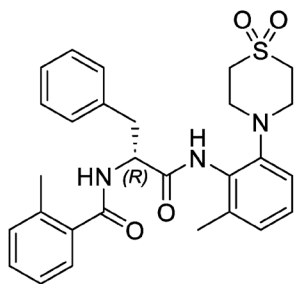
$^{13}\text{C}$  NMR (**Spectrum 34**) (101 MHz, Chloroform-*d*)  $\delta$  169.24, 165.63, 159.14 (d,  $J = 245.3$  Hz), 146.70, 138.56 (d,  $J = 2.8$  Hz), 136.54, 136.25, 130.90 (d,  $J = 9.0$  Hz), 129.81, 129.31, 128.89, 127.70, 127.43, 127.31, 126.39 (d,  $J = 2.8$  Hz), 123.73 (d,  $J = 17.0$  Hz), 118.43, 112.90 (d,  $J = 22.0$  Hz), 55.01, 51.97, 50.99, 37.55, 18.88, 18.85.

Mass: Calculated  $m/z$  for  $\text{C}_{28}\text{H}_{31}\text{FN}_3\text{O}_4\text{S}^+$   $[\text{M}+\text{H}]^+ = 524.2014$ ; found APCI: 524.4; found HRMS:  $[\text{M}+\text{H}]^+ 524.2010$

HPLC purity: 98.0 %;  $t_R = 2.8$  min (**HPLC-Trace 14**); (Agilent Poroshell 120, EC-C18, 3,0x50 mm, 2,7  $\mu$ m, acetonitrile/ water 15:85, 6 min,  $v = 1.2$  mL/min,  $\lambda = 254$  nm)

## 22

(2R)-N-[2-((1,1-dioxo-1 $\lambda^6$ -thiomorpholin-4-yl)-6-methylphenyl)-2-[(2-methylphenyl)formamido]-3-phenylpropanamide



### Synthesis:

**Quantities:** Boc-deprotected crude product of **19** (67 mg, 0.17 mmol, 1 eq.); **THF** (10 mL); **2-methylbenzoic acid** (28 mg, 0.21 mmol, 1.2 eq., TCI); **PyBOP** (135 mg, 0.26 mmol, 1.5 eq., Carbolution); **DIPEA** (88  $\mu$ L, 0.52 mmol, 3 eq., Aldrich)

**Procedure:** Dissolve the Boc-deprotected reactant of **19**, the **2-methylbenzoic acid** and **PyBOP** in 10 mL **THF**; add **DIPEA**; stir over night

After the reaction time the crude reaction mixture was directly evaporated on silica gel without previous washing.

### Purification:

Flash chromatography heptane/ethyl acetate gradient 75 % heptane to 30 % over 8 CV on 8 g normal phase silica gel 0.63 – 0.2  $\mu$ m particle size. Preparative HPLC afterwards. Yield: 14 mg; 16 %

### Analyses:

$R_f$  value: 0.20 heptane/ethyl acetate 1:1

$^1\text{H}$  NMR (**Spectrum 35**) (400 MHz, Chloroform-*d*)  $\delta$  8.11 (s, 1H), 7.41 – 7.26 (m, 6H), 7.23 – 7.12 (m, 4H), 7.04 (d,  $J$  = 7.6 Hz, 1H), 6.98 (dd,  $J$  = 7.9, 1.4 Hz, 1H), 6.31 (d,  $J$  = 7.6 Hz, 1H), 5.03 (q,  $J$  = 7.5 Hz, 1H), 3.42 (dd,  $J$  = 14.0, 7.1 Hz, 1H), 3.39 – 3.24 (m, 4H), 3.20 (dd,  $J$  = 14.0, 7.9 Hz, 1H), 3.18 – 3.09 (m, 4H), 2.32 (s, 3H), 2.15 (s, 3H).

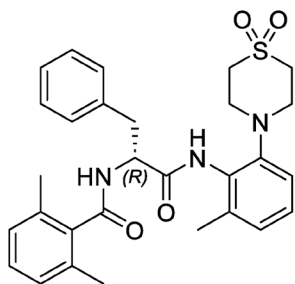
$^{13}\text{C}$  NMR (**Spectrum 36**) (101 MHz, Chloroform-*d*)  $\delta$  170.40, 169.57, 146.31, 136.49, 136.32, 136.25, 134.64, 131.33, 130.60, 129.81, 129.34, 128.99, 127.83, 127.44, 127.36, 126.72, 125.92, 118.33, 55.38, 52.06, 51.08, 37.37, 19.84, 18.99.

Mass: Calculated  $m/z$  for  $\text{C}_{28}\text{H}_{32}\text{N}_3\text{O}_4\text{S}^+$   $[\text{M}+\text{H}]^+ = 506.2108$ ;  $[\text{M}+\text{Na}]^+ = 528.1927$ ; found APCI: 506.1; found HRMS:  $[\text{M}+\text{H}]^+ 506.2112$ ;  $[\text{M}+\text{Na}]^+ 528.1932$

HPLC purity: 97.3 %;  $t_R = 2.8$  min (**HPLC-Trace 15**); (Agilent Poroshell 120, EC-C18, 3,0x50 mm, 2,7  $\mu$ m, acetonitrile/ water 15:85, 6 min,  $v = 1.2$  mL/min,  $\lambda = 254$  nm)

## 23

(2R)-2-[(2,6-dimethylphenyl)formamido]-N-[2-(1,1-dioxo-1 $\lambda^6$ -thiomorpholin-4-yl)-6-methylphenyl]-3-phenylpropanamide

**Synthesis:**

**Quantities:** Boc-protected crude product of **19** (74 mg, 0.19 mmol, 1 eq.); **DMF** (10 mL); **2,6-dimethylbenzoic acid** (35 mg, 0.23 mmol, 1.2 eq., TCI); **PyBOP** (198 mg, 0.38 mmol, 2 eq., Carbolution); **DIPEA** (97  $\mu$ L, 0.57 mmol, 3 eq., Aldrich)

**Procedure:** Dissolve the Boc-protected reactant of **19**, the **2,6-dimethylbenzoic acid** and **PyBOP** in 10 mL **DMF**; add **DIPEA**; stir over night

After the reaction time the crude reaction mixture was directly evaporated on silica gel without previous washing.

**Purification:**

Flash chromatography heptane/ethyl acetate gradient 70 % heptane to 30 % over 8 CV on 8 g normal phase silica gel 0.63 – 0.2  $\mu$ m particle size. Preparative HPLC afterwards. Yield: 76 mg; 77 %

**Analyses:**

$R_F$  value: 0.30 heptane/ethyl acetate 1:1

$^1\text{H}$  NMR (**Spectrum 37**) (400 MHz, Chloroform-*d*)  $\delta$  8.26 (s, 1H), 7.38 – 7.31 (m, 4H), 7.31 – 7.26 (m, 1H), 7.17 (t,  $J = 7.8$  Hz, 1H), 7.12 (t,  $J = 7.6$  Hz, 1H), 7.06 (d,  $J = 7.6$  Hz, 1H), 7.00 (d,  $J = 7.8$  Hz, 1H), 6.94 (d,  $J = 7.6$  Hz, 2H), 6.20 (d,  $J = 7.6$  Hz, 1H), 5.13 (ddd,  $J = 9.6, 7.6, 5.8$  Hz, 1H), 3.44 (dd,  $J = 14.3, 5.8$  Hz, 1H), 3.41 – 3.25 (m, 4H), 3.20 (s, 4H), 3.07 (dd,  $J = 14.3, 9.6$  Hz, 1H), 2.18 (s, 3H), 2.03 (s, 6H).

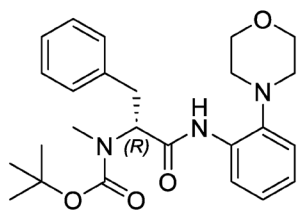
$^{13}\text{C}$  NMR (**Spectrum 38**) (126 MHz, Chloroform-*d*)  $\delta$  170.97, 169.82, 146.18, 136.33, 136.25, 136.15, 134.27, 129.80, 129.17, 129.07, 129.01, 127.88, 127.52, 127.42, 127.28, 118.29, 54.89, 52.07, 51.08, 37.76, 19.13, 18.81.

Mass: Calculated  $m/z$  for  $\text{C}_{29}\text{H}_{34}\text{N}_3\text{O}_4\text{S}^+$   $[\text{M}+\text{H}]^+ = 520.2265$ ;  $[\text{M}+\text{Na}]^+ = 542.2084$ ; found APCI: 520.5; found HRMS:  $[\text{M}+\text{H}]^+ 520.2271$ ;  $[\text{M}+\text{Na}]^+ 542.2088$

HPLC purity: 99.3 %;  $t_R = 3.0$  min (**HPLC-Trace 16**); (Agilent Poroshell 120, EC-C18, 3,0x50 mm, 2,7  $\mu$ m, acetonitrile/ water 15:85, 6 min,  $v = 1.2$  mL/min,  $\lambda = 254$  nm)

**24**

tert-butyl (*R*)-methyl(1-((2-morpholinophenyl)amino)-1-oxo-3-phenylpropan-2-yl)carbamate

**Synthesis:**

**Quantities:** Pyridine (5 mL); EtOAc (10 mL); **2-morpholinoaniline** (166 mg, 0.94 mmol, 1 eq.); **N-Boc-N-methyl-(R)-phenylalanine** (289 mg, 1.1 mmol, 1.1 eq.); **T3P 50 % m/v in EtOAc** (559  $\mu$ L, 1.88 mmol, 2.0 eq.)

**Procedure:** **2-Morpholinoaniline** and **N-Boc-N-methyl-(R)-phenylalanine** were dissolved in a 1:2 mixture of distilled pyridine and EtOAc. The mixture was cooled to -20 °C with an isopropanol dry-ice bath before **T3P 50 % m/v in EtOAc** was added. After the addition, the cooling bath was removed, and the mixture was stirred for 20 h at room temperature. Afterwards the mixture was washed with 0.25 M  $\text{KH}_2\text{PO}_4$  solution three times before the organic phase was evaporated on silica gel under reduced pressure for purification.

**Purification:**

Flash chromatography ethyl acetate/heptane gradient 80 % heptane to 40 % over 8 CV on 45 g. Yield: 162 mg; 39 %

**Analyses:**

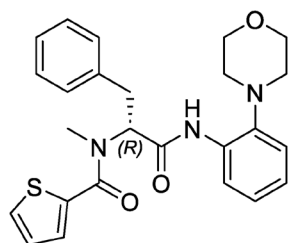
$R_f$  value: 0.25 ethyl acetate/heptane 1:1

$^1\text{H}$  NMR (**Spectrum 39**) (400 MHz, Chloroform-*d*)  $\delta$  9.25 – 9.14 (m, 1H), 8.51 – 8.41 (m, 1H), 7.32 – 7.05 (m, 8H), 5.27 – 5.20 (m, 1H), 4.86 – 4.78 (m, 0H), 3.89 – 3.75 (m, 4H), 3.59 – 3.47 (m, 1H), 3.01 – 2.93 (m, 1H), 2.91 – 2.66 (m, 7H), 1.42 – 1.10 (m, 9H).

Mass: Calculated  $m/z$  for  $\text{C}_{25}\text{H}_{34}\text{N}_3\text{O}_4^+$   $[\text{M}+\text{H}]^+ = 440.2544$ ; found APCI:  $[\text{M}+\text{H}]^+ 440.1$

**25**

(*R*)-*N*-methyl-*N*-(1-((2-morpholinophenyl)amino)-1-oxo-3-phenylpropan-2-yl)thiophene-2-carboxamide



**Synthesis:**

**Quantities:** DCM (2 mL); TFA (2 mL); **24** (100 mg, 0.23 mmol, 1.0 eq.); **thiophene-2-carboxylic acid** (30 mg, 0.23 mmol, 1.0 eq.); **PyBOP** (132 mg, 0.25 mmol, 1.1 eq.); **DMF** (5 mL), **DIPEA** (120  $\mu$ L, 0.69 mmol, 3.0 eq.)

**Procedure:** Dissolve **24** in **DCM** and add **TFA** under stirring; stir for 1 h and check for full conversion by TLC; after conversion evaporate the solvents under reduced pressure; followed by coevaporation with toluene 3x, DCM 3x; dissolve the Boc-protected reactant, the **thiophene-2-carboxylic acid** and **PyBOP** in **DMF**; add **DIPEA**; stir over night at 65 °C under argon and light protection.

After the reaction time the crude reaction mixture was directly evaporated on silica gel without previous washing.

**Purification:**

Flash chromatography ethyl acetate/heptane gradient 95 % heptane to 50 % over 10 CV on 45 g. Yield: 38 mg; 37 %

**Analyses:**

$R_F$  value: 0.25 ethyl acetate/heptane 1:1

$^1\text{H}$  NMR (**Spectrum 40**) (400 MHz, Chloroform-*d*)  $\delta$  9.44 (s, 1H), 8.46 (d,  $J = 8.1$  Hz, 1H), 7.46 (d,  $J = 5.0$  Hz, 1H), 7.36 – 7.26 (m, 4H), 7.24 – 7.05 (m, 5H), 7.03 – 6.97 (m, 1H), 5.63 (s, 1H), 3.93 (s, 4H), 3.51 (dd,  $J = 14.8, 6.7$  Hz, 1H), 3.23 (s, 1H), 3.19 (s, 3H), 2.88 – 2.75 (m, 4H).

$^{13}\text{C}$  NMR (**Spectrum 41**) (126 MHz, Chloroform-*d*)  $\delta$  168.1, 165.6, 141.4, 137.1, 134.0, 130.3, 129.0, 128.8, 127.1, 126.9, 125.8, 124.2, 121.2, 119.7, 67.4, 59.5, 52.9, 33.9.

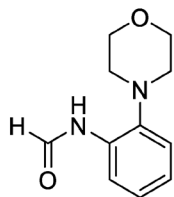
Additional HSQC is provided because of superimposed signals (**Spectrum 42**).

Mass: Calculated  $m/z$  for  $\text{C}_{25}\text{H}_{28}\text{N}_3\text{O}_3\text{S}^+$   $[\text{M}+\text{H}]^+ = 450.1846$ ;  $[\text{M}+\text{Na}]^+ = 472.1665$ ; found APCI:  $[\text{M}+\text{H}]^+ 450.1$ ; found HRMS:  $[\text{M}+\text{H}]^+ 450.1850$ ;  $[\text{M}+\text{Na}]^+ 472.1668$

HPLC purity: 98.4 %;  $t_R = 3.3$  min (**HPLC-Trace 17**); (Agilent Poroshell 120, EC-C18, 3,0x50 mm, 2,7  $\mu\text{m}$ , acetonitrile/ water 15:85, 6 min,  $v = 1.2$  mL/min,  $\lambda = 254$  nm)

**26**

*N*-(2-morpholinophenyl)formamide



#### Synthesis:

**Quantities:** **Formic acid** (422  $\mu$ L, 11.2 mmol, 4.0 eq.); **2-morpholinoaniline** (500 mg, 2.8 mmol, 1.0 eq.); **sodium formate** (38 mg, 0.56 mmol, 0.2 eq.)

**Procedure:** **2-morpholinoaniline** and **sodium formate** were suspended in **formic acid** and stirred at room temperature overnight.

#### Purification:

The reaction mixture was poured in ethyl acetate and washed with saturated  $\text{NaHCO}_3$  solution three times. Followed by flash chromatography ethyl acetate/DCM gradient 70 % ethyl acetate to 30 % over 13 CV on 45 g. Yield: 456 mg; 79 %

#### Analyses:

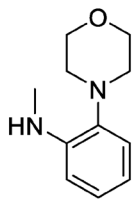
$R_f$  value: 0.15 ethyl acetate/DCM 9:1

$^1\text{H}$  NMR (**Spectrum 43**) (400 MHz, Chloroform- $d$ )  $\delta$  8.87 (d,  $J$  = 11.9 Hz, 0.4H), 8.51 (s, 1H), 8.39 (dd,  $J$  = 8.0, 1.5 Hz, 0.6H), 8.14 (s, 1H), 7.25 – 7.08 (m, 3H), 3.93 – 3.78 (m, 4H), 2.93 – 2.79 (m, 4H).

Mass: Calculated  $m/z$  for  $\text{C}_{11}\text{H}_{15}\text{N}_2\text{O}_2^+$   $[\text{M}+\text{H}]^+ = 207.1128$ ; found APCI:  $[\text{M}+\text{H}]^+ 207.0$

## 27

*N*-methyl-2-morpholinoaniline

**Synthesis:**

**Quantities:** **26** (457 mg, 2.21 mmol, 1.0 eq.); **LiAlH<sub>4</sub> 1 M in THF** (4.4 mL, 4.42 mmol, 2.0 eq.); **THF** (10 mL)

**Procedure:** **26** was dissolved in **THF** and **LiAlH<sub>4</sub> 1 M in THF** was added dropwise over 30 minutes at 0 °C under argon atmosphere. The reaction mixture was warmed to room temperature and stirred overnight.

**Purification:**

The reaction mixture was quenched by addition of water and the aqueous phase was extracted with ethyl acetate 3x. Followed by flash chromatography ethyl acetate/heptane gradient 95 % ethyl acetate to 50 % over 8 CV on 45 g. Yield: 219 mg; 51 %

**Analyses:**

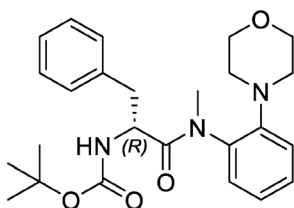
$R_f$  value: 0.45 ethyl acetate/heptane 1:1

<sup>1</sup>H NMR (**Spectrum 44**) (400 MHz, Chloroform-*d*)  $\delta$  7.08 (td,  $J = 7.7, 1.5$  Hz, 1H), 7.02 (dd,  $J = 7.8, 1.5$  Hz, 1H), 6.71 (td,  $J = 7.6, 1.4$  Hz, 1H), 6.64 (dd,  $J = 8.0, 1.4$  Hz, 1H), 4.73 (s, 1H), 3.85 (t,  $J = 4.5$  Hz, 4H), 2.92 – 2.88 (m, 4H), 2.87 (s, 3H).

Mass: Calculated  $m/z$  for  $C_{11}H_{17}N_2O^+$   $[M+H]^+ = 193.1335$ ; found APCI:  $[M+H]^+ 193.0$

**28**

tert-butyl (*R*)-(1-(methyl(2-morpholinophenyl)amino)-1-oxo-3-phenylpropan-2-yl)carbamate

**Synthesis:**

*Quantities:* **Pyridine** (5 mL); **EtOAc** (10 mL); **27** (125 mg, 0.65 mmol, 1.0 eq.); **N-Boc-(R)-phenylalanine** (189 µg, 0.72 mmol, 1.1 eq.); **T3P 50 % m/v in EtOAc** (774 µL, 1.30 mmol, 2.0 eq.)

*Procedure:* **27** and **N-Boc-(R)-phenylalanine** were dissolved in a 1:2 mixture of distilled **pyridine** and **EtOAc**. The mixture was cooled to -20 °C with an isopropanol dry-ice bath before **T3P 50 % m/v in EtOAc** was added. After the addition, the cooling bath was removed, and the mixture was stirred for 20 h at room temperature. Afterwards the mixture was washed with 0.25 M  $\text{KH}_2\text{PO}_4$  solution three times before the organic phase was evaporated on silica gel under reduced pressure for purification.

Purification:

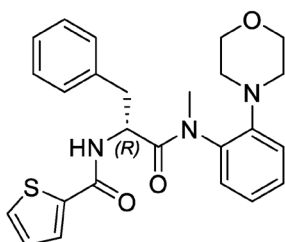
Flash chromatography ethyl acetate/heptane gradient 80 % ethyl acetate to 50 % over 9 CV on 45 g. Yield: 95 mg; 33 %

Analyses:

Mass: Calculated  $m/z$  for  $\text{C}_{25}\text{H}_{34}\text{N}_3\text{O}_4^+$   $[\text{M}+\text{H}]^+ = 440.2544$ ; found APCI:  $[\text{M}+\text{H}]^+ 440.2$

## 29

(R)-N-(1-(methyl(2-morpholinophenyl)amino)-1-oxo-3-phenylpropan-2-yl)thiophene-2-carboxamide



Synthesis:

*Quantities:* **DCM** (2 mL); **TFA** (2 mL); **28** (95 mg, 0.22 mmol, 1.0 eq.); **thiophene-2-carboxylic acid** (28 mg, 0.22 mmol, 1.0 eq.); **PyBOP** (125 mg, 0.24 mmol, 1.1 eq.); **DCM** (2 mL), **DIPEA** (114 µL, 0.66 mmol, 3.0 eq.)

*Procedure:* Dissolve **28** in **DCM** and add **TFA** under stirring; stir for 1 h and check for full conversion by TLC; after conversion evaporate the solvents under reduced pressure; followed by coevaporation with toluene 3x, DCM 3x; dissolve the Boc-protected reactant, the **thiophene-2-carboxylic acid** and **PyBOP** in **DMF**; add **DIPEA**; stir over night at 65 °C under argon and light protection.

After the reaction time the crude reaction mixture was directly evaporated on silica gel without previous washing.

Purification:

Flash chromatography ethyl acetate/heptane gradient 80 % heptane to 40 % over 7 CV on 45 g. Yield: 76 mg; 77 %

Analyses:

$R_f$  value: 0.45 ethyl acetate/heptane 4:1

$^1\text{H}$  NMR (**Spectrum 45**) (400 MHz, Chloroform-*d*)  $\delta$  7.52 (dd,  $J = 3.7, 1.0$  Hz, 1H), 7.47 (dd,  $J = 5.0, 1.1$  Hz, 1H), 7.24 – 7.18 (m, 4H), 7.11 – 7.02 (m, 2H), 7.02 – 6.93 (m, 3H), 6.86 (td,  $J = 7.6, 1.4$  Hz, 1H), 6.18 (dd,  $J = 7.8, 1.5$  Hz, 1H), 4.95 – 4.87 (m, 1H), 3.65 – 3.57 (m, 2H), 3.55 – 3.45 (m, 2H), 3.21 (s, 3H), 2.93 – 2.83 (m, 4H), 2.78 – 2.70 (m, 2H).

$^{13}\text{C}$  NMR (**Spectrum 46**) (126 MHz, Chloroform-*d*)  $\delta$  172.7, 160.4, 148.4, 139.1, 136.5, 136.5, 130.3, 129.7, 128.9, 128.5, 128.1, 128.1, 127.9, 126.9, 124.2, 120.4, 67.1, 52.5, 51.7, 41.0, 37.1.

Mass: Calculated  $m/z$  for  $\text{C}_{25}\text{H}_{28}\text{N}_3\text{O}_3\text{S}^+$   $[\text{M}+\text{H}]^+ = 450.1846$ ;  $[\text{M}+\text{Na}]^+ = 472.1665$ ; found APCI:  $[\text{M}+\text{H}]^+ 450.1$ ; found HRMS:  $[\text{M}+\text{H}]^+ 450.1850$ ;  $[\text{M}+\text{Na}]^+ 472.1670$

HPLC purity: 96.3 %;  $t_{\text{R}} = 2.9$  min (**HPLC-Trace 18**); (Agilent Poroshell 120, EC-C18, 3,0x50 mm, 2,7  $\mu\text{m}$ , acetonitrile/ water 15:85, 6 min,  $v = 1.2$  mL/min,  $\lambda = 254$  nm)



**5.4) Supplementary Information Publication III**

**Broad-Spectrum *In Vitro* Activity of *N*-aroyl-*N*-aryl-Phenylalanine Amides against Non-Tuberculous Mycobacteria and Comparative Analysis of RNA Polymerases**

Markus Lang, Uday S. Ganapathy, Lea Mann, Rüdiger W. Seidel, Richard Goddard, Frank Erdmann, Thomas Dick, Adrian Richter

**MDPI**

**Antibiotics**

*Antibiotics* **2024**, *13*(5), 404

Publication Date: 28.04.2024

DOI: [10.3390/antibiotics13050404](https://doi.org/10.3390/antibiotics13050404)

# Supplementary Information

Broad-Spectrum *In Vitro* Activity of  
*N*- $\alpha$ -aroyl-*N*-aryl-Phenylalanine Amides  
Against Non-Tuberculous Mycobacteria  
and Comparative Analysis of RNA  
Polymerases

---

**Table S 1.** MIC<sub>90</sub> values of a selection of AAPs against type strains of the *Mycobacterium abscessus* complex. Cell shading from green to red indicates high to low activity. The displayed values are average values of two technical replicates. For detailed information on the origin of clinical isolates see Materials & Methods section of the main manuscript.

	<i>M. abscessus</i> subsp. <b>abscessus</b> ATCC 19977	<i>M. abscessus</i> subsp. <b>massiliense</b> CCUG 48898-T	<i>M. abscessus</i> subsp. <b>bolletii</b> CCUG 50184-T
ID	MIC <sub>90</sub> [μM]	MIC <sub>90</sub> [μM]	MIC <sub>90</sub> [μM]
CLR	1.5	0.2	0.5
MMV	6.4	9.1	4.4
1	7.3	5.7	1.9
2	4.7	4.8	2.1
3	2.1	2.8	8.5
4	2.6	4.4	3.6
5	1.5	2.3	2.3
6	5.0	4.0	2.0
7	1.8	2.0	2.1
8	1.5	1.4	1.7
9	4.8	4.4	6.5
10	2.2	2.6	9.0

**Table S 2.** MIC<sub>90</sub> values of a selection of AAPs against a panel of *Mycobacterium abscessus* complex clinical isolates. Cell shading from green to red indicates high to low activity. The displayed values are average values of two technical replicates. For detailed information on the origin of clinical isolates see Materials & Methods section of the main manuscript.

	<i>M. abscessus</i> subsp. <b>abscessus</b> Bamboo	<i>M. abscessus</i> subsp. <b>abscessus</b> M9	<i>M. abscessus</i> subsp. <b>abscessus</b> M199	<i>M. abscessus</i> subsp. <b>abscessus</b> M337	<i>M. abscessus</i> subsp. <b>abscessus</b> M404
ID	MIC <sub>90</sub> [μM]	MIC <sub>90</sub> [μM]	MIC <sub>90</sub> [μM]	MIC <sub>90</sub> [μM]	MIC <sub>90</sub> [μM]
CLR	0.5	6.7	19.5	7.3	0.8
MMV	8.2	26.4	29.3	9.8	14.2
7	2.1	8.1	9.5	3.5	6.1
8	2.3	5.8	9.3	3.9	7.0

	<i>M. abscessus</i> subsp. <b>abscessus</b> M422	<i>M. abscessus</i> subsp. <b>bolletii</b> M232	<i>M. abscessus</i> subsp. <b>bolletii</b> M506	<i>M. abscessus</i> subsp. <b>massiliense</b> M111
ID	MIC <sub>90</sub> [μM]	MIC <sub>90</sub> [μM]	MIC <sub>90</sub> [μM]	MIC <sub>90</sub> [μM]
CLR	4.2	10.6	1.1	0.5
MMV	13.4	6.0	10.8	6.8
7	1.8	3.9	2.9	3.4
8	1.8	4.6	2.9	5.6

**Table S 3.** MIC<sub>90</sub> values of a selection of AAPs against type strains of the *Mycobacterium avium* complex. Cell shading from green to red indicates high to low activity. The displayed values are average values of two technical replicates. For detailed information on the origin of clinical isolates see Materials & Methods section of the main manuscript.

	<i>M. avium</i> subsp. <i>hominissuis</i> MAC109	<i>M. avium</i> subsp. <i>hominissuis</i> M. avium 11	<i>M. intracellulare</i> subsp. <i>intracellulare</i> ATCC 13950	<i>M. intracellulare</i> subsp. <i>chimaera</i> CCUG 50989
ID	MIC <sub>90</sub> [μM]	MIC <sub>90</sub> [μM]	MIC <sub>90</sub> [μM]	MIC <sub>90</sub> [μM]
CLR	1.7	0.4	0.6	0.5
MMV	> 50 <sup>a</sup>	3.2	3.2	2.0
1	19.0	1.7	3.4	1.4
2	14.1	1.6	1.9	1.3
3	13.5	1.4	1.2	0.8
4	14.4	1.4	1.0	0.7
5	8.5	1.2	0.9	0.7
6	9.6	1.2	1.4	0.7
7	12.5	1.0	1.2	0.6
8	6.3	0.6	0.5	0.3
9	22.6	1.5	1.7	1.1
10	9.6	1.0	1.1	0.6

<sup>a</sup> incubation of *M. avium* subsp. *hominissuis* MAC109 with MMV did not reach 90% growth inhibition. MIC<sub>75</sub> = 6.6 μM.

**Table S 4.** MIC<sub>90</sub> values of a selection of AAPs against type strains of the different NTM. Cell shading from green to red indicates high to low activity. The displayed values are average values of two technical replicates. For detailed information on the origin of clinical isolates see Materials & Methods section of the main manuscript.

	<i>M. chelonae</i> ATCC 35752	<i>M. fortuitum</i> ATCC 6841	<i>M. szulgai</i> ATCC 35799	<i>M. xenopi</i> ATCC 19250	<i>M. ulcerans</i> S4018	<i>M. marinum</i> ATCC 927	<i>M. simiae</i> <sup>a</sup> ATCC 25275	<i>M. malmoense</i> <sup>a</sup> ATCC 29571	<i>M. kansasii</i> ATCC 12478
ID	MIC <sub>90</sub> [μM]	MIC <sub>90</sub> [μM]	MIC <sub>90</sub> [μM]	MIC <sub>90</sub> [μM]	MIC <sub>90</sub> [μM]	MIC <sub>90</sub> [μM]	MIC <sub>90</sub> [μM]	MIC <sub>90</sub> [μM]	MIC <sub>90</sub> [μM]
CLR	0.1	2.9	0.2	0.1	0.12	9.1	> 100	3.4	0.4
MMV	0.8	1.5	1.6	48.8	0.47	2.2	> 100	> 100	0.5
1	0.4	2.0	2.8	24.1	0.16	9.6	> 100	> 100	2.6
2	0.3	0.9	1.4	21.2	0.09	3.2	43.0	> 100	0.6
3	0.2	1.5	1.1	6.9	0.08	2.7	54.1	16.1	0.7
4	0.4	1.7	1.8	7.0	0.13	6.5	> 100	18.2	0.7
5	0.4	1.4	0.9	3.3	0.10	2.4	45.7	> 100	0.3
6	0.5	1.5	9.0	1.8	0.05	13.9	> 100	> 100	2.8
7	0.2	0.8	0.5	8.0	0.06	1.2	> 100	2.3	0.2
8	0.2	0.6	0.5	3.3	0.02	1.4	20.9	4.9	0.2
9	0.5	1.6	1.2	10.0	0.14	3.1	> 100	> 100	0.8
10	0.4	1.0	0.7	5.2	0.08	1.9	33.5	5.8	0.5

<sup>a</sup> In some cases 90% growth inhibition was not reached for *M. simiae* ATCC 25275 and for *M. malmoense* ATCC 29571. MIC<sub>75</sub> values are displayed:

	<i>M. simiae</i> ATCC 25275	<i>M. malmoense</i> ATCC 29571
ID	MIC <sub>75</sub> [ $\mu$ M]	MIC <sub>75</sub> [ $\mu$ M]
<b>CLR</b>	29.3	0.6
<b>MMV</b>	25.2	3.1
<b>1</b>	36.9	2.8
<b>2</b>	13.7	1.7
<b>3</b>	16.4	1.8
<b>4</b>	17.9	2.2
<b>5</b>	11.0	1.7
<b>6</b>	20.9	5.5
<b>7</b>	6.3	1.1
<b>8</b>	6.9	0.6
<b>9</b>	20.5	1.7
<b>10</b>	11.2	1.3



**Table S 6.** Alignment of RpoC primary sequences of all tested strains from position 500-580. Position numbering refers to PDB: 5UHE. Dots represent amino acid identity.

RpoC		<i>M. tuberculosis</i> ATCC 25618/H37Rv PDB: 5UHE	<i>M. chelonae</i> ATCC 35752	<i>M. fortuitum</i> ATCC 6841	<i>M. szulgai</i> ATCC 35799	<i>M. xenopi</i> ATCC 19250	<i>M. ulcerans</i> S4018	<i>M. marinum</i> ATCC 927	<i>M. simiae</i> ATCC 25275	<i>M. malmoense</i> ATCC 29571	<i>M. kansasii</i> ATCC 12478	<i>M. intracellulare</i> ssp. <i>chimaera</i> CCUG 50989	<i>M. avium</i> ssp. <i>hominissus</i> MAC109	<i>M. abscessus</i> ssp. <i>abscessus</i> ATCC 19977	<i>M. intracellulare</i> ssp. <i>intracellulare</i> ATCC 13950	<i>E. coli</i> ATCC 11775
1	800	I	.	.	.	.	.	.	.	.	.	.	.	T	.	Y
2	801	T	.	.	.	.	.	.	.	.	.	.	.	L	.	M
3	802	I	.	.	.	.	.	.	.	.	.	.	.	L	.	M
4	803	V	.	.	.	.	.	.	.	.	.	.	.	P	.	A
5	804	D	E	K	.	E	.	.	.	.	.	.	.	K	.	.
6	805	S	.	.	.	.	.	.	.	.	.	.	.	.	.	.
7	806	G	.	.	.	.	.	.	.	.	.	.	.	.	.	.
8	807	A	.	.	.	.	.	.	.	.	.	.	.	.	.	.
9	808	T	.	.	.	.	.	.	.	.	.	.	.	.	.	R
10	809	G	.	.	.	.	.	.	.	.	.	.	.	.	.	.
11	810	N	.	.	.	.	.	.	.	.	.	.	.	.	.	S
12	811	F	.	L	.	.	.	.	.	.	.	.	.	M	.	A
13	812	T	.	.	.	.	.	.	.	.	.	.	.	.	.	A
14	813	Q	.	.	.	.	.	.	.	.	.	.	.	.	.	.
15	814	T	.	.	.	.	.	.	.	.	.	.	.	V	.	I
16	815	R	.	.	.	.	.	.	.	.	.	.	.	.	.	.
17	816	T	.	.	.	.	.	.	.	.	.	.	.	N	.	Q
18	817	L	.	.	.	.	.	.	.	.	.	.	.	.	.	.
19	818	A	.	.	.	.	.	.	.	.	.	.	.	.	.	.
20	819	G	.	.	.	.	.	.	.	.	.	.	.	.	.	.
21	820	M	.	.	.	.	.	.	.	.	.	.	.	.	.	.
22	821	K	.	.	.	.	.	.	.	.	.	.	.	.	.	R
23	822	G	.	.	.	.	.	.	.	.	.	.	.	.	.	.
24	823	L	.	.	.	.	.	.	.	.	.	.	.	.	.	.
25	824	V	.	.	.	.	.	.	.	.	.	.	.	.	.	M
26	825	T	.	.	.	.	.	.	.	.	.	.	.	.	.	A
27	826	N	.	.	.	.	.	.	.	.	.	.	.	.	.	K
28	827	P	.	.	.	.	.	.	.	.	.	.	.	.	.	.
29	828	K	.	.	.	.	.	.	.	.	.	.	.	.	.	D
30	829	G	.	.	.	.	.	.	.	.	.	.	.	.	.	.
31	830	E	.	.	.	.	.	.	.	.	.	.	.	.	.	S
32	831	F	.	.	.	.	.	.	.	.	.	.	.	Y	.	I
33	832	I	.	.	.	.	.	.	.	.	.	.	.	.	.	.
34	833	P	.	.	.	.	.	.	.	.	.	.	.	.	.	E
35	834	R	.	.	.	.	.	.	.	.	.	.	.	.	.	T
36	835	P	.	.	.	.	.	.	.	.	.	.	.	.	.	.
37	836	V	I	I	.	I	I	I	.	.	.	.	.	I	.	I
38	837	K	.	.	.	.	.	.	.	.	.	.	.	.	.	T
39	838	S	.	.	.	.	.	.	.	.	.	.	.	.	.	A
40	839	S	.	.	.	.	.	.	.	.	.	.	.	.	.	N
41	840	F	.	.	.	.	.	.	.	.	.	.	.	.	.	.
42	841	R	.	.	.	.	.	.	.	.	.	.	.	.	.	.
43	842	E	.	.	.	.	.	.	.	.	.	.	.	.	.	.
44	843	G	.	.	.	.	.	.	.	.	.	.	.	.	.	.
45	844	L	.	.	.	.	.	.	.	.	.	.	.	.	.	.
46	845	T	.	.	.	.	.	.	.	.	.	.	.	.	.	N
47	846	V	.	.	.	.	.	.	.	.	.	.	.	.	.	.
48	847	L	.	.	.	.	.	.	.	.	.	.	.	.	.	.
49	848	E	.	.	.	.	.	.	.	.	.	.	.	.	.	Q
50	849	Y	.	.	.	.	.	.	.	.	.	.	.	.	.	.
51	850	F	.	.	.	.	.	.	.	.	.	.	.	.	.	.
52	851	I	.	.	.	.	.	.	.	.	.	.	.	.	.	.
53	852	N	.	.	.	.	.	.	.	.	.	.	.	.	.	S
54	853	T	.	.	.	.	.	.	.	.	.	.	.	.	.	.
55	854	H	.	.	.	.	.	.	.	.	.	.	.	.	.	.
56	855	G	.	.	.	.	.	.	.	.	.	.	.	.	.	.
57	856	A	.	.	.	.	.	.	.	.	.	.	.	.	.	.
58	857	R	.	.	.	.	.	.	.	.	.	.	.	.	.	.
59	858	K	.	.	.	.	.	.	.	.	.	.	.	.	.	.
60	859	G	.	.	.	.	.	.	.	.	.	.	.	.	.	.
61	860	L	.	.	.	.	.	.	.	.	.	.	.	.	.	.
62	861	A	.	.	.	.	.	.	.	.	.	.	.	.	.	.
63	862	D	.	.	.	.	.	.	.	.	.	.	.	.	.	.
64	863	T	.	.	.	.	.	.	.	.	.	.	.	.	.	.
65	864	A	.	.	.	.	.	.	.	.	.	.	.	.	.	.
66	865	L	.	.	.	.	.	.	.	.	.	.	.	.	.	.
67	866	R	.	.	.	.	.	.	.	.	.	.	.	.	.	K
68	867	T	.	.	.	.	.	.	.	.	.	.	.	.	.	.
69	868	A	.	.	.	.	.	.	.	.	.	.	.	.	.	.
70	869	D	.	.	.	.	.	.	.	.	.	.	.	.	.	N
71	870	S	.	.	.	.	.	.	.	.	.	.	.	.	.	.
72	871	G	.	.	.	.	.	.	.	.	.	.	.	.	.	.
73	872	Y	.	.	.	.	.	.	.	.	.	.	.	.	.	.
74	873	L	.	.	.	.	.	.	.	.	.	.	.	.	.	.
75	874	T	.	.	.	.	.	.	.	.	.	.	.	.	.	.
76	875	R	.	.	.	.	.	.	.	.	.	.	.	.	.	.
77	876	R	.	.	.	.	.	.	.	.	.	.	.	.	.	.
78	877	L	.	.	.	.	.	.	.	.	.	.	.	.	.	.
79	878	V	.	.	.	.	.	.	.	.	.	.	.	.	.	.
80	879	D	.	.	.	.	.	.	.	.	.	.	.	.	.	.
81	880	V	.	.	.	.	.	.	.	.	.	.	.	.	.	.

Direct drug-target contacts

Reported resistance after mutation

7 Å distance from target bound D-AMP1



# Publication List

## Scientific Articles

**Lang, M.**, Ganapathy, U. S., Abdelaziz, R., Dick, T., & Richter, A. (2024). Broad-Spectrum *In Vitro* Activity of  $\alpha$ -aroyl-*N*-aryl-Phenylalanine Amides against Non-Tuberculous Mycobacteria and comparative Analysis of RNA Polymerases.

*Antibiotics*, 13(5), 404.

DOI: 10.3390/ANTIBIOTICS13050404

**Lang, M.**, Ganapathy, U. S., Mann, L., Seidel, R. W., Goddard, R., Erdmann, F., Dick, T., & Richter, A. (2024).

Synthesis and *in vitro* Metabolic Stability of Sterically Shielded Antimycobacterial Phenylalanine Amides.

*ChemMedChem*, 19(6), e202300593.

DOI: 10.1002/CMDC.202300593

**Lang, M.**, Goddard, R., Patzer, M., Ganapathy, U. S., Dick, T., Richter, A., & Seidel, R. W. (2024).

Polymorphism of an  $\alpha$ -Aroyl-*N*-Aryl-Phenylalanine Amide: An X-ray and Electron Diffraction Study.

*Molbank*, 2024(3), M1851.

DOI: 10.3390/M1851

**Lang, M.**, Ganapathy, U. S., Mann, L., Abdelaziz, R., Seidel, R. W., Goddard, R., Sequenzia, I., Hoenke, S., Schulze, P., Aragaw, W. W., Csuk, R., Dick, T., & Richter, A. (2023).

Synthesis and Characterization of Phenylalanine Amides Active against *Mycobacterium abscessus* and Other Mycobacteria.

*Journal of Medicinal Chemistry*, 66(7), 5079–5098.

DOI: 10.1021/ACS.JMEDCHEM.3C00009

Mann, L., Siersleben, F., **Lang, M.**, & Richter, A. (2024).

Determination of bactericidal activity against 3HC-2-Tre-labelled *Mycobacterium abscessus* (*Mycobacteroides abscessus*) by automated fluorescence microscopy.

*Journal of Microbiological Methods*, 107002

DOI: 10.1016/J.MIMET.2024.107002

Seidel, R. W., Goddard, R., **Lang, M.**, & Richter, A. (2024).

$\alpha$ -aroyl-*N*-aryl-phenylalanine amides: a promising class of antimycobacterial agents targeting the RNA polymerase.

*Chemistry & Biodiversity*, 21(6), e202400267.

DOI: 10.1002/CBDV.202400267

Mann, L., Ganapathy, U. S., Abdelaziz, R., **Lang, M.**, Zimmerman, M. D., Dartois, V., Dick, T., & Richter, A. (2022).

*In Vitro* Profiling of the Synthetic RNA Polymerase Inhibitor MMV688845 against *Mycobacterium abscessus*.

*Microbiology Spectrum*, 10(6), e02760.

DOI: 10.1128/SPECTRUM.02760-22

Mann, L., **Lang, M.**, Schulze, P., Halz, J. H., Csuk, R., Hoenke, S., Seidel, R. W., & Richter, A. (2021).

Racemization-free synthesis of *N*-2-thiophenoyl-phenylalanine-2-morpholinoanilide enantiomers and their antimycobacterial activity.

*Amino Acids*, 53(8), 1187–1196.

DOI: 10.1007/S00726-021-03044-1

### Oral Presentations

Research Symposium - NTM Drug Development – Hospital for Sick Children, Toronto, 07.2024

HIPS Symposium 2024, Helmholtz Institute for Pharmaceutical Research, Saarbrücken, 05.2024

CDI Leading Research Seminar Series, Center for Discovery and Innovation, Nutley, NJ, USA, 07.2023

Research Symposium - Antibiotic Drug Development - German University of Kairo, 07.2023

### Poster Presentations:

46<sup>th</sup> European Cystic Fibrosis Conference, Valetta, Malta, 03.2024

German Cystic Fibrosis Conference, Würzburg, 11.2023

Gordon Research Conference - Tuberculosis Drug Discovery and Development, Barcelona, 07.2023

Colorado Non-tuberculous Mycobacteria Conference 2022, Fort Collins, CO, USA, 06.2022

# Curriculum Vitae

<b>Name</b>	Markus Philipp Lang	
<b>Education</b>	08.2005 – 07.2013	Bertolt-Brecht-Gymnasium Schwarzenberg/Erzg.
	10.2013 – 10.2017	Pharmacy studies, Martin-Luther- Universität Halle-Wittenberg
	11.2017 – 04.2018	Diploma student under the supervision of Professor Dr. Lea Ann Dailey, MLU, Institute of Pharmacy, Biopharmacy, Thesis:  “The impact of the encapsulated semiconducting conjugated polymers CNPPV-2 and PCPDTBT on the biodegradability of different PEG-PLGA nanoparticle systems”
<b>Public Pharmacy</b>	05.2018 – 04.2019	Pharmacy trainee, IDT Biologika GmbH, Apotheke im Magistralen Carré
	07.2019 – 03.2023	Apotheke im Magistralen Carré, Halle (Saale)
<b>Doctoral Studies</b>	Since 10.2019	Doctoral student under the supervision of Professor Dr. Peter Imming, Institute of Pharmacy, Department of Pharmaceutical Chemistry, Thesis:  “Synthesis and Characterization of <i>N</i> α-aroyl- <i>N</i> -aryl-Phenylalanine Amides and Their Activity Against Different Mycobacteria”
	05.2023 – 09.2023	Guest researcher at the Center for Discover and Innovation, Nutley, NJ, USA Antimycobacterial inhibition assays against a broad library of NTM

Markus Philipp Lang

Halle (Saale), 28.12.2024

# Eidesstattliche Erklärung

Hiermit erkläre ich, dass ich die vorliegende kumulative Dissertation selbständig und ohne unerlaubte fremde Hilfe angefertigt habe. Ich habe keine anderen als die im Literaturverzeichnis angegebenen Quellen benutzt und alle Stellen, die veröffentlichten oder unveröffentlichten Werken wörtlich oder sinngemäß entnommen sind, sowie alle Angaben, die auf mündlichen Auskünften beruhen, als solche kenntlich gemacht. Ebenso sind alle von anderen zur Verfügung gestellten Materialien oder erbrachten Leistungen als solche gekennzeichnet. Für alle verwendeten Abbildungen, die von anderen Personen erstellt wurden, wurde die Erlaubnis zur Veröffentlichung in dieser Arbeit eingeholt. Bei der Auswahl und Beurteilung des Materials, bei der Erstellung des Manuskripts sowie bei der gedanklichen Ausarbeitung der vorgelegten Arbeit waren keine anderen Personen beteiligt. Insbesondere wurde weder die Hilfe eines Doktorvaters in Anspruch genommen, noch haben Dritte von mir unmittelbar oder mittelbar geldwerte Leistungen für Arbeiten erhalten, die im Zusammenhang mit dem Inhalt der vorgelegten Dissertation stehen. Die vorgelegte Dissertation hat in gleicher oder ähnlicher Form weder in Deutschland noch im Ausland einer anderen Prüfungsbehörde zum Zwecke der Promotion oder eines anderen Prüfungsverfahrens vorgelegen. Ich habe keine früheren erfolglosen Promotionsversuche unternommen.

Markus Philipp Lang

Halle (Saale), 28.12.2024